DOKUZ EYLÜL UNIVERSITY
GRADUATE SCHOOL OF NATURAL AND APPLIED SCIENCES

AN INVESTIGATION ON SELF-HEALING ABILITY OF CEMENT BASED COMPOSITES

Ahsanollah BEGLARIGALE

March, 2018
İZMİR

AN INVESTIGATION ON SELF-HEALING ABILITY OF CEMENT BASED COMPOSITES

A Thesis Submitted to the
Graduate School of Natural and Applied Sciences of Dokuz Eylül University
In Partial Fulfillment of the Requirements for the Degree of Doctor of Philosophy in Civil Engineering, Construction Materials Program

by
Ahsanollah BEGLARIGALE

March, 2018
İZMİR

Ph.D. THESIS EXAMINATION RESULT FORM

We have read the thesis entitled **"AN INVESTIGATION ON SELF-HEALING ABILITY OF CEMENT BASED COMPOSITES"** completed by **AHSANOLLAH BEGLARIGALE** under supervision of **PROF. DR. HALİT YAZICI** and we certify that in our opinion it is fully adequate, in scope and in quality, as a thesis for the degree of Doctor of Philosophy

Prof. Dr. Halit YAZICI
Supervisor

Prof. Dr. Selçuk TÜRKEL
Thesis Committee Member

Assist. Prof. Dr. Abdullah SÖNMEZ
Thesis Committee Member

Prof. Dr. İ. Özgür YAMAN
Examining Committee Member

Prof. Dr. Lutfullah GÜNDÜZ
Examining Committee Member

Prof.Dr. Kadriye ERTEKİN
Director
Graduate School of Natural and Applied Sciences

ACKNOWLEDGEMENTS

First and foremost I would like to express my deepest appreciation to my dear supervisor, Prof. Dr. Halit YAZICI, for his everlasting energy and valuable guidance. I would like to present my sincere thanks to him for all of his support since I came to İzmir. Special thanks to Prof. Dr. Yoldaş SEKİ for his support throughout my thesis.

I am grateful to Prof. Dr. Selçuk TÜRKEL and Assist. Prof. Dr. Abdullah SÖNMEZ for their comments and encouragement during the thesis follow-up meetings. I would like to thank C. Eng. Houtan VAHEDI and C. Eng. Doğa EYİCE for their valuable and generous support within the scope of the TÜBİTAK project. Thanks are due for my professors and friends at Construction Materials Division for their valuable contributions during my studies. Thanks are also given to M.A. KAPÇI, M.H. SUH, Ö.M. ÖNDÜN, V. SARUHAN, M. GÖKDUMAN, N. ARABACI, B. KARAHANÇER, C.E. GÜLER, N.Y. DEMİR, M. ÖZKAYA, and A.A AYTUĞ for their contributions within the scope of Undergraduate Graduation Projects.

I would like to acknowledge the financial support provided by The Scientific & Technological Research Council of Turkey (TÜBİTAK, Project No: 215M783). I would like to express my gratitude to Turkish Cement Manufacturers' Association (TÇMB) for their support within the "İz Bırakanlar Scholarships" program (2013-2016). I am also grateful to BASF (Turkey), Bekaert (Turkey), Pomza Export, Dere Concrete, and OYAK Denizli cement for their material supports.

Lastly, I would like to give my sincere thanks and deepest appreciation to my life partner, my dear wife Avat MOUSHEKAF. I would like to thank my merciful mother, loving father, and dear sisters (Aysan & Aylin) for all their love and unconditional support in my whole life.

This thesis dedicated to My Wife who filled my life with Love, Hope and Happiness.

Ahsanollah BEGLARIGALE

AN INVESTIGATION ON SELF-HEALING ABILITY OF CEMENT BASED COMPOSITES

ABSTRACT

The service life of constructions can be increased by many passive self-healing methods with lower costs and fewer problems. Encapsulation of self-healing agents by microencapsulation technology, restriction of the crack width with fibers, and ensuring the presence of unreacted cementitious materials in matrix were the self-healing techniques investigated within the scope of this study. Enhancing and characterization of self-healing ability of cementitious composites is the main aim of this research. The self-healing mechanisms of macro/micro cracks formed under tension and compression loads were investigated by various mechanical, permeability, and microstructure analysis. Ultra high performance concrete (UHPC) was used as the cement based composite. Different mix designs have been considered to increase the amount of unreacted cementitious materials in the matrix. In addition, the self-healing capacities of supplementary cementitious materials (SCM) were evaluated through a novel test method, which has been developed to assess the bonding capacity of self-healing products in cementitious composites.

The microencapsulation of sodium silicate as a self-healing agent with polymeric shell materials was one of the main objectives of this study. The synthesized microcapsules were optimized and characterized by various methods and analyses. This study has also dealt with the idea of possible microencapsulation of isophorone diisocyanate as a self-healing agent with silica-based shell for the first time in the literature.

In spite of the positive effect of SCMs on self-healing ability of UHPC, it was observed that the self-healing ratios depend on critical parameters such as damage type/level and the methods used to verify the phenomenon of self-healing. The sodium silicate, which has many advantages as a self-healing agent in cementitious materials, can be encapsulated via the interfacial polymerization of shell-forming monomer on

the aqueous sodium silicate droplets. In addition, promising results were obtained in the process of microencapsulation of isophorone diisocyanate in silica-based microcapsules.

Keywords: Cement based composite, self-healing, microencapsulation, pozzolan, microcapsule

ÇİMENTO ESASLI KOMPOZİTLERİN KENDİ KENDİNE İYİLEŞME KABİLİYETİNİN ARAŞTIRILMASI

ÖZ

Birçok pasif kendi kendine iyileşme (KKİ) yöntemi sayesinde, daha düşük maliyet ve daha az sorun ile yapıların servis ömrü arttırılabilir. KKİ ajanların mikrokapsülasyon teknolojisi ile kapsüllenmesi, kısa kesilmiş lifler ile çatlak genişliğinin kısıtlanması ve uzun süre matris içinde hidrate olmamış taneciklerin bulunmasının sağlanması KKİ yöntemleri olarak bu araştırma kapsamında incelenmiştir. Bu araştırmanın temel amacı, çimento esaslı kompozitlerin KKİ kabiliyetinin geliştirilmesi ve karakterize edilmesidir. Çekme ve basınç yükleri altında oluşan makro/mikro çatlakların KKİ mekanizmaları farklı mekanik, geçirimlilik ve içyapı analizler ile incelenmiştir. Bu çalışmada ultra yüksek performanslı beton (UYPB) çimento esaslı malzeme olarak kullanılmıştır. Hidrate olmamış puzolan ve çimento taneciklerin matris içinde yüksek miktarda bulunması için farklı tasarımlar düşünülmüştür. Ayrıca, puzolan veya mineral katkıların KKİ kapasiteleri, çimento esaslı kompozitlerdeki KKİ ürünlerin bağlama kapasitesini değerlendirmek üzere geliştirilen yeni bir deney yöntemi ile araştırılmıştır.

Sodyum silikatın bir KKİ ajanı olarak polimerik kabuk ile mikrokapsülasyonu bu çalışmanın temel amaçlarından biri olarak belirlenmiştir. Sentezlenen mikrokapsüller farklı metotlar ve analizler ile optimize ve karakterize edilmiştir. Bu çalışmada aynı zamanda, literatürde ilk kez silika esaslı kabuk ile KKİ ajanı olarak izoforon diizosiyanatın olası mikrokapsülasyonu fikri ele alınmıştır.

Puzolanların UYPB'nin KKİ kabiliyeti üzerinde olumlu etkileri olsa da, KKİ oranların hasar türü/düzeyi ve KKİ olgusunu doğrulamak için kullanılan yöntemler gibi kritik parametrelere bağlı olduğu gözlenmiştir. Çimento easalı malzemelerde bir KKİ ajanı olarak birçok avantaja sahip olan sodyum silikat, sulu sodyum silikat damlacıkları üzerinde kabuk oluşturan monomerin ara yüzey polimerizasyonu yoluyla

kapsüllenebilmiştir. Ayrıca, silika esaslı mikrokapsüllerde izofor diizosiyanatın mikrokapsülasyonu sürecinde umut verici sonuçlar elde edilmiştir.

Anahtar Kelimeler: Çimento esaslı kompozit, kendi kendine iyileşme, mikrokapsülasyon, puzolan, mikrokapsül

CONTENTS

Page

Ph.D. THESIS EXAMINATION RESULT FORM ii

ACKNOWLEDGEMENTS iii

ABSTRACT iv

ÖZ vi

LIST OF FIGURES xiii

LIST OF TABLES xxi

CHAPTER ONE - INTRODUCTION 1

1.1 Aim and Scope 2

CHAPTER TWO - LITERATURE REVIEW 3

2.1 Self-Healing Phenomena 3

2.2 Phenomenon of Self-Healing in Cement Based Composites 3

2.2.1 Significance of Self-Healing in Cement Based Composites 6

2.2.2 Self-Healing Approaches in Cement Based Composites 8

2.2.2.1 Autogenous Healing 8

2.2.2.2 Restriction of the Crack Width 10

2.2.2.3 Water Supply 14

2.2.2.4 Incorporation of Supplementary Cementitious Materials 14

2.2.2.5 Incorporation of Crystalline and Expansive Additives 19

2.2.2.6 Bacteria Based Self-Healing 19

2.2.2.7 Macrocapsule Based Self-Healing 20

2.2.2.8 Microcapsule Based Self-Healing 21

2.2.2.9 Vascular Systems 27

2.1.3 Methods Used to Verify Self-Healing in Cement-based Composites 29

2.3 Microencapsulation 30

2.3.1 Microencapsulation of Isophorone Diisocyanate 33

CHAPTER THREE - MATERIALS AND METHODS **37**

3.1 Ultra High Performance Concrete (UHPC) 37
3.1.1 Materials Used in UHPC Mixtures 37
3.1.1.1 Cement and Supplementary Cementitious Materials......................... 37
3.1.1.2 Aggregates 38
3.1.1.3 Steel fibers... 38
3.1.1.4 Chemical Admixture 39
3.1.2 Test Methods.. 39
3.1.2.1 Mixing Procedure and Mortar Flow Test.. 39
3.1.2.2 Compressive Strength Test 40
3.1.2.3 Direct Tension Test... 41
3.1.2.4 Novel “Self-Bonding” Test 43
3.1.2.5 Crack Closing Test.. 49
3.1.2.6 Total and Capillary water absorption Tests 52
3.1.2.7 Air Permeability Test 53
3.1.2.8 Ultrasonic Pulse Velocity Test.. 58
3.1.2.9 Water Permeability Test.. 59
3.2 Microencapsulation 61
3.2.1 Microencapsulation of Sodium Silicate with Urea-Formaldehyde Shell.. 61
3.2.1.1 Materials.. 61
3.2.1.2 Microencapsulation Method 62
3.2.2 Microencapsulation of Sodium Silicate with Polyurethane Shell............. 65
3.2.2.1 Materials.. 65
3.2.2.2 Microencapsulation Method 66
3.2.2.3 Characterization of Microcapsules.. 67
3.2.3 Microencapsulation of Isophorone Diisocyanate with Silica-based Shell 69
3.2.3.1 Materials.. 69
3.2.3.2 Microencapsulation Method 69
3.2.3.3 Characterization of Microcapsules.. 70

CHAPTER FOUR - RESEARCH PROGRAM **72**

CHAPTER FIVE - DESIGN OF ULTRA HIGH PERFORMANCE CONCRETE 75

5.1 Mix Designs and Fresh Properties 75
5.2 Compressive Strength Test Results.. 76
5.3 Direct Tension Test Results 76

CHAPTER SIX - INCORPORATION OF STEEL FIBERS 78

6.1 Mix Designs and Fresh Properties 78
6.2 Compressive Strength Test Results.. 80
6.3 Direct Tension Test Results 81
6.4 Discussion 83

CHAPTER SEVEN - INCORPORATION OF SUPPLEMENTARY CEMENTITIOUS MATERIALS 84

7.1 Mix Designs 84
7.2 Test Results and Discussion... 85

CHAPTER EIGHT - EVALUATION OF SELF-HEALING MECHANISM THROUGH VARIOUS METHODS 96

8.1 Evaluation of Self-Healing Mechanism Using Compressive Strength Test 96
8.2 Evaluation of Self-Healing Mechanism Using Direct Tension Test.............. 104
8.3 Evaluation of Self-Healing Mechanism Using Crack Closing Test............... 108
8.4 Evaluation of Self-Healing Mechanism Using Air Permeability Test........... 110
8.5 Evaluation of Self-Healing Mechanism Using Ultrasonic Pulse Velocity Test 112
8.6 Evaluation of Self-Healing Mechanism Using Water Permeability Test 113
8.7 Evaluation of Self-Healing Mechanism Using Total Water Absorption Test 115

8.8 Evaluation of Self-Healing Mechanism Using Capillary Water Absorption Test 121

CHAPTER NINE - MICROENCAPSULATION OF SODIUM SILICATE ... 127

9.1 Microencapsulation with Urea-Formaldehyde Polymer 127
9.1.1 Synthesis 127
9.1.2 Results and Discussion 130
9.2 Microencapsulation with Polyurethane Polymer 134
9.2.1 Optimization of Shell-Forming Monomer - Characterization of Microcapsules 134
9.1.1.1 Synthesis 135
9.1.1.2 FTIR Analysis Results 136
9.1.1.3 TG Analysis Results 137
9.1.1.4 XRD Analysis Results 139
9.1.1.5 SEM/EDS Analysis Results 140
9.1.1.7 Fracture Behavior of Microcapsules in Cementitious Matrix 143
9.2.2 Optimization of Core Material Components 146
9.2.3 Optimization of Stirring Speed 150
9.3 Incorporation of SS-loading Microcapsules in UHPC Mixtures 157
9.3.1 Second Washing/Drying Process of Microcapsules 158
9.3.2 Mix Designs and Fresh Properties of Microcapsule Containing Mixtures 160
9.3.3 The Effect of Microcapsules on Compressive Strength of UHPC mixtures 162
9.3.4 Evaluation of Self-Healing Mechanism Using Crack Closing Test 163

CHAPTER TEN - MICROENCAPSULATION OF ISOPHORONE DIISOCYANATE 170

10.1 Preliminary Tests 172
10.2 Optimization of IPDI/Silica Microcapsules 177

10.2.1 The Effect of Tween80 Weight Ratio on Properties of Microcapsules 177
10.2.1 The Effect of pH Value of Emulsion on Properties of Microcapsules . 182
10.2.3 The Effect of Stirring Speed for Emulsification on Samples................ 185

CHAPTER ELEVEN - CONCLUSIONS AND RECOMMENDATIONS 191

11.1 Conclusions 191
11.2 Recommendations 194

REFERENCES 196

LIST OF FIGURES

Page

Figure 2.1 The number of publications related to the self-healing phenomena in concrete materials between 2001 and 2011 4
Figure 2.2 The number of publications related to the self-healing materials between 1969 and 2012 5
Figure 2.3 Possible mechanisms for self-healing in concrete 6
Figure 2.4 Conceptual life-cycle models of structures made with traditional concrete 7
Figure 2.5 Conceptual life-cycle models of structure made with self-healing concrete 7
Figure 2.6. Precipitation of calcium carbonate in cracks 9
Figure 2.7 Self-healing capacity of mortars submerged in sea-water 10
Figure 2.8 An example of tensile stress–strain curve and cracks formation of ECC. 11
Figure 2.9 Tensile stress-strain relationship of air cured sound specimens, compared with that of preloaded specimens submerged in aggressive solutions and water for (a) 30 days, (b) 60 days, (c) 120 days 12
Figure 2.10 Crack-closure mechanism of shrinkable polymer tendons 13
Figure 2.11 Schematic illustration of self-sealing mechanism of cracks using SAP. 14
Figure 2.12 Healing in ECC cracks before and after subjecting to continuous wet (CW) curing.. 16
Figure 2.13 Change in compressive strength (f'c) and chloride permeability (RCPT) of preloaded specimens: (a) before healing period, (b) after 15-days healing period, (c) after 30-day healing period 18
Figure 2.14 Schematic illustration of capsule based self-healing mechanism 20
Figure 2.15 Schematic illustration of microcapsule based self-healing approach in structural composite 21
Figure 2.16 The self-healing concept of the dual component microcapsules in cementitious matrix 22

Figure 2.17 SEM images of the silica/epoxy microcapsules. a) a broken microcapsule; b) Elemental analysis (Si = blue, C = red, and Al = green); c, d, and e) microcapsules images with various magnification................................ 24
Figure 2.18 Relationship of microcapsule content of matrix with self-healing efficiency 25
Figure 2.19 Optical microscope images of a) microcapsules with solid SS core, b) microcapsules with liquid SS core 27
Figure 2.20 The schematic illustration of A) one channel and B) multiple channel vascular systems 28
Figure 2.21 A novel distribution apparatus for vascular systems: a) the cross section of model, b) side view of the apparatus, c) the apparatus is connected to tubes, and d) front view of the apparatus 29
Figure 2.22 Schematic illustration of a microcapsule 30
Figure 2.23 Microencapsulation applications in building materials 32
Figure 2.24 Reaction scheme for microencapsulation (a) and schematic diagram of microencapsulation process (b) 34
Figure 2.25 Synthesis process of the IPDI-loaded multilayer microcapsules............ 35
Figure 2.26 Schematic representation of oxygen plasma treatment and PUF microencapsulation procedure 36
Figure 3.1 Mini-flow table test... 40
Figure 3.2 Mold and details of dog bone shaped specimen 42
Figure 3.3 Direct tension test 43
Figure 3.4 The self-bonding test steel mould 44
Figure 3.5 The end plates of the mould and pins 45
Figure 3.6 The apparatus used for splitting.. 46
Figure 3.7 The connector apparatus 47
Figure 3.8 Tightening of bolts with a Torque Wrench... 47
Figure 3.9 Specimens after 30 days water curing process 48
Figure 3.10 Self-bonding test 49
Figure 3.11 The two-part apparatus use for holding pins 49
Figure 3.12 Splitting tensile strength test for introducing a crack 50
Figure 3.13 Specimens used for crack-closing test 51

Figure 3.14 Capillary water absorption test ... 53
Figure 3.15 Torrent air permeability tester ... 54
Figure 3.16 Schematic diagram of the chamber TAP tester ... 54
Figure 3.17 A) Plate-shaped specimens molds. B) Loading apparatus... 55
Figure 3.18 Casting of plate-shaped specimens ... 56
Figure 3.19 Schematic diagram of the plate-shaped specimens ... 56
Figure 3.20 TAP test conducted on the plate-shaped specimen... 57
Figure 3.21 The plate-shaped specimen under loading... 58
Figure 3.22 UPV test... 59
Figure 3.23 Schematic diagram of the water permeability test... 60
Figure 3.24 Water permeability test... 60
Figure 3.25 Preparation of the maleic copolymer solution ... 62
Figure 3.26 Setting the PH value of solution ... 63
Figure 3.27 Agitating emulsion at 55 °C for 4 h... 64
Figure 3.28 Microencapsulation process of SS with polyurethane shell: a) surfactants were to the oil phase; b) SS solution was poured to the oil phase for emulsification; c) shell-forming solution was poured to the emulsion; d, e) vacuum filtration and washing of microcapsules; f) the microcapsules were transferred to watch glasses for drying process... 67
Figure 3.29 Disc-shaped specimen ... 68
Figure 5.1 Compressive strength of mixtures ... 76
Figure 5.2 Direct tensile strengths of UHPC mixtures ... 77
Figure 6.1 Free flow test of the mixture containing 1.5% MF2 fiber ... 79
Figure 6.2 Free flow test of the mixture containing 2% MF2 fiber ... 79
Figure 6.3 Free flow test of the mixture containing 2% MF1 fiber ... 80
Figure 6.4 Compressive strength of fiber reinforced mixtures (7 days) ... 81
Figure 6.5 The stress-strain curves of fiber reinforced UHPC mixtures... 82
Figure 6.6 The average direct tensile strengths and the toughness values... 82
Figure 7.1 Compressive strengths of SCMs bearing plain mixtures... 86
Figure 7.2 The self-bonding test results... 87
Figure 7.3 The bond loads of SCMs bearing mixture as compared to bond load of the control mixture ... 88

Figure 7.4 The crack closing ratios 89
Figure 7.5 The OM and SEM images of a crack of control mixture A) before and B) after self-healing process.. 91
Figure 7.6 The OM and SEM images of a crack of FA-G1 A) before and B) after self-healing process 92
Figure 7.7 The OM and SEM images of a crack of GGBFS-G1 A) before and B) after self-healing process 93
Figure 7.8 The EDS analysis of self-healing products formed in A) control and B) FA1-G1 mixtures 94
Figure 7.9 The EDS analysis of self-healing products formed in GGBFS-G1 mixture 95
Figure 8.1 The compressive strengths of 7-day specimens before and after 30 days healing period.. 97
Figure 8.2 The compressive strengths of 90-day specimens before and after 30 days healing period.. 98
Figure 8.3 The average reductions in compressive strength of UHPC specimens due to preloading.. 99
Figure 8.4 The average percentage of regain in strength (first approach) 100
Figure 8.5 The average percentage of regain in strength (second approach)........... 102
Figure 8.6 Relative post-healing compressive strength of preloaded specimens as compared to the virgin specimens with the same curing period 103
Figure 8.7 Relative post-healing compressive strength of preloaded specimens as compared to the 7 days and 90 days cured virgin specimens............... 104
Figure 8.8 Tensile stress-strain curve of a 7-day Control specimen 106
Figure 8.9 The average percentage of regain in direct tensile strength 107
Figure 8.10 Tensile stress-strain curve of a 90-day Control specimen 108
Figure 8.11 The crack closing test results 109
Figure 8.12 The optical microscope images of a crack in Control, FA1-G1 and GGBFS-G1 mixtures A) before and B) after self-healing process 110
Figure 8.13 Water dripping from crack in a water permeability test 114
Figure 8.14 The permeability recovery values.. 115
Figure 8.15 The TWA percentages of 7-day specimens 116

Figure 8.16 The TWA percentages of 90-day specimens 117
Figure 8.17 The average increases in TWA percentages of UHPC specimens due to preloading 118
Figure 8.18 The average percentage of recovery in TWA (first approach) 120
Figure 8.19 The average percentage of recovery in TWA (second approach) 121
Figure 8.20 The CWA test results of Control mixture 122
Figure 8.21 The CWA test results of FA1-G1 mixture 123
Figure 8.22 The CWA test results of GGBFS-G1 mixture 124
Figure 8.23 The average percentage of recovery in CWA (first approach) 125
Figure 8.24 The average percentage of recovery in CWA (second approach) 126
Figure 9.1 Clogging of filter paper during vacuum filtration process 129
Figure 9.2 The particles transferred to watch glasses for drying process 130
Figure 9.3 SEM images of particles obtained from a) EP2, b) EAR2, and c) ET3 experiments 131
Figure 9.4 EDS spectrum of some particles obtained from a) EP2, b) EAR2, and c) ET3 experiments 132
Figure 9.5 SEM images of microencapsulation results of DCPD (a and b) and sodium silicate (c and d) as healing agents 133
Figure 9.6 Image of 0.4 g of MDI-3 microcapsules powder spread over a watch glass with 80 mm diameter 135
Figure 9.7 Yield values of microcapsules 136
Figure 9.8 FTIR spectra for the microcapsules 137
Figure 9.9 TGA curves for the microcapsule 138
Figure 9.10 XRD patterns of microcapsule samples 140
Figure 9.11 SEM images of (a) MDI-1, (b) MDI-2, (c) MDI-3, and (d) MDI-4 microcapsules 141
Figure 9.12 SEM image of the MDI-1 microcapsules. (b) The EDS spectrum presenting the chemical composition of a MDI-1 microcapsule 141
Figure 9.13 Crushed microcapsules 142
Figure 9.14 The EDS analyses conducted on a crushed microcapsule 142
Figure 9.15 SEM image of fractured surface of the disk-shaped specimens 144
Figure 9.16 Closer examination of a fractured microcapsule 144

Figure 9.17 SEM images of fractured microcapsule (×2000) 145
Figure 9.18 SEM images of fractured microcapsules (×430 and ×2000) 145
Figure 9.19 Yield values of microcapsules 147
Figure 9.20 SEM images of SS/W-50 (MDI-2) microcapsules 147
Figure 9.21 SEM images of SS/W-75 microcapsules 148
Figure 9.22 SEM images of SS/W-100 microcapsules 149
Figure 9.23 SEM images of SS/W-25 microcapsules 149
Figure 9.24 SEM images of SS/W-0 microcapsules 150
Figure 9.25 Yield values of microcapsules 152
Figure 9.26 The microcapsules synthesized via the EP6 procedure 152
Figure 9.27 The microcapsules synthesized via the EP7 procedure 153
Figure 9.28 The EDS spectrums presenting the chemical composition of EP7 microcapsules 154
Figure 9.29 The EDS spectrum presenting the chemical composition of irregular-shaped particles 154
Figure 9.30 The EDS spectrum presenting the chemical composition of cylindrical-like particle 155
Figure 9.31 A digital microscope image of the microcapsules synthesized via the EP7 procedures 155
Figure 9.32 A fractured microcapsule synthesized via the EP7 procedures 156
Figure 9.33 Cross section of a fractured microcapsule synthesized via the EP7 procedures 157
Figure 9.34 The aggregation and clumping of microcapsules synthesized via the EP7 procedures 158
Figure 9.35 The second washing/drying process of microcapsules 159
Figure 9.36 Microcapsules powder after the second washing/drying process 159
Figure 9.37 EDS image and spectrum of a microcapsule after the second washing/drying process 160
Figure 9.38 Compressive strengths of microcapsule containing UHPC mixtures 163
Figure 9.39 The crack closing ratios 164
Figure 9.40 SEM image captured from fractured surface of WM_Control mixture after healing period 165

Figure 9.41 Healing products at the fractured surfaces of WM_Control mixture ... 166
Figure 9.42 Healing products like Ettringite at the fractured surfaces of WM_Control mixture ... 166
Figure 9.43 Healing products (mainly $CaCO_3$) formed at the surface of a fractured aggregate ... 167
Figure 9.44 Massive $CaCO_3$ formation; and Ca-rich products with rose petal-like morphology ... 168
Figure 9.45 A dome-shaped empty covered by massive healing products ... 169
Figure 9.46 SEM image of two dome-shaped empties captured at the M_GGBFS-G1 mixture ... 169
Figure 10.1 Schematic illustration of preparing silica shell-based microcapsules via interfacial polycondensation ... 172
Figure 10.2 SEM/EDS spectrum images of the particles (possible microcapsules) synthesized via the P-EP4 experiment ... 174
Figure 10.3 DM image of the particles/microcapsules synthesized via the P-EP4 experiment ... 174
Figure 10.4 SEM/EDS spectrum images of a microcapsule synthesized via the P-EP4 experiment ... 175
Figure 10.5 DM and SEM images of the microcapsule synthesized via the P-EP5 experiment ... 176
Figure 10.6 SEM/EDS spectrum images of a microcapsule synthesized via the P-EP5 experiment ... 176
Figure 10.7 Digital microscope image of Control microcapsules ... 179
Figure 10.8 SEM/EDS spectrum images of a Control microcapsule ... 180
Figure 10.9 TGA curves for the samples (effect of Tween80) ... 181
Figure 10.10 FTIR spectra for the samples (effect of Tween80) ... 182
Figure 10.11 Digital microscope and SEM images of M-PH2.6 sample ... 183
Figure 10.12 TGA curves for the samples (effect of pH) ... 184
Figure 10.13 FTIR spectra for the samples (effect of pH) ... 185
Figure 10.14 SEM image and EDS spectrum of the M-SE800 microcapsules ... 186
Figure 10.15 Digital microscope images of A) M-SE800 and B) Control microcapsules ... 187

Figure 10.16 SEM image of the M-SE110 sample 188
Figure 10.17 TGA curves for the samples (effect of SS-E)..................................... 189
Figure 10.18 FTIR spectra for the samples (effect of SS-E).................................... 190

LIST OF TABLES

Page

Table 3.1 Physical and chemical properties of cement ... 37
Table 3.2 Properties of SCMs ... 38
Table 3.3 Properties of steel micro-fibers ... 38
Table 3.4 Properties of superplasticizer ... 39
Table 5.1 Mix design of UHPC mixtures (kg/m^3) ... 75
Table 6.1 Mix design of fiber reinforced UHPC mixtures (kg/m^3) ... 78
Table 7.1 Mix design of SCM containing mixtures (kg/m^3) ... 85
Table 8.1 Mix design of SCM and fiber containing UHPC mixtures (kg/m^3) ... 96
Table 8.2. Torrent air permeability test results ... 111
Table 8.3 The ultrasonic pulse velocity test results ... 113
Table 8.4 The water permeability test results ... 114
Table 9.1 The variables of microencapsulation process ... 128
Table 9.2 TGA data for the microcapsule samples ... 139
Table 9.3 The stirring procedures performed in each experiment ... 151
Table 9.4 Mix design of microcapsule containing UHPC mixtures ... 162
Table 10.1 The parameters examined in the preliminary tests ... 173
Table 10.2 Sample codes, varieties, and yield values (effect of Tween80) ... 179
Table 10.3 The effect of Tween80 weight ratio on TGA data ... 180
Table 10.4 Sample codes, varieties, and yield values (effect of pH) ... 182
Table 10.5 The effect of pH value on TGA data ... 184
Table 10.6 Sample codes, varieties, and yield values (effect of SS-E) ... 185
Table 10.7 The effect of SS-E on TGA data ... 189

CHAPTER ONE
INTRODUCTION

Macro and micro cracks that can be formed due the various reasons in the cement based composites are the most important problem which affects the performance of these low tensile strength materials. Existence of these cracks leads to penetration of aggressive liquid and gases that can cause lots of durability and structural problems like reinforcement corrosion. The repair of cracks formed in cement based construction materials is a complex, high cost and high labor operation (Cailleux & Pollet, 2009; V. C. Li & Herbert, 2012; Van Breugel, 2007). In addition, it can lead to many environmental and social problems. The repair operations in important infrastructures such as bridges and tunnels which have massive traffic jam or underground structures and hazardous liquid containers can be very difficult or dangerous (Freyermuth, 2001; Mihashi & Nishiwaki, 2012; Sangadji & Schlangen, 2012; Van Tittelboom & De Belie, 2013). Additionally, in many cases, the cracks are not visible or accessible (S. Zhou, Zhu, & Yan, 2014).

The service life of constructions can be increased by many passive self-healing methods with lower costs and fewer problems. Formations of calcium carbonate or calcium hydroxide, further hydration of the unreacted cement or cementitious materials or expansion of the hydrated cementitious matrix in the crack flanks are well known autogenous self-healing mechanisms in conventional concrete materials (Ter Heide, 2005). It was discovered by many researchers that the autogenous self-healing phenomena is not a constant mechanism. Also, it has not a great effect on recovery of mechanical properties. There are many self-healing methods that can be applied consciously during the production of cementitious materials. Techniques such as restriction of the crack width (Kuang & Ou, 2008b; T. Nishiwaki, Koda, Yamada, Mihashi, & Kikuta, 2012; Van Tittelboom & De Belie, 2013), usage of various pozzolans (X. Liu, Yao, Zheng, & Wu, 2005; Sahmaran, Keskin, Ozerkan, & Yaman, 2008; Sahmaran, Yildirim, & Erdem, 2013; Termkhajornkit, Nawa, Yamashiro, & Saito, 2009; Z. H. Zhou, Li, Xu, & Yu, 2011), and expansive agents (T.-H. Ahn & T. Kishi, 2010; Kishi, Ahn, Hosoda, Suzuki, & Takaoka, 2007; K. Sisomphon, Copuroglu, & Koenders, 2012, 2013) can be used for reducing the drawbacks of the autogenous healing. Novel methods such as incorporating internal curing materials, bacteria, and microcapsules are in the research development stage. In many developed countries, the problems encountered in the repairing of infrastructures such as the high cost and the invisible/inaccessible deterioration will become more important. It will be possible to eliminate these problems through a self-healing system.

1.1 Aim and Scope

Encapsulation of self-healing agents by microencapsulation technology, restriction of the crack width with micro fibers, and ensuring the presence of unreacted cementitious materials in matrix were the self-healing techniques investigated within the scope of this study. These techniques were designed in a way to support each other as a self-healing system. Enhancing and characterization of self-healing ability of ultra-high performance concrete (UHPC) mixtures is the main aim of this research. Novel test methods were also developed to assess the self-healing capacity of cementitious mixtures. In addition, besides optimization of sodium silicate bearing microcapsules, a new microcapsule was developed for self-healing materials. It is expected that some of the gaps in the related literature can be filled by new approaches, solutions and analysis presented in this study.

CHAPTER TWO
LITERATURE REVIEW

This chapter has two main sections as follows: Section 1) The phenomenon of self-healing was discussed in general terms. It was aimed to emphasize the background, significance, and different approaches of self-healing mechanisms in cement based composites. Section 2) Microencapsulation technology and its applications were explained as well as the methods used for preparing microcapsules.

2.1 Self-Healing Phenomena

The phenomenon of self-healing is the ability of living plants, animals, manmade materials (self-healing materials) to recover and/or repair damages itself (de Rooij, Van Tittelboom, De Belie, & Schlangen, 2013; Ghosh, 2009). Hager, Greil, Leyens, van der Zwaag, and Schubert (2010) stated that “in nature, self-healing can take place either at the level of single molecules (e.g. , repair of DNA) or at the macroscopic level: Merging of broken bones, closure and healing of injuries of blood vessels” (p. 5424).

Self-healing materials must be able to heal certain damages automatically/autonomously or with the minimal help of an external trigger (de Rooij et al., 2013; Ghosh, 2009). In order to design a self-heling material, different strategies and approaches can be used in the various engineering materials such as polymers, ceramics, metals, and especially cement-based materials.

2.2 Phenomenon of Self-Healing in Cement Based Composites

In 1836, the self-healing mechanism, autogenous healing of cracks, has been observed by the French Academy of Science in fractured concrete structures such as retaining structures, culverts and pipes (de Rooij et al., 2013; Van Breugel, 2007). In addition, Hearn (1998) has stated that self-healing had already observed by Hyde and Smith (1889). According to Huang, Ye, Qian, and Schlangen (2016) a more systematic study on self-healing was carried out by Glanville (1931) in 1920s. Although, self-healing is not a new issue in cement based materials, it has become an attractive and promising topic since 2001 in the field of construction materials. V. C. Li and Herbert (2012) have emphasized the increasing of the number of publications dealt with self-healing concrete between 2001 and 2011 according to Google Scholar on-line (Figure 2.1). It should be noted that there are hundreds of studies have published since 2013.

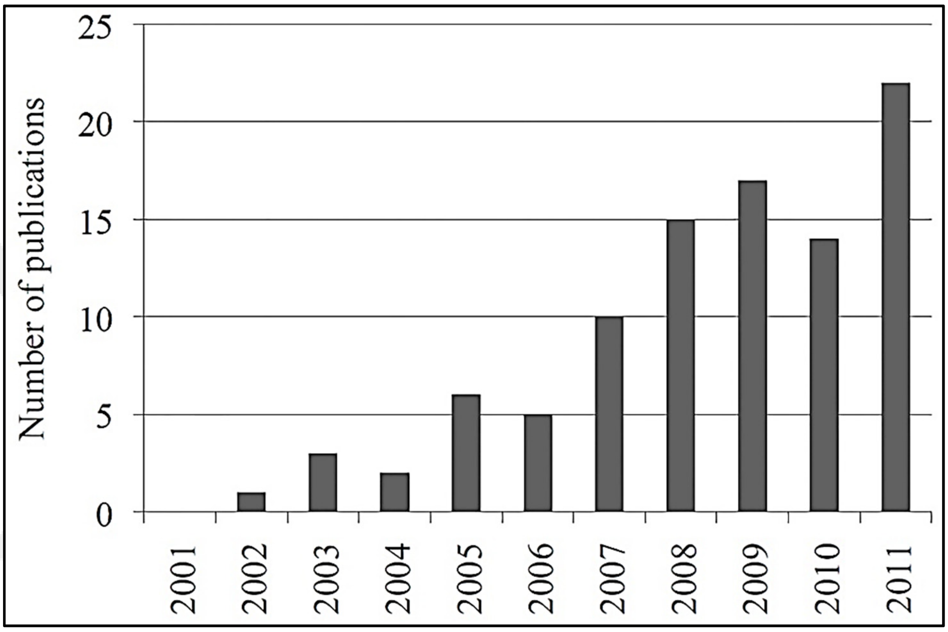

Figure 2.1 The number of publications related to the self-healing phenomena in concrete materials between 2001 and 2011 (V. C. Li & Herbert, 2012)

Van Tittelboom and De Belie (2013) have reported that self-healing properties were used for the first time in polymeric materials by Malinskii, Prokopenko, Ivanova, and Kargin (1970). They have also stated that the studies dealt with self-healing materials increased rapidly after the paper published at 2011 by White et al. (2001) in Nature (Figure 2.2). Dry (1994) started his investigation on self-healing concrete in the 90's. In addition, in the 90's, Hearn and Morley (1997) have carried out an experimental study about self-sealing property of concrete. Generally, as can be seen from Figures 2.1 and 2.2 the importance of self-healing materials has been noticed mainly after 2001.

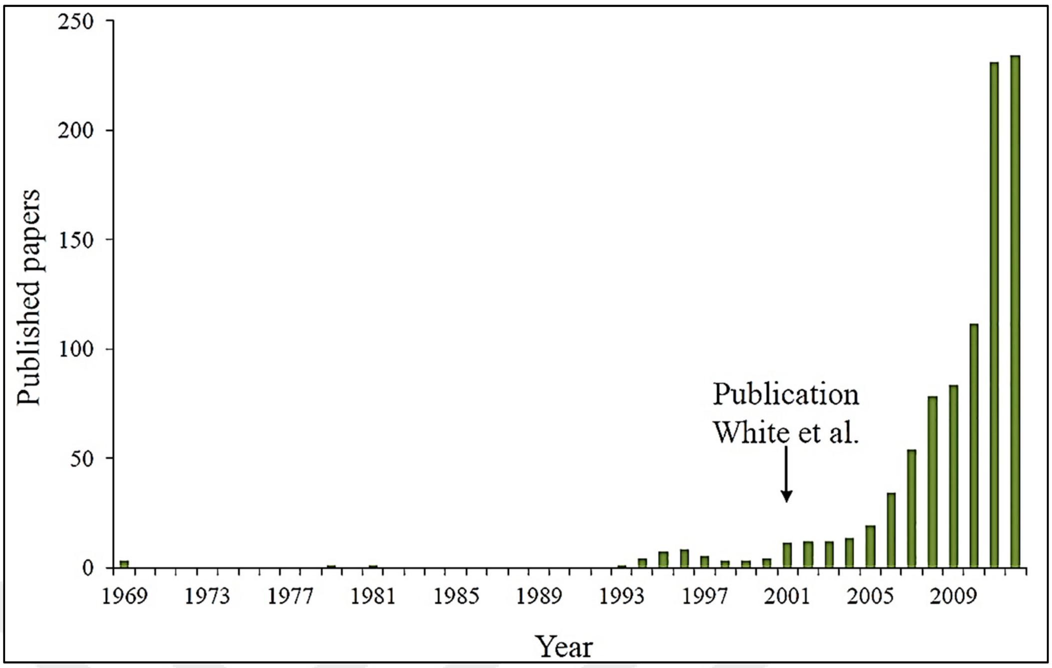

Figure 2.2 The number of publications related to the self-healing materials between 1969 and 2012 (Van Tittelboom & De Belie, 2013)

There is an autogenous self-healing mechanism in concrete due to its nature. Ter Heide (2005) has illustrated the self-healing of cracks in concrete as follows: i) Calcium carbonate or calcium hydroxide formations. ii) Cracks can be clogged by the particles and impurities suspended in the water. iii) Further hydration of unreacted particles such as cement and supplementary cementing materials iv) Swelling of calcium-silicate-hydrate in the crack flanks. In young concrete, further hydration of unreacted cement particles is the main healing mechanism, while the $CaCO_3$ formation becomes the major mechanism at later ages (Neville, 2002). Van Tittelboom and De Belie (2013) has emphasized that "autogenous healing is limited to small cracks, is only effective when water is available and is difficult to control" (p. 2183). Therefore, it seems that the autogenous self-healing mechanism should be improved by various approaches.

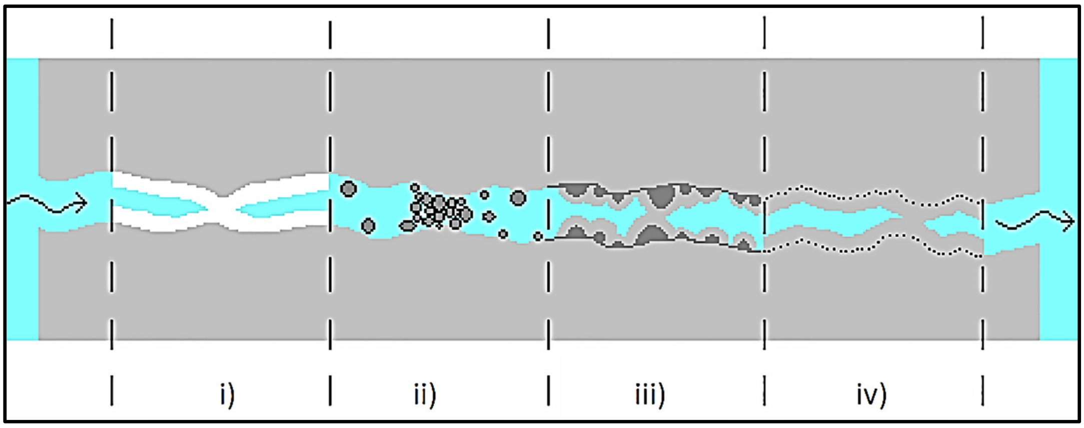

Figure 2.3 Possible mechanisms for self-healing in concrete (Ter Heide, 2005)

2.2.1 Significance of Self-Healing in Cement Based Composites

In many developed countries, the annual cost of repair and maintenance has outstripped the cost of new infrastructure construction (V. C. Li & Herbert, 2012). Christopher Joseph, Gardner, Jefferson, Isaacs, and Lark (2010) have also stated that the outlay for repair and maintenance in Great Britain is approximately 45% of the all expenditure of construction works. Similar statistics were reported for Europe by Cailleux and Pollet (2009).

As mentioned earlier, the repair operations in important infrastructures such as bridges and tunnels which have massive traffic jam or underground structures and hazardous liquid containers can be very difficult or dangerous (Freyermuth, 2001; Mihashi & Nishiwaki, 2012; Sangadji & Schlangen, 2012; Van Tittelboom & De Belie, 2013). Van Tittelboom and De Belie (2013) stated that "in addition to the direct costs, also the indirect costs due to loss in productivity and occurrence of traffic jams carry a severe economic penalty" (p. 2183). The cost associated with the traffic jam is estimated to be 10 times higher than the cost of repair and maintenance works (Freyermuth, 2001). Additionally, in many cases, the cracks are not visible or accessible (Van Tittelboom & De Belie, 2013).

Van Breugel (2007) has compared the performance and cost of structures by means of conceptual life-cycle models. As can be seen in Figure 2.4, the gradual deterioration in structures requires first repair after a certain period of time (curve A). In most cases, a second repair is required after 10-15 years. If a high-quality structure is constructed at a higher cost, the maintenance-free period can be extended and the first major repair operation can be postponed (curve B). A higher quality material significantly reduces the cost of repair and maintenance. The extreme case is a smart structure that can exhibit self-healing behavior that does not require repair and maintenance costs (Figure 3.5). As seen in Figure 3.5, over time, the material will repair itself and thus will not have the cost of repair and maintenance. Although the initial cost of reinforced concrete construction showing self-healing behavior will be high, it can be a financially positive situation for the project owner by eliminating costs of maintenance and repair.

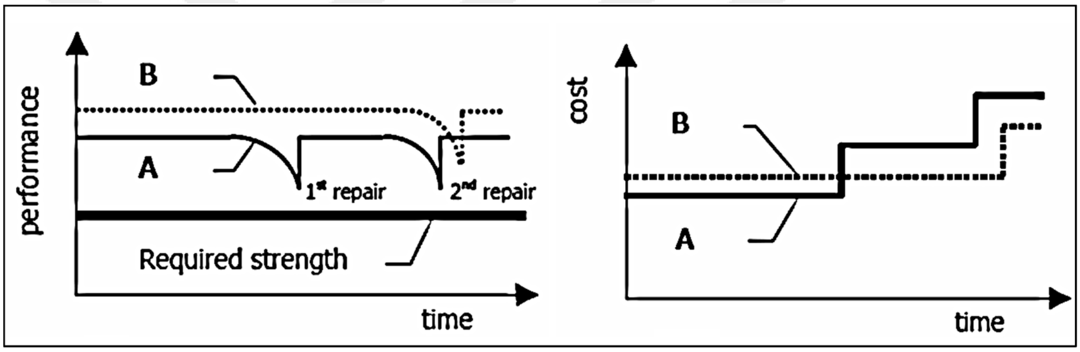

Figure 2.4 Conceptual life-cycle models of structures made with traditional concrete (Van Breugel, 2007)

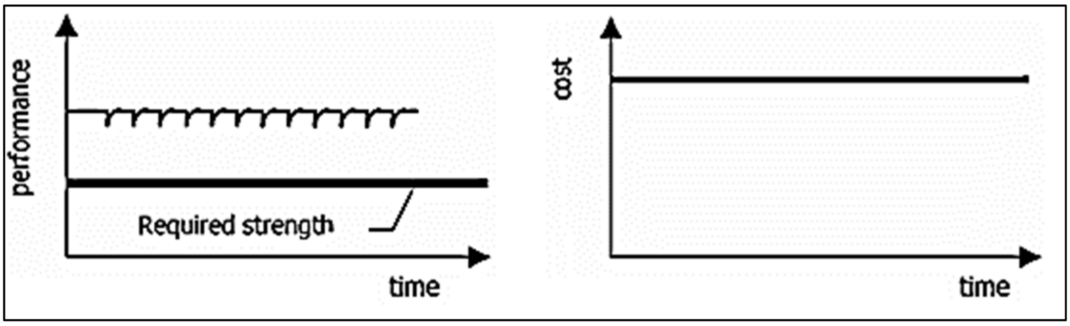

Figure 2.5 Conceptual life-cycle models of structure made with self-healing concrete (Van Breugel, 2007)

2.2.2 Self-Healing Approaches in Cement Based Composites

Van Tittelboom and De Belie (2013) has categorized the main and well-known self-healing mechanisms in cementitious materials as follows: 1) Intrinsic healing: Autogenous healing, improved autogenous healing, and healing in polymer modified concrete. Improved autogenous healing can be achieved by restriction of the crack width, water supply, improving the possibility of further hydration and crystallization. Further hydration and crystallization can be promoted by using supplementary cementitious materials, expansive additives, and bacteria. 2) Capsule based self-healing: Macroencapsulation and microencapsulation. 3) Vascular based self-healing.

Huang, Ye, Qian, et al. (2016) has also categorized self-healing of cracks in cementitious materials according to mechanisms as follows: “1) autogenous self-healing, 2) self-healing based on mineral admixtures, 3) self-healing based on bacteria, 4) self-healing based on adhesive agents” (p. 500).

2.2.2.1 Autogenous Healing

As mentioned earlier, the autogenous self-healing in concrete is a mechanism originated from the nature of cement based composites. Similar to the hypothesis of Neville (2002), there is an agreement in literature that autogenous self-healing can be mainly attributed to further hydration of unhydrated cement particles and carbonation $Ca(OH)_2$.

Calcium hydroxide, which is one of the cement hydration products dissolved in water, is present throughout the cracking surfaces. Wu, Johannesson, and Geiker (2012) has summarized the reaction of carbon dioxide with calcium ions in cracks as follows: “then free calcium ions from cement hydration react with dissolved carbon dioxide, so ‘selfhealed’ crystals are formed, growing at both surfaces of the cracks and finally filling into the gaps” (p. 573). As can be seen from figure 2.6, Edvardsen (1999) illustrated the above-mentioned mechanism in schematic figure.

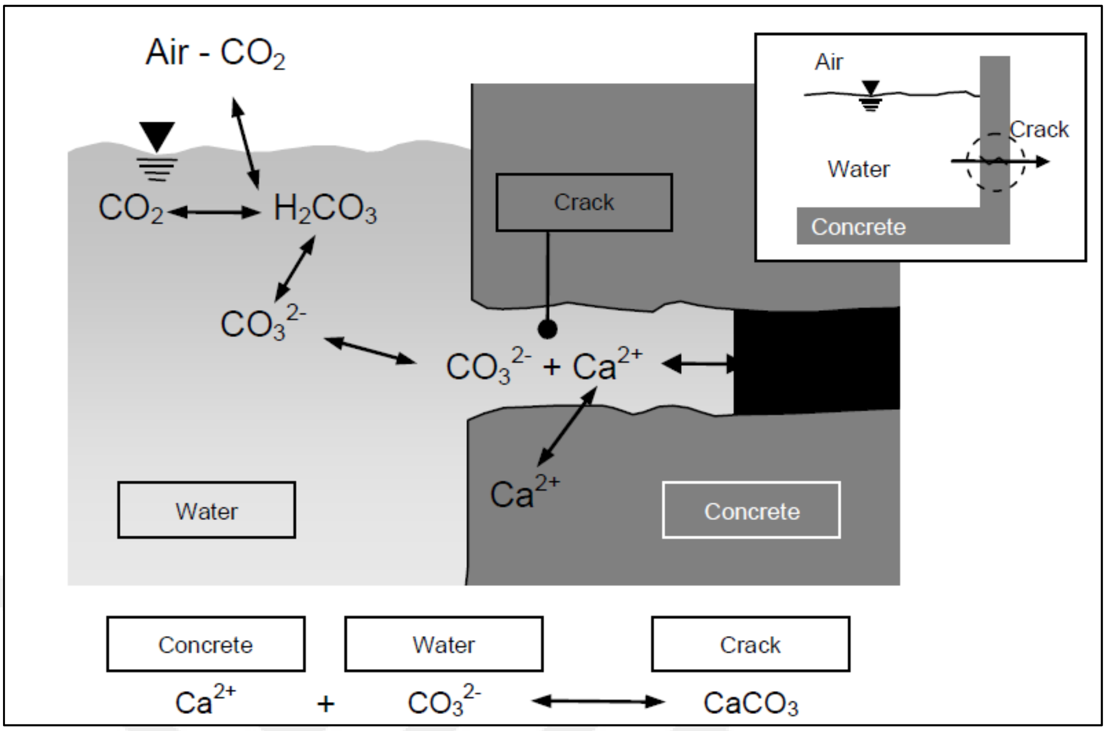

Figure 2.6. Precipitation of calcium carbonate in cracks (Edvardsen, 1999). This figure was reprinted from the paper of Mihashi and Nishiwaki (2012)

The autogenous self-healing mechanism is now a well-known mechanism owing to the studies carried out by researchers all over the world (Aldea, Song, Popovics, & Shah, 2000; Clear, 1985; Edvardsen, 1999; Hearn, 1993; Hearn & Morley, 1997; Huang, Ye, & Pel, 2016; Jacobsen, Marchand, & Boisvert, 1996; Jacobsen & Sellevold, 1996; Neville, 2002; Nijland, Larbi, van Hees, Lubelli, & de Rooij, 2007; Ramm & Biscoping, 1998; Reinhardt & Jooss, 2003; Sahmaran, Li, & Li, 2007; Y. Z. Yang, Lepech, Yang, & Li, 2009). Besides the well-known above-mentioned phenomena, different mechanism can lead to an autogenous self-healing process depending on the environment in which structures are located. Palin, Wiktor, and Jonkers (2015) evaluated the autogenous self-healing capacity of mortar specimens immersed in fresh- and sea-water. As can be seen from Figure 2.7 the ordinary Portland cement mortar specimens immersed in sea-water displayed the maximum healing capacity. They emphasized the ions such as magnesium, calcium, and carbonate in sea-water can precipitate as minerals. Palin et al. (2015) has stated that “these precipitates give cementitious materials in sea-water a greater healing potential over those in fresh-water” (p. 22).

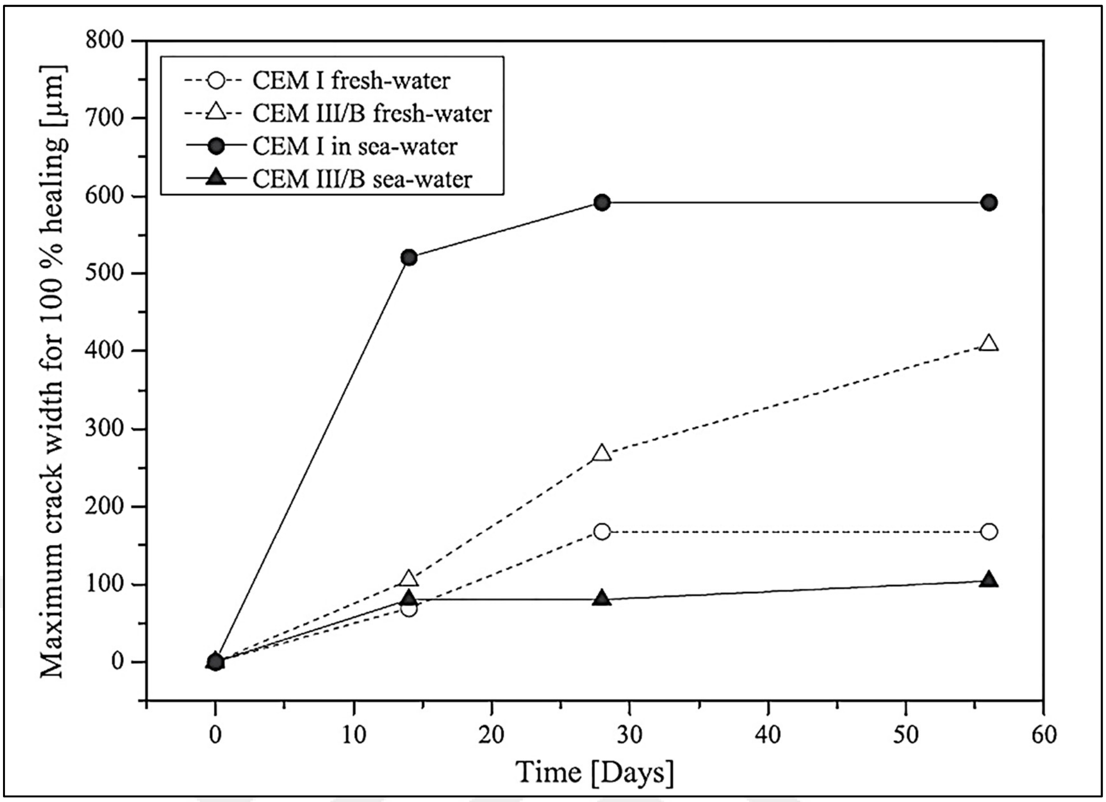

Figure 2.7 Self-healing capacity of mortars submerged in sea-water (Palin et al., 2015)

2.2.2.2 Restriction of the Crack Width

The efficiency of autogenous self-healing mechanism can be enhanced by restriction of the crack width. In other words, the narrower cracks are more likely to be closed by the autogenous self-healing mechanism (Van Tittelboom & De Belie, 2013). the use of different fibers is greatly contributing to the autogenous self-healing by restricting the crack width (Kunieda, Choonghyun, Ueda, & Nakamura, 2012). Fiber reinforced cementitious composite (FRCC) can be categorized as a self-healing material. T. Nishiwaki et al. (2012) have stated that "FRCC has mechanical characteristics that can control crack propagation in the cement matrix through bridging with short fibers. Since the self-healing process requires crack widths that are sufficiently small, FRCCs are expected to have great self-healing capability" (p. 195).

A typical and successful example for above-mentioned approach is the Engineered Cementitious Composite (ECC). ECC is an ultra ductile fiber reinforced cement based composites with tensile strain-hardening behavior, originally developed at the University of Michigan (V. C. Li, Lim, & Chan, 1998). In contrast with the other FRCCs, Multiple cracks is form in the ECC with a maximum crack width below 60 μm. An example of tensile stress–strain curve and cracks formation of ECC are shown in Figure 2.8. V. C. Li et al. (1998) carried out a study on the self-healing capacity of ECC and reveled the superior self-healing behavior it. (H. Z. Liu, Zhang, Gu, Su, & Li, 2017b) have analyzed the self-healing behavior of ECC exposed to aggressive chloride and sulfate conditions. The mechanical properties were experimentally evaluated for ECC specimens that were preloaded to 1% strain and submerged in sulfate and sulfate-chloride solutions for 30, 60 or 120 days. Control specimens were also prepared and immersed in water. As can be seen from Figure 2.9, the tensile strain capacity of preloaded ECC exposed to aggressive solutions and water (after self-healing) was higher than that of specimen that were reloaded after 1 day after preloading.

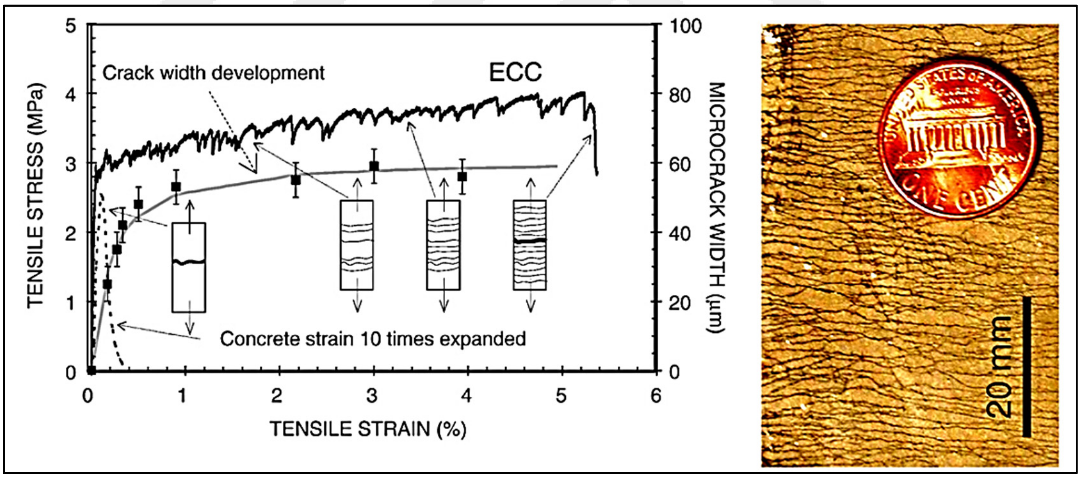

Figure 2.8 An example of tensile stress–strain curve and cracks formation of ECC (Sahmaran & Li, 2009)

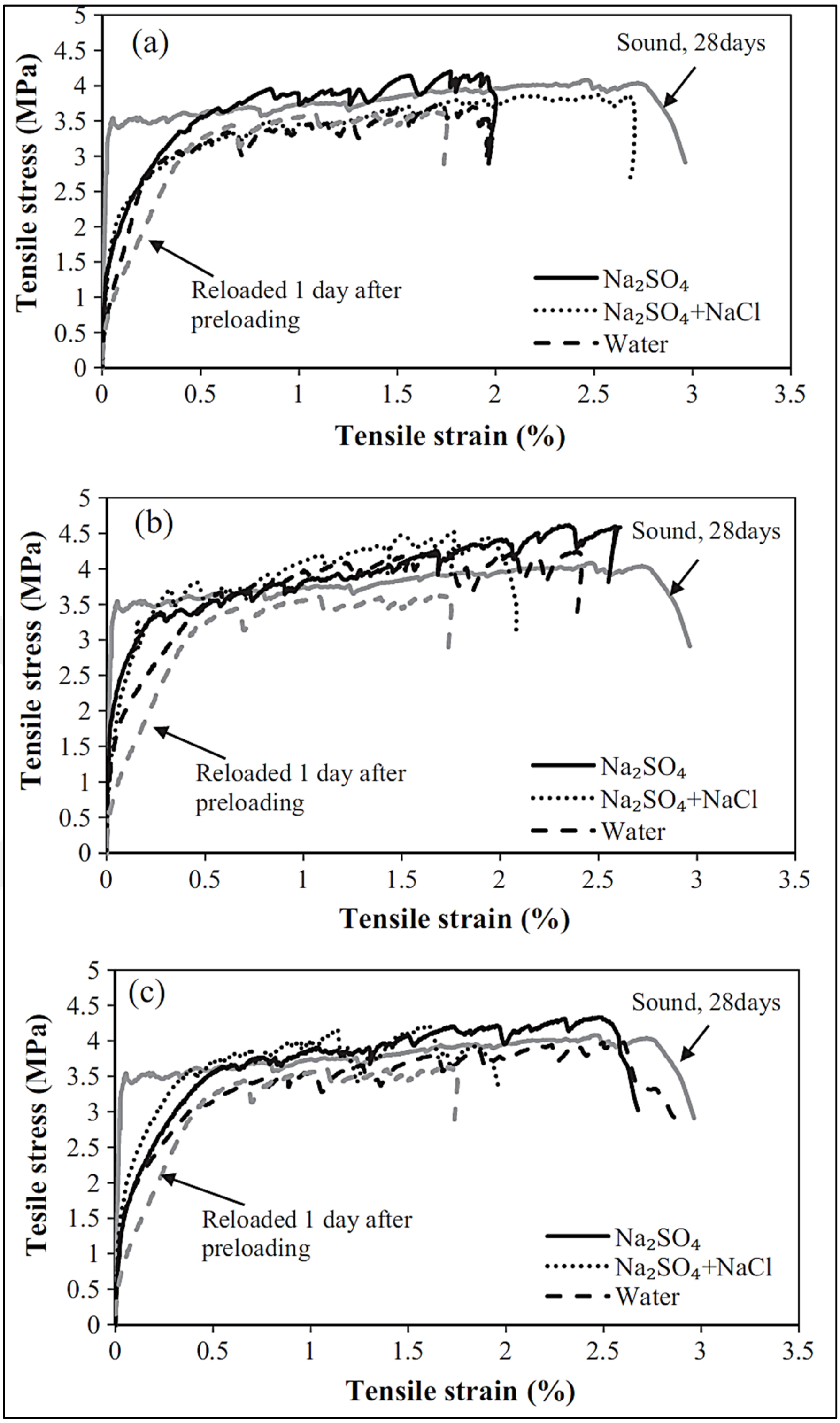

Figure 2.9 Tensile stress-strain relationship of air cured sound specimens, compared with that of preloaded specimens submerged in aggressive solutions and water for (a) 30 days, (b) 60 days, (c) 120 days (H. Z. Liu et al., 2017b)

Besides the many studies that have dealt with the self-healing behavior of synthetic fibers reinforced ECC, (Hung, Su, & Hung, 2017; M. Li & Li, 2011; V. C. Li et al., 1998; H. Z. Liu, Zhang, Gu, Su, & Li, 2017a; H. Z. Liu et al., 2017b; Qian, Zhou, & Schlangen, 2010; Sahmaran et al., 2007; Sahmaran & Li, 2009; Siad, Lachemi, Sahmaran, & Hossain, 2017; Y. Z. Yang et al., 2009), the self-healing efficiency of different steel fibers reinforced cementitious composites were investigated in some researches (Homma, Mihashi, & Nishiwaki, 2009; Kim, Kang, & Ahn, 2014; T. Nishiwaki, Kwon, Homma, Yamada, & Mihashi, 2014). Kim et al. (2014) the crack self-healing capacity of high-performance steel-fiber reinforced cement composites (HPSFRC) was examined by means of the mechanical recovery. In order to introduce multiple micro cracks, they pretensioned all of the specimens at the age of 90-day up to 0.3% tensile strain. Then, the specimens were re-tensioned after 3, 7, and 14 days. Kim et al. (2014) reported that the first cracking strength can be recovered up to 36% at 14-day of water healing, while this recovery ratio was 100% for post cracking strength.

In another approach, the cracks can be restricted at the time of unloading with shape memory alloys or polymers (Isaacs, Lark, Jefferson, Davies, & Dunn, 2013; Jefferson et al., 2010; C. Joseph, Jefferson, Isaacs, Lark, & Gardner, 2010; Kuang & Ou, 2008a, 2008b; Teall et al., 2017). Jefferson et al. (2010) has summarized the crack-closure mechanism of shrinkable polymer tendons in cement based composites as follows (Figure 2.10): “The shrinkage mechanism in the anchored embedded polymer tendon (or tendons) is activated by heating, which results in crack closure and compressive stresses being developed across the closed crack faces” (p. 796).

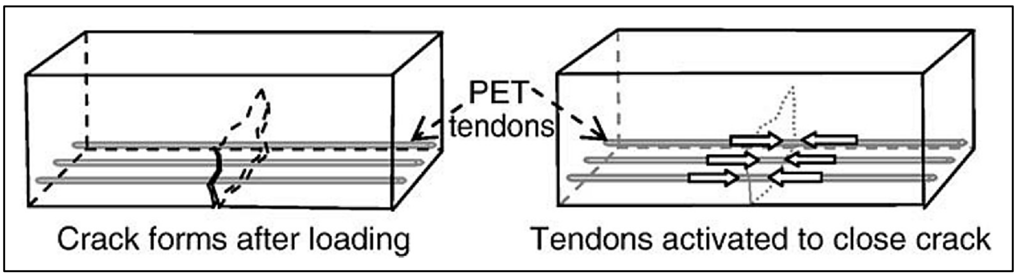

Figure 2.10 Crack-closure mechanism of shrinkable polymer tendons (Jefferson et al., 2010)

2.2.2.3 Water Supply

Superabsorbent polymers (SAP), which absorb a huge amount of liquid from their surroundings, can be used in cement based materials to block cracks and provide additional water for autogenous self-healing mechanism (H. Lee, Wong, & Buenfeld, 2010; H. X. D. Lee, Wong, & Buenfeld, 2016; Snoeck, Steuperaert, Van Tittelboom, Dubruel, & De Belie, 2012). As can be seen from the schematic illustration presented in Figure 2.11-a, the SAPs, which are added to fresh concrete mixtures, releases its adsorbed water and shrinks, leaving behind hundreds of micronmetres pores in the matrix. The cracks are likely to propagate through those pores during the service life of concrete (Figure 2.11-b). Ingress of moisture and fluids through the cracks can lead to swell SAP significantly depending on the ionic concentration of the liquid. As can be seen from Figure 2.11- c, the expanded SAP can directly block the crack and prevent further ingress of water (H. Lee et al., 2010). During dry periods, the swollen SAP can release its absorbed water through the crack, resulting more effective autogenous healing (Van Tittelboom & De Belie, 2013).

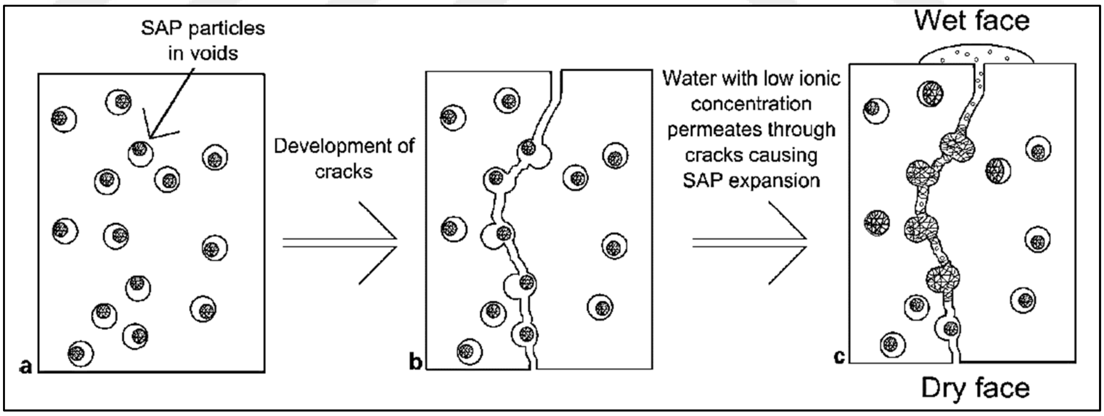

Figure 2.11 Schematic illustration of self-sealing mechanism of cracks using SAP (H. Lee et al., 2010)

2.2.2.4 Incorporation of Supplementary Cementitious Materials

Pozzolans or supplementary cementitious materials (SCM) such as fly ash (FA) and ground granulated blast furnace slag (GGBFS) are widely used in cement based composites. It is now well-known that the SCMs provides many advantages for cementitious composites. As considerable amounts of SCMs remains unhydrated for a long period of time, the autogenous self-healing due to further hydration can be promoted (Van Tittelboom & De Belie, 2013). Thanks to these properties of pozzolans, they can provide great advantages for the self-healing mechanism. When any cracks occur, existing unhydrated pozzolanic particles in the surfaces of cracks may form secondary C-S-H as a result of reaction with calcium hydroxide. The self-healing mechanism that can be formed as a result of using SCMs depends on the existence of water, ambient temperature, substitution amount, chemical and physical properties of SCMs.

Sahmaran et al. (2013) have investigated comprehensively the effects of Class-F FA, Class-C FA and GGBFS on the self-healing capabilities of Engineered Cementitious Composite (ECC) exposed to various environmental conditions. The ECC cylindrical specimens with Ø100×50 mm dimensions were preloaded (up to failure) at the age of 60 days by means of splitting tensile test, and then exposed to freeze/thaw cycle, continuous air and wet conditions (CW) for 30 and 60 days. The self-healing capability were assessed by measuring of rapid chloride permeability test. They revealed that the type of SCMs has great effects on the self-healing capability of cement based composites as measured by the rapid chloride permeability test. Sahmaran et al. (2013) have emphasized that “although ECC samples with fly ash have more unhydrated cementitious materials, and therefore, expectedly, a higher capacity for self-healing, more evident self-healing product was observed from the ECC mixture incorporating slag” (p. 89). As can be seen from Figure 2.12, depending on the crack width and type of SCMs, self-healing was observed in all of ECC mixtures under CW condition up to certain level. Sahmaran et al. (2013) have also stated “decrease in the crack width suggests that CW curing have greatly promoted the self-healing process and therefore enhanced the chloride ion transport properties after precracking” (p. 99). Z. G. Zhang, Qian, and Ma (2014) has revealed that self-healing behavior of ECC mixture can be remarkably enhanced with FA to cement ratio of four by weight. The superior effect of FA on the self-healing behavior of ECC was also reported in other studies (Alyousif, Lachemi, Yildirim, & Sahmaran, 2015; Hung, Su,

& Su, 2018; Ozbay, Sahmaran, Lachemi, & Yucel, 2013; Yildirim, Sahmaran, & Ahmed, 2015).

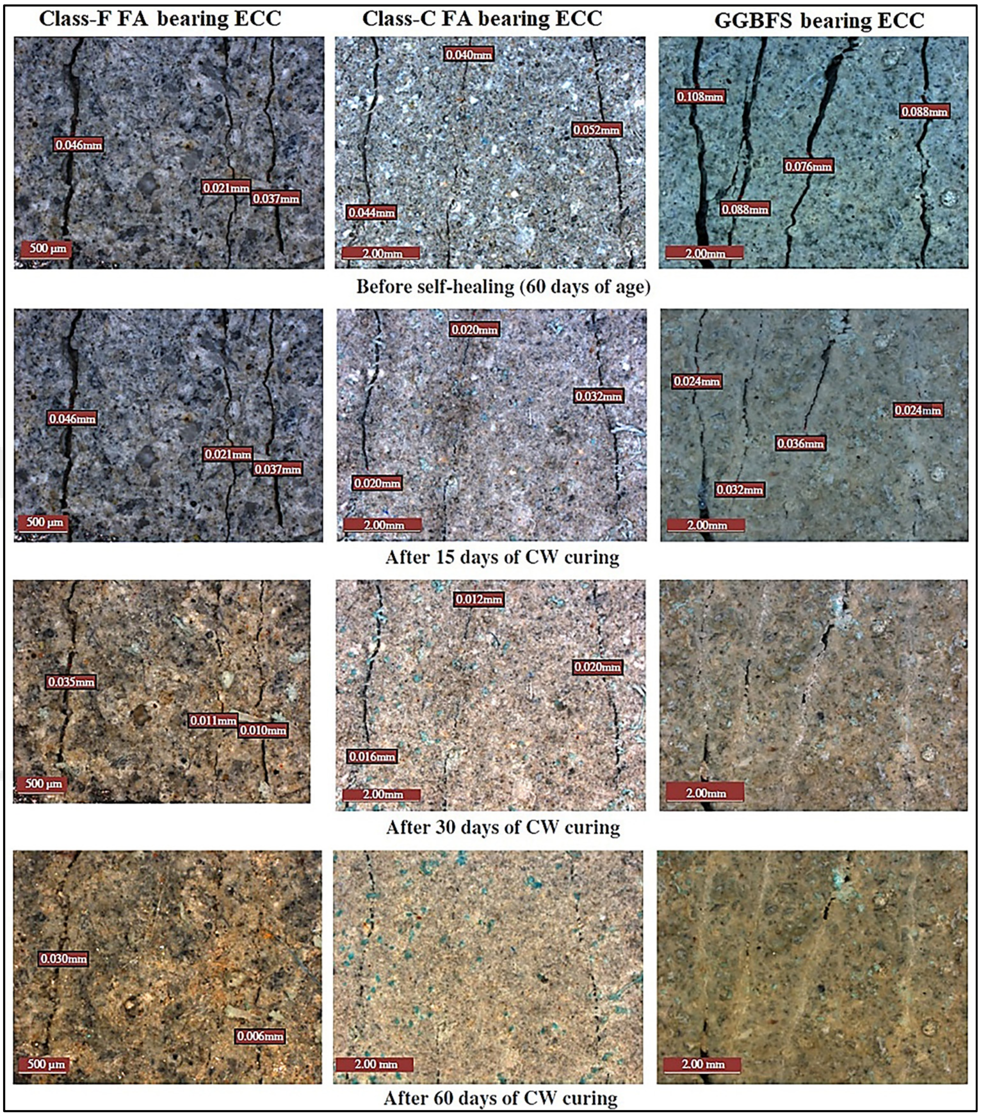

Figure 2.12 Healing in ECC cracks before and after subjecting to continuous wet (CW) curing (Sahmaran et al., 2013)

Termkhajornkit et al. (2009) have investigated the self-healing capacity of FA bearing mixtures (pastes) by focusing on the their porosity, compressive strength, chloride diffusion coefficient, and hydration reactions after shrinkage cracking occurs (after 28 days). Termkhajornkit et al. (2009) have concluded that “fly ash–cement system has the self-healing ability for micro cracks that occur from shrinkage” (p. 202).

Sahmaran et al. (2008) have analyzed the phenomenon of self-healing in self-consolidating concrete mixtures in which low-lime FA was used with 0%, 35%, and 55% replacement ratios. After preloading of specimens under uniaxial compression loads up to 70% and 90% of their ultimate compressive load, they were stored in water for 30 days. As can be seen from Figure 2.13, Sahmaran et al. (2008) evaluated the self-healing behavior of preloaded specimens by means of change in measured parameter (compared to the virgin specimens at the same ages) before and after 15 and 30 days water curing (healing period). They reported that FA bearing mixtures lost strength up to 27% in the case of 90% preloading level. After 30-day healing period, the strength loss was 7% as result of the self-healing mechanism. In the case of mixtures without FA, the strength loss before and after healing period was 19% and 13%, respectively. Sahmaran et al. (2008) have observed similar behaviors through the rapid chloride permeability test (RPCT). Na et al. (2012) have investigated the hydration process of four different FA in paste mixtures, while the self-healing ability of the FAs were evaluated in mortar mixtures. They have concluded that "to ensure proper self-healing performance, practical fly ash replacement ratios in fly ash concrete could be 10% to 15% and 11% to 20% for water to cement ratios 0.50 to 0.55 and 0.55 to 0.60, respectively" (p. 252).

Huang, Ye, and Damidot (2014) made artificial planar gaps in a GGBFS cement paste (containing 66% of slag) cubic specimen to separate the healing products from the matrix. For this purpose, the specimen was sliced and then the slices were grounded to achieve flat surfaces. The slices were put together and cured saturated $Ca(OH)_2$ solution for 200 h. Huang et al. (2014) reported that "the reaction products formed in cracks are mainly composed of C-S-H, ettringite, hydrogarnet and OH–hydrotalcite. The fraction of C-S-H in reaction products is much larger than the other minerals, which is similar to the bulk paste" (p. 81). Salama, Hilloulin, Medjigbodo, and Loukili (2017) have investigated the self-healing potential of mortar mixtures incorporating GGBFS and metakaolin (25% replacement ratio) through mechanical and permeability tests. Their test results revealed that the GGBFS bearing mixture had self-healing capacity as compared to the control mixtures while the performance metakaolin bearing mortar was relatively close to the control mixture (Salama et al., 2017).

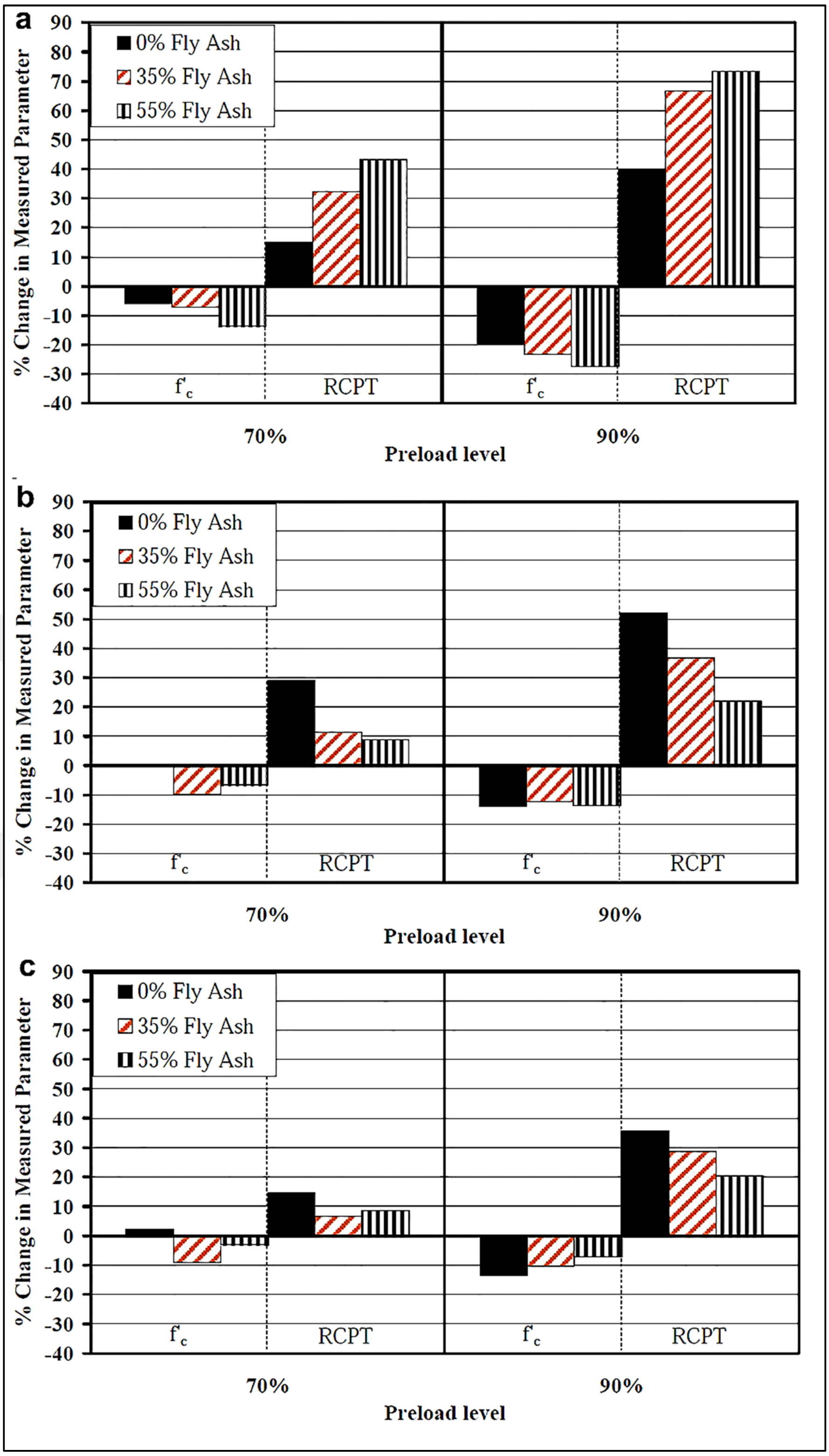

Figure 2.13 Change in compressive strength (f'c) and chloride permeability (RCPT) of preloaded specimens: (a) before healing period, (b) after 15-days healing period, (c) after 30-day healing period (Sahmaran et al., 2008)

2.2.2.5 Incorporation of Crystalline and Expansive Additives

Alternative cementitious additives can be used in cement based composites to enhance the self-healing mechanism. K. Sisomphon et al. (2012) used a calcium sulfoaluminate based expansive additive and a reactive silica containing crystalline additive for crack-closing purpose. The same authors, in another study (K. Sisomphon et al., 2013), reported that the self-healing products are composed of ettringite, $CaCO_3$, and C–S–H gel. K. Sisomphon et al. (2013) have stated that "the proportion of healing minerals depends on exposure condition and the type of cementitious materials used" (p. 217). In addition to above-mentioned additives, MgO type expansive agents (Sherir, Hossain, & Lachemi, 2016, 2017a, 2017b), geo-materials (T. H. Ahn & T. Kishi, 2010), and a blend of microsilica-cement-sand (Ferrara, Krelani, & Moretti, 2016) were used in some studies. Van Tittelboom and De Belie (2013) have nicely summarized the self-healing mechanism of them as follows: "when water enters into the crack, the expansive agent expands, the geo-materials swell and the chemical agents cause precipitation of crystals leading to crack closure" (p. 2186-2187).

2.2.2.6 Bacteria Based Self-Healing

The idea of using $CaCO_3$ precipitating bacterial spores as a healing agents in concrete was firstly proposed by Ramachandran, Ramakrishnan, and Bang (2001). Jonkers (2007) has summarized the general mechanism of bacteria based self-healing as follow: "bacteria on fresh crack surfaces become activated due to water ingression, start to multiply and precipitate minerals such as calcite ($CaCO_3$), which eventually seal the crack and protect the steel reinforcement from further external chemical attack" (p. 199). This approach has drawn the attention of many researchers all over the world. Thanks to this attention many novel methods and materials such as encapsulation of bacterial spores and new nutrients for bacteria have been developed up to now (Bhaskar, Hossain, Lachemi, Wolfaardt, & Kroukamp, 2017; Sangadji, Wiktor, Jonkers, & Schlangen, 2017; J. Wang, Jonkers, Boon, & De Belie, 2017; J. Y. Wang, Snoeck, Van Vlierberghe, Verstraete, & De Belie, 2014; J. Y. Wang, Soens, Verstraete, & De Belie, 2014; Wiktor & Jonkers, 2011; Xu & Yao, 2014).

2.2.2.7 Macrocapsule Based Self-Healing

Capsule or macrocapsule based self-healing is an approach in which a healing agent are surrounded and protected by a shell material. In the event of any crack occur, the capsule breaks and the healing agent release into the crack (Figure 2.14). The healing mechanisms of agents were nicely summarized by Van Tittelboom and De Belie (2013) as follows: “some agents react upon contact with moisture or air or due to heating or upon contact with the cementitious matrix itself, other agents react when making contact with a second component which is present in the matrix or provided by additional capsules” (p. 2188).

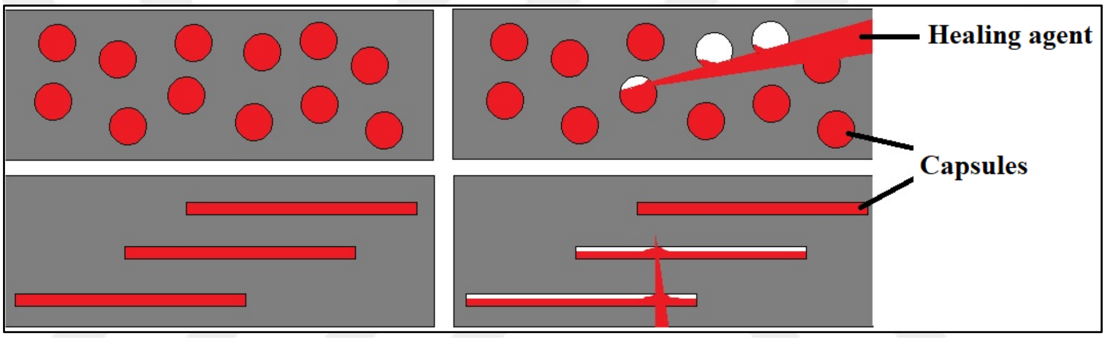

Figure 2.14 Schematic illustration of capsule based self-healing mechanism

In 1990s, the first applications of cylindrical capsules in cementitious composites were investigated in few studies (Dry, 1994, 1999). The capsules can be cylindrical (hollow pipettes or tubes) spherical made with various range of materials such as glass, polymers, and even lightweight porous aggregates. (Choi, Oh, & Choi, 2017; Gilabert et al., 2017; C. Joseph et al., 2010; V. C. Li et al., 1998; Tomoya Nishiwaki, Mihashi, Jang, & Miura, 2006; Savija et al., 2017).

Choi et al. (2017) have encapsulated cement powder in a cement-based capsule an then, used in a mortar mixture to proof their method. In the study carried out by Sisomphon, Copuroglu, & Fraaij, (2011), sodium monofluorophosphate solution was impregnated into a cement coated expanded clay aggregate to produce a self-healing system in GGBFS bearing mortars. Alghamri, Kanellopoulos, and A-Tabbaa (2016) have also used lightweight aggregates as host for healing agent (sodium silicate).

2.2.2.8 Microcapsule Based Self-Healing

Storing healing agents in capsules is one of the most promising self-healing methods in cementitious materials. Because of the considerable advantage of microencapsulation, it has become more interested as compared to the other encapsulation methods. For the first time, White et al. (2001) have proposed the microcapsule based self-healing methods for polymer composites. White et al. (2001) have described the healing concept of their proposed method as follows (Figure 2.15): "a, Cracks form in the matrix wherever damage occurs; b, the crack ruptures the microcapsules, releasing the healing agent into the crack plane through capillary action; c, the healing agent contacts the catalyst, triggering polymerization that bonds the crack faces closed" (p. 794).

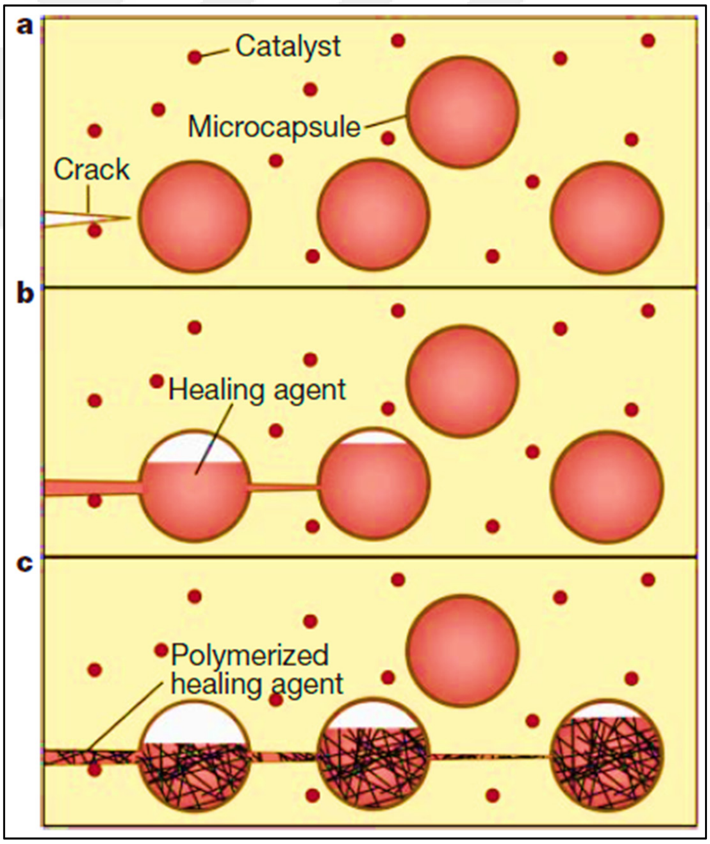

Figure 2.15 Schematic illustration of microcapsule based self-healing approach in structural composite (White et al., 2001)

Since 2001, hundreds of studies have been carried out all over the world to develop the microcapsule based self-healing system in various range of materials especially polymer based composites. Zhu, Rong, and Zhang (2015) have provided a comprehensive literature review related with the microcapsule based self-healing approaches in polymeric materials.

The microcapsule based self-healing approach in cement based composites is relatively new topic as compared to the polymer composites. Before 2011, there are few studies (Xing et al., 2008; Z. X. Yang, Holler, He, & Shi, 2010) that have dealt with microcapsule based self-healing method in cement-based composites. Because the cementitious materials have completely different nature, most of the microcapsule used in polymer composites cannot provides effective self-healing mechanism in cement based composites. Z. X. Yang, Hollar, He, and Shi (2011) have encapsulated methylmethacrylate monomer and triethylborane as the healing agent and the catalyst through an interfacial self-assembly process. The shell of these microcapsules was a silica based material as results of sol–gel reaction. As can be seen from Figure 2.16, there were two kind of microcapsules embedded the cementitious matrix. Z. X. Yang et al. (2011) have summarized the concept of their suggested method as follows (Figure 2.16): "for the hardened mortar, self-healing can be triggered by crack propagation through the microcapsules, which then releases the healing agent and the catalyst from their respective stress-ruptured reservoir upon crack intrusion" (p. 507).

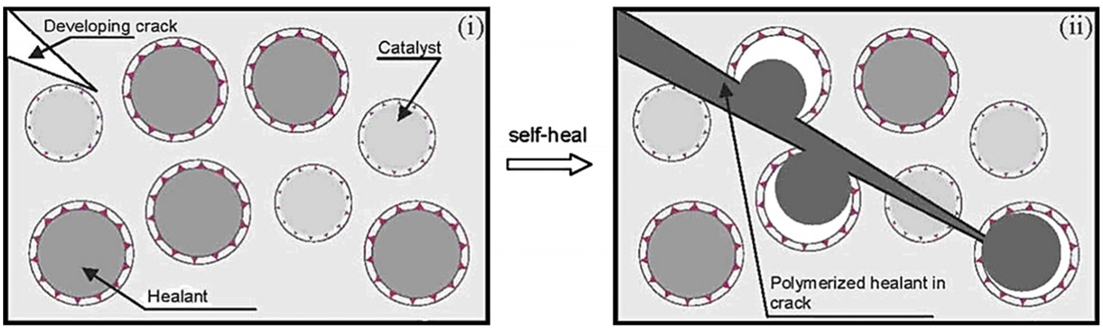

Figure 2.16 The self-healing concept of the dual component microcapsules in cementitious matrix (Z. X. Yang et al., 2011)

Z. X. Yang et al. (2011) have reported significant self-healing ratios in the preloaded specimens. It was also stated that the silica based shell of microcapsules form a stronger bond with the cementitious matrix. The shell can chemically and physically bonded to the matrix, allowing the microcapsule to remain stable for years without deterioration. The adherence between the shell and the matrix must be strong. If the wall-matrix bond strength is low, the crack will advance from the interface and the microcapsule will not break (S. Zhou et al., 2014). Perez, Erkizia, et al. (2015) have also synthesized a type of microcapsules with silica based shell for self-healing mechanism in cement based composites (Figure 2.17). They have encapsulated Epothin® (epoxy compound) as healing agent through a sol-gel reaction. Similar to the hypothesize of Z. X. Yang et al. (2011), Perez, Erkizia, et al. (2015) have stated that "a good bond will be formed between the shell of the capsules and the matrix, but the silica capsules remain stable in a high proportion upon reaction with lime" (p. 47). The self-healing efficiency of these microcapsules were investigated in different studies (Calvo et al., 2017; Perez, Gaitero, Erkizia, Jimenez, & Guerrero, 2015). Calvo et al. (2017) have reported that although the silica/epoxy microcapsules are well integrated in the matrix, they can causes a decreasing in the mechanical performance of cementitious composite.

Dong et al. (2016) and Gilford et al. (2014) have encapsulated, respectively, epoxy resin E-51 and dicyclopentadiene monomer healing agents with urea–formaldehyde polymer (shell material). In both of the studies a certain amount of self-healing in cementitious composites. Dong et al. (2017), in another study, have analyzed the self-healing capacity of the urea-formaldehyde/Epoxy resin E-51 microcapsules through the chloride permeability method. Based in the test results, Dong et al. (2017) have concluded that "the healing efficiency of permeability increases to a maximum level of 19.8%, indicating that the system actually works on decreasing permeability" (p. 95). As can be seen from Figure 2.18 the self-healing efficiency was improved with an increase in the microcapsule content of cementitious matrix.

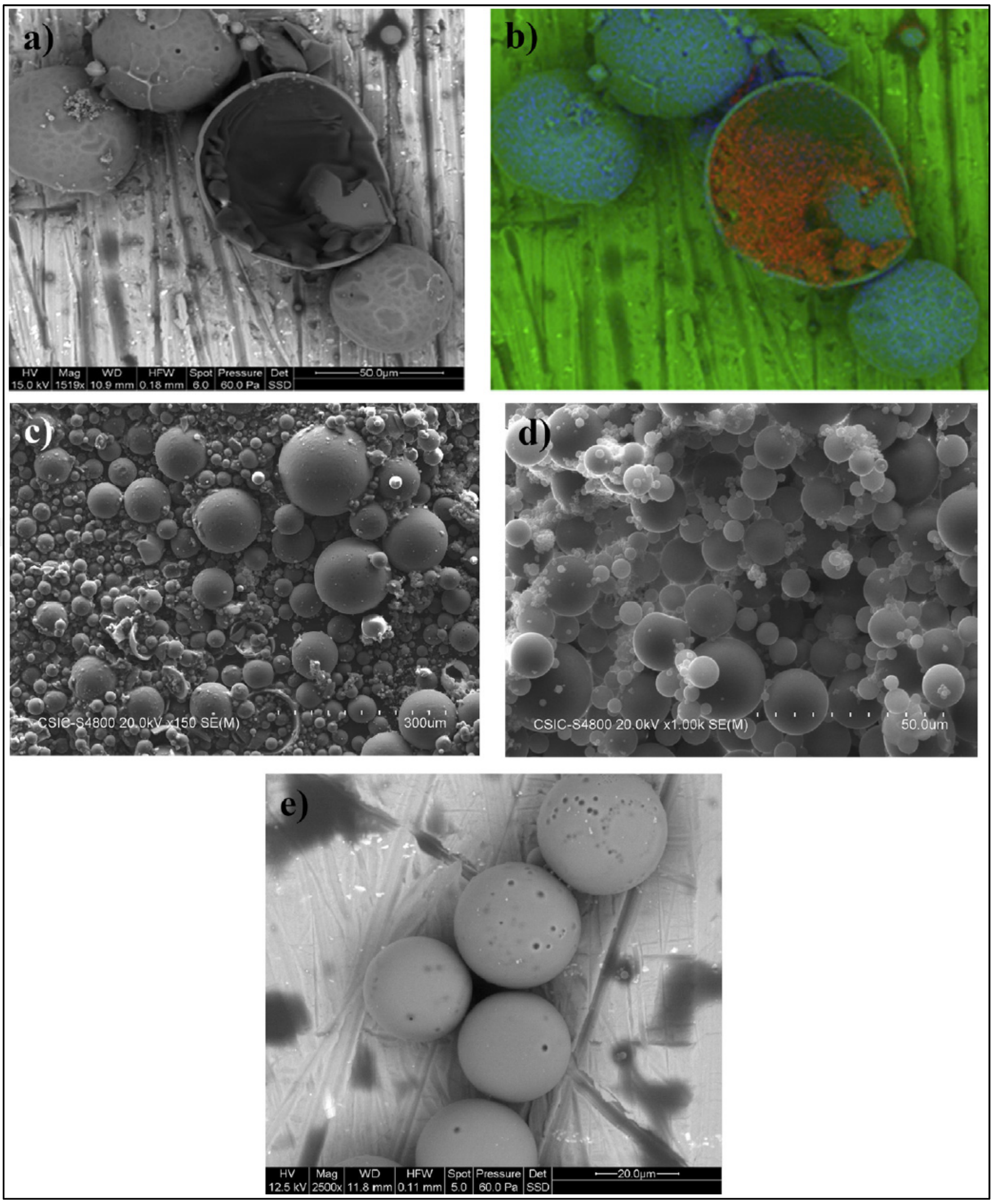

Figure 2.17 SEM images of the silica/epoxy microcapsules. a) a broken microcapsule; b) Elemental analysis (Si = blue, C = red, and Al = green); c, d, and e) microcapsules images with various magnification (Perez, Erkizia, et al., 2015)

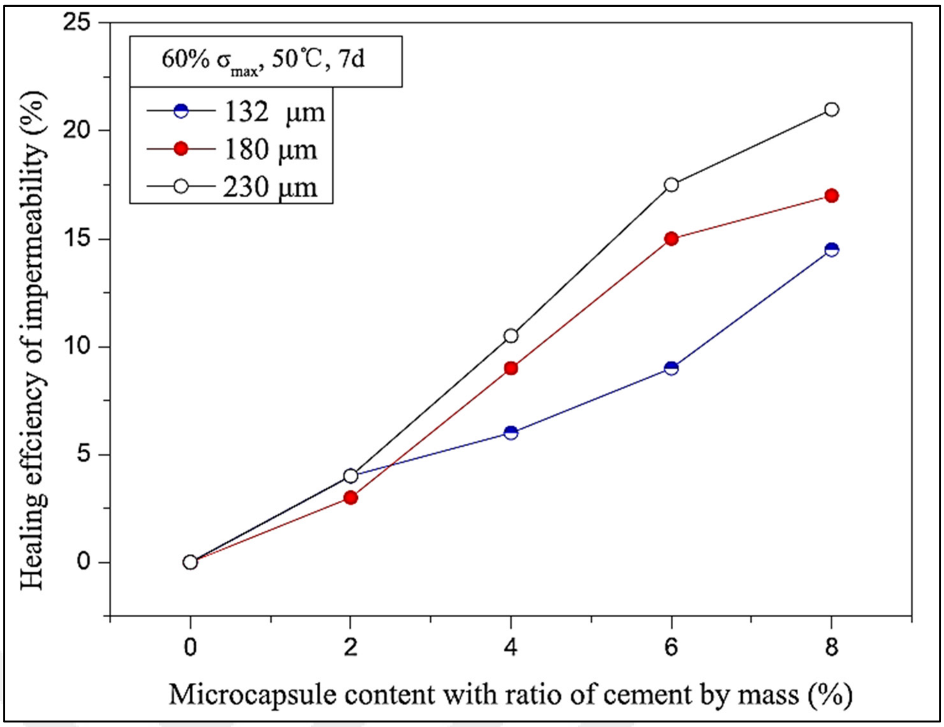

Figure 2.18 Relationship of microcapsule content of matrix with self-healing efficiency (Dong et al., 2017)

Dicyclopentadiene, as healing agent for cementitious materials, was also encapsulated within phenol-formaldehyde resin shell in the scope of the study carried out by Lv et al. (2016). They put the microcapsules in simulated concrete pore solution and cement paste samples to examine the stability performance of the microcapsules. Their test results revealed that the microcapsules has superior stability performance in simulated pore solution as well as in the real cement environment (Lv et al., 2016).

All of the above mentioned healing agents can only react with the second component (microencapsulated) or a catalyst embedded in the cementitious matrix. In two-component agents, the ratio of the first component to the second component is usually uncontrolled. Especially for epoxy resins, this ratio is an important factor for the complete polymerization. Therefore, single component agents can be considered to be more appropriate agents because they do not need a second component. $Ca(OH)_2$, a product of hydrated cement, can react with SiO_2 provided by pozzolanic materials such as fly ash (Sahmaran et al., 2008; Termkhajornkit et al., 2009; Z. H. Zhou et al., 2011) and ground-granulated blast-furnace slag (Sahmaran et al., 2013; Z. H. Zhou et al., 2011). In past years, a few studies have dealt with the incorporating of silica-based microcapsules, as SiO_2 source, in cement-based composites (Giannaros, Kanellopoulos, & Al-Tabbaa, 2016; Kanellopoulos, Giannaros, & Al-Tabbaa, 2016; Kanellopoulos, Giannaros, Palmer, Kerr, & Al-Tabbaa, 2017; Pelletier, Brown, Shukla, & Bose, 2011; Tan, Keung, Choi, Lam, & Leung, 2016). Pelletier et al. (2011) have introduced the idea of encapsulation of aqueous sodium silicate (SS) solution in polyurethane microcapsules through an interfacial polymerization. Colloidal silica was also used as a healing agent and a SiO_2 source in similar microcapsules (Tan et al., 2016). In addition, Kanellopoulos et al. (2017) have encapsulated SS solution in gelatin/acacia gum microcapsule through a complex coacervation technique. The self-healing mechanisms of these microcapsules are based on the rupture of their shell during the crack formation in cementitious matrix, and then the reaction of released SS or colloidal silica with $Ca(OH)_2$ to form secondary calcium-silicate-hydrate gel.

In addition, the microencapsulation of aqueous sodium silicate (SS) with urea-formaldehyde shell was tried by Gilford et al. (2014). In order to encapsulate SS as healing agent, they have tried to adopt a well-developed in situ poly(urea-formaldehyde) microencapsulation method recommended by Brown, Kessler, Sottos, and White (2003) to encapsulate dicyclopentadiene (DCPD) monomer.

As can be seen from Figure 2.19, Giannaros et al. (2016) have used two different kinds of microcapsules with solid (mean size of 130 μm) and liquid (mean size of 500 μm) core SS. The shell materials of these microcapsules was poly-urea and gelatin-gum Arabic, respectively. Giannaros et al. (2016) have reported that "addition of 4% (with respect to cement volume) microencapsulated sodium silicate was shown to reduce sorptivity of cracked specimens over a 28 day healing period. Thus, the efficacy of microencapsulated sodium silicate to close cracks and provide sealing was quantified" (p. 11).

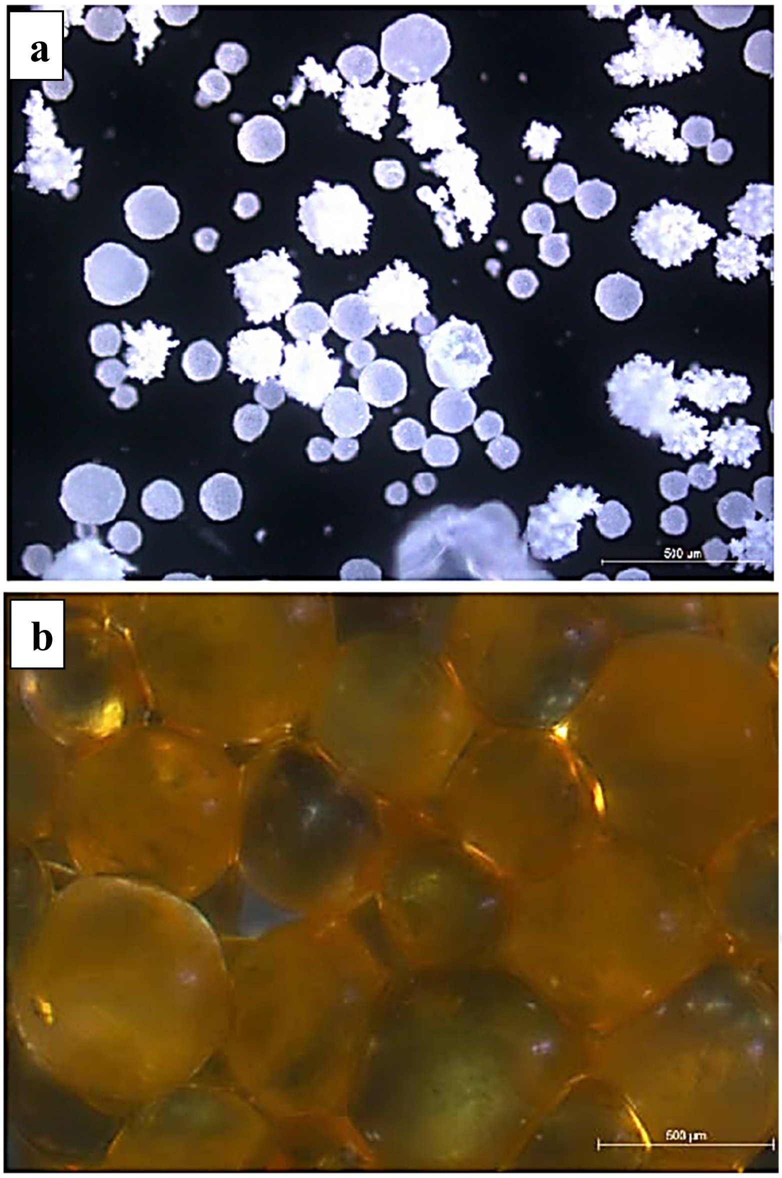

Figure 2.19 Optical microscope images of a) microcapsules with solid SS core, b) microcapsules with liquid SS core (Giannaros et al., 2016)

2.2.2.9 Vascular Systems

The vascular based self-healing approach is very similar to the cylindrical capsule (hollow tubes) based approach. In vascular systems, the hollow tubes embedded in matrix are connect to a healing agent supplier at the exterior of composite. As can be seen from Figure 2.20, Van Tittelboom and De Belie (2013) have illustrated the concept of this approach via a schematic figure. The release of healing materials from the supplier tank is provided by vascular systems through the damaged zone as result of three main mechanisms: a) gravitational force, b capillary forces, and c) hydrostatic pressure (Van Tittelboom & De Belie, 2013).

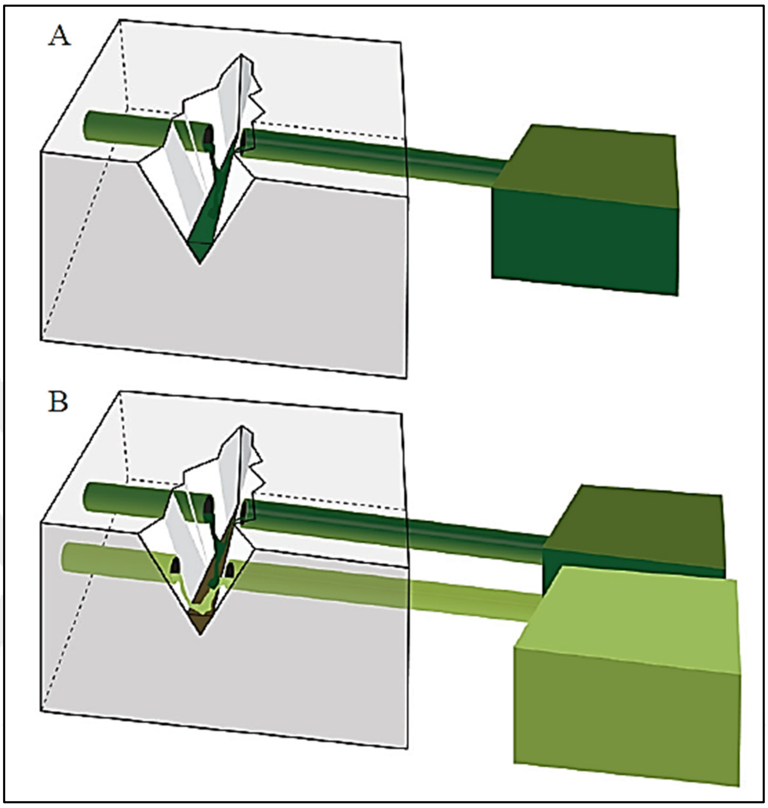

Figure 2.20 The schematic illustration of A) one channel and B) multiple channel vascular systems (Van Tittelboom & De Belie, 2013)

Minnebo et al. (2017) have recently proposed a vascular healing network connected to a novel 3D printed distribution apparatus. As can be seen from Figure 2.21, the distribution apparatus has one inlet accessible from exterior of concrete for supplying healing agent and has four outlets connected to vascular systems (tubes). In addition, they have investigated the advantages of using different types of tubes such as inorganic phosphate cement and alumina based tubes. Minnebo et al. (2017) have reported the suggested vascular system can provide a successful self-healing mechanism for cementitious composites. In addition, in some studies, tube-shaped holes or porous concrete were used as a vascular system inside the cementitious materials (Dry & McMillan, 1996; Sangadji & Schlangen, 2012).

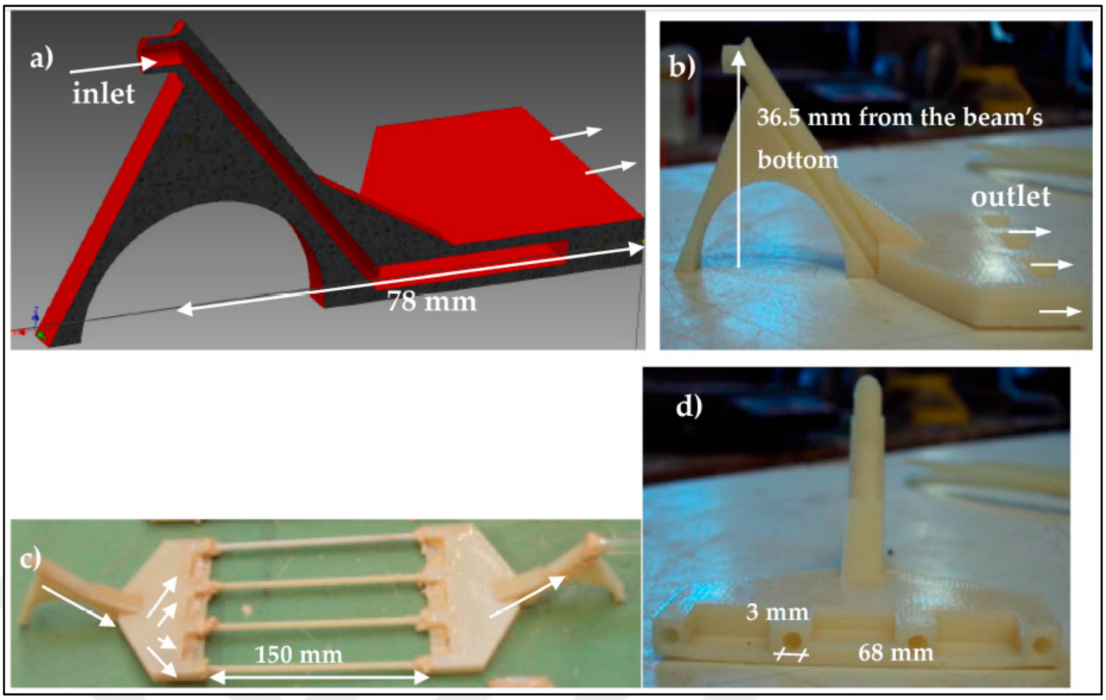

Figure 2.21 A novel distribution apparatus for vascular systems: a) the cross section of model, b) side view of the apparatus, c) the apparatus is connected to tubes, and d) front view of the apparatus (Minnebo et al., 2017)

2.1.3 Methods Used to Verify Self-Healing in Cement-based Composites

There are many methods to analyses the self-healing mechanism in various cementitious materials. Çopuroğlu et al. (2013) categorized these methods as follows: 1) Techniques used to examine crack healing such as microscopy, X-ray diffraction and Raman Spectroscopy 2) Techniques used to verify recovery against environmental actions such as water permeability tests, air permeability, osmosis, capillary water absorption, resonant frequency analysis, ultrasonic measurements, electrochemical impedance measurements, computed tomography, resistance against corrosion, and Fourier-Transform Infrared spectroscopy. 3) Techniques used to verify recovery against mechanical actions such as regain in strength and stiffness, fatigue resistance, and acoustic emission analysis.

Rapid chloride permeability (Sahmaran et al., 2013; Termkhajornkit et al., 2009), nuclear magnetic resonance (Huang, Ye, & Pel, 2016), μ-XRF (Danner, De Weerdt,

& Geiker, 2017) analyses were successfully used in studies to assess the extent of self-healing. Besides, Termkhajornkit et al. (2009) examined the self-healing ability of fly ash bearing mixture through the Mercury Intrusion Porosimetry test and considering hydration reactions. Muhammad et al. (2016) and Tang, Kardani, and Cui (2015) have provide comprehensive literature review on the evaluation methods for self-healing in cement based composites. The lack of standard assessment methods was emphasized in both of the review papers.

2.3 Microencapsulation

Microencapsulation is the process of coating a wide range of materials with protective membranes called shell or wall. Therefore, as can be seen from Figure 2.22 a microcapsule consists of core/inner and shell/coating material. The core material can be liquid, solid or even gaseous components. Jia et al. (2016) have summarized the function of microcapsules as follows: “theoretically, microcapsules could both isolate inner active species with high loading from outer environment and hold long-term storage and processing stability to achieve controlled release of their latent functionality at targeted location and/or at desired time upon an external stimulus” (p. 221-222).

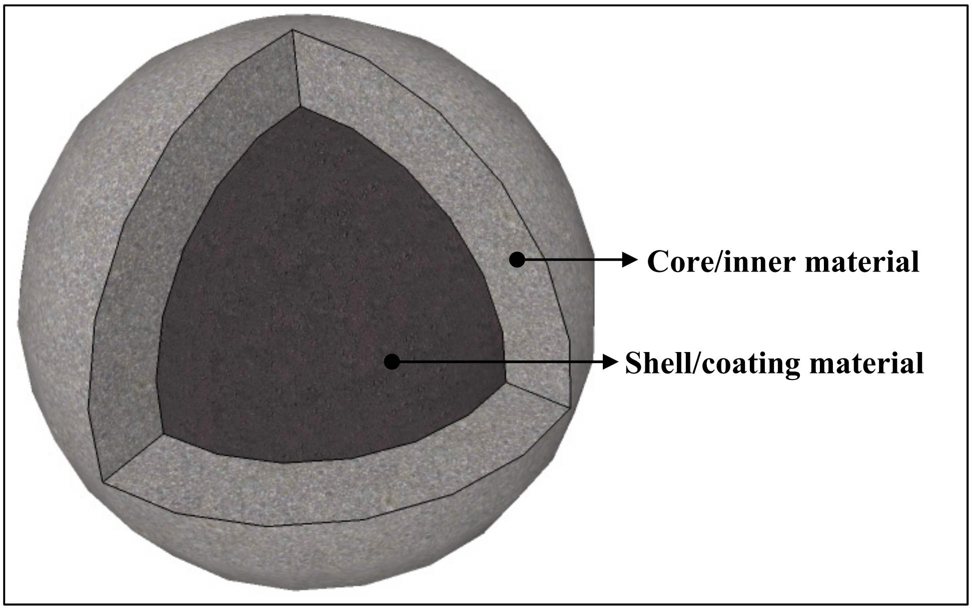

Figure 2.22 Schematic illustration of a microcapsule

In the past two decades microcapsules has gained a considerable amount of interest in diverse spectrum of applications (Kanellopoulos et al., 2017). Various types of microcapsules are being using in many industries such as pharmaceutical, medical, food, cosmetic, textile, paint, and construction. For example, the advantage of using microcapsules as a drug delivery systems can be summarized as follows: (a) protection of active agent (core material) against degradation, (b) controlling the release rate of encapsulated drug, and (c) providing pre-programmed release profiles for drugs (Singh, Hemant, Ram, & Shivakumar, 2010). In addition, a review paper published by Boh and Šumiga (2008) have focused on the applications of microcapsules in construction materials available in literature up to 2008 . As can be seen from Figure 2.23, various types of microcapsules were used for a wide range of purposes in building/constructions materials.

Using microcapsules as a self-healing method in engineering materials is one of the most striking application of them. As discussed in detail earlier, because of the considerable advantage of microencapsulation, it has become more interested as compared to the other encapsulation methods in self-healing materials. For the first time, White et al. (2001) have proposed the microcapsule based self-healing methods for polymer composites. The concept of microcapsule based self-healing materials was discussed in details at section 2.2.2.9. The microcapsule based self-healing approach in cement based composites is relatively new topic as compared to the polymer composites. Before 2011, there are few studies (Xing et al., 2008; Z. X. Yang, Holler, He, & Shi, 2010) that have dealt with microcapsule based self-healing method in cement-based composites. In addition, as can be seen from Figure 2.23, the microcapsule based self-healing had not been applied in construction materials up to 2008.

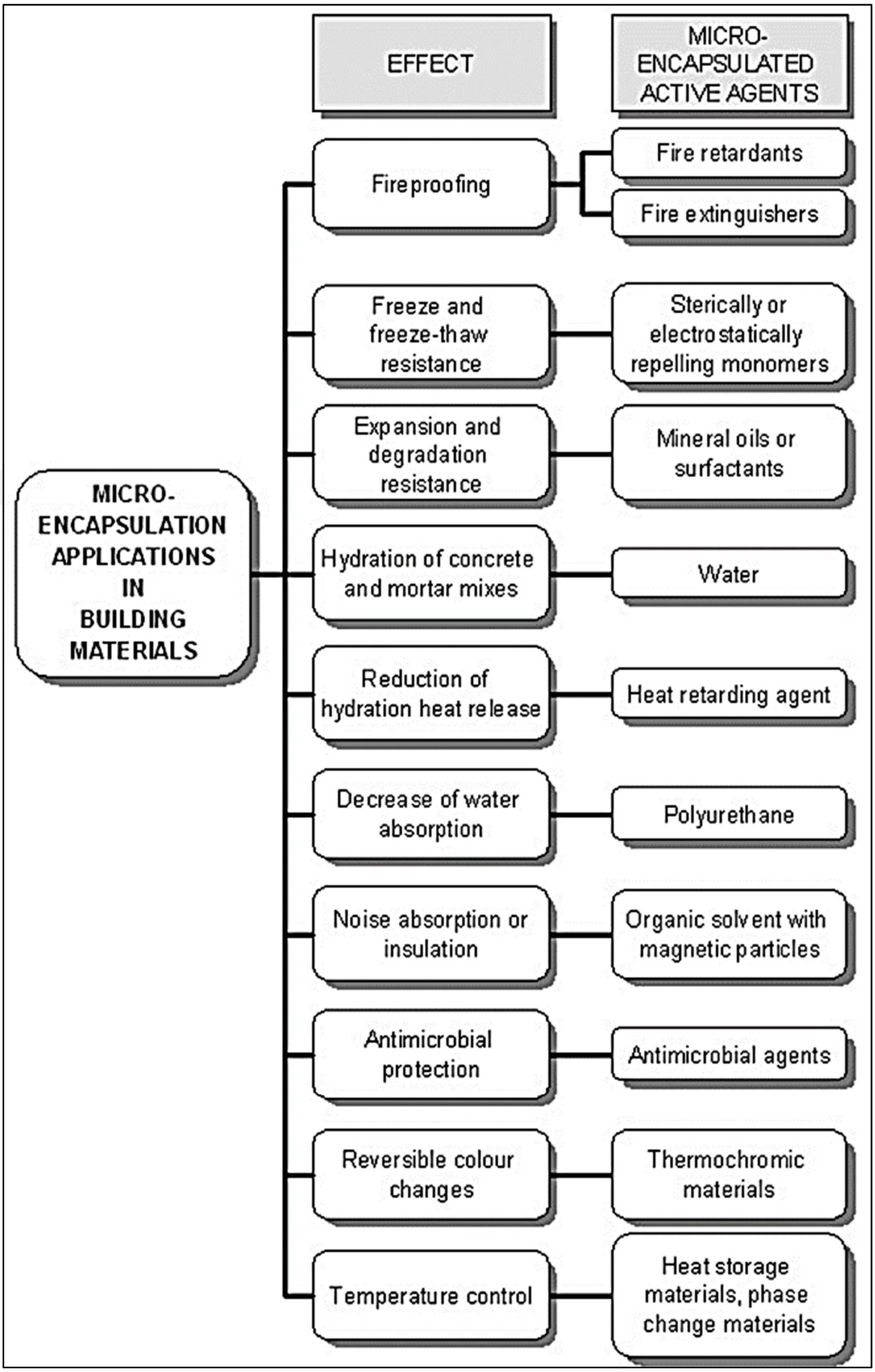

Figure 2.23 Microencapsulation applications in building materials (Boh & Šumiga, 2008)

The microencapsulation methods can be categorized into physical and chemical groups (Boh & Šumiga, 2008; Tyagi, Kaushik, Tyagi, & Akiyama, 2011). Technologies such as pan coating, spray drying, centrifugal extrusion, air-suspension coating, and vibrational nozzle can be categorized as the physical microencapsulation methods (T. H. Ahn & T. Kishi, 2010; Boh & Šumiga, 2008; Tyagi et al., 2011). In situ polymerization, interfacial polymerization, miniemulsion polymerization, pickering emulsion templating, sol–gel encapsulation, and solvent evaporation/solvent extraction methods are the most common chemical microencapsulation methods (Boh & Šumiga, 2008; Zhu et al., 2015). In addition, Kanellopoulos et al. (2017) have put the ionic gelation and complex coacervation methods in the physicochemical microencapsulation category. Selection of an appropriate production methods or technology depends mostly on the properties of core materials. Kanellopoulos et al. (2017) has listed these properties as follows: “the cargo material state (liquid or solid), type (organic or inorganic), miscibility as well as its chemical compatibility with the shell materials” (p. 2).

2.3.1 Microencapsulation of Isophorone Diisocyanate

Isophorone diisocyanate (IPDI), a monomeric aliphatic diisocyanate, has been used as a catalyst free healing agent in a few studies since 2008. The liquid phase diisocyanate monomer healing agent, IPDI, was microencapsulated for the first time via interfacial polymerization of polyurethane in a stabilized aqueous emulsion by J. L. Yang, Keller, Moore, White, and Sottos (2008). J. L. Yang et al. (2008) have emphasized that “diisocyanates are reactive with water, introducing the possibility of one-part, catalyst-free self-healing system that is functional in an aqueous or moisture-laden environment” (p. 9650). As can be seen from Figure 2.24 microcapsules were synthesized by interfacial polymerization of a toluene diisocyanate (polyurethane prepolymer) in an oil-in-water emulsion. They have successfully synthesized high yields (~70%) of a free-flowing powder of microcapsules which contain a liquid core (IPDI) content of 70 wt % (J. L. Yang et al., 2008). Kardar (2015) has also produced similar IPDI-loaded polyurethane microcapsules using different polyol monomers. In addition, these kinds of microcapsules have been synthesized with different prepolymers (Alizadegan, Pazokifard, Mirabedini, Danaei, & Farnood, 2017; Di Credico, Levi, & Turni, 2013; Haghayegh, Mirabedini, & Yeganeh, 2016a, 2016b)

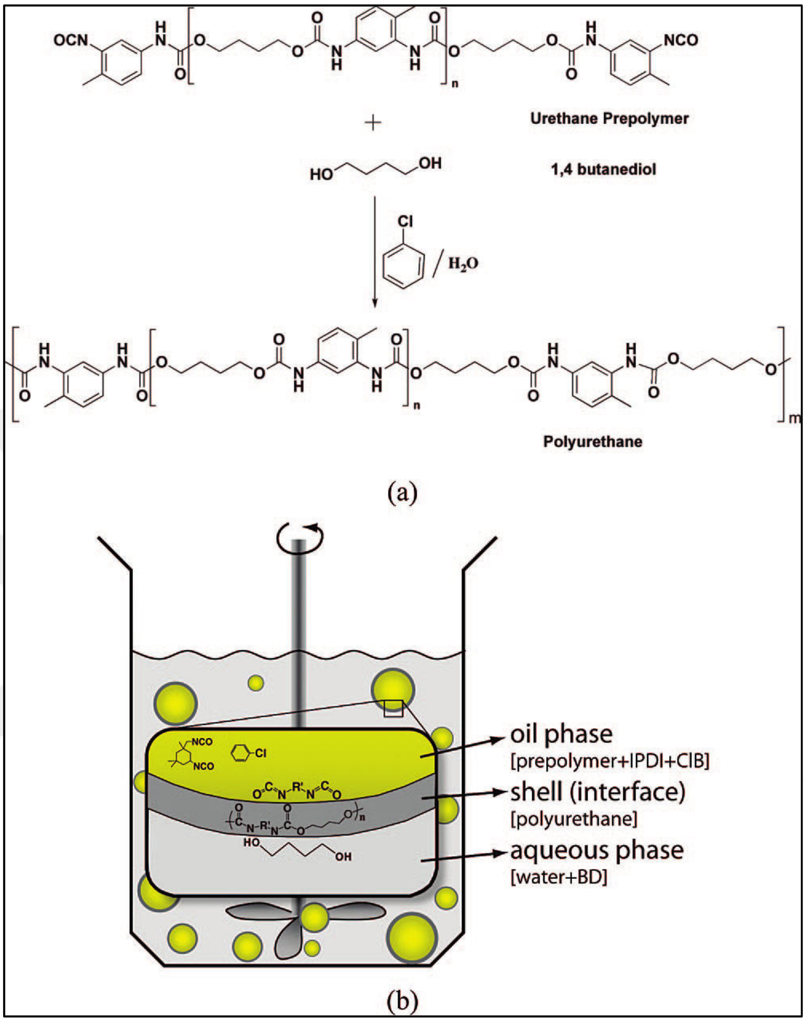

Figure 2.24 Reaction scheme for microencapsulation (a) and schematic diagram of microencapsulation process (b) (J. L. Yang et al., 2008)

Yi, Yang, Gu, Huang, and Wang (2015) have proposed IPDI-loaded multilayer microcapsules synthesized by Pickering emulsion templates. As can be seen from Figure 2.25 lignin nanoparticles were used to prepare the oil-in-water Pickering emulsion template. In other words, lignin nanoparticles were used as an emulsion stabilizer instead of classical surfactants. Yi et al. (2015) have stated that “alkaline lignin is chosen as an emulsion stabilizer for its inexpensiveness and abundance, which makes it even more suitable for applying this method to practical applications” (p.

13750). The oil phase was a mixture of diphenyl methane diisocyanate (MDI) and the IPDI (core material). Because of the higher reactivity of MDI as compared to IPDI, isocyanate groups of MDI can preemptively react with hydroxyls of lignin or water at the interface of emulsion droplets and form thin polyurethane membrane (Yi et al., 2015). Therefore, the IPDI remained as the only liquid core material. At the end of process, the emulsion was added to the polyvinyl alcohol (PVA) solution that contains melamine formaldehyde prepolymer (pre-MF). Microcapsules were formed by firstly interfacial polymerization of isocyanate groups and pre-MF (forming tightly cross-linked polyuria), and then in situ polymerization of pre-MF on the surface of microcapsules (forming melamine-formaldehyde polymer).

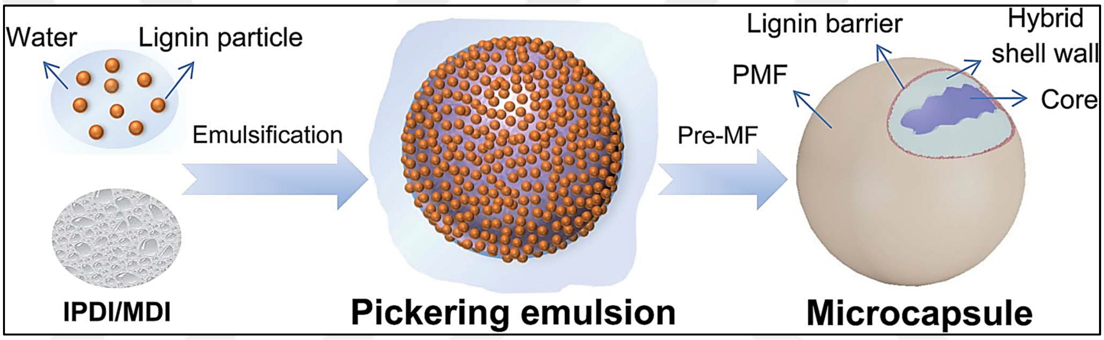

Figure 2.25 Synthesis process of the IPDI-loaded multilayer microcapsules (Yi et al., 2015)

W. Wang, Xu, Liu, Li, and Xing (2013) have prepared a novel IPDI-loaded poly(urea-formaldehyde) (PUF) microcapsule. Micromechanical behavior of the shell of microcapsules were enhanced by embedding oxygen plasma treated carbon nanotubes (OPCNTs). As can be seen from Figure 2.26, W. Wang et al. (2013) have illustrated the synthesis process as follows: Step 1) Carbon nanotubes were treated with oxygen plasm. Step 2) The OPCNTs were dispersed in a certain amount of water (20 mL). Step 3) The continuous phase (aqueous phase) was prepared by adding surfactant to 50 mL of water. Step 4) The shell-forming materials (urea etc.) were dissolved in aqueous phase. Step 5) IPDI, core material, was added to the solution to obtain an oil/water emulsion. Step 6) The pH were adjusted to desired value and then, the formaldehyde aqueous solution was added to the emulsion to begin in situ polymerization.

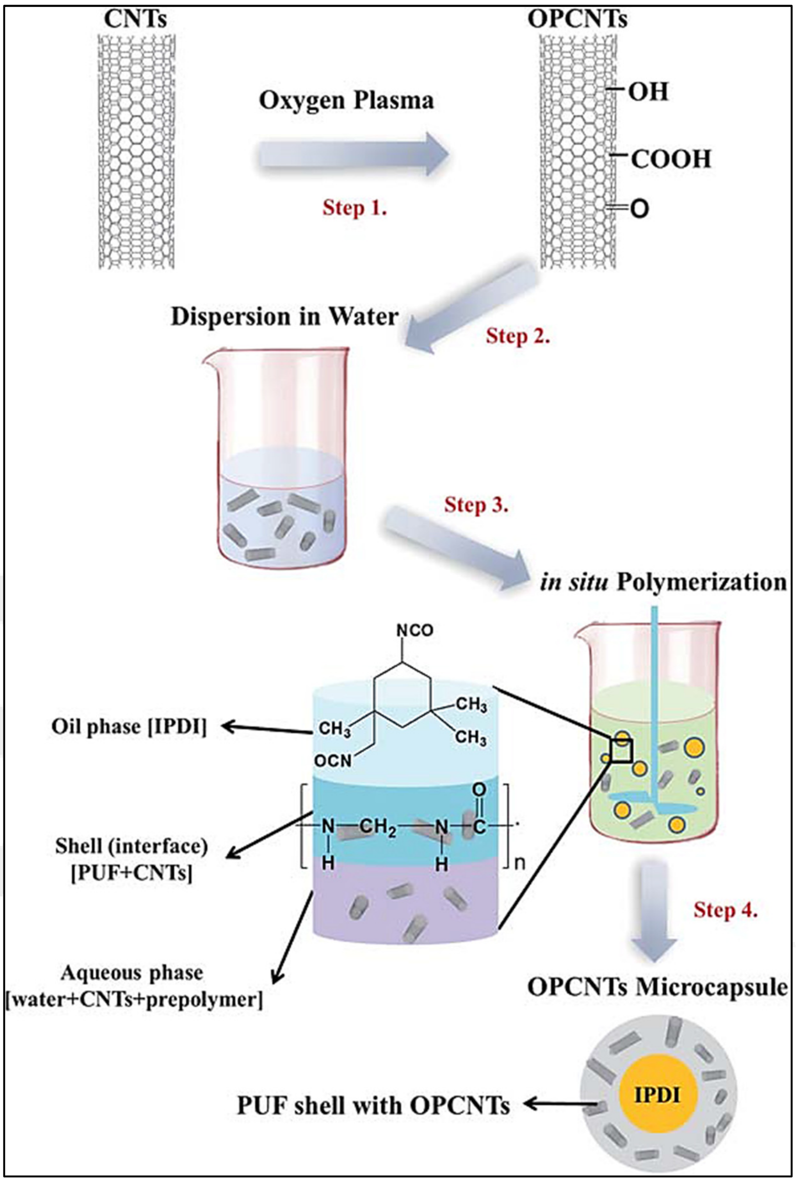

Figure 2.26 Schematic representation of oxygen plasma treatment and PUF microencapsulation procedure (W. Wang et al., 2013)

CHAPTER THREE
MATERIALS AND METHODS

3.1 Ultra High Performance Concrete (UHPC)

In this section, the materials used for preparing UHPC mixtures are described. In addition, the test methods applied to characterize the properties of UHPC mixtures and to assess the self-healing mechanisms are also present.

3.1.1 Materials Used in UHPC Mixtures

3.1.1.1 Cement and Supplementary Cementitious Materials

CEM I 42.5 R type Portland cement supplied from Denizli Cement was used. The properties of cement are presented in Table 3.1. A ground granulated blast furnace slag (GGBFS) obtained from Iskenderun iron and steel factory (Turkey) was used. In addition, the class C and F fly ashes (FA) obtained, respectively, from thermal power plants of Soma (FA1) and İzenerji (FA2) were used. The properties of supplementary cementitious materials (SCM) are presented in Table 3.2.

Table 3.1 Physical and chemical properties of cement

Chemical Composition (%)		**Physical Properties**	
SiO_2	19.1	Specific surface (Blaine) (m^2/kg)	369
Al_2O_3	4.40	Initial setting time (min)	110
Fe_2O_3	3.96	Final setting time (min)	166
CaO	61.85	Volume expansion (mm)	1.00
MgO	2.05		
Na_2O	0.27		
K_2O	0.70	**Compressive Strength**	
SO_3	3.72	2 days (MPa)	27.1
Cl^-	0.0004	7 days (MPa)	43.3
Loss on Ignition	1.82	28 days (MPa)	56.0

Table 3.2 Properties of SCMs

Chemical Composition (%)	FA1	FA2	GGBFS
SiO_2	41.96	48.95	39.95
Al_2O_3	19.55	28.68	11.46
Fe_2O_3	4.38	3.61	0.54
CaO	26.18	8.44	34.07
MgO	2.11	1.81	6.45
Na_2O	0.38	0.54	0.30
K_2O	1.46	1.06	1.02
SO_3	1.27	0.20	0.55
Cl^-	0.0181	0.0289	0.0246
Free CaO	1.66	1.01	0.13
Loss on Ignition	1.69	2.93	2.95

3.1.1.2 Aggregates

Three different sizes (0-0.4, 0.5-1, and 1-3 mm) of quartz aggregate obtained from Pomza Export were used in the UHPC mixtures. The specific gravity and water absorption of the aggregate are 2.66 and 0.10, respectively. The chemical composition of quartz aggregate consists by more than 99% of SiO_2.

3.1.1.3 Steel fibers

Two type of straight brass-coated steel micro-fibers were used in the fiber reinforced UHPC mixtures. The properties of the fibers (reported by manufacturer) are presented in Table 3.3.

Table 3.3 Properties of steel micro-fibers

Code	Length (mm)	Diameter (mm)	Aspect Ratio (L/d)	Tensile Strength (MPa)
MF1	6	0.16	37.5	2000
MF2	13	0.20	65	2750

3.1.1.4 Chemical Admixture

A new generation of Polycarboxylic ether based superplasticizer (MasterGlenium® ACE 450) supplied from BASF was used. The properties of the superplasticizer (SP) (reported by manufacturer) are presented in Table 3.4.

Table 3.4 Properties of superplasticizer

Properties	Explanations
Form	liquid
Structure of materials	Polycarboxylic ether based
Color	Amber
pH value	5 – 7 (20 °C)
Density	1.069 – 1.109 kg/lt (20 °C)
Solubility in water	Miscible

3.1.2 Test Methods

3.1.2.1 Mixing Procedure and Mortar Flow Test

Dry ingredients of mixtures were premixed for five minutes. Then, half of mixing water was added to the dry mixtures. The remaining water was mixed with the required amount of superplasticizer and then, poured into the mixer. After normal speed for about 5 minutes, mixing continued for another 15 min in high speed. The workability of each mixture was controlled by the mini-flow table test. The required amount of superplasticizer was used to achieve 260 ±10 mm free flow value (Figure 3.1). It should be noted that the mixing procedure of microcapsule containing mixture were discussed in details at Chapter 9, section 9.3.2.

Figure 3.1 Mini-flow table test (Personal archive, 2016)

3.1.2.2 Compressive Strength Test

The self-compacting UHPC mixtures were poured into 50×50×50 mm cubic molds. The compressive strength of all mixture in different ages were determined on these cubic specimens. In addition, the compressive strength test was one of the test methods applied in Chapter 8 to assess the self-healing (regain in compressive strength) ability of selected UHPC mixtures.

In order to assess the self-healing capacity of fiber reinforced UHPC mixtures in terms of compressive strength, 18 cubic specimens were prepared for each variable. After 7 and 90 days standard water curing, 15 specimens were taken out form the lime saturated water and left to dry in laboratory air for 1 day. Seven specimens were used to determine the average compressive strength of mixtures. Eight of the specimens were pre-loaded up to ~100% of their corresponding compressive strength. The load was carefully monitored and released at the required predetermined load value (~100%) to avoid further damage. Immediately after preloading, half of the preloaded specimens were subjected to the compressive strength test to determine the damage ratio due to the preloading. The other half of the preloaded specimens (4 specimens) were immersed in the lime saturated water. After 30 days, the preloaded specimens and the remaining specimens from 18 specimens (3 virgin specimens) were subjected to compressive strength test. The self-healing ratios were evaluated by two different approaches that can be seen in 8.1 section. It should be noted that another series of specimens were pre-loaded up to 90% of the ultimate compressive load that its details are also presented in 8.1 section.

3.1.2.3 Direct Tension Test

The tensile strength and stress-strain curves of UHPC specimens were obtained through a direct tension test. In addition, the crack width restriction capacity of steel micro fibers were analyzed through the direct tension test.

The direct tension test was also one of the test methods applied in Chapter 8 to assess the self-healing (regain in tensile strength) ability of selected mixtures. The tests were determined on special designed dog-bone shaped specimens with a gage length of 80 mm. The mold and details of the dog-bone shaped specimen are shown in Figure 3.2.

In order to assess the self-healing capacity of fiber reinforced UHPC mixtures in terms of direct tensile strength, seven dog-bone shaped specimens were prepared for each variety. After 7 and 90 days standard water curing, specimens were taken out form the lime saturated water and left to dry in laboratory air for 1 day. The specimens were subjected to direct tension test to introduce a crack with 100 µm ± 10 width. The pre-cracked specimens were immersed in the lime saturated water for 30 days and then, were subjected to direct tension test to observe any regain in strength.

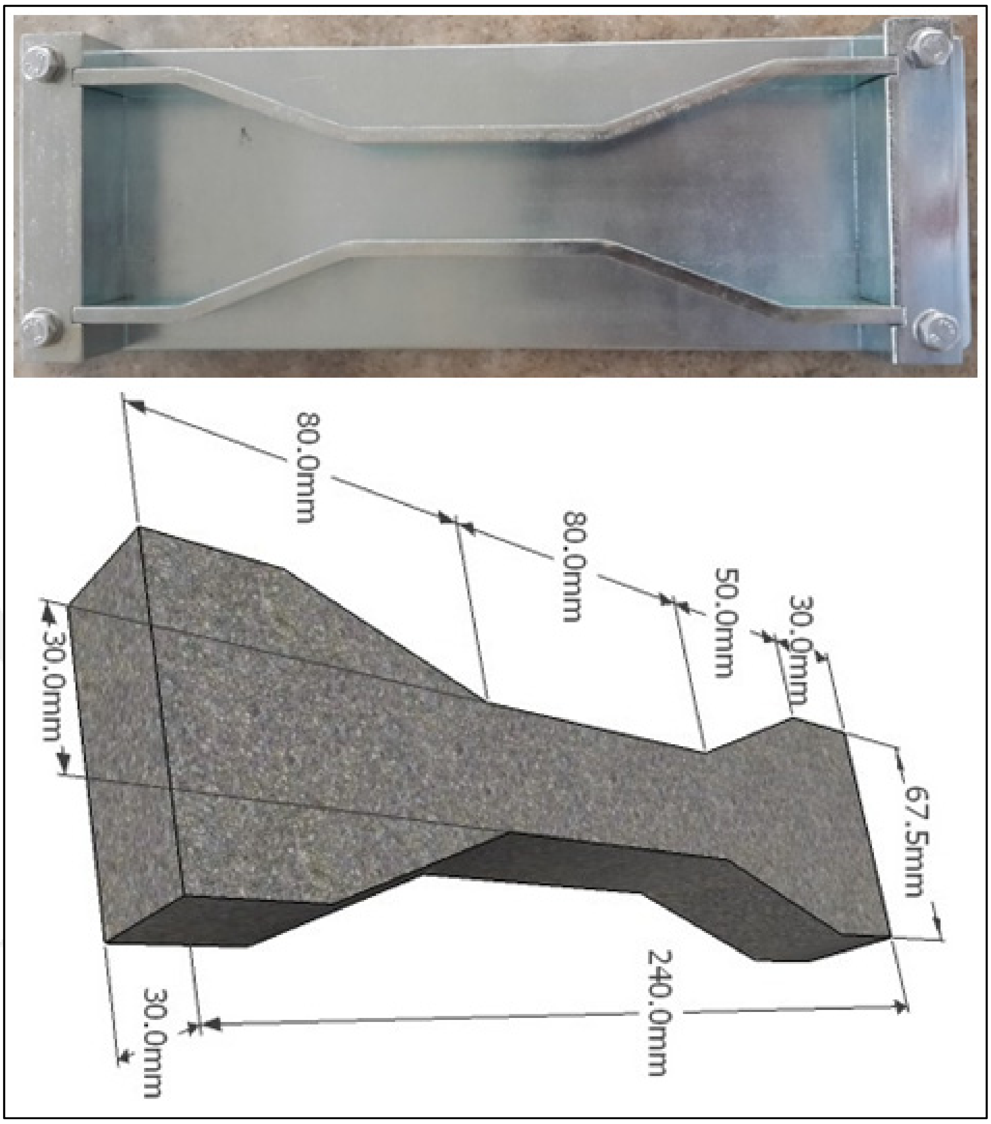

Figure 3.2 Mold and details of dog bone shaped specimen (Personal archive, 2016)

Direct tension tests were carried out by an electro mechanic closed-loop testing system (loading rate: 0.2 mm/min). Elongation was measured using with two optical encoder (Figure 3.3).

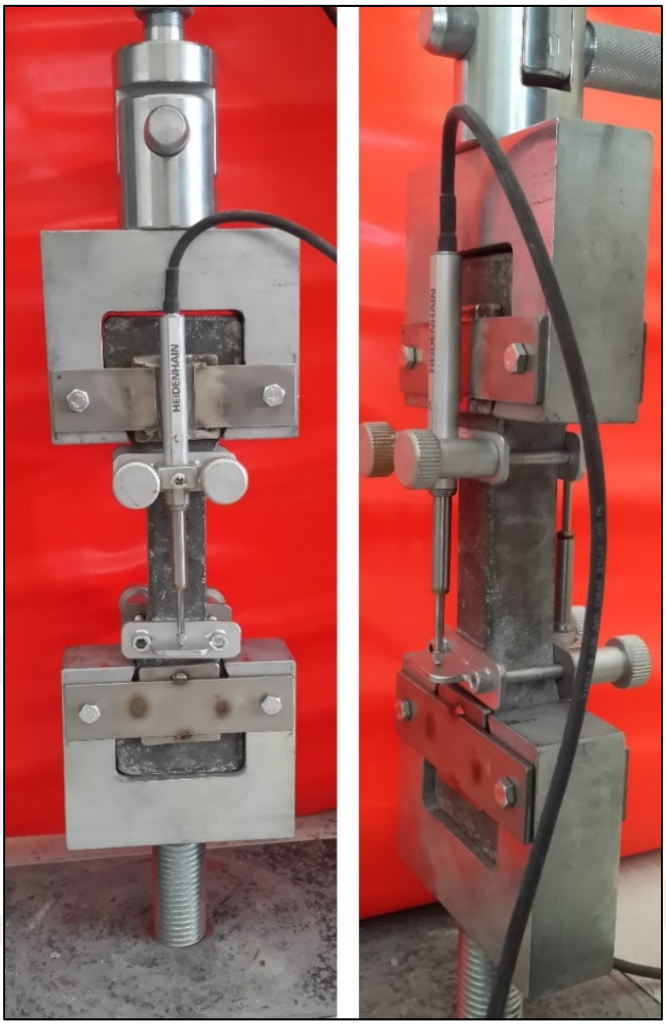

Figure 3.3 Direct tension test (Personal archive, 2016)

3.1.2.4 Novel "Self-Bonding" Test

This novel test method, hereafter called "self-bonding" method, was designed to evaluate the bonding capacity of healing products that can be formed in very tight cracks. The higher bonding capacity means the higher self-healing capacity of the cementitious matrix. The principle of this method lies in the bonding capacity of self-healing products under direct tension loads. This method was applied in Chapter 6 to observe the bonding capacity of nine different UHPC mixtures.

A cylinder steel mould (height of 100 mm and a diameter of 100 mm) with a triangle bulge at the middle of the inner lateral surface was designed (Figure 3.4). The purpose of the triangle bulge, which has 3 mm base and 2 mm height, was for creating a groove in the specimens. This groove was designed to split of the specimens easier. In addition, the end plates of the mould have holes in the centers to take chromium coated steel pins of 16 mm diameter and 75 mm length (Figure 3.5). The upper part of pin has a groove for holding it in the ending plates by a screw. This groove also allows hanging the specimens by the testing machine. In addition, these pins, which were embedded in both base of the cylinder specimens, have four grooves with 3 mm width and 4 mm depth at the bottom of them to create a strong bond with matrix (Figure 3.5).

Figure 3.4 The self-bonding test steel mould (Personal archive, 2016)

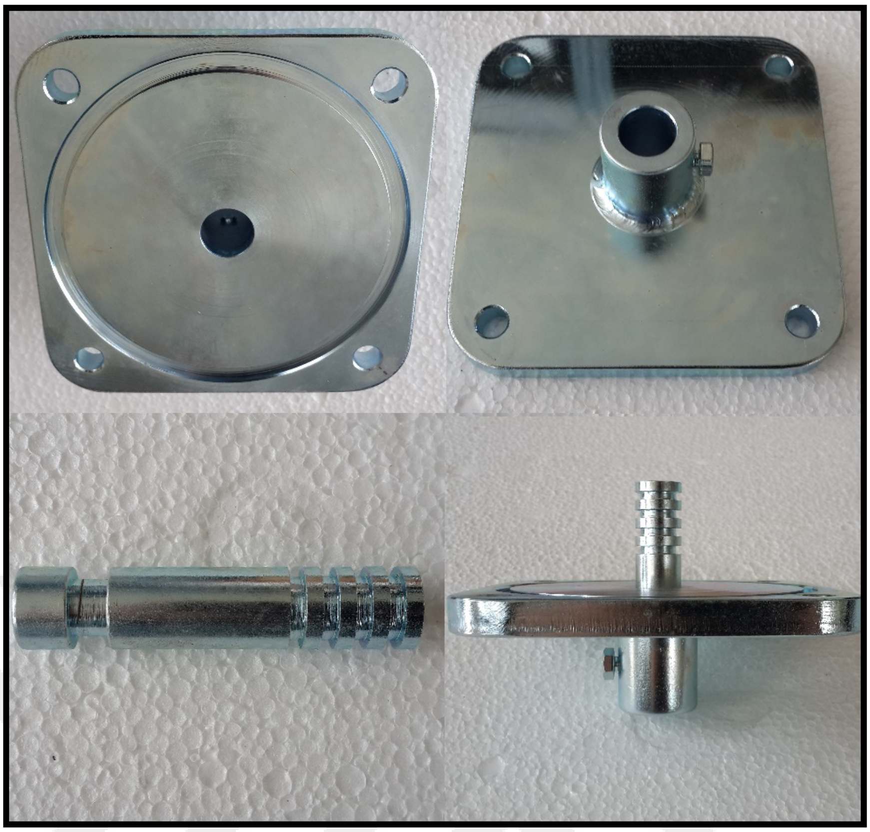

Figure 3.5 The end plates of the mould and pins (Personal archive, 2016)

The self-compacting UHPC mixtures were poured into the cylinder molds in two layers without any vibration. The top base of mould, which holds a pin just like the bottom base, was placed after pouring the final layer of the fresh UHPC. These bases allow the pins to be centrally embedded and become perpendicular to the surface of the specimen. Specimens were demolded after 24h and then, cured in standard water curing for 7 days. Four specimens were prepared for each mixture.

Specimens should be split from the groove which had been formed in the middle of lateral surfaces in the casting process. For this purpose, a rigid apparatus with crescent type blade were designed for splitting (Figure 3.6). This apparatus was mounted on an electro mechanic closed-loop testing system. The specimens were split by a loading rate of 0.1 mm/min (Figure 3.6).

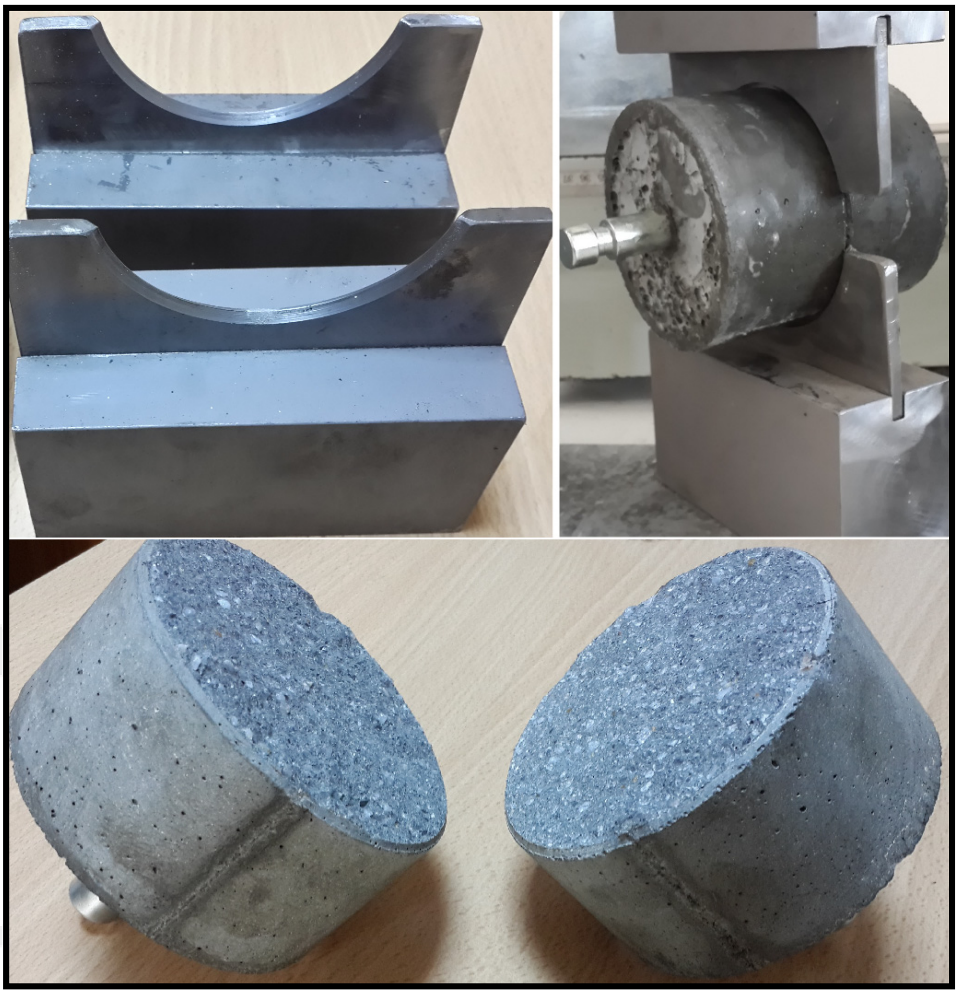

Figure 3.6 The apparatus used for splitting (Personal archive, 2016)

The two parts of the split specimen were carefully put together, immediately after splitting. For this purpose, stainless steel connector apparatus was designed to keep the surface of each part connected together with equal pressure for 30 days in water. The connector apparatus consists of two individual parts which holds each part of the divided specimen (Figure 3.7). The two parts of apparatuses were connected together with three long bolts which were tightened with a Torque Wrench to a torque of 2.7 N.m (Figure 3.8).

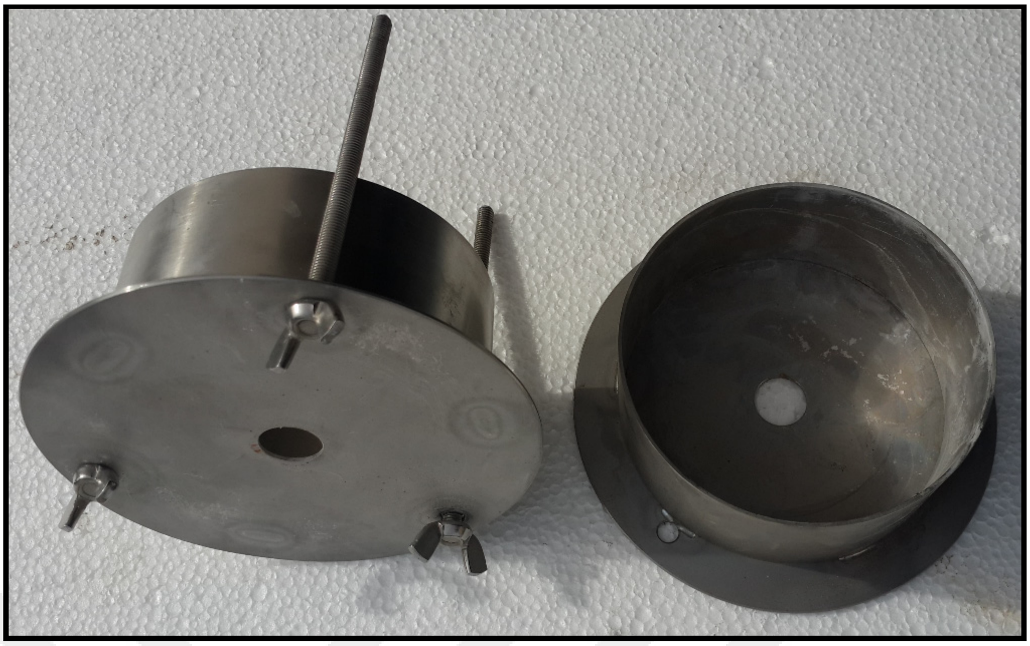

Figure 3.7 The connector apparatus (Personal archive, 2016)

Figure 3.8 Tightening of bolts with a Torque Wrench (Personal archive, 2016)

After 30 days, the specimens were taken out of the water and left to dry for 3 days (Figure 3.9). In order to determine the bond loads, a two-part apparatus was mounted on the electro mechanic closed-loop testing system to hold the embedded pins (Figure 3.10). The upper part, which had been mounted to a load cell with 6 kN capacity, held one of the embedded pins from the groove (Figure 3.11). In other words, the specimen was hanged to the upper part of apparatus to minimize any residual stresses. The other embedded pin was strongly held by the lower part of apparatus which had been mounted the bottom platen of the machine (Figures 3.10 and 3.11). It must be mentioned that the bolts of the connector apparatus were released just before the test began in order to avoid any possible damage in the specimens (Figure 3.10). The self-bonding test was carried out by moving upward of the upper part with a rate of 1 mm/min under closed loop control system.

Figure 3.9 Specimens after 30 days water curing process (Personal archive, 2016)

Figure 3.10 Self-bonding test (Personal archive, 2016)

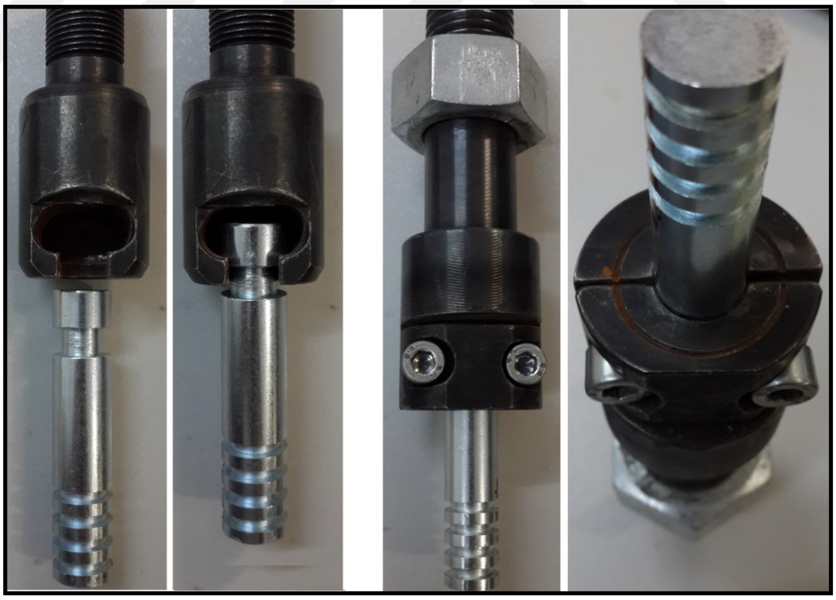

Figure 3.11 The two-part apparatus use for holding pins (Personal archive, 2016)

3.1.2.5 Crack Closing Test

Crack closing test was applied in Chapter 7 along with the self-bonding test to assess the self-healing capacity of seven different SCMs containing UHPC mixtures.

Furthermore, it was one of the methods used in Chapter 8 to assess the self-healing capacity of selected mixtures. In addition, the crack closing test method was the only test method to assess the self-healing capacity of Microcapsules bearing UHPC mixtures.

The fiber reinforced UHPC mixture were poured into disc-shaped plastic moulds with 30 mm diameter and a height of about 10 mm. The reason of using such a small specimen was to analyze the healing products formed in cracks by putting the specimens itself in the chamber of scanning electron microscope. The specimens were cured for 7 and 90 days and then were subjected to the splitting tensile strength test in order to create a crack (Figure 3.12). The width of the crack was monitored and measured by a digital optical microscope during the splitting process (Figure 3.12). For this purpose, a line was drawn by a red marker on the diameter of specimen and perpendicular to the force direction. The cracks at the marked point was restricted to width of 100 µm ± 10 (Figures 3.12 and 3.13). The surface area of the cracks was measured at five marked positions on the surface (Figures 3.13). Immediately after measurements, the specimens were immersed in water for 30 days self-healing process.

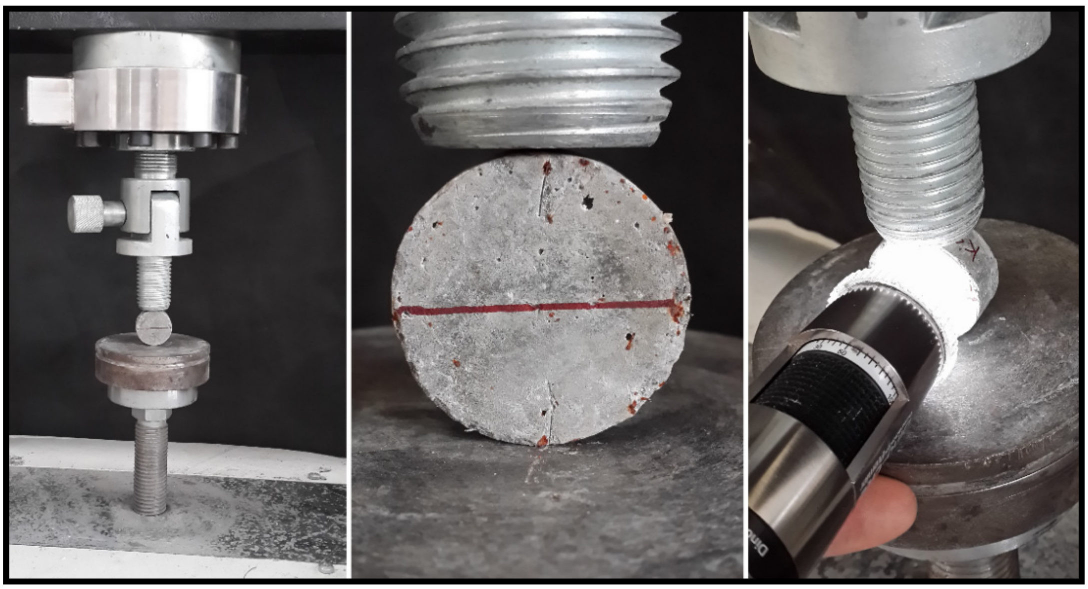

Figure 3.12 Splitting tensile strength test for introducing a crack (Personal archive, 2016)

Figure 3.13 Specimens used for crack-closing test (Personal archive, 2016)

The crack self-healing capacity of each UHPC mixture was determined by calculating the crack-closing ratio at each position of four specimens (20 position) using the following Equation:

$$H = \frac{a - b}{a} \times 100 \tag{3.1}$$

Where, H= healing percentage, a= the original crack surface area, and b = the crack surface area after healing.

The scanning electron microscope (SEM) and energy-dispersive X-ray spectroscopy (EDS) analyses were conducted on the disc-shaped specimens. SEM observations was made by using a scanning electron microscope (Carl Zeiss 300VP, Germany) operated at 3 kV. Prior to SEM imaging, gold sputtering was performed on the disc-shaped specimens.

3.1.2.6 Total and Capillary water absorption Tests

The total water absorption (TWA) and capillary water absorption (CWA) tests were used in Chapter 8 to observe the extent of self-healing. For this purpose, at least 18 cubic specimens with 50×50×50 mm dimensions were prepared for each variable. After 7 and 90 days standard water curing, at least 16 specimens were taken out form the lime saturated water and left to dry in laboratory air for 1 day. Seven specimens were used to determine the average compressive strength of mixtures. Eight of the specimens were pre-loaded up to ~100% of their corresponding compressive strength. The load was released at the required predetermined load value to avoid further damage. Immediately, all of the specimens were immersed in water for at least 24 h and then, the saturated surface dry weight of them was weighted. After that, they were kept in oven at 50°C for three days. It is well known that the oven-dried weight of cementitious materials are usually measured after drying them in an oven at 105ºC for 24 h. If the specimens were dried at 105ºC, it would affect the hydration of unreacted cement and SCMs. Therefore, the specimens were dried at 50°C to minimize the effect of temperature. After measuring the oven-dried weight of specimens, they were subjected to CWA test from their preloaded surfaces (Figure 3.14). The increase in mass of specimens due to absorption of water (capillary suction) was registered at 30, 60, 90, 120, 150, 180, 240, 300, and 360 min. After CWA test, all of the specimens were immersed in water. After 30 days (healing period), all of the specimens, include virgin specimens, were examined by the TWA and CWA tests. It should be noted that there were two types of undamaged (virgin) specimens: a) two specimens tested before and after the 30-day additional water curing (healing process) similar to the damaged specimens b) two specimens tested only after the 30-day additional water curing (healing process). The purpose of the second group of control specimens was to observe the effect of drying process on water transport behavior of UHPC mixtures.

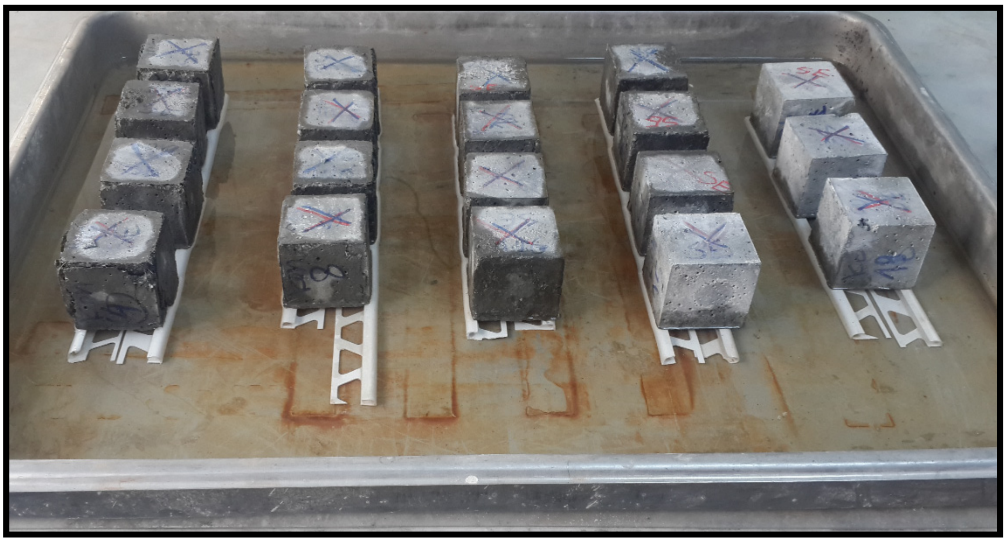

Figure 3.14 Capillary water absorption test (Personal archive, 2017)

3.1.2.7 Air Permeability Test

The air permeability test was on the test methods used in Chapter 8 to assess the extent of self-healing. Kunieda et al. (2012) applied the Torrent Air Permeability Method (Torrent, 1992) to assess the autogenous healing behavior of cracked Ultra High Performance-Strain Hardening Cementitious Composites (UHP-SHCC). Special designed plate-shaped specimens were cracked by a special uniaxial tensile test (Kunieda et al., 2012). The pre-damaged UHP-SHCC had multiple fine cracks with widths less than 30 microns resulting from its multiple-cracking behavior.

In this study, it was aimed to examine self-healing of a single crack in selected UHPC mixtures through the Torrent air permeability (TAP) method. For this purpose, special plate-shaped specimens were designed.

As can be seen from figure 3.15 the TAP tester consists of a vacuum pump, a pressure sensor, a logger and a two-cell chamber (Figure 3.15). The chamber, which is put on the concrete during measurement, has an inner chamber and an outer chamber (Figure 3.16). A unidirectional air-flow into the measuring (inner) chamber is possible as result of absorbing lateral perturbations by the outer chamber (Torrent, 1992). The result of test is the coefficient of air permeability (kT. [10^{-16} m^2]) according to the model proposed by Torrent (1992).

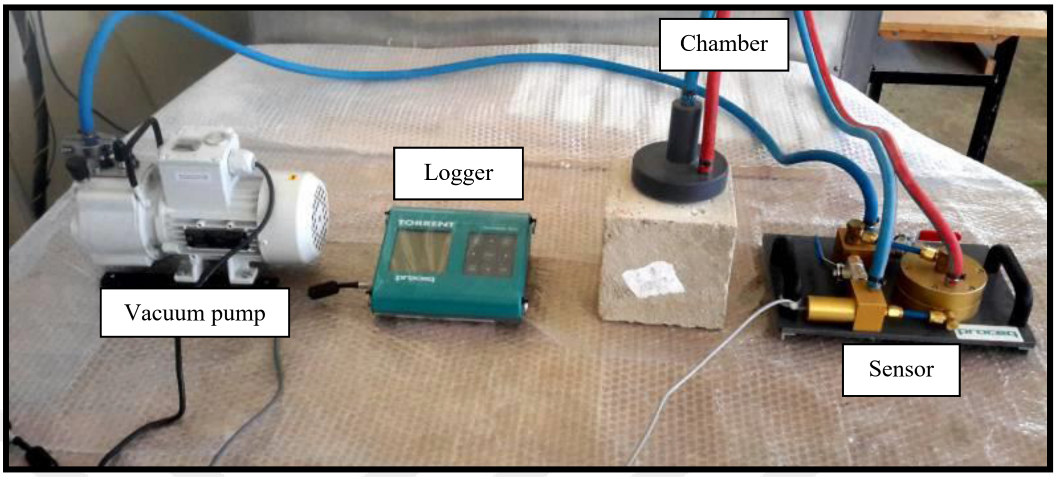

Figure 3.15 Torrent air permeability tester (Personal archive, 2014)

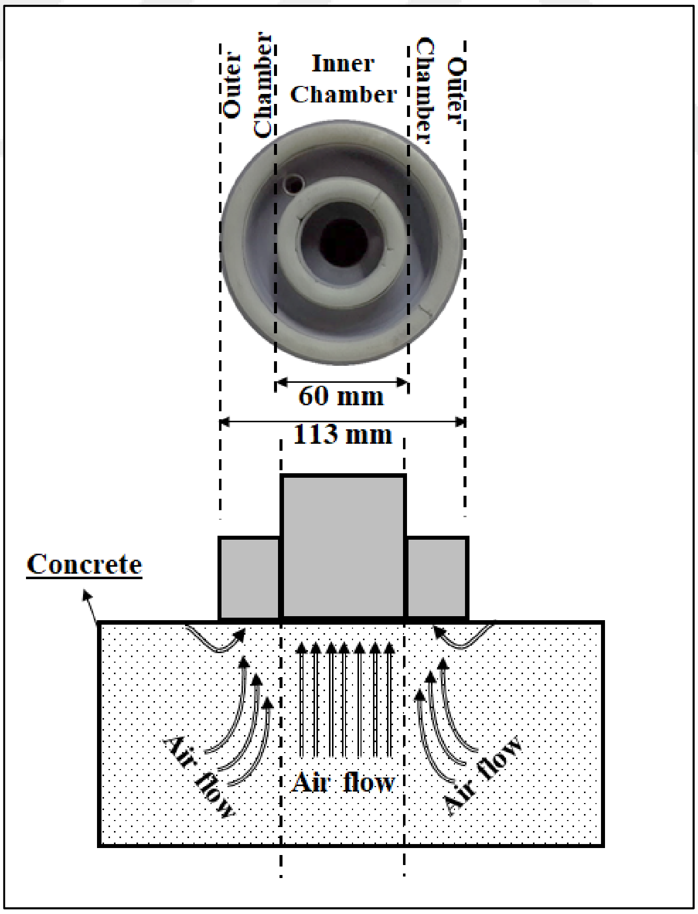

Figure 3.16 Schematic diagram of the chamber TAP tester

As mentioned earlier special plate-shaped specimens were designed and cracked to assess the self-healing capacity of selected UHPC mixtures through the air permeability test. According to preliminary experiments, it is important that the length of such a crack with 100 μm do not exceed the diameter of the TAP chamber. Otherwise, the tester do not vacuum the concrete. Therefore, it aimed to introduce a crack with maximum 65 mm length in the middle of the plate-shaped specimens. For this purpose, before the casting, special stainless steel made loading apparatus were embedded in molds. The UHPC mixture were cast (Figure 3.18) and then, cured in lime saturated water for 7 and 90 days following by demolding 24 h after casting. The details of the specimens are presented in Figure 3.19. In order to assess the self-healing capacity of fiber reinforced UHPC mixtures in terms of air permeability, three plate-shaped specimens were prepared for each variety. It must be noted that the ultrasonic pulse velocity and water permeability tests (see next sections) were conducted on the same plate-shaped specimens.

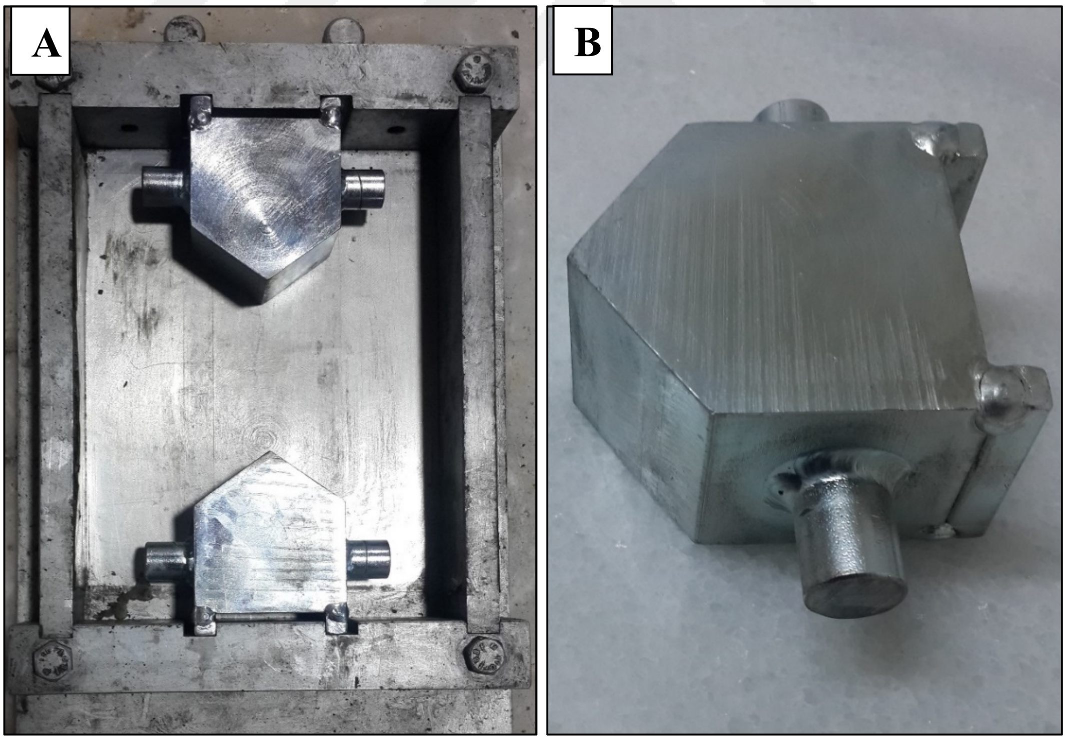

Figure 3.17 A) Plate-shaped specimens molds. B) Loading apparatus (Personal archive, 2017)

Figure 3.18 Casting of plate-shaped specimens (Personal archive, 2017)

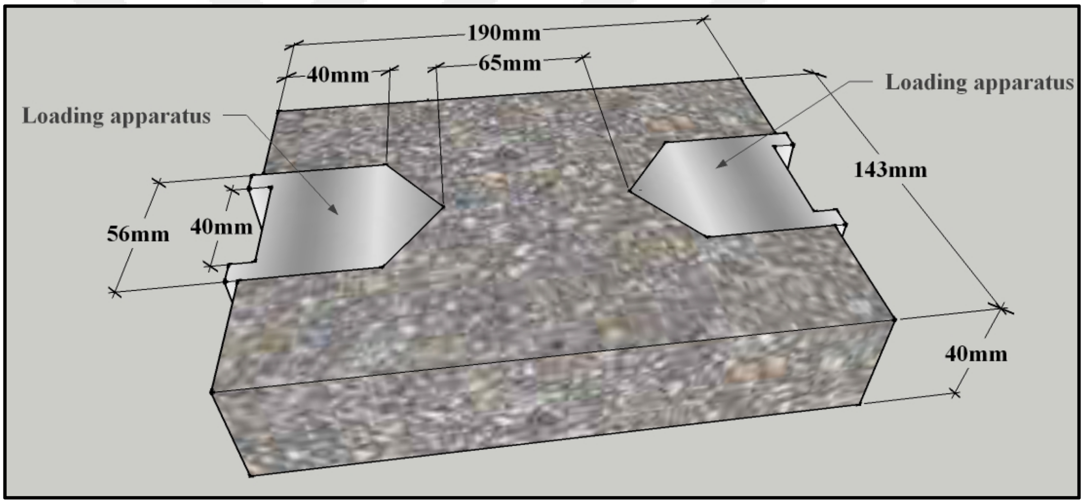

Figure 3.19 Schematic diagram of the plate-shaped specimens

After curing periods, the plate-shaped specimens were taken out of the water and then, dried in oven at 50°C for two days. The drying process is necessary for an appropriate air permeability and also and water permeability tests. As can be seen from Figure 3.20 the TAP test were conducted on the undamaged plate-shaped specimens. It should be noted that ultrasonic pulse velocity and water permeability tests were respectively applied on the same specimens following by TAP test.

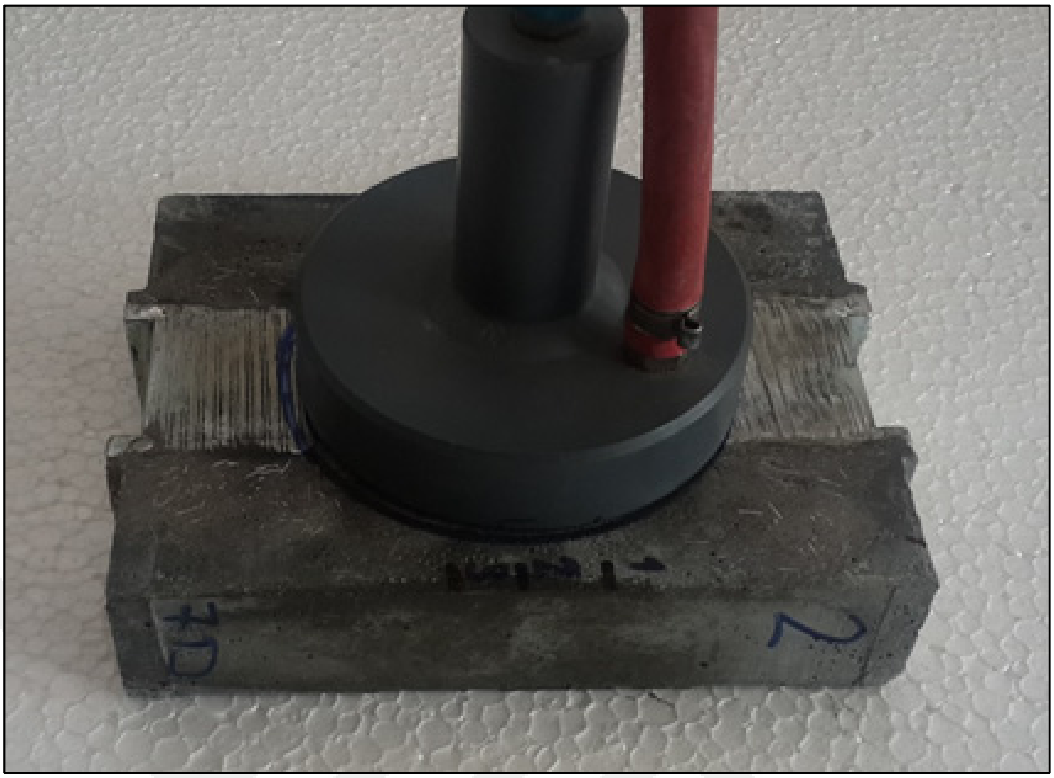

Figure 3.20 TAP test conducted on the plate-shaped specimen (Personal archive, 2017)

As can be seen from Figure 3.21 the plate-shaped specimens were loaded from the embedded loading apparatuses. The loading was continued until introducing a crack with 100 ± 20 μm width. Immediately, the pre-damaged specimens were subjected to the TAP, ultrasonic pulse velocity, and water permeability tests. After measurements, the specimens were immersed in water for self-healing process. After 30 days, the preloaded specimens were subjected to the TAP, ultrasonic pulse velocity, and water permeability tests to assess the extent of self-healing.

Figure 3.21 The plate-shaped specimen under loading (Personal archive, 2017)

3.1.2.8 Ultrasonic Pulse Velocity Test

The ultrasonic pulse velocity (UPV) test was one the test methods used in Chapter 8 to observe the extent of self-healing. As can be seen from Figure 2.22 the UPV test was conducted on the same plate-shaped specimens following by the TAP test. Similar to the TAP test, the UPV was applied on the specimens before and after introducing crack to determine the damage ratio. After 30 days water curing, the extent of self-healing was determined by repeating the tests. The UPV test were carried out by placing the transducers (55 KHz) at three points along the cracks. It should be emphasized that the TAP, UPV, and water permeability tests were conducted on dry specimens.

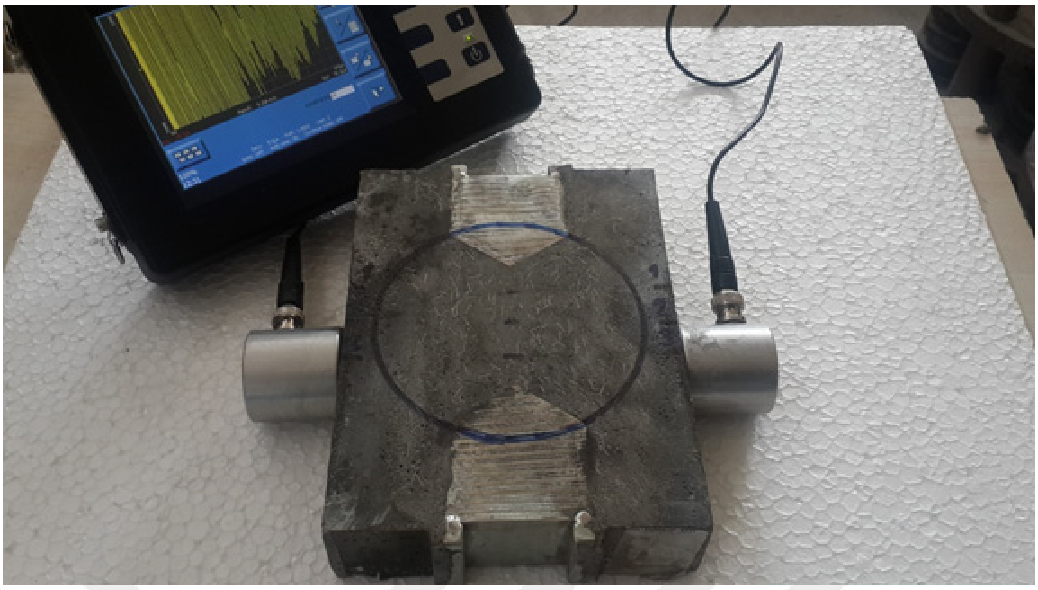

Figure 3.22 UPV test (Personal archive, 2017)

3.1.2.9 Water Permeability Test

Kunieda et al. (2012) have also used the surface penetrant test method recommended by the Japan Society of Civil Engineers (JSCE, 2004) as water permeability test. They applied the water permeability test to assess the autogenous healing behavior of the same UHP-SHCC specimens that were analyzed by the air permeability test. The similar water permeability setup was also used in this study to assess the extent of self-healing in the plate-shaped specimens (Figure 3.23). After TAP and UPV tests, the water permeability test was conducted on the same plate-shaped specimens. A plastic funnel with 80 mm diameter was connected to a plastic measuring pipette (25 ml) by silicon sealant and then, followed by sealing with paraffin. As can be seen from Figure 3.24 the funnel was attached to the center of the surface of the plate-shaped specimens by silicone sealant and then, water was poured until the water head of 250 mm (Kunieda et al., 2012). It should be noted that using of appropriate silicone sealant is essential in terms of efficient sealing. As can be seen from Figure 3.24 the red and white color high temperature resistance silicone sealants were successfully used for this purpose. The change of water level in measuring pipette was registered after 24 hours.

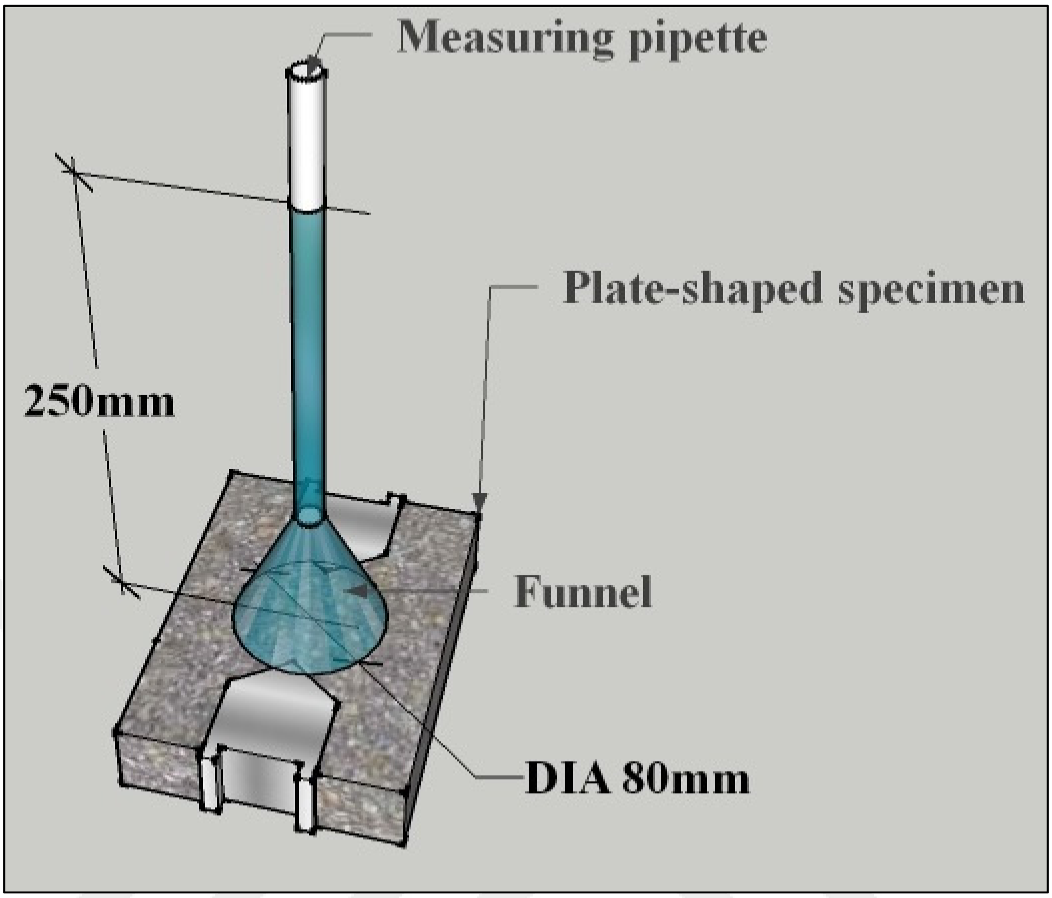

Figure 3.23 Schematic diagram of the water permeability test

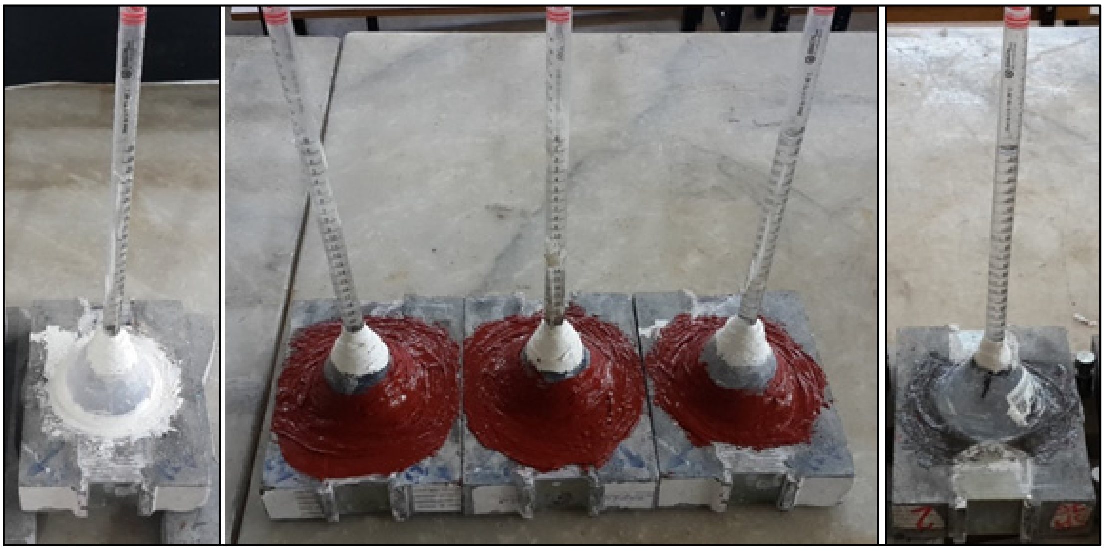

Figure 3.24 Water permeability test (Personal archive, 2017)

3.2 Microencapsulation

Materials and methods used for microencapsulation of sodium silicate and isophorone diisocyanate (IPD) as healing agent are present in this section.

3.2.1 Microencapsulation of Sodium Silicate with Urea-Formaldehyde Shell

The microencapsulation of aqueous sodium silicate (SS) with urea-formaldehyde shell was tried by Gilford et al. (2014). In order to encapsulate SS as healing agent, they have tried to adopt a well-developed in situ poly(urea-formaldehyde) microencapsulation method recommended by Brown et al. (2003) to encapsulate dicyclopentadiene (DCPD) monomer. The adopted synthesis method used by Gilford et al. (2014) was tried in the scope of this thesis.

3.2.1.1 Materials

Shell-forming materials, urea as monomer and formaldehyde solution (36.5-38% in H_2O) as condensing agent were purchased from Sigma-Aldrich. Ammonium chloride and resorcinol obtained from Sigma-Aldrich were used in the polymerization process of urea-formaldehyde. Deionized water was the continuous phase of the emulsion.

The healing agent or core material was sodium silicate solution purchased from Sigma-Aldrich. The SS solution contains ~10.6% Na_2O and ~26.5% SiO_2. A maleic copolymer (poly(E-MA)), poly(ethylene-alt-maleic anhydride), supplied from Sigma-Aldrich was used as emulsifier (polymeric surfactant) in synthesis process. In addition, Gilford et al. (2014) have declared that the copolymer improves mechanical properties of microcapsules.

1-octanol, hydrochloric acid (HCL), and sodium hydroxide (NaOH) obtained from Sigma-Aldrich were used as the surface bubbles remover, pH reducer, and pH enhancer agents, respectively.

3.2.1.2 Microencapsulation Method

A 50 ml of 2.5 wt% aqueous solution of maleic copolymer was prepared by using simultaneously ultrasonic bath and IKA RW 20 digital mixer (at least 2 h) and then, magnetic stirrer (DAIHAN - MSH-20D) over a night (Figure 3.25). The solution was added to 200 ml deionized water in 1000 ml beaker (water or continuous phase of the emulsion).

Figure 3.25 Preparation of the maleic copolymer solution (Personal archive, 2016)

Under agitation with IKA RW 20 digital mixer (three-bladed mixing propeller), 5.00 g urea, 0.50 g ammonium chloride, and 0.50 g resorcinol were added to the solution. In a typical procedure, the pH value of solution was set to 3.50 by dropwise addition of NaOH and HCI (Figure 3.26). WTW Inolab pH 7110 Set 2 was used for or the pH measurements. One drop of 1-octanol was added to the solution for eliminating surface bubbles.

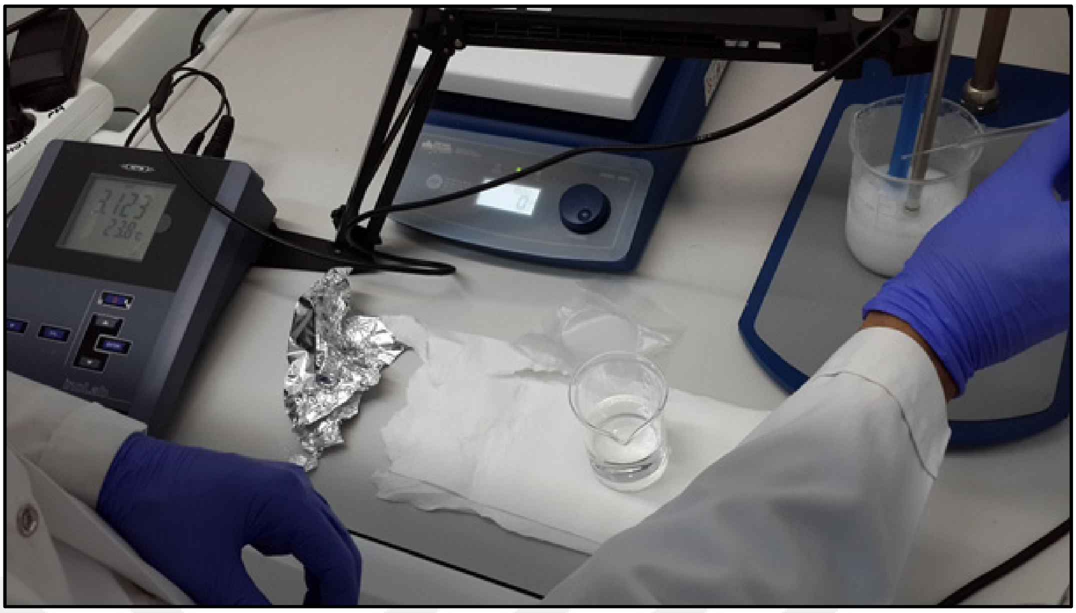

Figure 3.26 Setting the PH value of solution (Personal archive, 2016)

It should be noted that in the reference method recommended by Brown et al. (2003), the water-miscible core material, dicyclopentadiene (DCPD), were added to the water phase to prepare an oil-in-water emulsion. In other words, the core material, oil phase, were dispersed as micro droplets in water phase. The poly(E-MA) adsorbs on the interface between oil and water phases acts as polymeric surfactant to stabilize the emulsion and also works as a reaction site of polymerization (Yoshizawa, Kamio, Hirabayashi, Jacobson, & Kitamura, 2004). In the case of using the aqueous SS solution instead of the DCPD as core material, it can not be added directly to the water phase due to the fact that SS is a water-miscible liquid. In other words, the aqueous SS cannot dispersed as micro droplets in water phase. Therefore, in the adopted method, Gilford et al. (2014) slowly added HCL to a solution contains deionized water (170 ml) and aqueous SS (60 ml) to form a gel/aqueous solution. After that, 100 ml of gel/aqueous SS solution were added to the main solution (continuous or water) phase. In the reference method (Brown et al., 2003), there is no need to monitor again the pH level of emulsion when the core materials (DCPD) is added to the water phase. However, it is so critical maintaining pH of emulsion at desired value (3.0 – 4.0) in the case of using gel/aqueous SS solution as core material.

After agitation (10 min) with desired rate (250, 350, 450, 550, 650, 700 and 750 rpm), which is the most important factor in terms of the size of microcapsules, 12.7 g of the formaldehyde solution were added to the emulsion. The molar ratio of formaldehyde to urea is 1:1.9 as recommended in the reference method (Brown et al., 2003) according to a study carried out by Sanghvi and Nairn (1992).

At end the of microencapsulation process, the beaker was wrapped and covered with aluminum foil and the emulsion was slowly heated up to the desired temperature (50, 51, 52, 53, 54, 55 and 56 °C) under continuous agitation. After 4 h continuous agitation, the suspension of particles (possible microcapsules) was cooled to ambient temperature, and then was tried to be separated under vacuum with different filter papers and decantation with distilled water. As can be seen from Figure 3.27 the microencapsulation process were carried out with IKA RW 20 digital mixer (three-bladed mixing propeller) and magnetic stirrer (cylindrical magnetic stirring bar with 30 mm length) to evaluate the effect of mixing type. The decanted particles (possible microcapsules) were dried at room temperature for 72 h

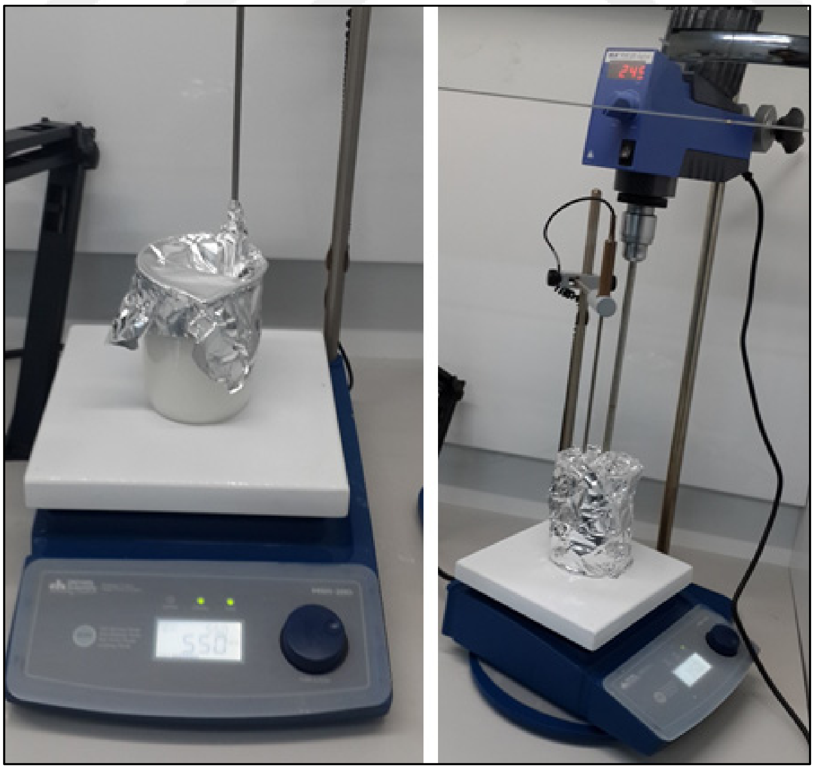

Figure 3.27 Agitating emulsion at 55 °C for 4 h (Personal archive, 2016)

The scanning SEM and EDS analyses were conducted on the dried powder (possible microcapsules). SEM observations was made by using a scanning electron microscope (Carl Zeiss 300VP, Germany) operated at 3 kV. Prior to SEM imaging, gold sputtering was on the samples.

3.2.2 Microencapsulation of Sodium Silicate with Polyurethane Shell

Pelletier et al. (2011) have prepared the aqueous SS-loaded polyurethane microcapsules according to the method suggested by Saihi, Vroman, Giraud, and Bourbigot (2006) for the microencapsulation of di-ammonium hydrogen phosphate. Pelletier et al. (2011) emulsified the aqueous SS in toluene, which is immiscible in water, using a combination of two different surfactants. After dispersing of SS in the organic phase, the shell-forming monomer, methylene diphenyl diisocyanate (MDI), was added to initiate the interfacial reaction of MDI and water at the interface of drops of the aqueous SS (Saihi et al., 2006). Similar interfacial polymerization method was also used by Tan et al. (2016) for microencapsulation of colloidal silica instead of SS. This section have dealt with the microencapsulation of sodium silicate as healing agent in polyurethane microcapsules.

3.2.2.1 Materials

Sodium silicate solution (SS) purchased from Sigma-Aldrich (Na2O, ~10.6% and SiO2, ~26.5%) was used as a core material with deionized water. Shell-forming monomer, 4,4′-Methylenebis(phenyl isocyanate) 98%, and surfactants, Span 85 (Sorbitanetrioleate) and Poly(ethylene glycol) dioleate (POEDO) were also supplied from Sigma-Aldrich. In addition, Dibutyltindilaurate (95%) obtained from Sigma-Aldrich was used as catalyst. Organic phase for emulsifying of SS was toluene (Sigma-Aldrich) which was used without further purification.

3.2.2.2 Microencapsulation Method

The synthesis process was based on in situ interfacial polymerization method introduced by Saihi et al. (2006). However, some necessary modifications were performed in the process. In typical process, the synthesis of microcapsules was performed in a 100 mL beaker by using a digital hotplate stirrer (DAIHAN - MSH-20D) and a magnetic cylindrical stirrer bar (30 mm). This method has two main steps as follows: 1) dispersion of the aqueous solution of SS in organic phase, 2) addition of shell-forming solution. It must be noted that many preliminary tests were carried out to find out the material ratios and stirring speeds. Three solutions were prepared in the synthesis process as follows: 1) S1 is a solution of surfactants, which are Span 85 (2 g) and POEDO (1 g), in 45 mL of toluene, 2) S2 is a solution of shell-forming substances, which are MDI (various amounts were analyzed) and a few droplets of catalyst, in 7.5 mL of S1 and 12.5 g of additional toluene, 3) S3 is solution of SS (7.5 g) in 7.5 mL of deionized water, called core material. It must be mentioned that various SS/water ratios were analyzed in the core material solution. In addition, the morphology optimization tests were carried out in 250 mL beaker (doubled materials) by using various type of magnetic stirrer bars. The details are present in Chapters 9.

In a typical microencapsulation procedure, S3 was emulsified in S1 solution at a speed of 1000 rpm (various stirrer speeds were analyzed) for 20 min. After dispersion and stabilization of aqueous SS micro droplets in the organic phase, S2 solution was added to the primary emulsion. Based on the preliminary test results, various amounts of MDI were used to determine the effect of diisocyanate monomer on the properties of the microcapsules. The mixture was stirred at a speed of 900 rpm (various stirrer speeds were analyzed) for 20 min at room temperature to form the primary membrane (Saihi et al., 2006). Then, temperature was gradually increased to 63°C, while the stirring speed was reduced to 800 rpm (various stirrer speeds were analyzed). The stirring was continued at 63°C and 800 rpm for 4 h to grow the membrane. The microcapsules were vacuum filtered, and then washed with toluene for removal of MDI residue and ethanol/water for removal of surfactant residue and non-encapsulated SS. The microcapsules were dried at room temperature for 48 h, and then weighed for yield calculation. Figure 3.29 shows a brief of microencapsulation process of SS with polyurethane shell.

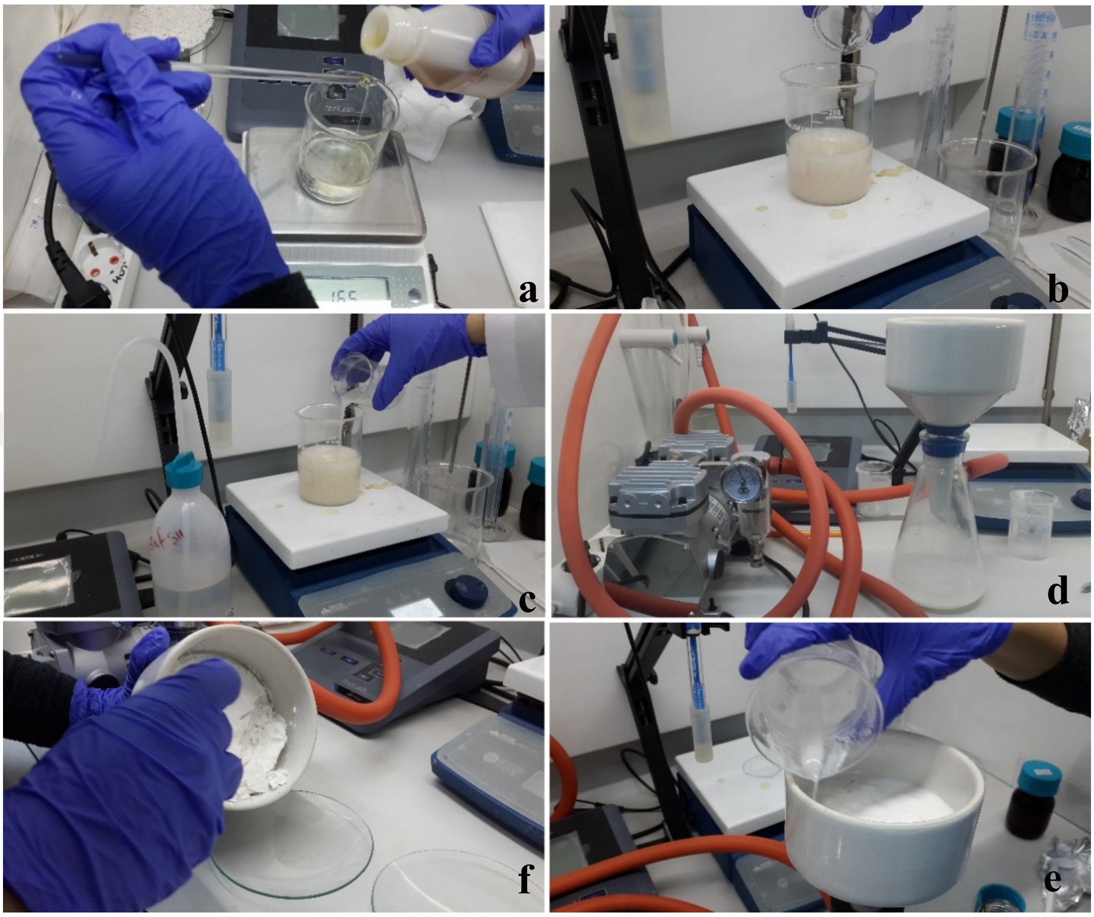

Figure 3.28 Microencapsulation process of SS with polyurethane shell: a) surfactants were to the oil phase; b) SS solution was poured to the oil phase for emulsification; c) shell-forming solution was poured to the emulsion; d, e) vacuum filtration and washing of microcapsules; f) the microcapsules were transferred to watch glasses for drying process (Personal archive, 2017)

3.2.2.3 Characterization of Microcapsules

FTIR-ATR analyses of the samples were made by using Fourier transform infrared spectrometer (Perkin Elmer Spectrum BX) in the range 4.000-650 cm^{-1}.

Thermal stability of microcapsules was analyzed by TGA using a DTG-60/60 Simultaneous Thermogravimetry/Differential Thermal Analyzer (Shimadzu). The analyses were carried out at a heating rate of 10°C/min from room temperature to 800°C under nitrogen atmosphere.

The crystallographic properties of microcapsules were examined by X-ray diffractometer (RIGAKU, D-Max 2200 PC with CuK$_{\alpha}$ radiation (λ = 1.54Å).

SEM observation of the microcapsules was made by using a scanning electron microscope (SEM) (Carl Zeiss 300VP, Germany) operated at3 kV. Prior to SEM imaging, gold sputtering was performed on the samples.

Fracture behavior of microcapsules was analyzed in cement paste matrix. Optimized microcapsules were added in a cement paste mixture (water/cement ratio=0.3) at a concentration of 5% with respect to cement weight. The microcapsules were mixed with cement to obtain a homogenous dry mixture, and then water containing superplasticizer was added to the mixture. The cement past was poured into disk shaped molds with 30 mm diameter as shown in Figure 3.29. The specimens were demolded after 24 h and subjected to water curing for 7 days, and then were dried in air for 1 day. The specimens were split by means of the splitting tensile method. SEM analyses were performed on the fracture surface of the specimens (Figure 3.29).

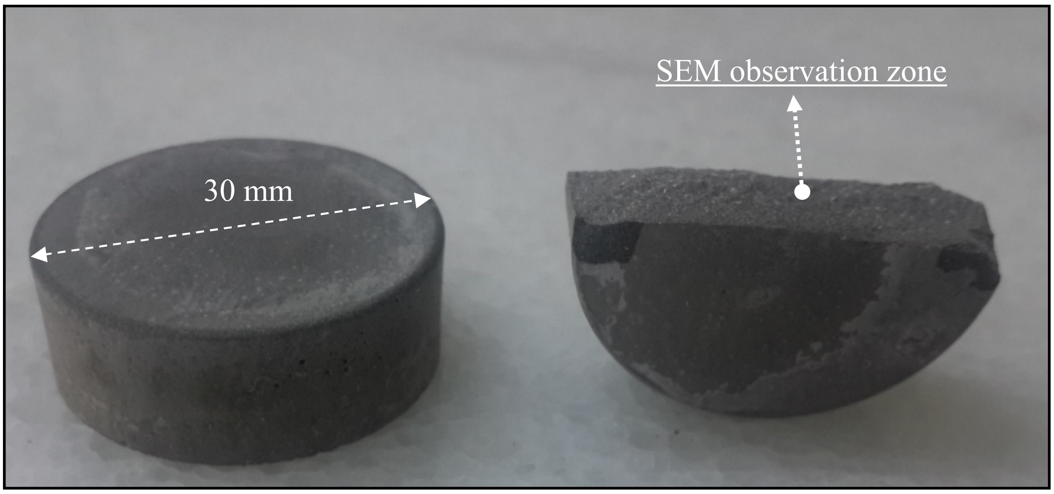

Figure 3.29 Disc-shaped specimen (Personal archive, 2017)

3.2.3 Microencapsulation of Isophorone Diisocyanate with Silica-based Shell

Microcapsules based on isophorone diisocyanate core (healing agent) and silica shell were synthesized via the interfacial polycondensation of a silica precursor. Similar procedures have also carried out by H. Z. Zhang, Sun, Wang, and Wu (2011) for encapsulation of n-octadecane with inorganic silica.

3.2.3.1 Materials

Isophorone diisocyanate (IPDI), core material (catalyst-free healing agent), was purchased from Sigma-Aldrich. Shell-forming material (silica precursor), tetraethyl orthosilicate (TEOS), were also obtained from Sigma-Aldrich. Tween80 (Fluka chemika) was used the non-ionic surfactant (emulsifier material). Hydrochloric acid (HCL) purchased from Sigma-Aldrich were used as the pH reducer material. Deionized water was the continuous phase of the emulsion.

3.2.3.2 Microencapsulation Method

In typical process, the synthesis of microcapsules was performed in a 100 mL beaker by using a digital hotplate stirrer (DAIHAN - MSH-20D) and a magnetic oval stirrer bar (30 mm). This method has two main steps as follows: 1) dispersion of the oil phase (IPDI+TEOS) in water phase, 2) reducing the pH of emulsion to desired value solution to initiate the condensation of silica hydrolysates. It must be noted that many preliminary tests were carried out to find out the material ratios, pH values, and stirring speeds. Two solutions were prepared in the synthesis process as follows: 1) S1 is a solution of surfactant, Tween80, in 50 mL of deionized water. Various amounts (0.3, 0.5, 0.6, 0.8, 0.9, 1.0, and 1.2 g) of Tween80 were examined 2) S2 is a solution of 4.5 g of shell-forming (TEOS) and 4.5 g of core material (IPDI). In addition, the optimization of pH control times were carried out in 250 mL beaker (doubled materials) by using a magnetic oval stirrer bar with 40 mm length.

In a typical microencapsulation procedure, S2 was emulsified in S1 solution at a speed of 800 rpm (various stirrer speeds were analyzed) for 20-30 min. After dispersion and stabilization of TEOS/IPDI micro droplets in the water phase, the stirring speed were reduced to 500 rpm and then, pH was adjusted to the desired value by adding (dropwise) of the HCL aqueous solutions with various concentrations. WTW Inolab pH 7110 Set 2 was used for or the pH measurements. The emulsion was continuously stirred at 40 °C for 24 h to complete the interfacial polycondensation of silica precursor. It must be noted that, adjusting the pH value continuously to desired value for at least 30 min after raising temperature to 40 °C has remarkably positive effect on microencapsulation.

The microcapsules were vacuum filtered, and then washed ethanol/water for removal of surfactant residue and non-encapsulated materials. The microcapsules were transferred to watch glasses and dried at room temperature for 48 h or in oven at 40 °C, and then weighed for yield calculation.

3.2.3.3 Characterization of Microcapsules

FTIR-ATR analyses of the samples were made by using Fourier transform infrared spectrometer (Perkin Elmer Spectrum BX) in the range 4.000-650 cm^{-1}.

Thermal stability of microcapsules was analyzed by TGA using a DTG-60/60 Simultaneous Thermogravimetry/Differential Thermal Analyzer (Shimadzu). The analyses were carried out at a heating rate of 10°C/min from room temperature to 800°C under nitrogen atmosphere.

SEM observation of the microcapsules was made by using a scanning electron microscope (SEM) (Carl Zeiss 300VP, Germany) operated at3 kV. Prior to SEM imaging, gold sputtering was performed on the samples.

The optical microscope images were captured by digital microscope. The microcapsules were dispersed in water, and then few droplets of the suspension were analyzed by the optical microscopes.

CHAPTER FOUR
RESEARCH PROGRAM

The research program of this study has six sections as follows:

Section 1: It was aimed to design a flowable ultra high performance concrete (UHPC) mixture with 800 kg/m^3 cement dosage. The fresh and mechanical properties of four mixtures were determined. A mixture with optimum superplasticizer content and a compressive strength higher than 100 MPa was selected as the control cementitious matrix for the second and third section of research. The details are presented in Chapter 5.

Section 2: The selected UHPC mixture were reinforced by 0.5, 1.0, 1.5, and 2 vol.% of two different steel micro fiber. The fresh and mechanical properties of mixtures were determined. In addition, the crack restriction capacity of steel fibers were also analyzed. A type of steel micro-fiber and a certain volume fraction of fiber were selected for next sections of research. The details are presented in Chapter 6.

Section 3: In order to enhance the self-healing mechanism, the binder dosage of the UHPC mixture selected mixture from section one was increased to 1200 kg/m^3 by addition of various supplementary cementitious materials (SCM). The first group of mixtures (G1) contain 800 kg/m^3 of cement and 400 kg/m^3 of SCM. On the other hand, the binder phase of second group of mixtures (G2) consists of 400 kg/m^3 cement and 800 kg/m^3 SCM. The self-healing capacity of nine different UHPC mixtures were examined through a novel test method (please see 3.1.2.4) as well as the crack closing test. In addition, the compressive strength of mixtures were determined at 7 and 28 days. Besides the control mixture, a fly ash bearing mixture and a ground granulated blast furnace slag bearing mixture were selected for the next section of the research. The details are presented in Chapter 7.

Section 4: The self-healing capacity of the three selected UHPC mixtures were determined through the uniaxial compressive, direct tension, crack closing, total water absorption, capillary water absorption, air permeability, ultrasonic pulse velocity, and water permeability tests. A fiber reinforced UHPC mixture with better self-healing capacity was selected as the cementitious matrix in which the self-healing efficiency of microcapsules will be analyzed in next sections of thesis. In addition, the efficiency of above-mentioned methods were analyzed in terms of self-healing assessment. The details are presented in Chapter 8.

Section 5: This section has dealt with the microencapsulation of sodium silicate (SS) as healing agent with polymer based shells. For this purpose, two methods were used in this study:

a) The microencapsulation of aqueous SS with urea-formaldehyde shell was tried by Gilford et al. (2014). In order to encapsulate SS as healing agent, they have tried to adopt a well-developed in situ poly(urea-formaldehyde) microencapsulation method recommended by Brown et al. (2003) to encapsulate dicyclopentadiene monomer. The adopted synthesis method used by Gilford et al. (2014) was tried in the scope of this thesis. Parameter such as stirring speed of emulsification, pH value of emulsion, and polymerization temperature were investigated. The problems of this method were discussed in details in Chapter 9.

b) Pelletier et al. (2011) have prepared aqueous SS-loaded polyurethane microcapsules according to the method suggested by Saihi et al. (2006) for the microencapsulation of di-ammonium hydrogen phosphate. Pelletier et al. (2011) have used a certain amount of MDI in their synthesis procedure. However, it is well known that the amount of shell-forming monomer is a key factor in terms of the yield, shell thickness, and mechanical properties of microcapsule. In the scope of this study, various amounts of MDI were used in the synthesis of SS-loaded poly(urea-urethane) microcapsules. Moreover, Pelletier et al. (2011) have not studied the characterization of microcapsules in detail. Therefore, the microcapsules synthesized in this research were characterized through the microencapsulation yields, scanning electron microscopy, energy-dispersive X-ray spectroscopy, X-ray diffraction, thermogravimetric, and Fourier transform infrared (FTIR) analyses. Besides, the fracture behavior of the optimized microcapsule was examined in a cement paste matrix. In addition, the effect of parameters such as stirring speed of emulsification and core materials components ratios were examined.

c) The sodium silicate/polyurethane microcapsules, which its synthesis parameter such as shell-forming monomer, core material (healing agent), and stirring procedures have been optimized, were incorporated in UHPC mixtures. The details are presented in Chapter 9.

Section 6: In this section, microcapsules based on isophorone diisocyanate core (healing agent) and silica shell were synthesized via the interfacial polycondensation of a silica precursor. After many preliminary tests, the effect of Tween80 (surfactant) weight ratio, pH value, and stirring speed for emulsification were examined through the yield, microscopy, TGA, and FTIR analysis. The details are presented in Chapter 10.

CHAPTER FIVE
DESIGN OF ULTRA HIGH PERFORMANCE CONCRETE

As mentioned earlier, a flowable ultra high performance concrete (UHPC) mixture with 800 kg/m^3 cement dosage were designed in this section. Preliminary experiments were carried out to design four different mixture. The fresh and mechanical properties of four mixtures were determined. A mixture with optimum superplasticizer content and a compressive strength higher than 100 MPa was selected as the main cementitious matrix for this research.

5.1 Mix Designs and Fresh Properties

In the preliminary experiments made, four different mixtures were designed especially considering the free flow values. For this purpose, the water-to-binder ratio (W/B) of mixtures was adjusted to be 0.20 or 0.22. In addition, two different combinations of aggregates were investigated such that the maximum grain diameter was 1 mm and 3 mm. The mix design of mixtures are presented in Table 5.1.

The workability of each mixture was controlled by the mini-flow table test. The required amount of superplasticizer was used to achieve 260 ±10 mm free flow values. Considering that the amount of superplasticizer can be increased by the use of fibers throughout the study, the high superplasticizer requirement was considered as a disadvantage.

Table 5.1 Mix design of UHPC mixtures (kg/m^3)

Mixtures	Water	Cement	W/B	Quartz aggregate			SP
				0-0.4 (mm)	0.4-1 (mm)	1-3 (mm)	
0.20-1mm	160	800	0.20	415	969	-	35
0.20-3mm	160	800	0.20	352	493	563	25
0.22-1mm	176	800	0.22	410	956	-	25
0.22-3mm	176	800	0.22	345	483	552	19

5.2 Compressive Strength Test Results

The compressive strength test results are the average of three 50×50×50 mm cubic specimens. The compressive strength of the 0.22-3mm mixture at 7 and 28 days, which its superplasticizer dosage was at the optimum level, was found to be 90 MPa and 104 MPa, respectively (Figure 5.1). On the other hand, the compressive strength of the 0.22-3mm mixture is higher than the other three mixture.

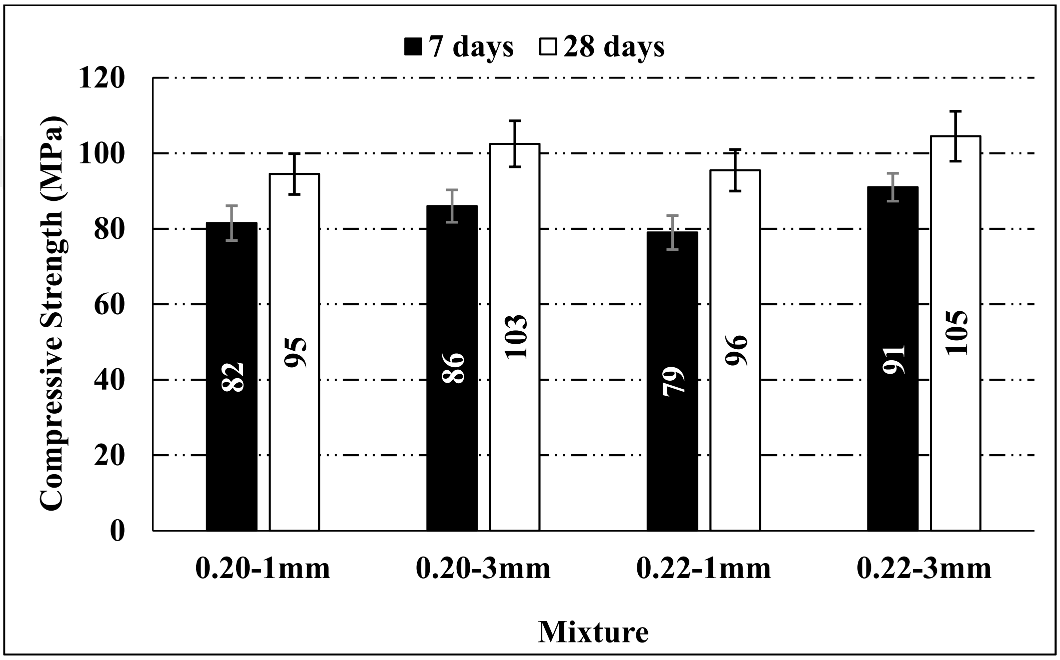

Figure 5.1 Compressive strength of mixtures

5.3 Direct Tension Test Results

The direct tension test results are the average of six dog-bone shaped specimens. As shown in Figure 5.2, the direct tensile strengths of the 0.22-3mm and 0.20-3mm mixtures at 7 and 28 days were found to be close to each other and higher than those of other mixtures.

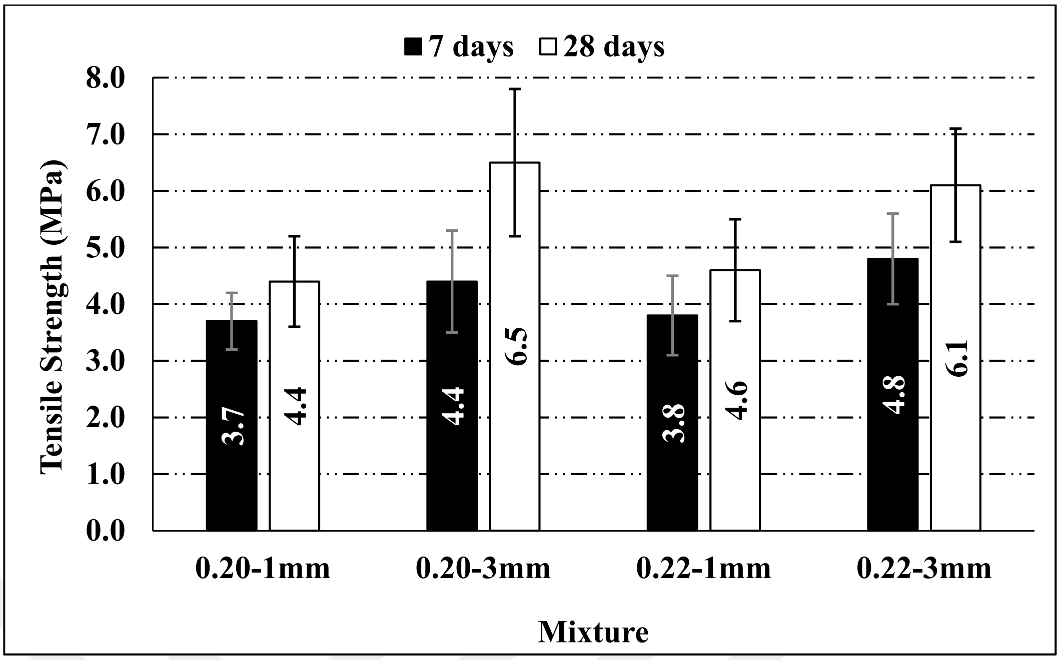

Figure 5.2 Direct tensile strengths of UHPC mixtures

Taking into consideration of the fresh properties, amount of required superplasticizer, compressive strength, and tensile strength, the 0.22-3mm mixture was selected as the main UHPC mixture for this study.

CHAPTER SIX
INCORPORATION OF STEEL FIBERS

The selected UHPC mixture were reinforced with two different steel micro fibers. The fresh and mechanical properties of mixtures were determined. In addition, the crack restriction capacity of steel fibers were also analyzed. A type of steel micro-fiber and a certain volume fraction of fiber were selected for next sections of this research.

6.1 Mix Designs and Fresh Properties

The 0.22-3mm mixture selected in the previous were reinforced by 0.5, 1.0, 1.5, and 2.0 vol.% of two different steel micro fibers with 6 mm and 13 mm lengths, hereafter called MF1 and MF2, respectively. Mix designs (using MF1) are presented in Table 6.1.

Table 6.1 Mix design of fiber reinforced UHPC mixtures (kg/m^3)

Mixtures	Water	Cement	Fiber	Quartz aggregate			SP
				0-0.4 (mm)	0.4-1 (mm)	1-3 (mm)	
F-0.0	176	800	-	345	483	552	19
F-0.5	176	800	36	340	476	544	22
F-1.0	176	800	72	337	472	539	22
F-1.5	176	800	108	334	467	534	22
F-2.0	176	800	143	330	463	529	23

As mentioned earlier, micro fibers having a length of 6 mm (MF1), as well as micro fibers having length of 13 mm (MF2), have also been tested in preliminary experiments. While the MF1 fiber did not affect the superplasticizer ratio very much (Table 6.1), the use of MF2 fiber greatly increased the need for superplasticizer. On the other hand, with the use of MF2 at a volume fraction of 1%, a free flow value of 260 ±10 mm could not be achieved despite the high superplasticizer dosage. As can be seen in Figure 6.1, the use of 13 mm fibers at 1.5% volume fraction affected adversely the flow of fresh mixture. This problem was more obvious in the case of using MF2 fiber at 2% volume fraction (Figure 6.2). It is obvious that higher binder dosage must be used for using these fibers. As can be seen from Figure 6.3, a free flow value of 260 ±10 mm could be achieved using MF1 fiber at volume fraction of 2%. Therefore, the MF1 fiber was used in continuation of the research.

Figure 6.1 Free flow test of the mixture containing 1.5% MF2 fiber (Personal archive, 2016)

Figure 6.2 Free flow test of the mixture containing 2% MF2 fiber (Personal archive, 2016)

Figure 6.3 Free flow test of the mixture containing 2% MF1 fiber (Personal archive, 2016)

6.2 Compressive Strength Test Results

The compressive strength test results are the average of three 50×50×50 mm cubic specimens. In subsequent sections of research, the self-healing assessment tests will be based on 7 days specimens, so the experiments were carried out on the 7 days water cured specimens (Figure 6.4). Taking into consideration that the plain mixture has a 7-day compressive strength of 90 MPa, the addition of fibers increased the compressive strength. The highest 7-day compressive strength was obtained with 2% fiber (98 MPa).

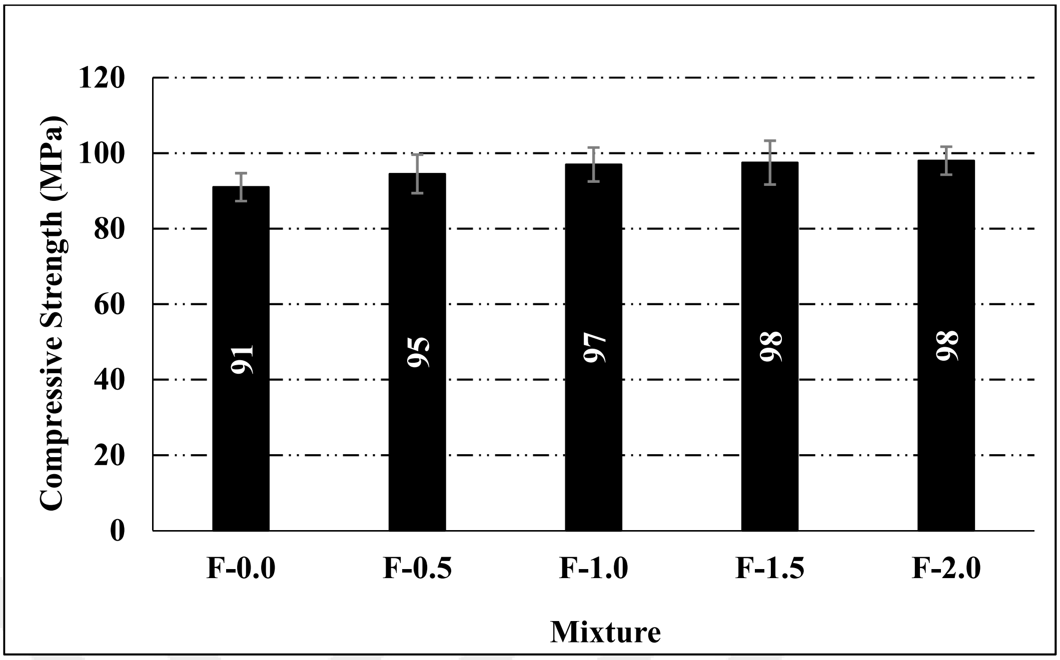

Figure 6.4 Compressive strength of fiber reinforced mixtures (7 days)

6.3 Direct Tension Test Results

The crack width restriction capacity of steel micro fibers were analyzed through the direct tension test. After 7 day water curing, 6 specimens were taken out form the lime saturated water and left to dry in laboratory air for 1 day. The specimens were subjected to direct tension loads until formation of a crack with 100 µm ± 10 width. In Figure 6.5, the curves of specimens that best represent the stress-strain behavior of the mixtures are presented. As can be seen from the figure, the mixture containing 2% fiber exhibited a better performance than the other mixtures. In other words, crack width control under direct tensile loads can be achieved more easily with a 2% fiber ratio. Nevertheless, it is obvious that the crack width control can be much easier and reliable in a composite that can exhibit deformation hardening behavior under direct tensile loads.

Figure 6.6 shows the average direct tensile strengths and the toughness values up to crack formation (100 ± 20 µm). It should be noted that the results are the average of six dog-bone shaped specimens. As can be seen, better performance can be achieved with a 2% fiber content.

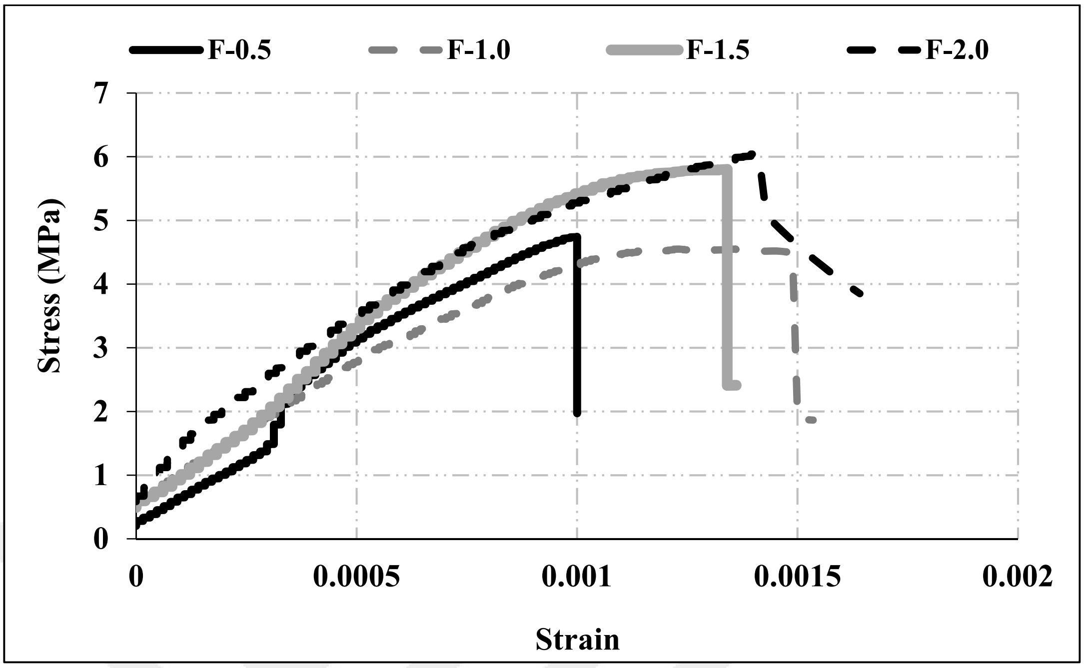

Figure 6.5 The stress-strain curves of fiber reinforced UHPC mixtures

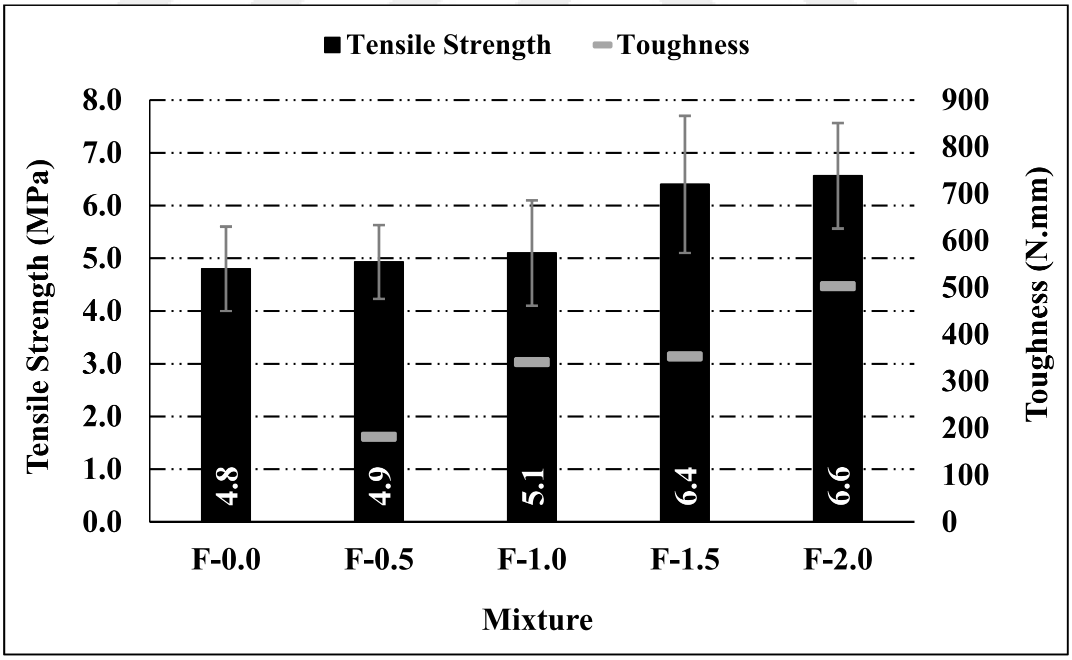

Figure 6.6 The average direct tensile strengths and the toughness values

6.4 Discussion

Incorporation of the steel micro fiber improved significantly compressive strength of the 0.22-3mm mixture. This behavior can be explained by the well-known crack-bridging effect of fibers. It has long been recognized that the behavior of cementitious materials can be improved by the addition various discontinuous fibers. However, as can be seen from test results, the direct tensile strength improvement was not as much as the compressive strength one. Mechanical properties of these composites are dramatically influenced by the fiber–matrix bond that provides the stress transferring between the fiber and matrix phases. Especially, the direct tensile strength of these composites is more dependent on the fiber-matrix bond strength. Beglarigale and Yazıcı (2015) have stated that the fiber-matrix bond characteristics improves as the embedment length of the fiber increases. They also reported that the effect of the embedment length of the fiber on the bond performance is much more noticeable for the smooth fibers. Therefore, the lower positive effect of micro fibers on direct tensile strength can be attributed to the lower length of the MF1 fibers. It must be mentioned that the purpose of using fiber in this study was different. The efficiency of autogenous self-healing mechanism can be enhanced by restriction of the crack width. In other words, the narrower cracks are more likely to be closed by the autogenous self-healing mechanism (Van Tittelboom & De Belie, 2013). The use of different fibers is greatly contributing to the autogenous self-healing by restricting the crack width (Kunieda et al., 2012).

Taking into consideration of the compressive strength, direct tensile behavior, and especially fresh properties of mixtures, the MF1 fibers (2 vol.%) was used in the next sections of this research.

CHAPTER SEVEN
INCORPORATION OF SUPPLEMENTARY CEMENTITIOUS MATERIALS

As mentioned earlier, in order to enhance the self-healing mechanism, the binder dosage of the UHPC mixture selected mixture from section one was increased to 1200 kg/m^3 by addition of various supplementary cementitious materials (SCM). The self-healing capacity of nine different UHPC mixtures were examined through a novel test method (please see 3.1.2.4) as well as the crack closing test (please see 3.1.2.5). This novel test method, hereafter called "self-bonding" method, was designed to evaluate the bonding capacity of healing products that can be formed in very tight cracks. The higher bonding capacity mean the higher self-healing capacity of the cementitious matrix. The principle of this method lies in the bonding capacity of self-healing products under direct tension loads. The efficiency of the method was analyzed in various SCMs bearing mixtures. The results of suggested new test method was compared with the crack closing test that was characterized through the microscopic analysis. In addition, the compressive strength of mixtures were determined at 7 and 28 days. Besides the control mixture, a fly ash (FA) bearing mixture and a ground granulated blast furnace slag (GGBFS) bearing mixture were selected for the next section of this research.

7.1 Mix Designs

A ground granulated blast furnace slag (GGBFS) obtained from Iskenderun iron and steel factory (Turkey) was used. In addition, the class C and F fly ashes (FA) obtained, respectively, from thermal power plants of Soma (FA1) and İzenerji (FA2) were used. The first group of mixtures (G1) contain 800 kg/m^3 of cement and 400 kg/m^3 of SCM. On the other hand, the binder phase of second group of mixtures (G2) consists of 400 kg/m^3 cement and 800 kg/m^3 SCM. The mix design of mixtures are presented in Table 7.1. It must be mentioned that the crack closing test can be carried out on the fiber reinforced mixture. Therefore, the UHPC mixtures, which were used to prepare the disk-shaped specimens, were reinforced by 2 vol.% of micro steel fiber.

Table 7.1 Mix design of SCM containing mixtures (kg/m^3)

Mixtures	Water	Cement	SCMs		Quartz aggregate			SP
			FA	GGBFS	0-0.4 (mm)	0.4-1 (mm)	1-3 (mm)	
Control	176	800	-	-	345	483	552	19
FA1-G1	264	800	400	-	192	269	307	4
FA1-G2	264	400	800	-	172	241	275	4
FA2-G1	264	800	400	-	190	266	303	8
FA2-G2	264	400	800	-	171	240	274	5
GGBFS-G1	264	800	-	400	203	285	326	9
GGBFS-G2	264	400	-	800	197	276	315	10

7.2 Test Results and Discussion

The compressive strengths of plain mixtures are presented in Figure 7.1. As expected the 7-day compressive strength of the second group of mixtures, which half of their cement content had been replaced by the SCMs, decreased as compared to the control mixture. In spite of the fact that the cement content of the first group of mixtures had not been reduced, the 7-day compressive strength of SCMs bearing mixtures (Except GGBFS-G1 mixture) decreased slightly. Pozzolanic reactions of the SCMs is limited during 7-day. As can be seen from Figure 7.1, the 28-day compressive strength of first group of SCMs bearing mixtures are similar or even higher than the compressive strength of control mixture. In the other words, the amount of C-S-H liberated by the pozzolanic reaction of SCMs with $Ca(OH)_2$ was as enough as that it can enhance the 28-day compressive strengths of mixtures.

As mentioned earlier the 7-day compressive strengths of the second group of mixtures with 400 kg/m^3 cement and 800 kg/m^3 SCMs content are low as compared to the control mixture with 800 kg/m^3 cement content. The 28-day compressive strength of GGBFS-G2 mixture reached to the 28-day strength of control mixture. However, the compressive strengths of second group of FA bearing mixtures (FA1-G1 and FA2-G2) are almost 20% lower the strength of control mixture. It can be explained by the lower pozzolanic reaction rate of FA as compared to the GGBFS one.

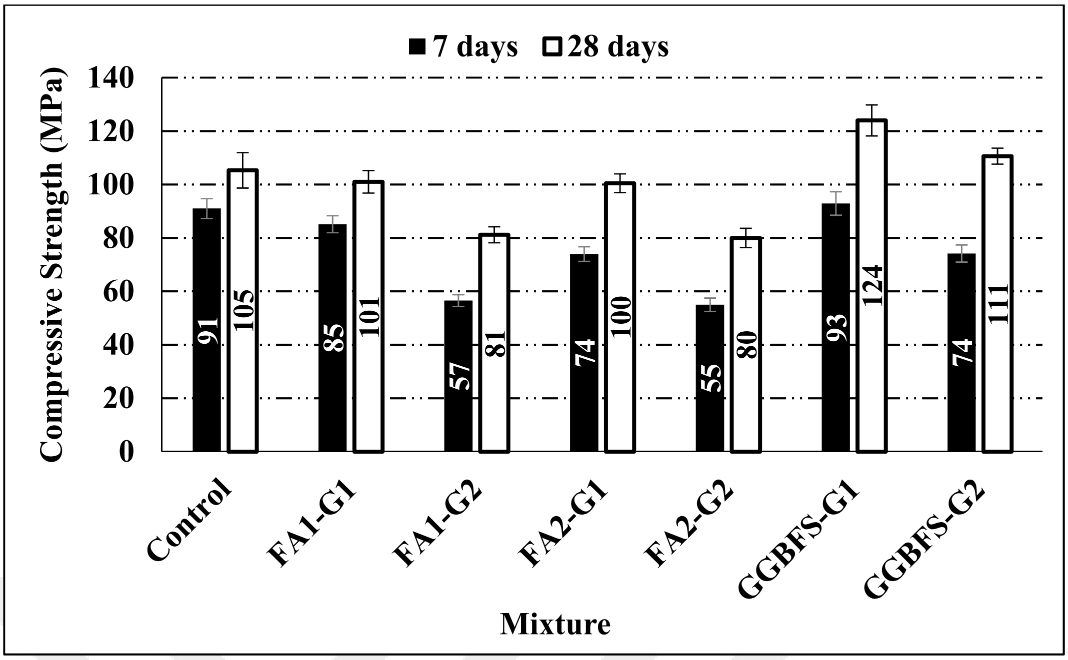

Figure 7.1 Compressive strengths of SCMs bearing plain mixtures

The self-bonding test results are presented in Figure 7.2. As can be seen from the test results a bond load due to bonding ability of healing products can be obtained in this novel test method. Huang, Ye, and Damidot (2013) made artificial planar gaps in a cement paste cubic specimen to separate the healing products from the matrix. For this purpose, the specimen was sliced and then the slices were ground to achieve flat surfaces. The slices were put together and cured in water for 200 h. Their microstructure analysis revealed that the healing product, which mainly consists of calcium hydroxide (CH) crystals and calcium silicate hydrate gels (C-S-H), can be formed by further hydration of unhydrated cement particles in the gaps. Therefore, the formation of these healing products can be considered as the main reason of the 81 N bond load of the control mixture. It is obvious that the amount of unhydrated cement particles at the fracture surface of each parts of the split specimens is the main factor that can affect the bond loads.

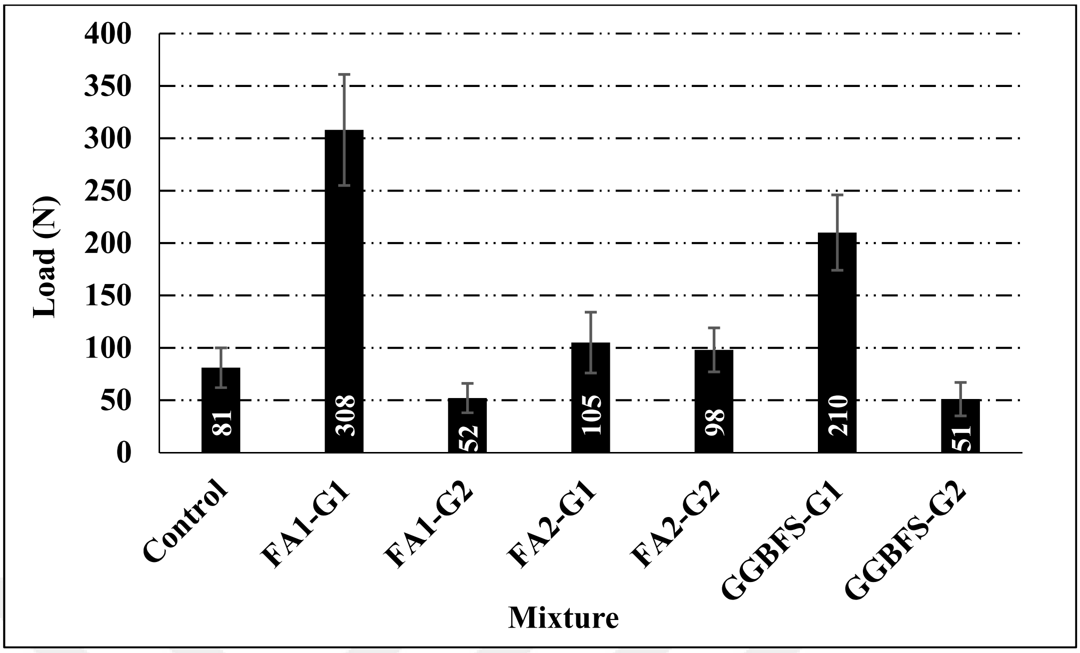

Figure 7.2 The self-bonding test results

Test results showed that the splitting process is very important point that can affect test results of the suggested self-bonding test method. As discussed earlier (see section 3.1.2.4), the specimens were split from the groove that had been formed in the middle of lateral surfaces in the casting process. It is very critical to obtain fracture surfaces with minimum losing of fragments. Forasmuch as the two parts of the split specimens must be carefully put together, any spalling on the fracture surfaces leads to reduce the contact area. It was observed that the 28-day cured UHPC specimens could not be spilt without spalling. The development of hydration process over time increased the rigidity and brittleness of the specimens. The splitting process was successfully applied on the 7 days water curing specimens with a low amount of losing of fragments from the fractured surfaces of the specimens. These 7-day specimens have compressive strength value below 100 MPa (Figure 7.1). Therefore, according to the test results of this study, the splitting step can be applied on such specimens that have compressive strength value at least below 100 MPa.

The maximum bond loads were observed in the FA-G1 mixture (Average load = 308 N). In other words, increasing the binder dosage of UHPC by addition of 400 kg/m^3 FA1 lead to a 280% increment in the bond load (Figure 7.3). This remarkable increment can be explained by the following mechanisms; 1) Further hydration of unhydrated cement particles similar to the control mixture 2) Further pozzolanic reaction of unhydrated fly ash with $Ca(OH)_2$ 3) High CaO content of FA1. In addition, as can be seen from Figure 7.4 the healing products sealed 84% of the surface crack of the Control mixture after 30 days, while this ratio is 93% for the FA1-G1 one.

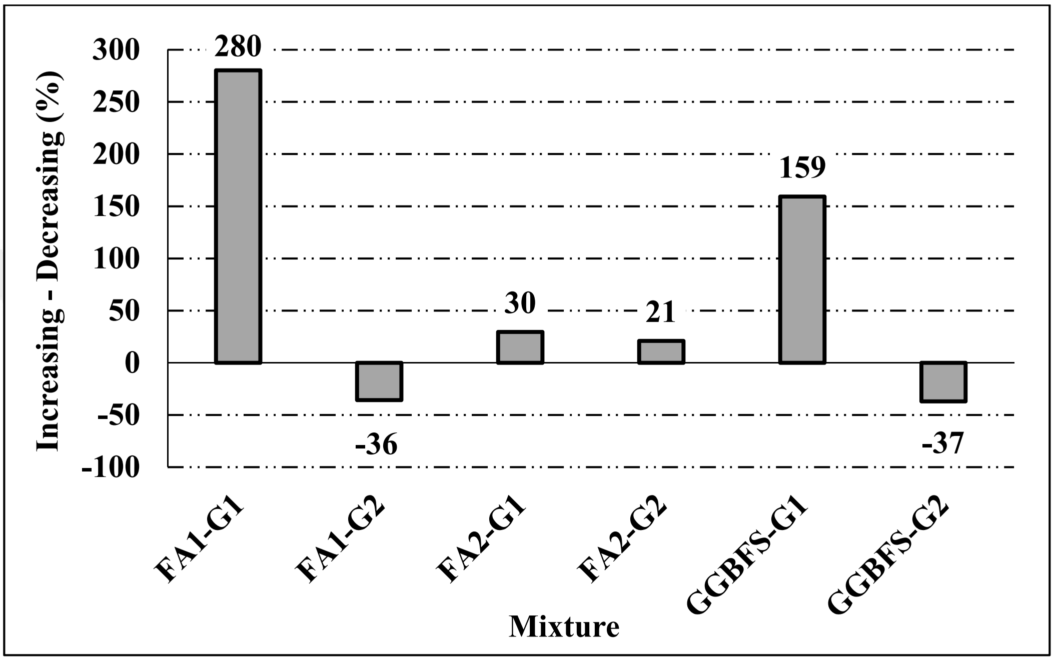

Figure 7.3 The bond loads of SCMs bearing mixture as compared to bond load of the control mixture

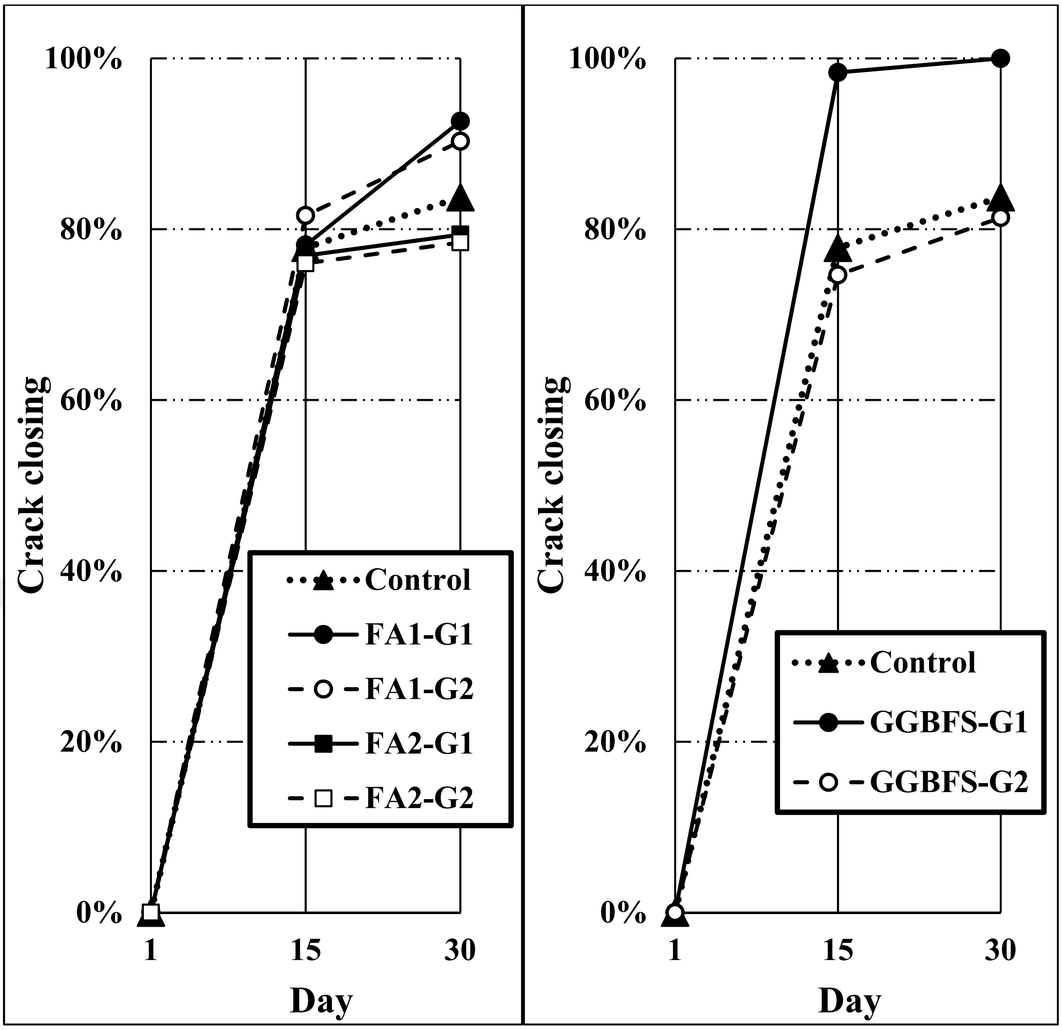

Figure 7.4 The crack closing ratios

Figure 7.5 shows the optical microscope (OM) and scanning electron microscopy (SEM) images of a crack of control mixture before and after self-healing process. The EDS analyses conducted on the healing products revealed that the main products are $CaCO_3$ and $Ca(OH)_2$. In spite of the products with different morphology, the main products in the FA1-G1 mixtures are also $Ca(OH)_2$ and $CaCO_3$ crystals similar to the control mixture (Figure 7.6). The second mixture that its bond load is higher than control mixture is GGBFS-G1 mixture. In other words, increasing the binder dosage of UHPC by addition of 400 kg/m^3 GGBFS lead to a 159% increment in the bond load (Figure 7.3). The higher bond loads observed in the FA1-G1 and GGBFS-G1 mixtures as compared to the FA2-G1 mixture can be mainly attributed to the higher CaO content of the FA1 and GGBFS. The maximum crack closing ratio was measured in the

GGBFS-G1 mixture (100%). Figure 7.7 shows the OM and SEM images of a crack of GGBFS-G1 mixture before and after self-healing process. The EDS analysis revealed that the self-healing products mainly consists of $CaCO_3$ and $Ca(OH)_2$ crystals similar to the Control and FA1-G1 mixtures and very low amount of C-S-H.

As can be seen from Figure 7.3 the bond load of FA1-G2 mixture was 36% lower than the control mixture. However, the crack closing ratio of FA1-G2 mixture (90%) was higher than the control mixture (84%). In addition, the bond performance of the class F fly ash bearing mixtures (FA2-G1 and FA2-G2) are better than the FA1-G2 and GGBFS-G2 mixtures. However, this is not valid in the case of crack closing test results. It should be mentioned that the maximum bond loads were observed in the FA-G1 mixture. However, the maximum crack closing ratio was measured in the GGBFS-G1 mixture (100%). It is obvious that the healing mechanism in the novel self-bonding test is different from the crack closing one. As mentioned earlier the healing process in the novel test, which can simulate self-healing of very tight cracks, differ from the other test method. In addition, the suggested test method is trying to evaluate the bonding capacity of healing products, not directly the amount of them. In contrast, the amount of self-healing products are more important in the determining the self-healing ratios of crack-closing test method which is based on the microscopic observations. However, it can be seen from test results that the performance FA1-G1 and GGBFS-G1 mixtures are better than the other mixtures in both of the test methods. Therefore, it can be concluded that the self-healing capacity of FA1-G1 and GGBFS-G1 mixture can be better than the other five mixtures in the case of evaluating them in the other test method used for analyzing the self-sealing mechanism.

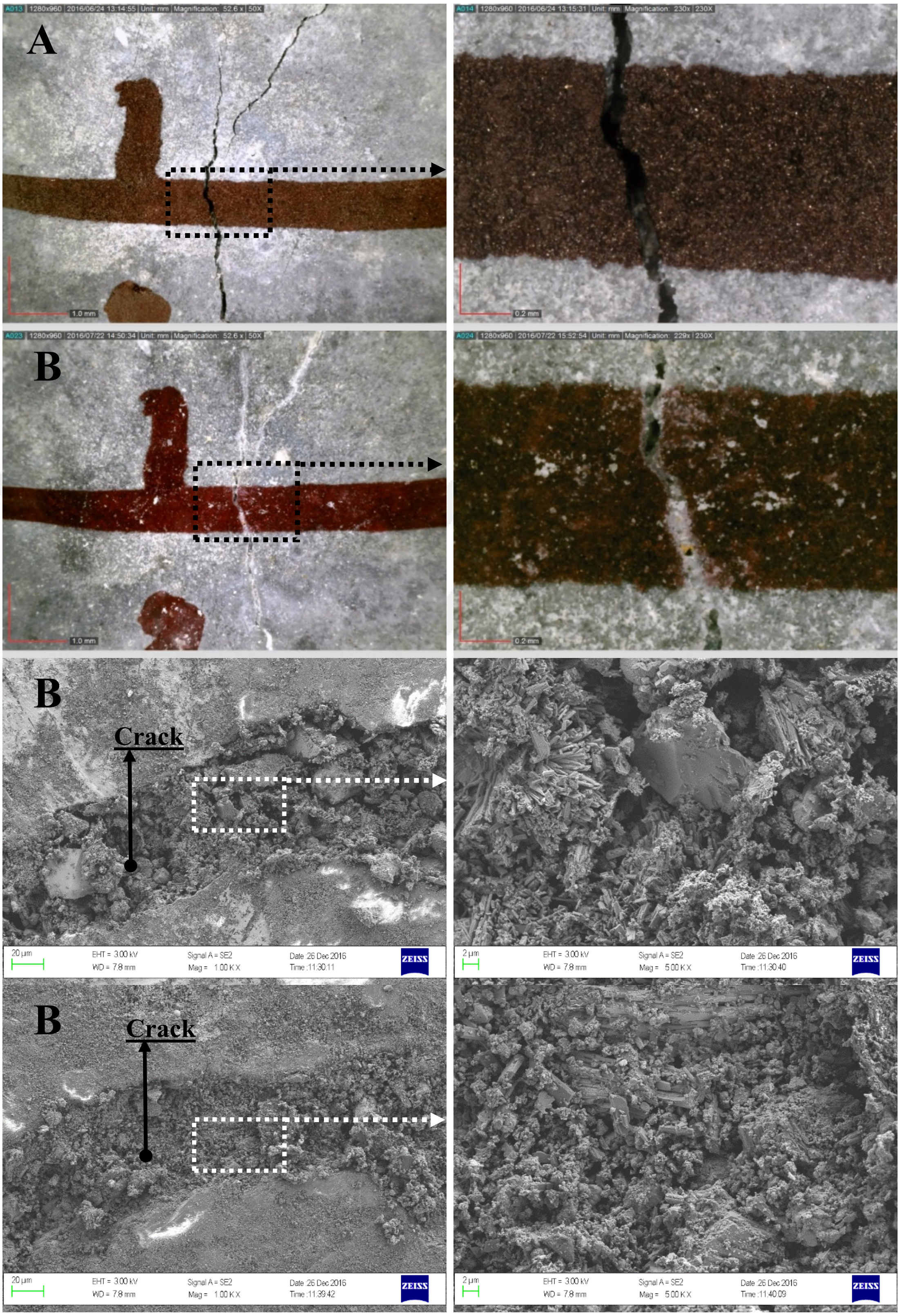

Figure 7.5 The OM and SEM images of a crack of control mixture A) before and B) after self-healing process

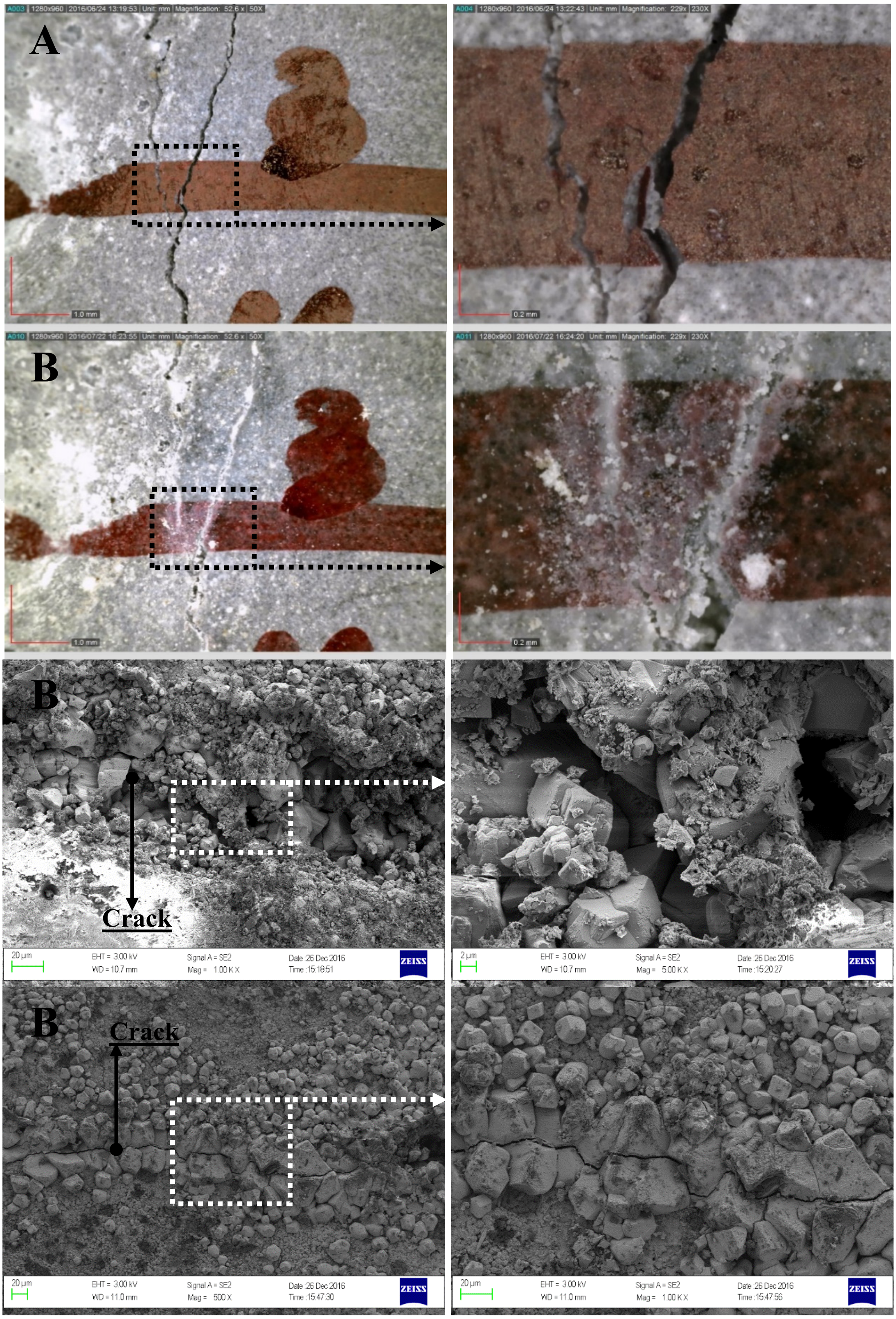

Figure 7.6 The OM and SEM images of a crack of FA-G1 A) before and B) after self-healing process

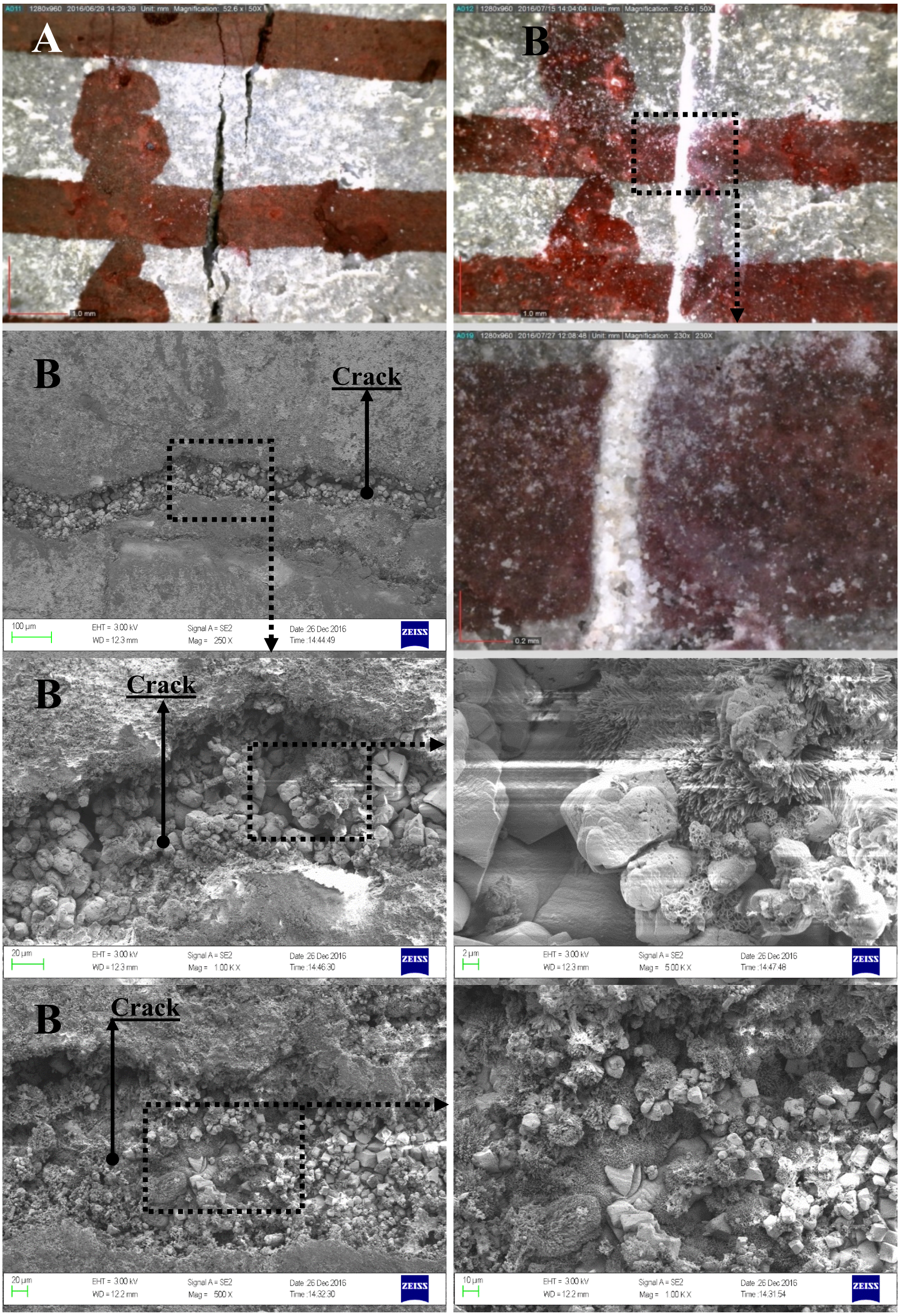

Figure 7.7 The OM and SEM images of a crack of GGBFS-G1 A) before and B) after self-healing process

As mentioned earlier, the EDS analyses conducted on the healing products formed in the control mixture revealed that the main products are $CaCO_3$ and $Ca(OH)_2$ (Figure 7.8). In spite of the products with different morphology, the main products in the FA1-G1 mixtures are also $Ca(OH)_2$ and $CaCO_3$ crystals (Figure 7.8). In addition, the EDS analysis conducted on different zone of cracks of GGBFS-G1 mixture revealed that the self-healing products mainly consists of $CaCO_3$ and $Ca(OH)_2$ crystals similar to the Control and FA1-G1 mixtures and also very low amount of C-S-H (Figure 7.9). It is possible to come across different results in the literature about the products that cause the cracks to heal. Sahmaran et al. (2013) have found that C-S-H formation was predominant in crack healing in FA containing mixtures, while in GGBFS containing mixtures $CaCO_3$ was the main composition of healing products. On the other hand, Huang et al. (2014) have shown that self-healing products formed in cracks of GGBFS containing mixtures are predominantly composed of C-S-H gel. Hung et al. (2018) have compared the EDS spectra of cracks with different widths. They have found that as the crack width increases, the $CaCO_3$ ratio of the newly formed crystals increases and the C-S-H ratio decreases. The reason for this was explained by the fact that $CaCO_3$ formation requires a larger area than C-S-H.

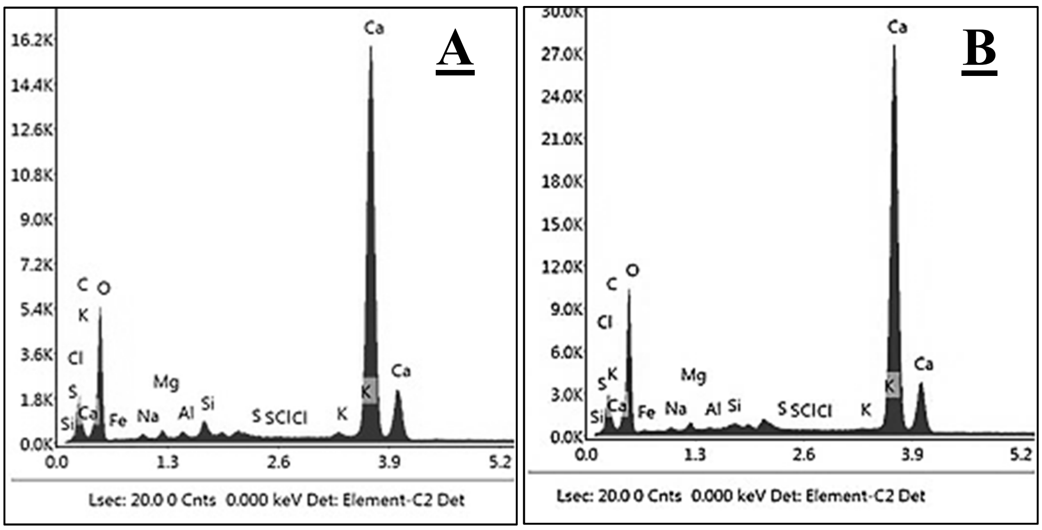

Figure 7.8 The EDS analysis of self-healing products formed in A) control and B) FA1-G1 mixtures

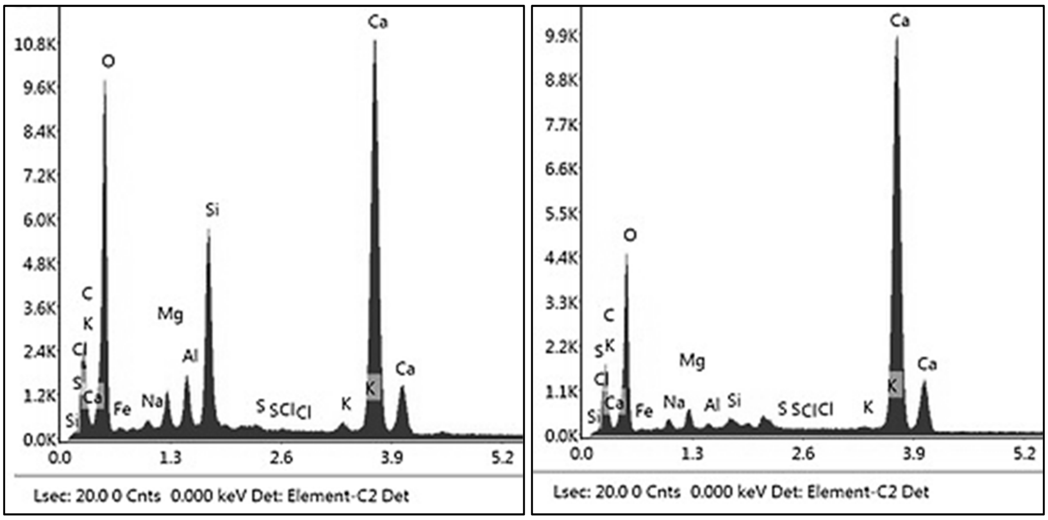

Figure 7.9 The EDS analysis of self-healing products formed in GGBFS-G1 mixture

The mixtures to be used in the next section were chosen not only considering of the self-bonding test results but also the compressive strength and crack closing test results. Among the FA containing mixtures, the mixture with the highest compressive strength at 7 and 28 days was FA1-G1 mixture. Given the results of the self-bonding and crack closing analyzes, the FA1-G1 mixture has exhibited the best performance. On the other hand, the performance of GGBFS-G1 mixture in all three tests was found much better than the GGBFS-G2 mixture. In addition, the FA1-G1 and GGBFS-G1 mixtures have exhibited the best performance among the other mixture in all three tests. Given the results, the control mixture as well as the FA1-G1 and GGBFS-G1 mixtures were selected for use in the next section of the study.

CHAPTER EIGHT
EVALUATION OF SELF-HEALING MECHANISM THROUGH VARIOUS METHODS

The self-healing capacity of the three UHPC mixtures (Control, FA1-G1 and GGBFS-G1 mixtures) selected from previous chapter were investigated through the uniaxial compressive, direct tension, crack closing, total water absorption, capillary water absorption, air permeability, ultrasonic pulse velocity, and water permeability tests. In addition, the efficiency of above-mentioned methods were analyzed in terms of self-healing assessment.

Control, FA1-G1 and GGBFS-G1 mixtures were reinforced with the MF1 steel micro-fibers (2 vol.%) selected from the sixth section. The mix design are presented in Table 8.1.

Table 8.1 Mix design of SCM and fiber containing UHPC mixtures (kg/m^3)

Mixtures	Water	Cement	Fiber	SCMs		Quartz aggregate			SP
				FA	GGBFS	0-0.4 (mm)	0.4-1 (mm)	1-3 (mm)	
Control	176	800	143	-	-	330	463	529	23
FA1-G1	264	800	143	400	-	178	249	284	6
GGBFS-G1	264	800	143	-	400	189	265	303	11

8.1 Evaluation of Self-Healing Mechanism Using Compressive Strength Test

As mentioned earlier, a series of UHPC specimens were preloaded up to 90% of their corresponding compressive strength. The load was released at the required predetermined load value. Immediately after preloading, half of the preloaded specimens were subjected to the compressive strength test to determine the damage ratio due to the preloading. However, there was not any reduction in compressive strength of specimens. Therefore, another series of UHPC specimens were preloaded up to ~100% of their corresponding compressive strength. The load was carefully monitored and released at the required predetermined load value (~100%) to avoid further damage. Similar to the previous procedure, immediately after preloading, half of the preloaded specimens were subjected to the compressive strength test to determine the damage ratio due to the preloading. Depending on the mixture type and the age of specimens, considerable damage (reduction in strength) were observed in specimens due to the preloading. The other half of preloaded specimens were immersed in the lime saturated water. After 30 days (healing period), the preloaded specimens and virgin specimens were subjected to compressive strength test. Figure 8.1 shows the compressive strength test results of 7-day specimen. In spite of the fact that the cement content of the SCMs bearing mixtures had not been reduced, the 7-day compressive strength of them decreased slightly (see the virgin specimens test results). It is well known that pozzolanic reactions of the SCMs is limited during 7-day. In continuation of this section, the reduction in strength due to preloading as well as the regain in strength (after healing period) are discussed in details.

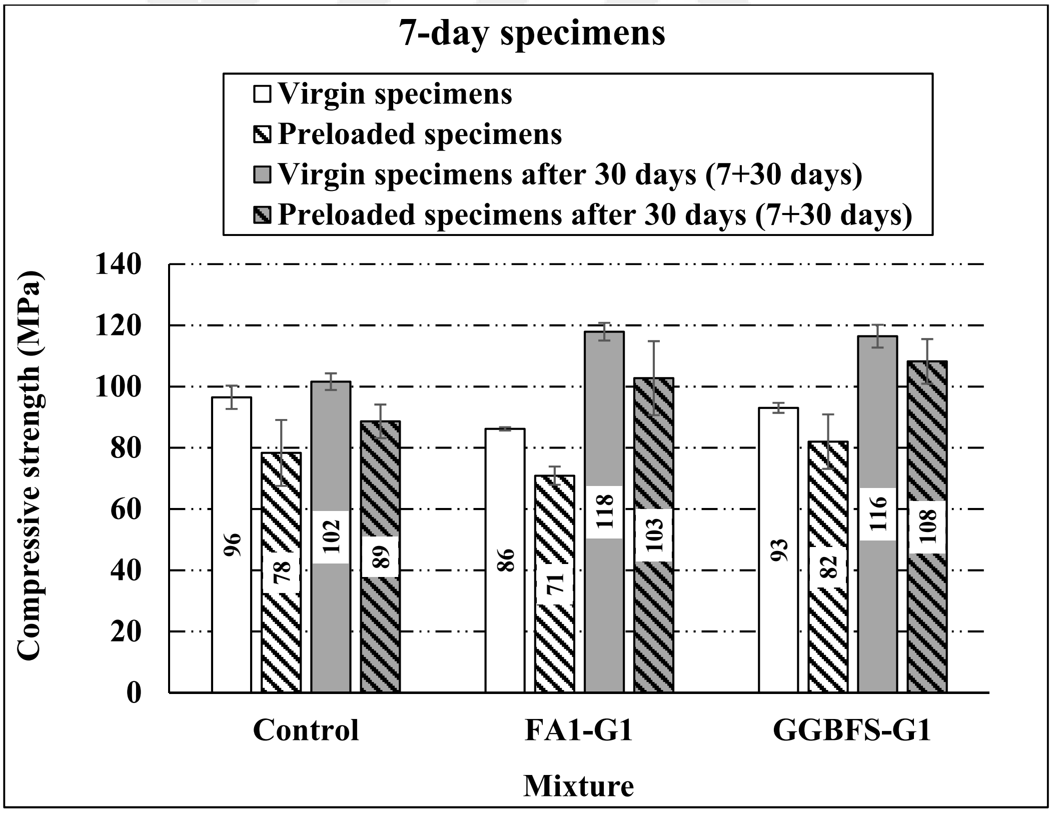

Figure 8.1 The compressive strengths of 7-day specimens before and after 30 days healing period

The 90-day compressive strength of SCMs bearing mixtures are higher than the compressive strength of control mixture (Figure 8.2). In other words, the amount of C-S-H liberated by the pozzolanic reaction of SCMs with $Ca(OH)_2$ was as enough as that it can enhance the 90-day compressive strengths of mixtures.

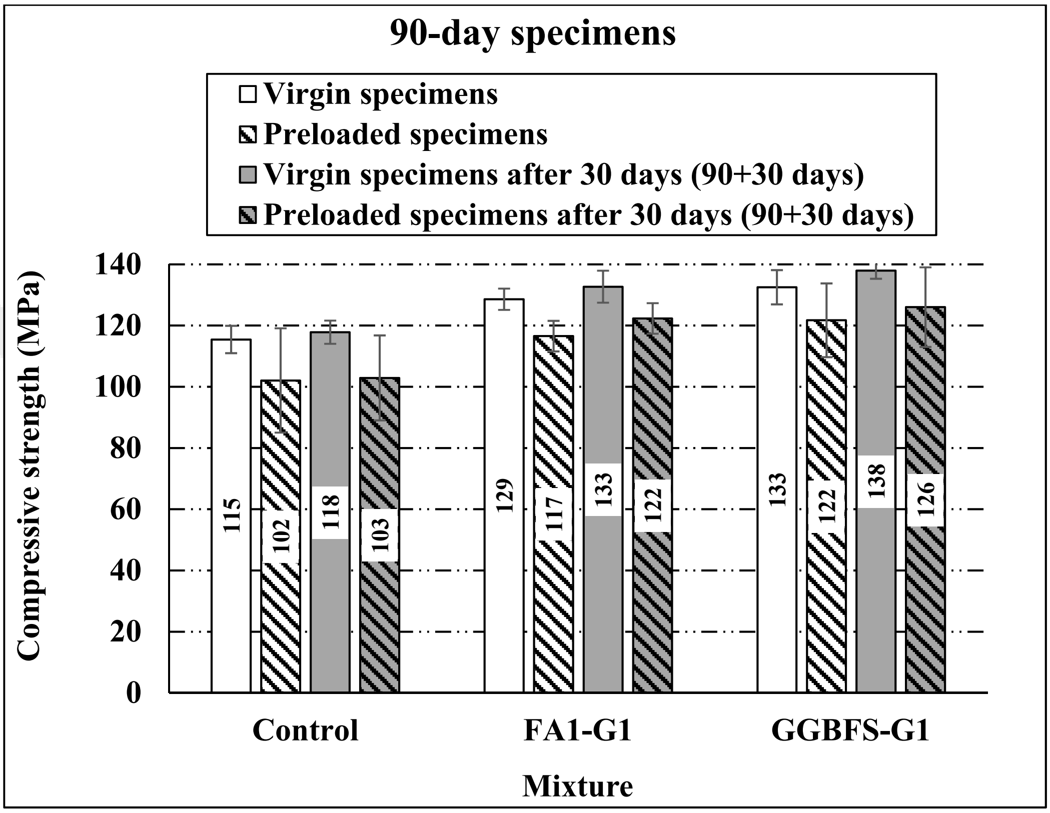

Figure 8.2 The compressive strengths of 90-day specimens before and after 30 days healing period

As can be seen from Figure 8.1, a preloading of up to ~100% of the average strength resulted in a certain extent of damage in the specimens. In spite of such a huge preloading level up to ~100% of the average corresponding compressive strength, the reduction in strength did not exceed 19% (Figure 8.3). It is well-known that plain (without any fiber) concretes or generally cement based materials are extremely brittle construction material. It has long been recognized that the problem can be mitigated by the incorporating of various types of discontinuous fibers in cementitious matrices. The damage ratios observed in compressive strength test are compared later at section 8.7 with the damage ratios observed in total water absorption test.

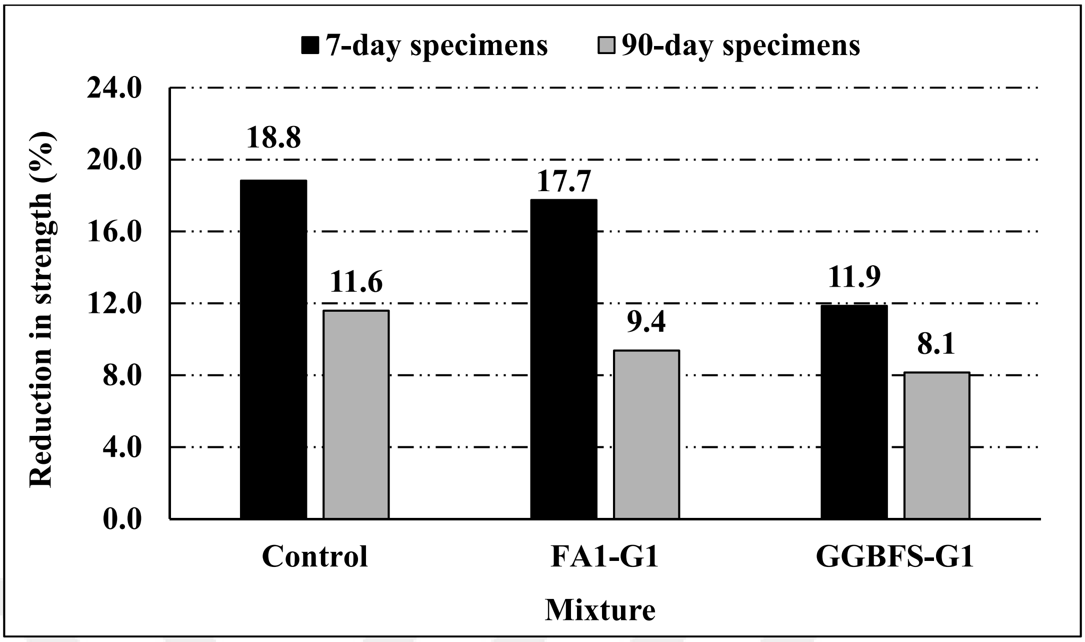

Figure 8.3 The average reductions in compressive strength of UHPC specimens due to preloading

It is only possible from a correct viewpoint to determine a realistic ratio of self-healing. In continuation of this section of report, the percentages of regain in compressive strengths (self-healing ratios) are expressed in two different approaches.

First approach:

$$RS(\%) = \frac{c - b}{d - b} \times 100 \tag{8.1}$$

Where "RS" is the percentage of regain in strength, "b" and "c" is, respectively, the compressive strengths of preloaded specimens before and after healing period (30 days), and "d" is the compressive strength of virgin specimens after healing period (7+30 or 90+30 days cured specimens).

The average percentages of regains in strengths expressed with the first approach are presented in Figure 8.4. As can be seen from Figure 8.4, despite a preloading up to ~100% of the compressive strength of specimens, a significant ratio of self-healing was detected in the 7-days specimens of all three mixtures. As expected, the self-healing ratios of FA1-G1 (68%) and GGBFS-G1 (76%) containing mixtures are higher than the control (44%) mixture. These ratios were significantly decreased for the 90-day specimens. However, the ratios in both of the FA and GGBFS containing mixtures are higher than the control mixture. It must be noted that these healing ratios are considerably depend on the specific damage level of each mixture. For example, the reduction in strength for 7-day cured specimens of FA1-G1 and GGBFS-G1 mixtures was 17.7% and 11.9%, respectively (Figure 8.3). Therefore, the damage ratio that should be healed in FA1-G1 mixture is higher than in GGBFS-G1 mixture. The higher self-healing ratio in the GGBFS-G1 mixture as compared to the FA1-G1 mixture can be explained by the higher pozzolanic reaction rate of GGBFS (used in this study) at early ages as well as the lower damage ratio in the 7-day cured GGBFS-G1 specimens. On the other hand, the reduction in strength for 90-day specimens of FA1-G1 and GGBFS-G1 mixtures was 9.4% and 8.1%, respectively. It can be seen that the difference in damage ratios decreased in the 90-day cured specimens. Because of approximately the same damage ratios, it can be concluded that the self-healing capacity of FA1-G1 mixture might be more than GGBFS-G1 mixture at mid-term ages.

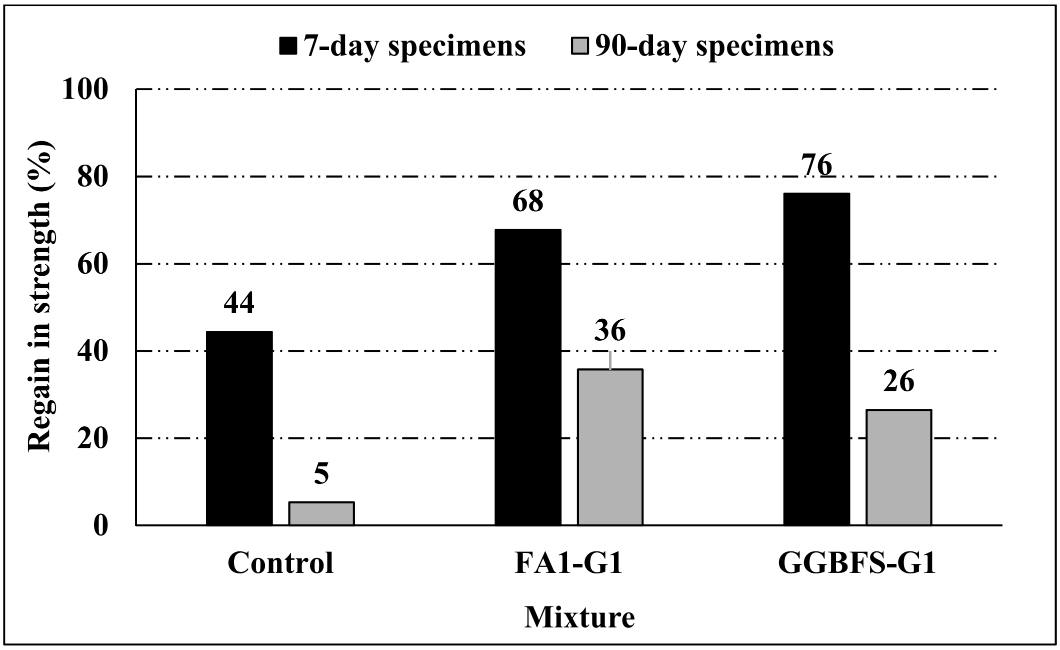

Figure 8.4 The average percentage of regain in strength (first approach)

It should be noted that the above mentioned conclusions are valid in the compressive strength test results, not necessarily in all of the test methods used in this study. The damage characteristic, level, and healing mechanism are different in various test methods.

Second approach:

$$RS(\%) = \frac{c - b}{a - b} \times 100 \tag{8.2}$$

Where "RS" is the percentage of regain in strength, "b" and "c" is, respectively, the compressive strengths of preloaded specimens before and after healing period (30 days), and "a" is the compressive strength of virgin specimens before healing period (7 days or 90 days cured specimens).

The average percentages of regains in strengths expressed with the second approach are presented in Figure 8.5. As can be seen from Equation 8.2 the regain in strength ratio was determined considering the compressive strength of 7 days or 90 days virgin specimens. In other words, 30 days healing period was ignored in determining compressive strength of virgin specimens used in the equation. Therefore, the undergoing hydration reactions and especially pozzolanic reactions during 30 days healing period in virgin specimens were not considered in the second approach. As can be seen from Figure 8.5 over-optimistic results can be obtained in 7-day specimens with the second approach. It is obvious that a significant proportion of the pozzolanic reactions in 7-day specimens occur during the healing period (30 days). However, these over-optimistic results were not seen in the 90-day specimens. As the majority of the pozzolanic reactions are completed up to 90 days, the first approach results are very close to the self-healing ratios obtained from the second approach.

Sahmaran et al. (2008) has emphasized that "comparing the properties of pre-loaded specimens by age will not necessarily point out any self-healing, as the hydration reactions continue even in the undamaged specimens. For this reason, the extent of any self-healing could be best detected, by comparing the results of pre-loaded and virgin specimens' properties at a particular age" (p. 876-877). Therefore, the first approach is absolutely the correct viewpoint to determine a realistic ratio of self-healing in compressive strength test.

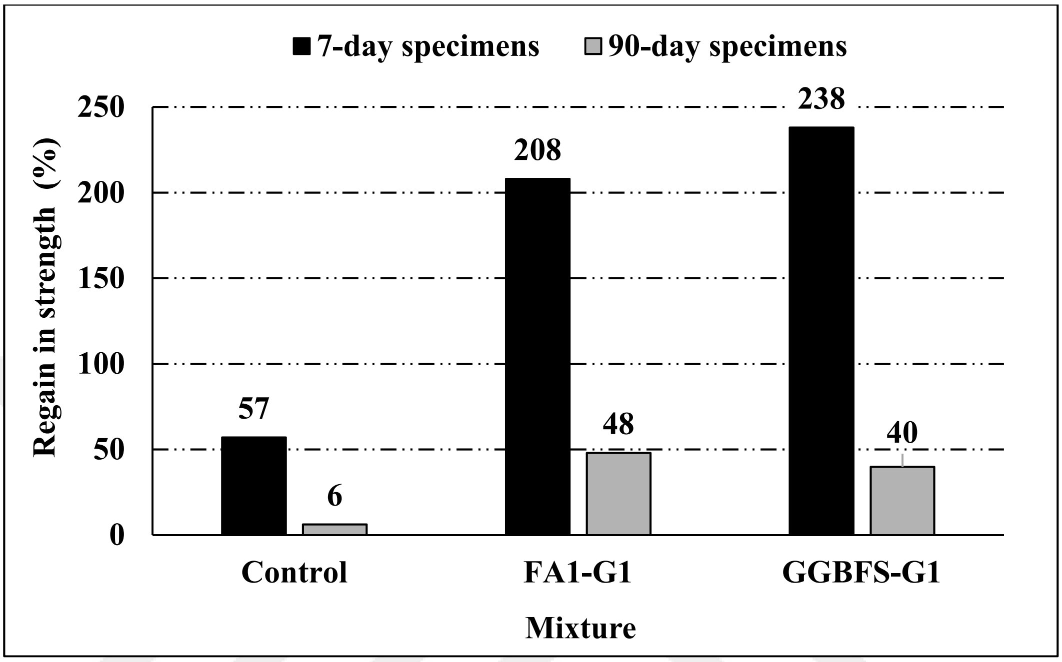

Figure 8.5 The average percentage of regain in strength (second approach)

Besides the above mentioned approaches, the strength development of preloaded specimens can be compared with virgin specimens. Figure 8.6 shows the relative post-healing compressive strength of preloaded specimens as compared to the virgin specimens with the same curing period (7+30 and 90+30). As can be seen from Figure 8.6 the relative compressive strength of 7-day and 90-day preloaded specimens of Control mixtures were both 87%. In the case of GGBFS-G1 mixture, the relative strengths were 93% and 91% for the 7-day and 90-day specimens. Surprisingly, the relative strength of 90-day preloaded specimens was higher the 7-day one. As can be seen from the relative strength results, it is not possible to monitor the self-healing ratios. It is essential to determine the compressive strength of preloaded specimens immediately after preloading (before healing). Only, if any relative strengths were 100%, it would be concluded that there was a 100% healing ratio. It is not possible to figure out a correct self-healing ratio with relative strength below the 100%.

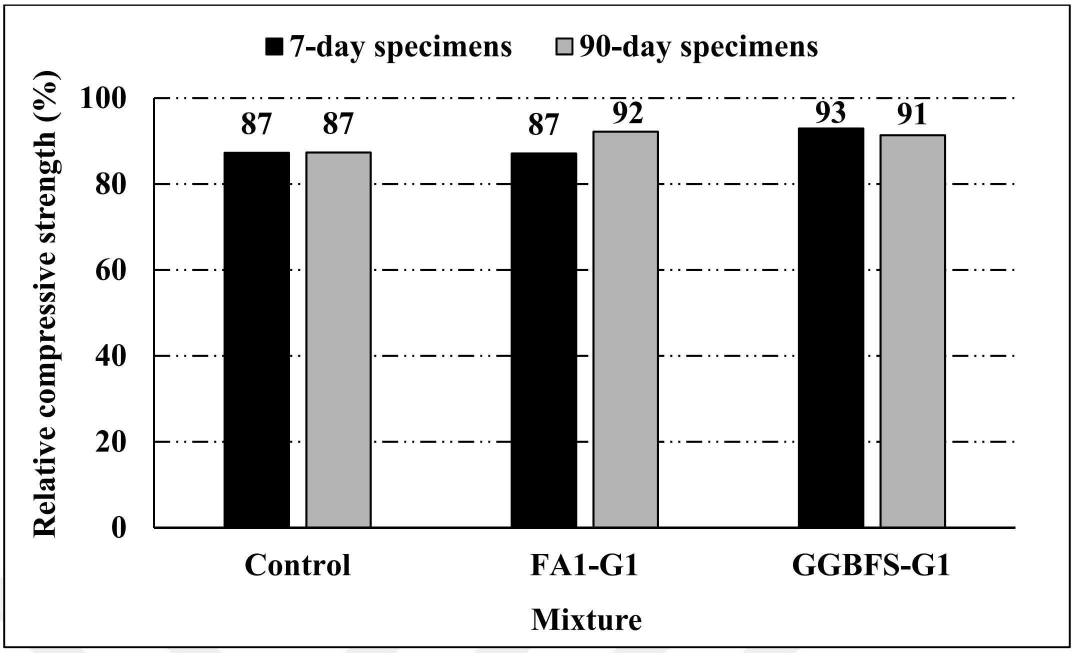

Figure 8.6 Relative post-healing compressive strength of preloaded specimens as compared to the virgin specimens with the same curing period

Figure 8.7 shows the relative post-healing compressive strength of preloaded specimens as compared to the 7 days and 90 days cured virgin specimens. The undergoing hydration reactions and especially pozzolanic reactions during 30 days healing period in virgin specimens were not considered. Therefore, unrealistic results were obtained in 7-day specimens of FA1-G1 (119%) and GGBFS-G1 (116%) mixtures.

It can be concluded that the first approach must be used for determining realistic self-healing ratios, especially in early age specimens. However, it should not be ignored that damage level in compressive strength is an important factor that can affect the self-healing ratios.

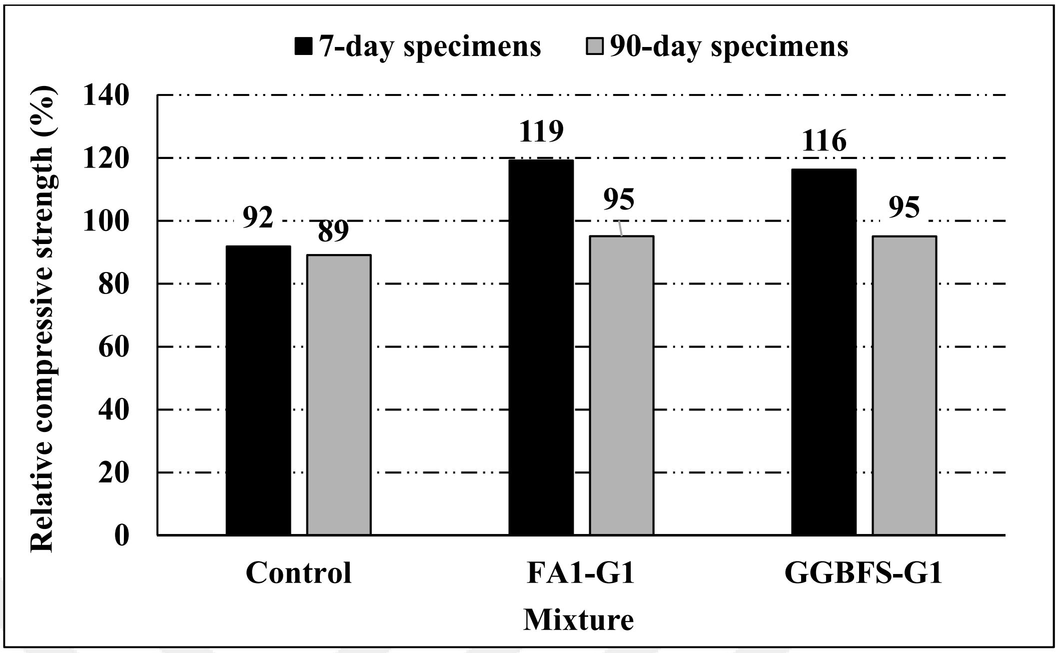

Figure 8.7 Relative post-healing compressive strength of preloaded specimens as compared to the 7 days and 90 days cured virgin specimens

8.2 Evaluation of Self-Healing Mechanism Using Direct Tension Test

Details of the direct tensile test are presented in section 3.1.2.3. As mentioned earlier in Chapter 3, in order to assess the self-healing capacity of fiber reinforced UHPC mixtures in terms of direct tensile strength, seven dog-bone shaped specimens were prepared for each variety. After 7 and 90 days standard water curing, specimens were taken out form the lime saturated water and left to dry in laboratory air for 1 day. The specimens were subjected to direct tension test to introduce a crack with 100 µm ± 10 width. The pre-cracked specimens were immersed in the lime saturated water for 30 days and then, were subjected to direct tension test to observe any regain in strength.

Although crack width control was relatively easy in 7-day specimens, since the mixture did not exhibit deformation hardening behavior, the load suddenly decreased after maximum stress (Figure 8.8). If there was a composite that can exhibit deformation hardening behavior under direct tensile loads, the load drop and crack width control would be much more easy and reliable. This problem became more evident in 90-day specimens. Particularly as the strength of the matrix increases, a more brittle behavior was observed (Figure 8.9). The sudden load drops in the direct tension test, which is a very sensitive and difficult experiment due to its nature, negatively affected the examination of the self-healing mechanism. Especially in the case of 90-day specimens, the above-mentioned problem made crack width control virtually impossible. If it was possible to use 13 mm length micro fibers (MF2), consequently it would be possible to obtain mixtures with deformation hardening behavior under direct tension loads. As described in the relevant section, higher binder dosage must be used for using these fibers. Otherwise, it was observed that the use of 13 mm fibers affected adversely the flow of fresh mixture.

In the direct tensile tests, the self-healing ratios were determined by the following relation between the maximum tensile stress, the tensile stress after crack formation, and the maximum tensile stress of preloaded specimens after 30 days healing period:

$$RS(\%) = \frac{C - B}{A - B} \times 100 \tag{8.3}$$

Where “RS” is the percentage of regain in strength, "A" is the maximum tensile stress obtained in the crack formation step (preloading), “B” is the tensile stress where the crack is 100 µm ± 10 width, and “C” refers to the maximum tensile stress at the end of the 30 days healing period (reloading). They were also shown on the tensile stress-strain curves of a specimen (Figure 8.8).

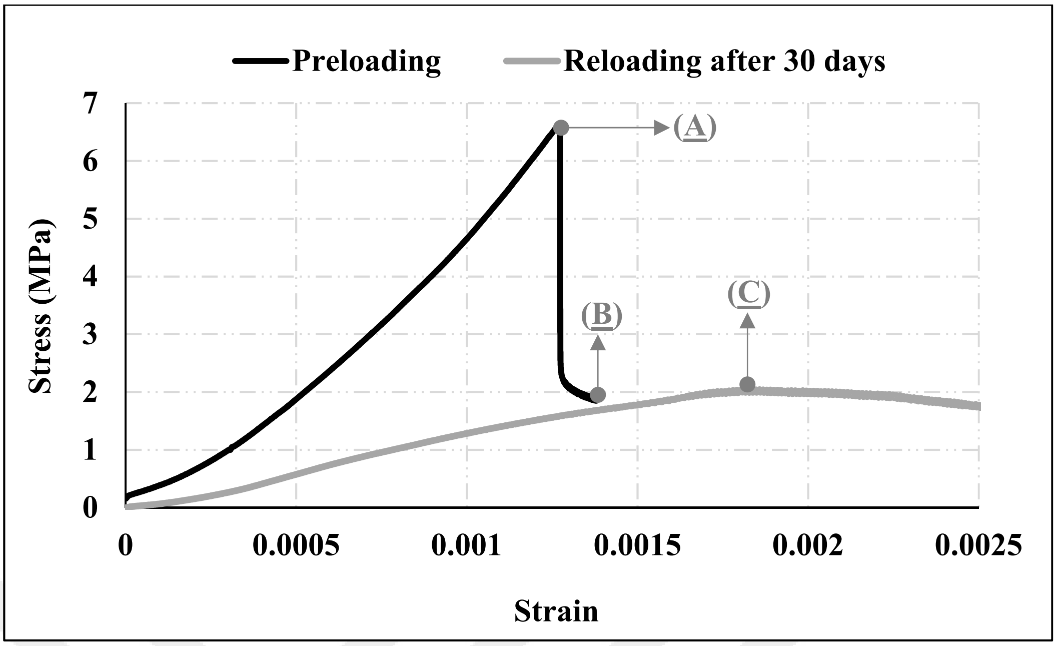

Figure 8.8 Tensile stress-strain curve of a 7-day Control specimen

The average percentages of regains in strengths are presented in Figure 8.9. As can be seen from the results of the 7-day specimens, the self-healing ratio in the direct tensile strength of the control mixture is about twice that of the pozzolan containing mixtures, unlike the results obtained in previous experiments (compressive strength, self-bonding, and crack closing). Maximum self-healing ratio (13.0%) was observed in the 7-day specimens of Control mixture. As mentioned earlier, the sudden load drop and the fact that the crack width could not be precisely controlled may have significantly affected these results. On the other hand, the self-healing verifying in direct tension test is completely different with other tests. The damage under compression loads was in the form of numerous micro-cracks, while the damage in the direct tensile test was a continuous single crack throughout the cross section and visible to the naked eye. The formation of secondary C-S-H wıth binding capacity in micro cracks is more likely to occur. Secondary C-S-H formation is virtually impossible without additional methods in a single continuous crack with a width of at least 100 μm. The most important factor is that the self-healing products make a substantial contribution to the strength recovery of preloaded specimens under compression loads. However, this hypothesis cannot be valid in the case of direct tension test of this study. In other words, even if a certain amount of the second C-S-

H was formed in the cracks of direct tension specimens, it has a very low tensile strength due to its nature. The self-healing ratios obtained in the direct tensile test can be explained by the possible improvement in the fiber-matrix interface during healing period.

As can be seen in Figure 8.10, sudden load drops have become more pronounced in 90 day samples. As discussed before, the sudden load drops in the direct tension test negatively affected the examination of the self-healing mechanism. As expected, the regain in strength ratio of 90- day control specimens were decreased as compared to the 7-day specimens. However, there is not significance difference between the 7-day and 90-day specimens of FA1-G1 and GGBFS-G1 mixtures. It is obvious that above-mentioned problems in direct tension test affects the results.

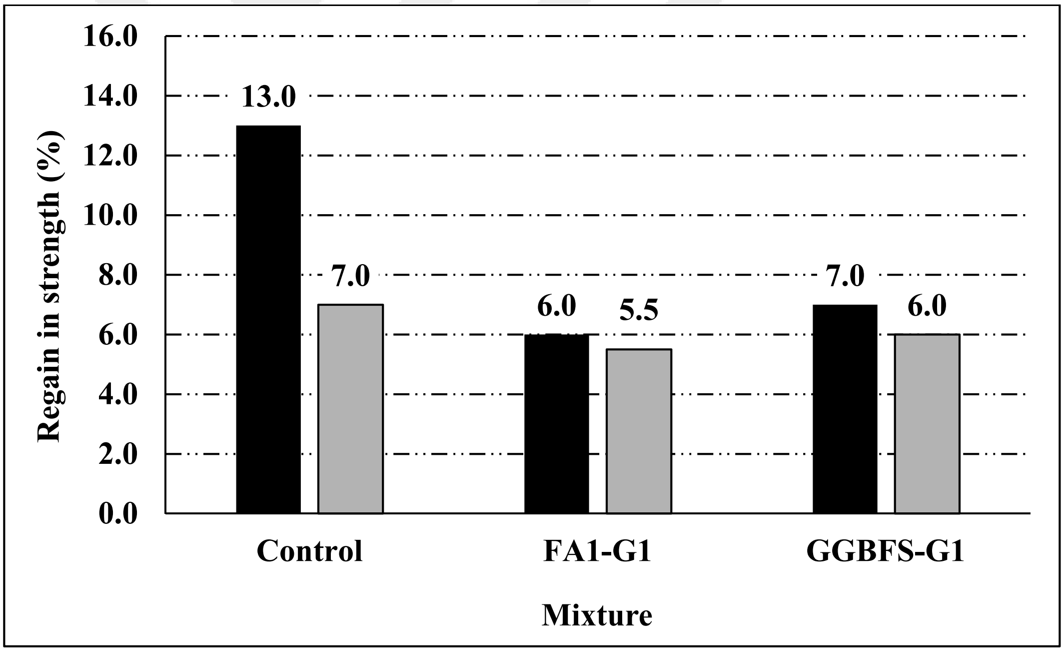

Figure 8.9 The average percentage of regain in direct tensile strength

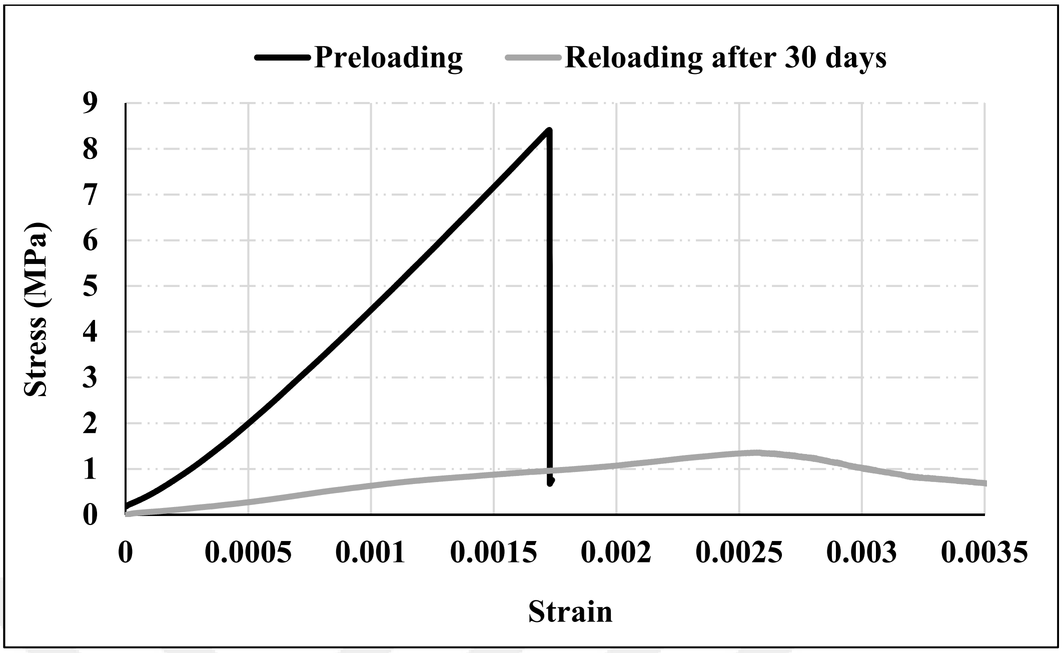

Figure 8.10 Tensile stress-strain curve of a 90-day Control specimen

8.3 Evaluation of Self-Healing Mechanism Using Crack Closing Test

The crack closing analysis of 7-day specimens has already been carried out in Chapter 7. In the scope of this section, crack closing analyzes of 90 day samples of Control, FA1-G1, GGBFS-G1 mixtures were performed. The test results of 7-day and 90-day specimen are presented in Figure 8.11. As expected, the crack closing ratio of 90-day specimens decreased as compared to the 7-day specimens. The most important point is that the self-healing percentages of all three mixtures are close to each other in 90-day specimens. The superior performance of 7-day specimens of FA1-G1 and GGBFS-G1 mixtures were not observed in the 90-day specimens due to the fact that most of the pozzolanic reactions have already been completed up to 90 days. The superior performance of 7-day specimens of FA1-G1 and GGBFS-G1 mixtures were not observed in the 90-day specimens. It can explained by the fact that most of the pozzolanic reactions in 90-day specimens have already been completed before introducing crack. Figure 8.12 shows the optical microscope images of a crack in Control, FA1-G1 and GGBFS-G1 mixtures before and after self-healing process to give only an opinion.

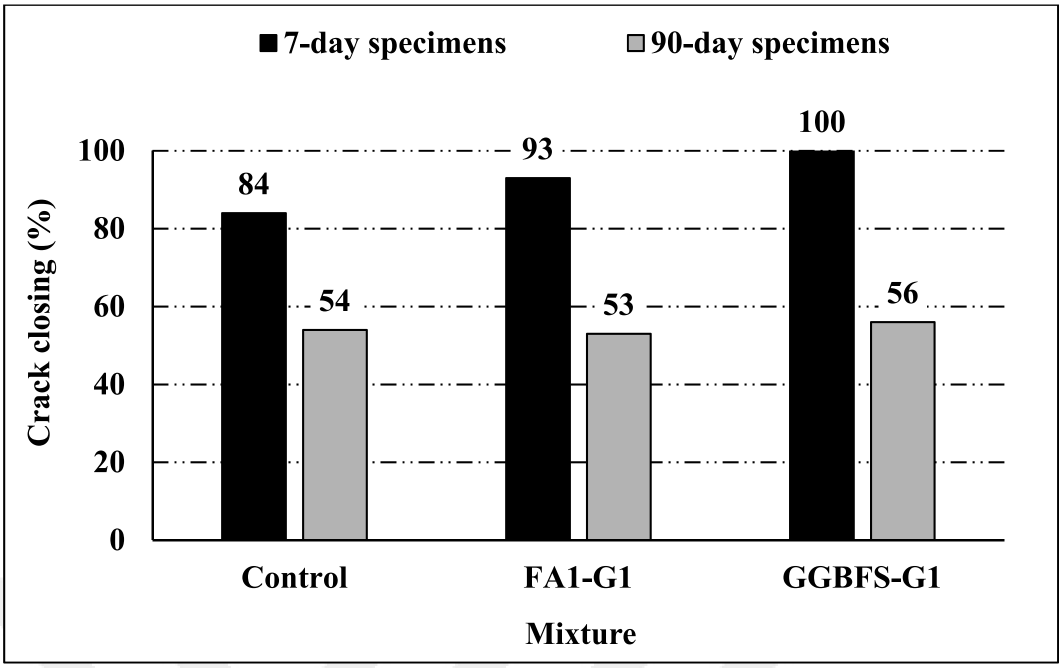

Figure 8.11 The crack closing test results

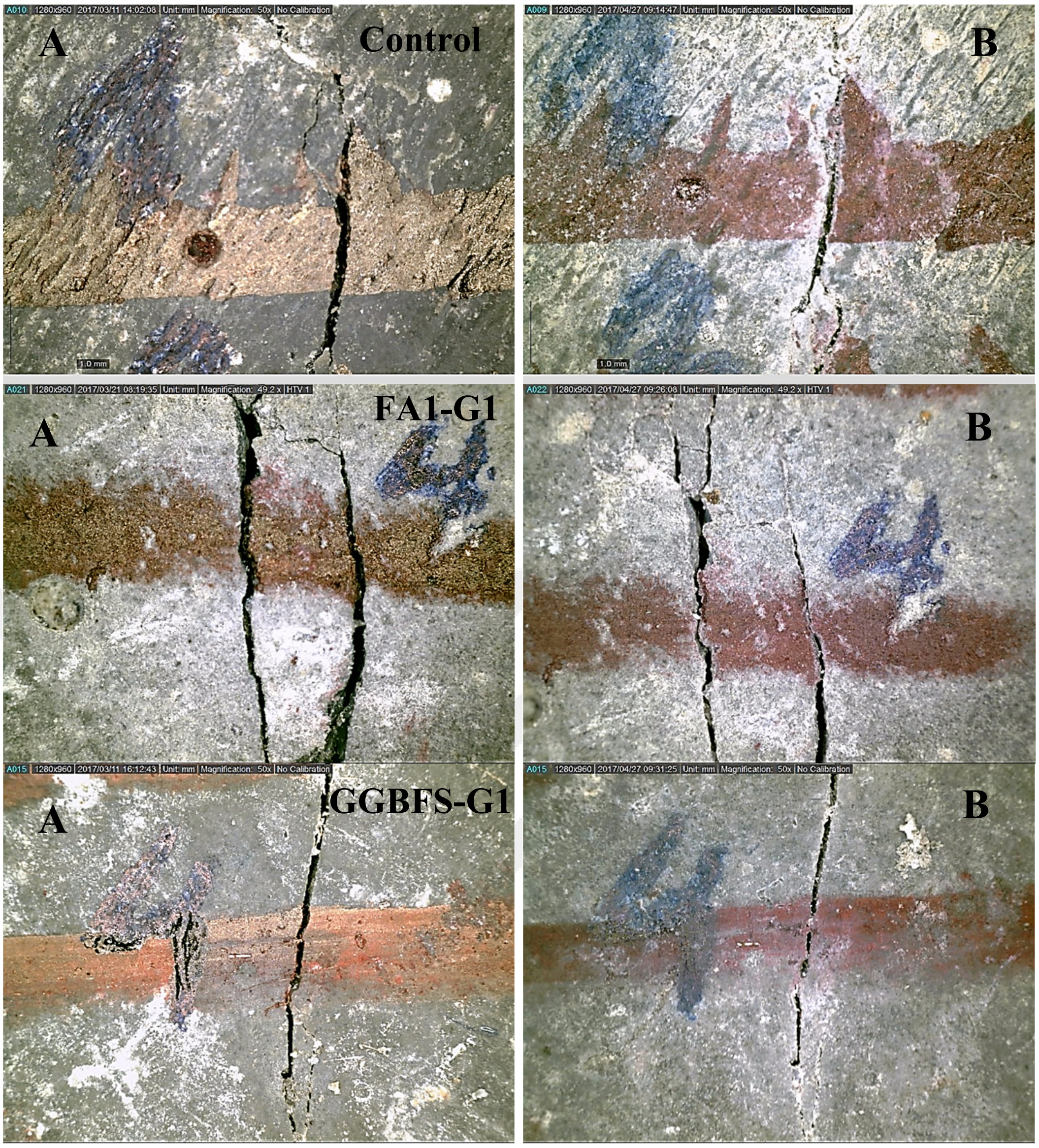

Figure 8.12 The optical microscope images of a crack in Control, FA1-G1 and GGBFS-G1 mixtures A) before and B) after self-healing process

8.4 Evaluation of Self-Healing Mechanism Using Air Permeability Test

As discussed earlier in details at section 3.1.2, special plate-shaped specimens were designed and cracked to assess the self-healing capacity of selected UHPC mixtures through the Torrent air permeability (TAP) test. It should be noted that ultrasonic pulse velocity and water permeability tests were respectively applied on the same specimens following by TAP test. The test results of all specimens are presented in Table 8.2. As can be seen from the TAP test results, no matter which one of mixture tested, the K_T

value of all specimen before cracking are very low due to the superior permeability behavior of UHPC mixtures. However, the K_T could not be measured after cracking due to the fact that air was flowing from other side of the crack. In other words, the air permeability of specimens were extremely increased and as result, it exceed the measuring capacity of the instrument.

Table 8.2. Torrent air permeability test results

	Mixture	Specimen number	Before cracking (Virgin) K_T	After cracking (Preloaded) K_T	After healing (Preloaded) K_T
7-days specimens	Control	1	0.001	-------	1.251
		2	0.001	6.049	-------
		3	0.002	-------	-------
	FA1-G1	1	0.012	-------	0.731
		2	0.01	-------	7.821
		3	0.005	-------	0.001
	GGBFS-G1	1	0.046	-------	2.214
		2	0.026	-------	0.623
		3	0.004	-------	8.235
90-days specimens	Control	1	0.092	-------	-------
		2	0.041	-------	-------
		3	0.052	-------	6.35
	FA1-G1	1	0.034	-------	8.674
		2	0.002	-------	-------
		3	0.012	-------	-------
	GGBFS-G1	1	0.071	-------	-------
		2	0.19	-------	-------
		3	0.01	-------	9.112

After 30 days healing period, K_T values could be obtained in all of the 7-day specimens of FA1-G1 and GGBFS-G1 mixtures. However, the values are very variable. It is obvious that this test method cannot be used to assess the self-healing ratio of such cracks examined in this study. Kunieda et al. (2012) applied the TAP to assess the autogenous healing behavior of cracked Ultra High Performance-Strain

Hardening Cementitious Composites (UHP-SHCC). Special designed plate-shaped specimens were cracked by a special uniaxial tensile test (Kunieda et al., 2012). The pre-damaged UHP-SHCC had multiple fine cracks with width less than 30 microns resulting from its multiple-cracking behavior. Therefore, they have successfully measured the K_T values of pre-damaged specimens before and after healing.

8.5 Evaluation of Self-Healing Mechanism Using Ultrasonic Pulse Velocity Test

The ultrasonic pulse velocity (UPV) test was conducted on the plate-shaped specimens following by the TAP test. Similar to the TAP test, the UPV was applied on the specimens before and after introducing crack to determine the damage ratio. After 30 days water curing, the extent of self-healing was determined by repeating the tests.

The average test results are presented in Table 8.3. Significant reductions in UPV values (15% -70%) were observed due to the cracks. The crack creates significant voids in cementitious matrix. Surprisingly, after the 30 days healing period, no matter which mixture tested, the UPV of all 7-day and 90-day specimens returned to the pre-damage values. In other words, it can be concluded that there is 100% self-healing ratio in all cracks. However, as can be seen from TAP test results, it is not possible that the cracks healed 100%. It is obvious that over optimistic self-healing ratio were obtained by the UPV test. The optimistic results may be related to the number and structure of the cracks. As expected, there were considerable decreases in UPV values after single crack formation. Filling this single crack with even low amount of products such as $Ca(OH)_2$, $CaCO_3$, C-S-H, and the particles and impurities suspended in the water can lead to obtain over optimistic self-healing ratios with UPV test.

Table 8.3 The ultrasonic pulse velocity test results

		Before cracking (Virgin)	After cracking (Preloaded)	After healing (Preloaded)
		UPV (km/s)	UPV (km/s)	UPV (km/s)
7-day specimens	Control	4.59	2.63	4.66
	FA-G1	4.42	3.22	4.44
	GGBFS-G1	4.48	3.06	4.50
90-day specimens	Control	4.90	3.75	4.93
	FA-G1	4.57	3.94	4.59
	GGBFS-G1	4.75	3.66	4.75

8.6 Evaluation of Self-Healing Mechanism Using Water Permeability Test

The water permeability (WP) test was conducted on the plate-shaped specimens following by the UPV test. The self-healing ratios were calculated by considering the results of the 24-hour water permeability test before and after healing period. The average test results (water passing) are presented in Table 8.4. As can be seen, no water passing (decrease of water in the measuring pipette) in undamaged specimens was observed. In other words, the WP values of all specimens before cracking were zero. After the formation of the cracks, a decrease in the water height in measurement pipette, or in other words, water passing was observed. Figure 8.13 shows the water droplets passing through a crack during the WP test. The permeability recovery or self-healing ratios were calculated by the following equation:

$$PR(\%) = \frac{A - B}{A} \times 100 \qquad (8.4)$$

Where, "PR" is the permeability recovery or self-healing ratio, "A" is the WP value immediately after cracking, and "B" is the WP value after healing period. The PR ratios are presented Figure 8.14. The maximum PR (89%) was observed in the 7-day specimens of FA1-G1 mixture. The PR values in 7-day specimens of Control and GGBFS-G1 mixtures were 74% and 81%, respectively. As expected, the PR ratios of 7-day specimens are higher than 90-day specimens. Similar to the crack closing test, the differences between self-healing ratios of mixture in 7-day specimens were considerably decrease in the 90-day specimens. The PR values of 90-day specimens were in range of 38-43 %.

Table 8.4 The water permeability test results

		Before cracking (Virgin)	After cracking (Preloaded)	After healing (Preloaded)
		WP (mL)	WP (mL)	WP (mL)
7-day specimens	Control	0	9.5	2.6
	FA-G1	0	12.2	1.4
	GGBFS-G1	0	11	2.1
90-day specimens	Control	0	9	5.6
	FA-G1	0	10.7	6.2
	GGBFS-G1	0	8.5	4.8

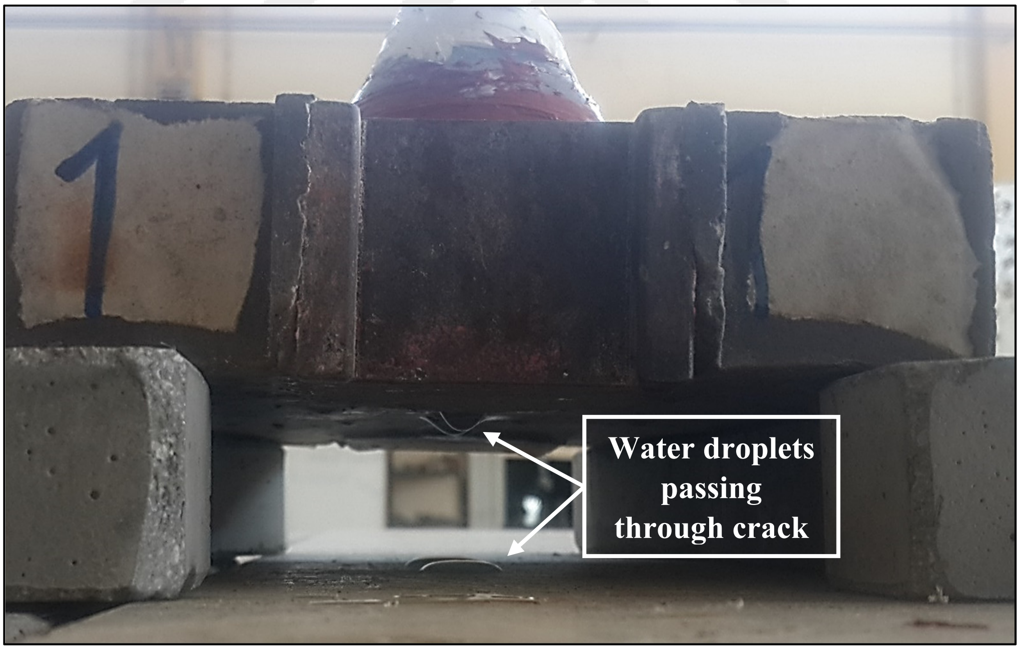

Figure 8.13 Water dripping from crack in a water permeability test (Personal archive, 2017)

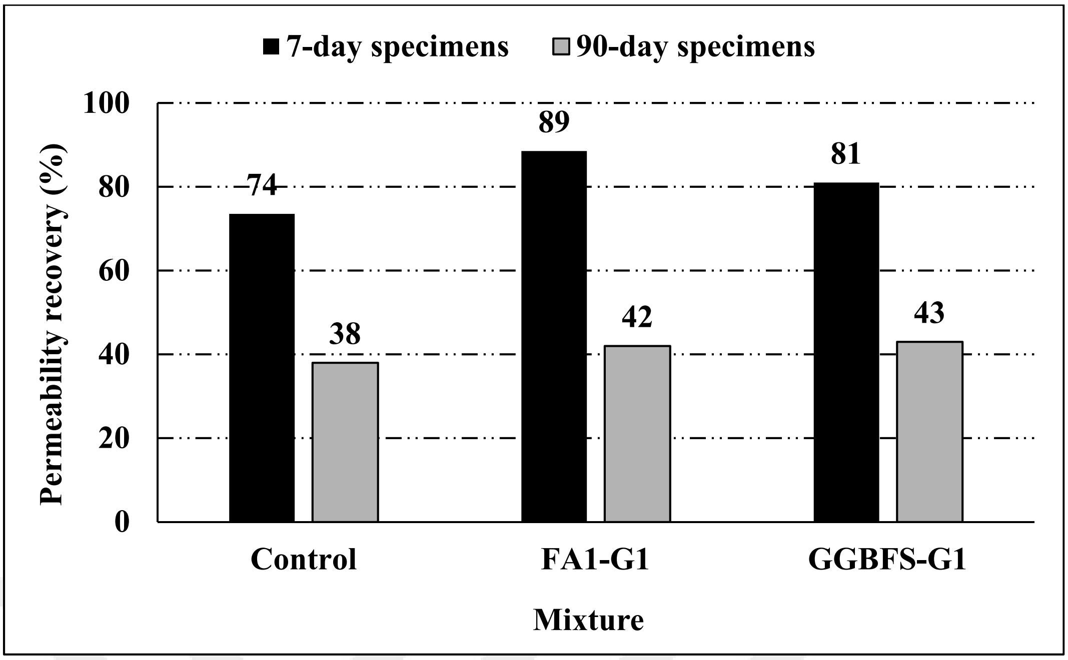

Figure 8.14 The permeability recovery values

8.7 Evaluation of Self-Healing Mechanism Using Total Water Absorption Test

The average total water absorption (TWA) percentages of 7-day specimens are presented in Figure 8.15. As can be seen from Figure 8.15 the TWA of Control UHPC mixture was very low (0.56%). However, the TWA percentages of FA1-G1 and GGBFS-G1 mixtures were almost 3 and 2 times higher than the Control mixture. In spite of the fact that the cement content of the SCMs bearing mixtures had not been reduced, the TWA percentages of them are higher than the Control mixture one. It is well known that pozzolanic reactions of the SCMs, especially FAs, is limited at early ages. Therefore, replacing a certain amount of quartz aggregate, which has water absorption of 1%, with FA or GGBFS increased the early age TWA of UHPC mixture. In continuation of this section, the increases in TWA percentages due to preloading as well as the recovery in TWA (after healing period) are discussed in details.

As mentioned in earlier chapters, there were two types of undamaged (virgin) specimens: a) two specimens tested before and after the 30-day additional water curing (healing process) similar to the preloaded specimens b) two specimens tested only after the 30-day additional water curing (healing process). The purpose of preparing the second group of control specimens was to observe the effect of drying process on water absorption behavior of UHPC mixtures. However, it was observed there is negligible differences between the TWA of two groups of virgin specimens. Therefore, the first group of virgin specimens were used in graphs and calculations.

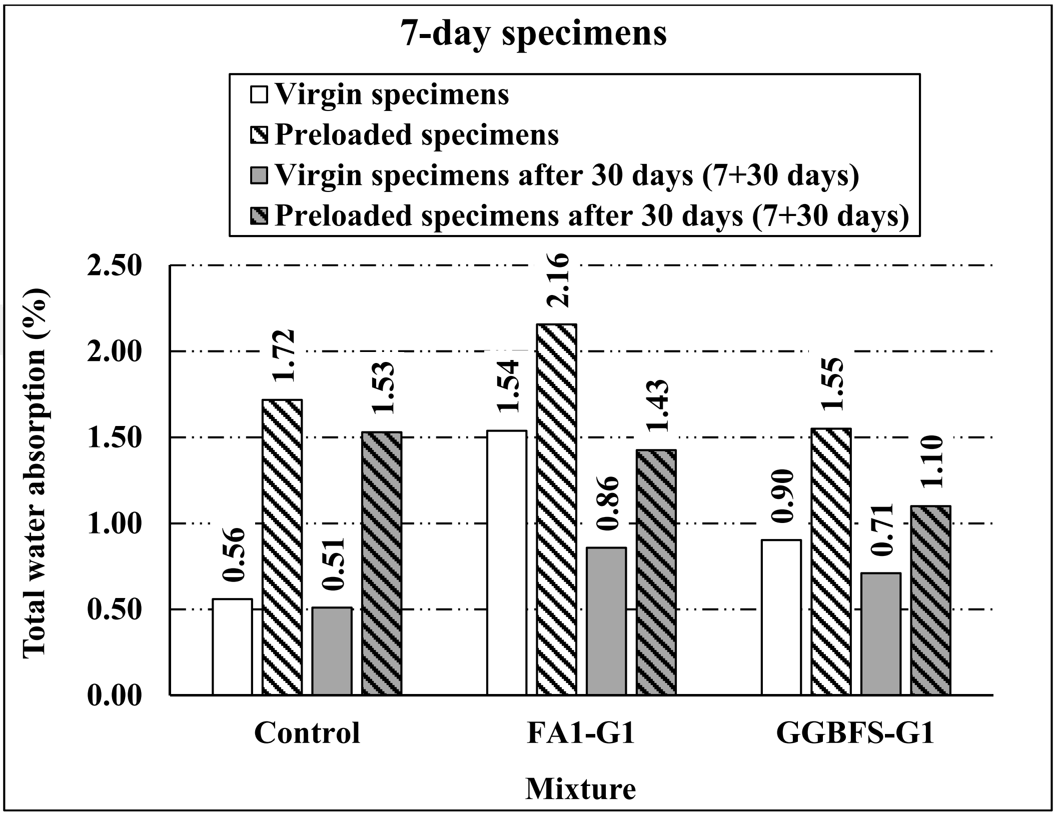

Figure 8.15 The TWA percentages of 7-day specimens

The average TWA percentages of 90-day specimens are presented in Figure 8.16. The TWA percentages of 90-day specimens of Control, FA1-G1, and GGBFS-G1 mixtures are 0.45%, 0.45%, and 0.37%, respectively. As can be seen the 90-day TWA percentages of SCMs bearing mixtures are similar or even higher than the Control mixture one. It is obvious that the amount of C-S-H liberated by the pozzolanic reaction of SCMs with $Ca(OH)_2$ was as enough as that it can enhance the 90-day TWA of UHPC mixtures.

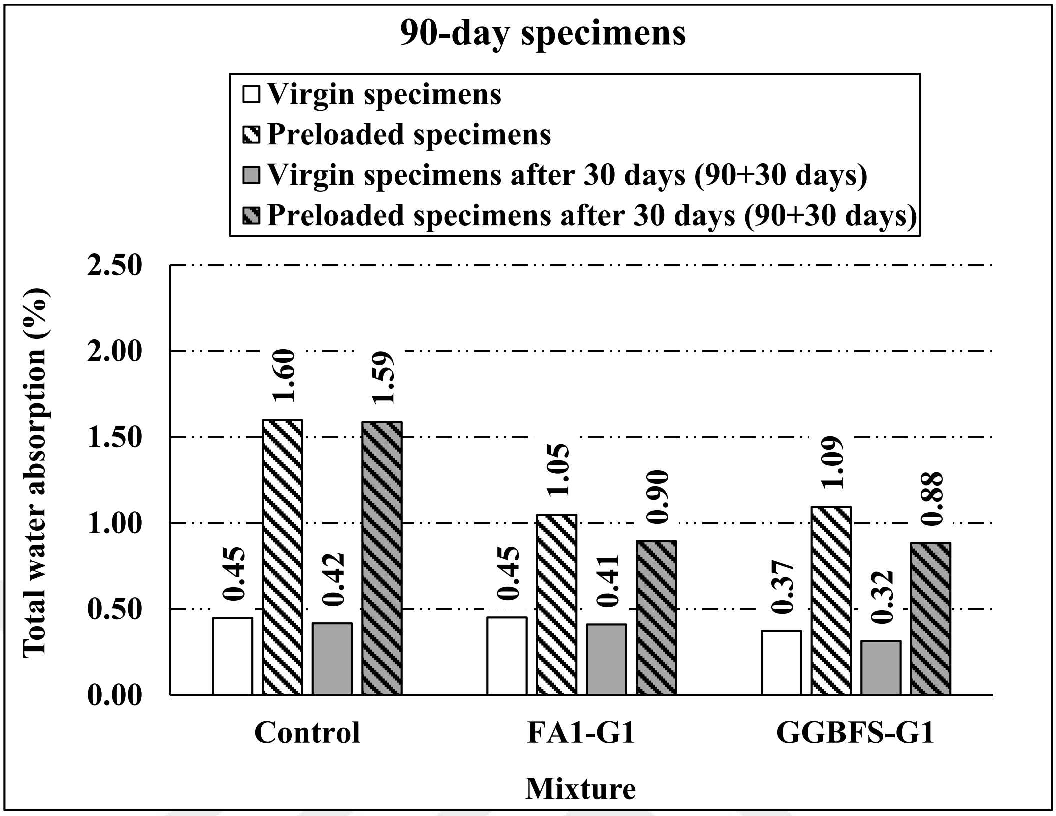

Figure 8.16 The TWA percentages of 90-day specimens

As can be seen from Figure 8.17, a preloading of up to ~100% of the average compressive strengths of specimens resulted in huge increases (40%-257%) in the TWA percentages. The most important point is that the TWA of 90-day preloaded specimens were higher than the 7-day preloaded specimens, especially in the case of SCMs containing mixtures. In other words, more micro cracks have been formed in the 90-day specimens. Therefore, the 90-day preloaded specimens have absorbed more water than the 7-day preloaded specimens.

The increases in TWA can also be considered as the damage ratios obtained from TWA test. As discussed earlier (section 8.1), in spite of such a huge preloading level up to ~100% of the average corresponding compressive strength, the reduction in strength did not exceed 19%. In addition, in contrast with the TWA test, the damage ratios (reduction in strength) in 7-days specimens were higher than in the 90-days specimens. It is obvious that, despite the similar specimens and preloading process/level, the concept of “damage” is totally different in compressive strength and

TWA tests. Simply speaking, comparing with the compressive strength property, the water absorption property of cement based materials is much more sensitive to micro cracks. For example, as expected, the 90-days specimens of FA1-G1 and GGBFS-G1 mixtures are denser and more brittle than the 7-days specimens. Therefore, a preloading of up to ~100% of the average compressive strengths of specimens resulted in formation of more micro cracks in 90-day specimens as compared to the 7-days specimens. Therefore, the 90-day preloaded specimens have absorbed more water than the 7-day preloaded specimens. In other words the "damage" ratios in 90-day specimen were higher than in 7-day specimens. In the case of compressive strength, the parameters such as the maturity of matrix and the fiber-matrix bond strength were more predominant than the formation of micro cracks. The maturity of cementitious matrix and the fiber-matrix bond strength are much higher in 90-day specimens as compared to the 7-day specimens. Herewith, the "damage" ratios, reductions in strength, were lower in the 90-days specimens than in the 7-days specimens.

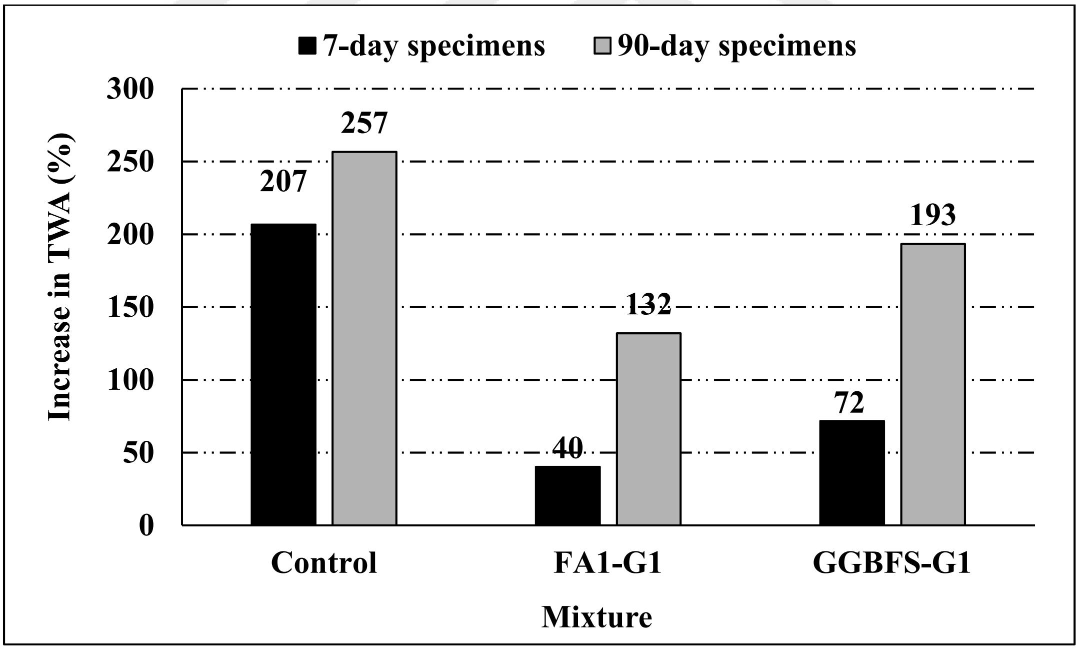

Figure 8.17 The average increases in TWA percentages of UHPC specimens due to preloading

Similar to the compressive strength test, it is only possible from a correct viewpoint to determine a realistic ratio of self-healing. In continuation of this section, the recovery in TWA (self-healing ratios) are expressed in two different approaches.

First approach:

$$RTWA(\%) = \frac{c - b}{d - b} \times 100 \tag{8.5}$$

Where "RTWA" is the percentage of recovery in TWA, "b" and "c" is, respectively, the TWA percentages of preloaded specimens before and after healing period (30 days), and "d" is the TWA percentage of virgin specimens after healing period (7+30 or 90+30 days cured specimens).

The average percentages of recovery in TWA expressed with the first approach are presented in Figure 8.18. As can be seen from Figure 8.18, the self-healing ratio (recovery in TWA) of Control mixture in 7-day specimens is 15.5%. As discussed earlier in section 8.1, the regain in compressive strength (self-healing ratio) of the similar specimens was 44%. It can explained by the fact that the "damage" ratios observed in TWA (increase in TWA percentage) were much higher than the "damage" ratios observed in compressive strength (reduction in strength). Furthermore, as mentioned earlier, comparing with the compressive strength property, the water absorption property of cement based materials is much more sensitive to micro cracks. As expected that self-healing ratios (recovery in TWA) of FA1-G1 (56.3%) and GGBFS-G1 (53.6%) mixtures are much higher than the Control mixtures (Figure 8.18). On the other hand, the self-healing ratios (regain in strength) observed in compressive strength were 68% and 76% for FA1-G1 and GGBFS-G1, respectively.

It can be seen from Figure 8.18 that the self-healing ratios were dramatically decreased in the 90-day specimens. While there was almost no any healing/recovery (1.1%) in the 90-day specimens of Control mixture, the self-healing ratios in FA1-G1 and GGBFS-G1 mixture were 24% and 26.9%, respectively.

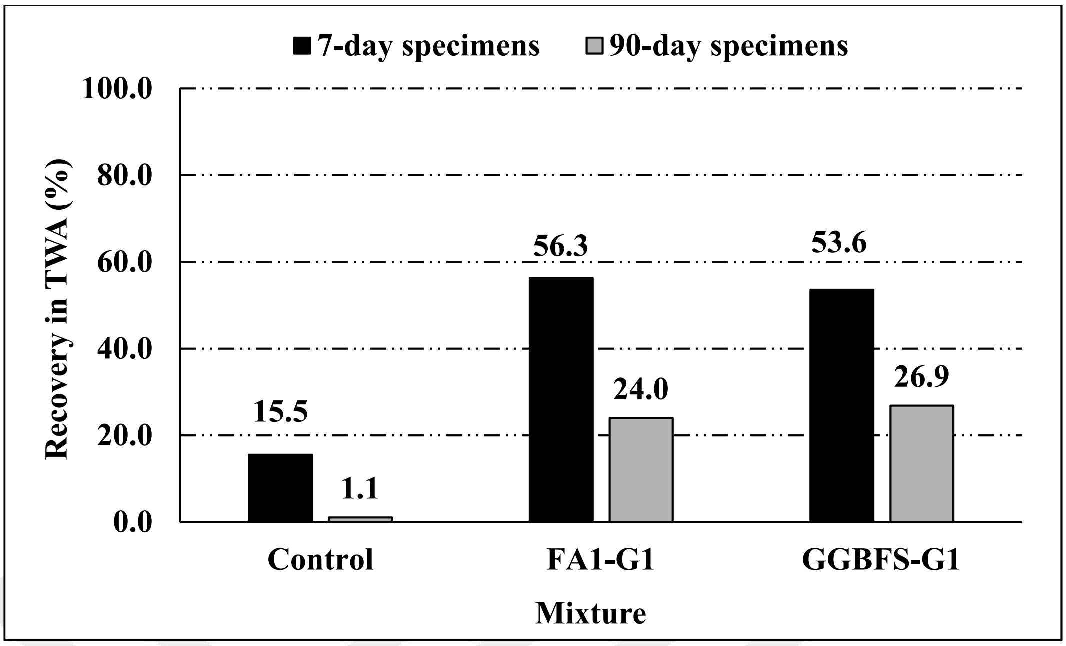

Figure 8.18 The average percentage of recovery in TWA (first approach)

Second approach:

$$RTWA(\%) = \frac{c - b}{a - b} \times 100 \tag{8.6}$$

Where "RTWA" is the percentage of recovery in TWA, "b" and "c" is, respectively, the TWA percentages of preloaded specimens before and after healing period (30 days), and "a" is the TWA percentage of virgin specimens before healing period (7 days or 90 days cured).

The average percentages of recovery in TWA expressed with the second approach are presented in Figure 8.19. As can be seen from Equation 8.6 the self-healing ratio was determined considering the TWA percentage of virgin specimens before healing period. In other words, 30 days healing period was ignored in determining TWA percentage of virgin specimens used in the equation. Therefore, the undergoing hydration reactions and especially pozzolanic reactions during 30 days healing period in virgin specimens were not considered in the second approach. As can be seen from Figure 8.19 over-optimistic results (especially in FA1-G1 mixture) were be obtained in 7-day specimens with the second approach. It is obvious that a significant proportion of the pozzolanic reactions in 7-day specimens occur during the healing period (30 days). However, these over-optimistic results were not seen in the 90-day specimens. As the majority of the pozzolanic reactions are completed up to 90 days, the first approach results are very close to the self-healing ratios obtained from the second approach.

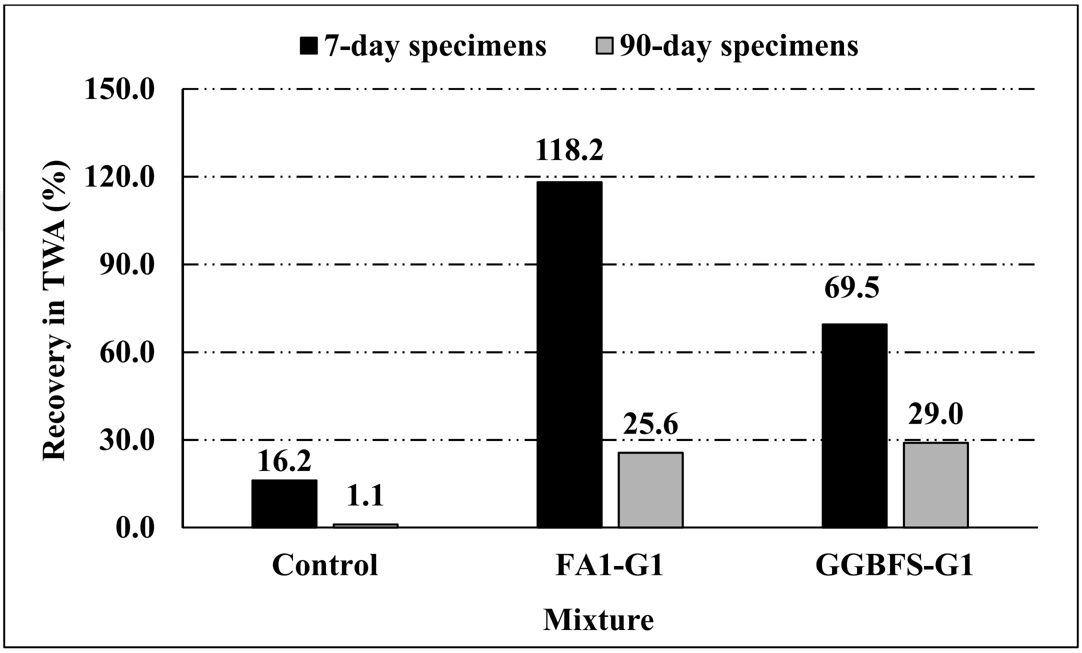

Figure 8.19 The average percentage of recovery in TWA (second approach)

8.8 Evaluation of Self-Healing Mechanism Using Capillary Water Absorption Test

The capillary water absorption (CWA) test results (CWA vs. time curves) of Control, FA1-G1, and GGBFS-G1 mixture are presented in Figures 8.20, 8.21, and 8.22, respectively. As can be seen from the figures, a preloading of up to ~100% of the average compressive strengths of specimens resulted in huge increases in the CWA values of all mixtures. In contrast with the TWA, the increases in CWA values due to the preloading were higher in the 7-day specimens than in the 90-day specimens. It can be explained by the fact that the water suction behavior of a specimen immersed in water differs from its suction behavior through the capillary.

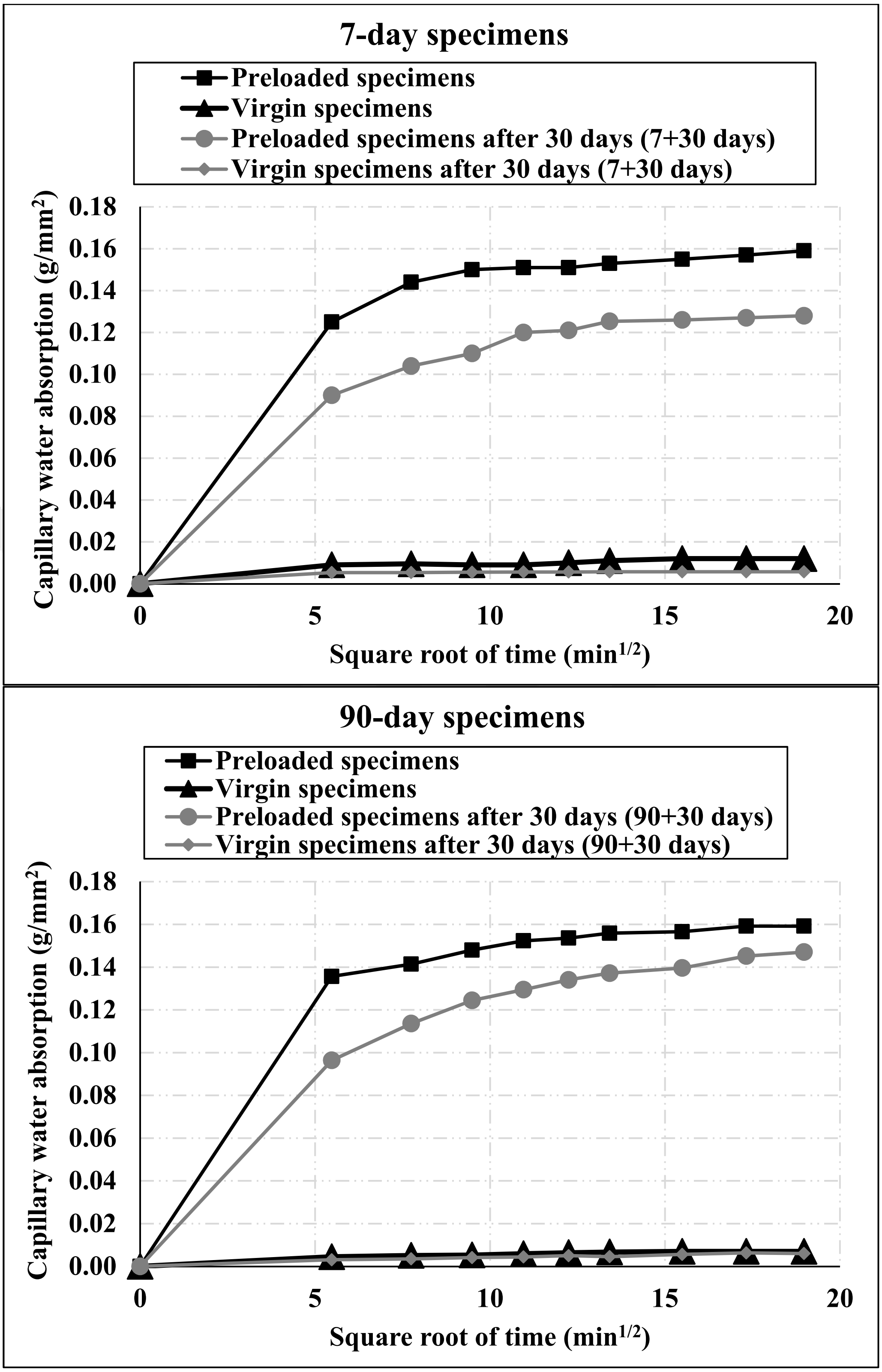

Figure 8.20 The CWA test results of Control mixture

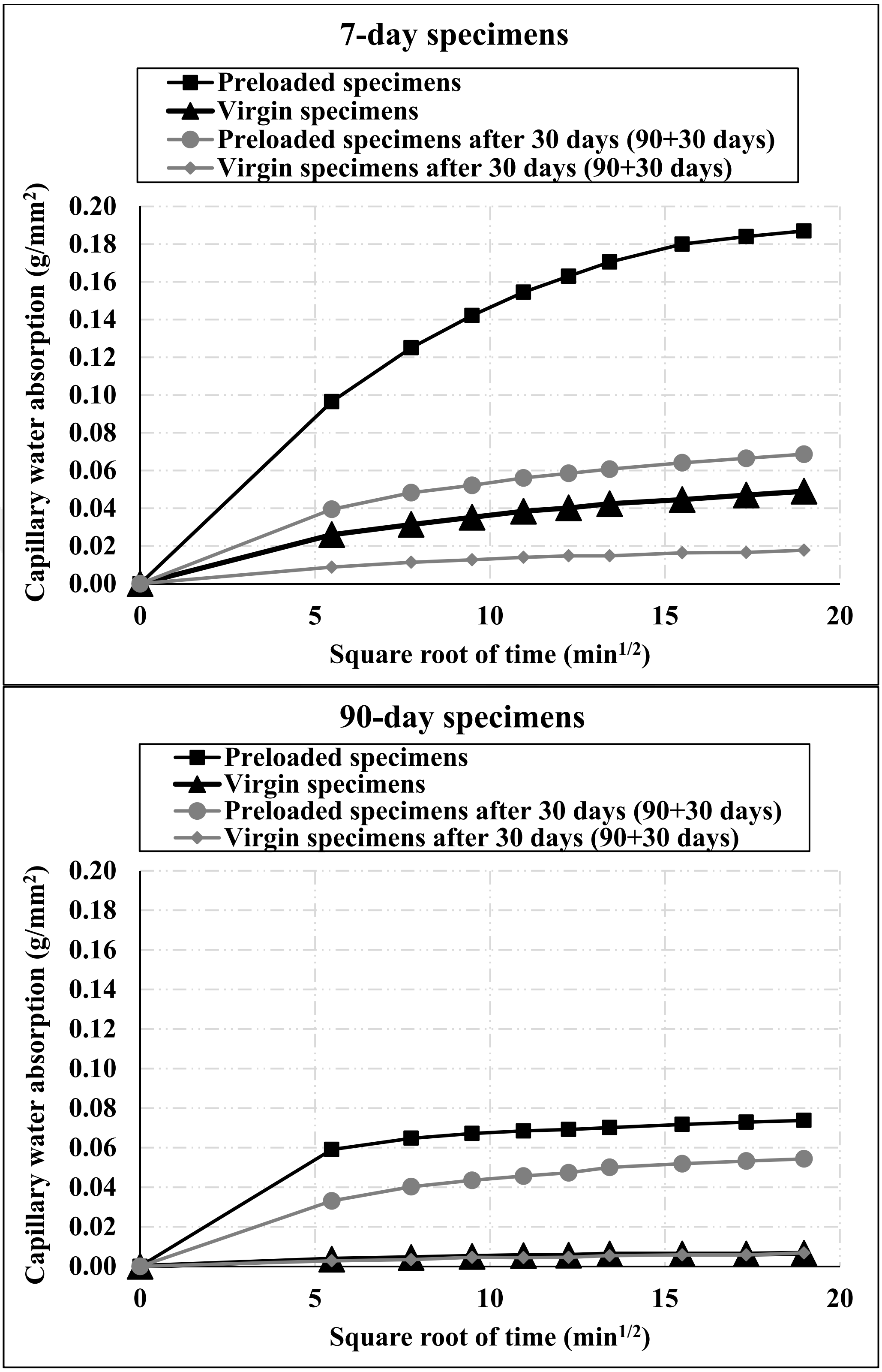

Figure 8.21 The CWA test results of FA1-G1 mixture

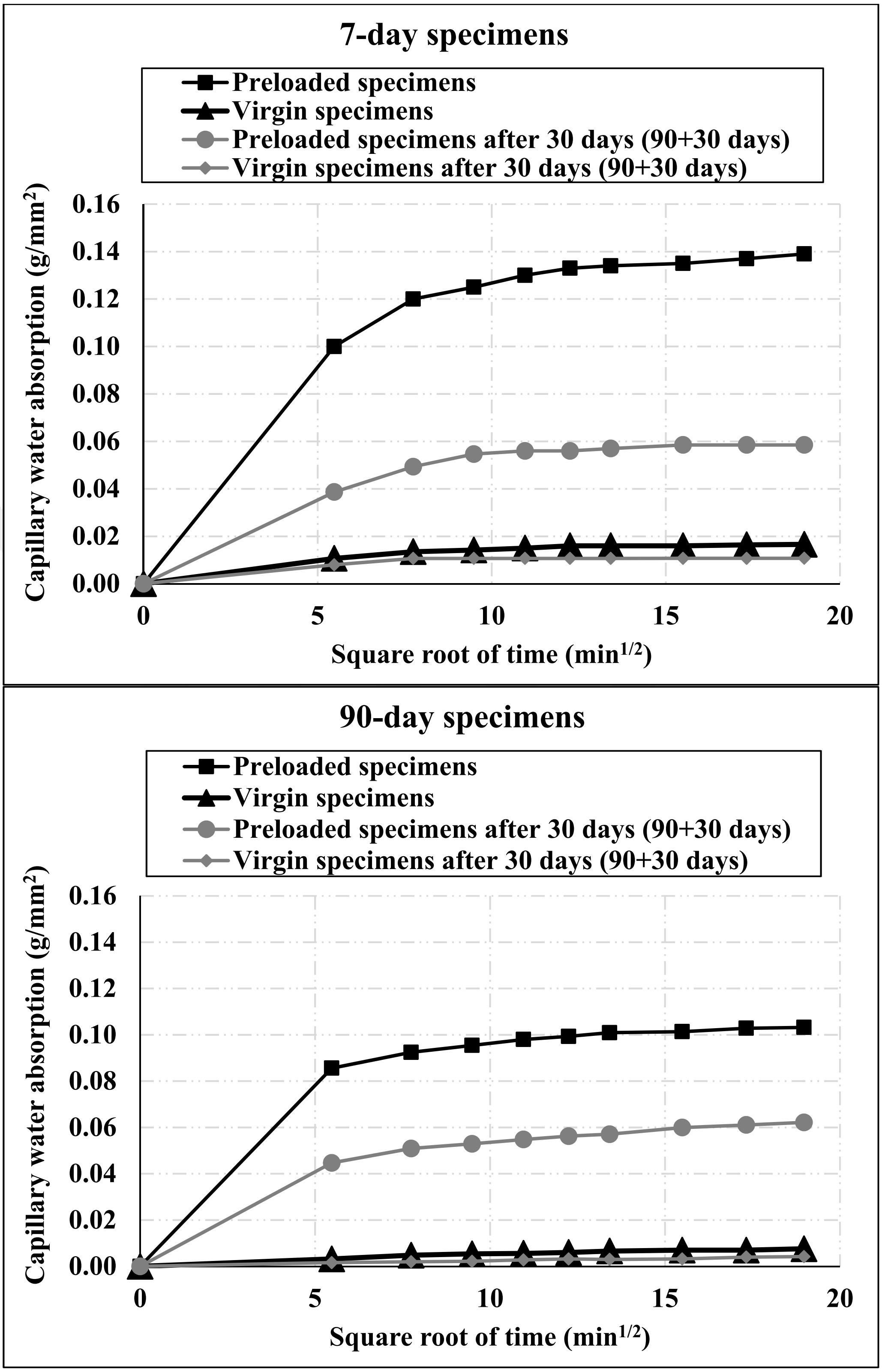

Figure 8.22 The CWA test results of GGBFS-G1 mixture

The recovery ratios in CWA (self-healing ratios) were also calculated via the two different approaches used in the TWA test. It must be noted that the CWA values at the end of 360 minutes (18.97 min$^{1/2}$) were used in the Equations 8.5 and 8.6. The average percentages of recovery in CWA expressed with the first approach are presented in Figure 8.23. As can be seen from Figure 8.23, the self-healing ratio (recovery in TWA) of Control mixture in 7-day specimens is 20.2%. As expected that self-healing ratios (recovery in CWA) of FA1-G1 (69.9%) and GGBFS-G1 (62.8%) mixtures are much higher than the Control mixtures (Figure 8.23). Despite the higher "damage" ratios in CWA as compared to the TWA, the self-healing ratios in CWA are slightly higher in the TWA.

It can be seen from Figure 8.23 that the self-healing ratios were dramatically decreased in the 90-day specimens. While there was very low healing/recovery (7.9%) in the 90-day specimens of Control mixture, the self-healing ratios in FA1-G1 and GGBFS-G1 mixture were 29.0% and 41.4%, respectively.

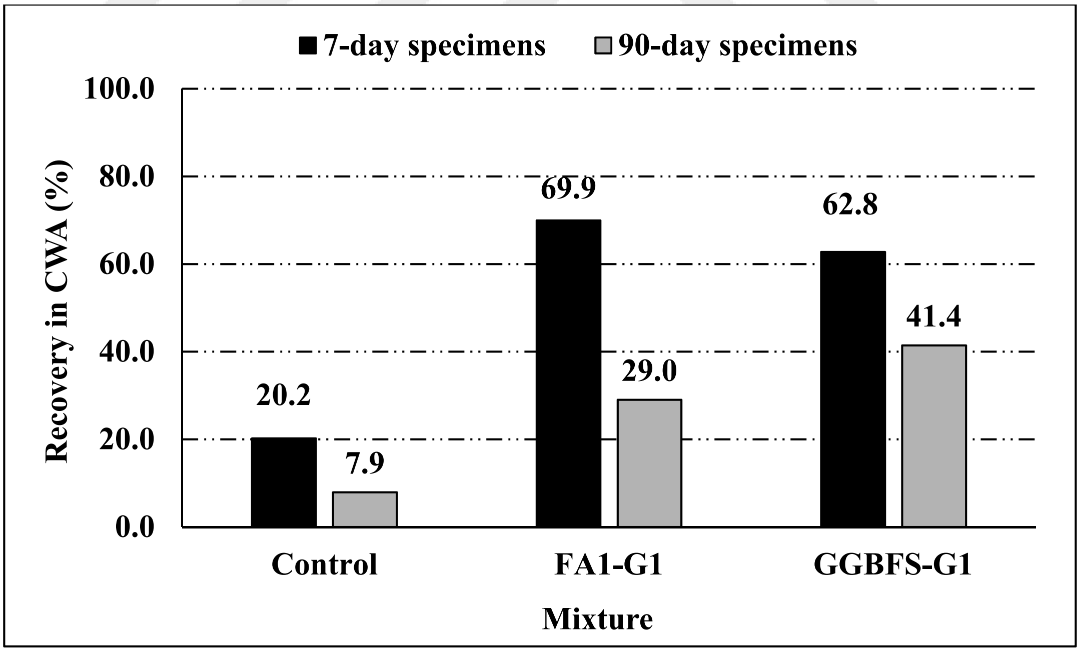

Figure 8.23 The average percentage of recovery in CWA (first approach)

The average percentages of recovery in CWA expressed with the second approach are presented in Figure 8.24. As can be seen from Figure 8.24, except the 7-day specimens of FA-G1 mixture, the recovery ratios are almost the same with recovery ratios expressed with the first approach. The superior effect of SCMs on self-healing ability of UHPC mixture can be seen in both of the approach. As discussed in details earlier, the second approach can lead to obtain over-optimistic self-healing ratios. However, it seems that this finding, which were observed in the compressive strength and TWA test result, was not valid in the CWA test results.

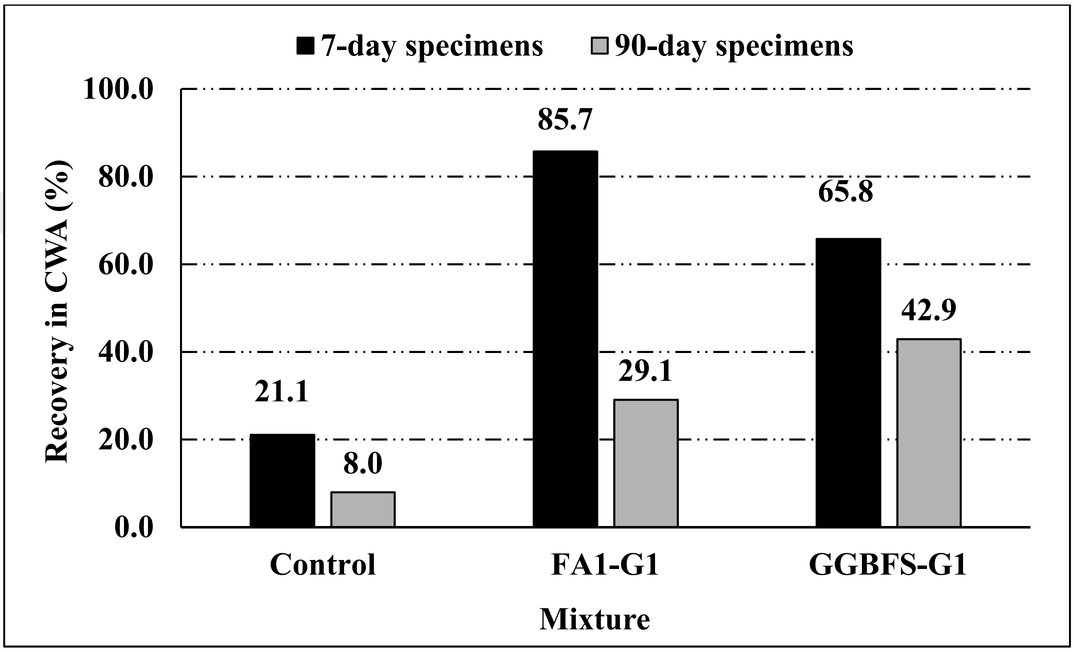

Figure 8.24 The average percentage of recovery in CWA (second approach)

CHAPTER NINE
MICROENCAPSULATION OF SODIUM SILICATE

This chapter has dealt with the microencapsulation of sodium silicate (SS) as healing agent with two different polymeric shell. The microencapsulation processes were explained earlier in details at sections 3.2.1 and 3.2.2

9.1 Microencapsulation with Urea-Formaldehyde Polymer

As mentioned in earlier sections, the microencapsulation of aqueous SS with urea-formaldehyde shell was tried by Gilford et al. (2014). In order to encapsulate SS as healing agent, they have tried to adopt a well-developed in situ poly(urea-formaldehyde) microencapsulation method recommended by Brown et al. (2003) to encapsulate dicyclopentadiene (DCPD) monomer. The adopted synthesis method used by Gilford et al. (2014) to encapsulate SS was tried within the scope of this thesis.

9.1.1 Synthesis

In the reference method recommended by Brown et al. (2003), the water-miscible core material, DCPD, were added to the water phase to prepare an oil-in-water emulsion. In other words, the core material, oil phase, were dispersed as micro droplets in water phase. The poly(E-MA) adsorbs on the interface between oil and water phases acts as polymeric surfactant to stabilize the emulsion and also works as a reaction site of polymerization (Yoshizawa et al., 2004). In the case of using the aqueous SS solution instead of the DCPD as core material, it cannot be added directly to the water phase due to the fact that SS is a water-miscible liquid. In other words, the aqueous SS cannot dispersed as micro droplets in water phase. Therefore, in the adopted method, Gilford et al. (2014) slowly added HCL to a solution contains deionized water and aqueous SS to form a gel/aqueous solution. After that, a certain amount of gel/aqueous SS solution were added to the main solution (continuous or water) phase. In the reference method (Brown et al., 2003), there is no need to monitor again the pH level of emulsion when the core materials (DCPD) is added to the water phase. However, it is so critical maintaining pH of emulsion at desired level in the case of using gel/aqueous SS solution as core material. The gel/aqueous SS solution immediately increases the pH of emulsion due to the alkaline nature of SS.

In spite of many investigations on the microencapsulation parameters such as pH level, agitation rate, and polymerization temperature, it was observed that the SS could not be efficiently encapsulated with the urea-formaldehyde through the methods proposed by Gilford et al. (2014) due to the above-mentioned problems. As can be seen from Table 9.1, besides the parameters examined by Gilford et al. (2014), many additional experiments were performed in the scope of this study.

Table 9.1 The variables of microencapsulation process

Experiment Code	pH value	Agitation rate (rpm)	Temprature (°C)	Description
Control	3.0	550	55	Suggested by Gilford et al. (2014)
EP1	3.1	550	55	Suggested by Gilford et al. (2014)
EP2	3.2	550	55	Suggested by Gilford et al. (2014)
EP3	3.3	550	55	Additional experiment
EP4	3.4	550	55	Additional experiment
EP5	3.5	550	55	Additional experiment
EP6	4.0	550	55	Additional experiment
EAR1	3.0	250	55	Suggested by Gilford et al. (2014)
EAR2	3.0	350	55	Suggested by Gilford et al. (2014)
EAR3	3.0	450	55	Suggested by Gilford et al. (2014)
EAR4	3.0	650	55	Additional experiment
EAR5	3.0	700	55	Additional experiment
EAR6	3.0	750	55	Additional experiment
ET1	3.0	550	50	Suggested by Gilford et al. (2014)
ET2	3.0	550	51	Suggested by Gilford et al. (2014)
ET3	3.0	550	52	Suggested by Gilford et al. (2014)
ET4	3.0	550	53	Additional experiment
ET5	3.0	550	54	Additional experiment
ET6	3.0	550	56	Additional experiment

In addition to the experiments presented in Table 9.1, many unsystematic experiments were also carried to find out any possible solution for the problems encountered during syntheses. Moreover, to observe the effect of mix type, the experiments suggested by Gilford et al. (2014) were carried out by both of the magnetic stirrer and mechanical (digital) mixer. However, the problems encountered in the microencapsulation process could not be eliminated.

As the final step of synthesis process, the resulting particles (possibly microcapsules) are separated by vacuum filtration. In the case of complete encapsulation of core materials, this step can be done without any problem. For example, if the DCPD, which was encapsulated in the reference method, was used as the core material instead of SS, the filtration process would be successfully done without any clogging in the filter paper. As mentioned earlier the SS cannot be added directly to the water phase because SS is a water-miscible liquid. Therefore, it should be added in the form of a gel/aqueous solution. Therefore, a considerable amount of SS may be mixed in water phase (emulsion). It can also be proved by the fact that the pH level of water phase increases rapidly with addition of SS gel/aqueous solution. For this reason, the filter paper used in the vacuum filtration, no matter which procedure (Table 9.1) used, was immediately clogged (Figure 9.1).

Figure 9.1 Clogging of filter paper during vacuum filtration process (Personal archive, 2016)

As a different solution for separating the resulting particles (possible microcapsules), the mixture was decanted at least 5 times by adding distilled water and then, the particles in the bottom of beaker were transferred to watch glasses for drying (Figure 9.2). Centrifuging was also tried for this purpose, but the decantation was more effective method.

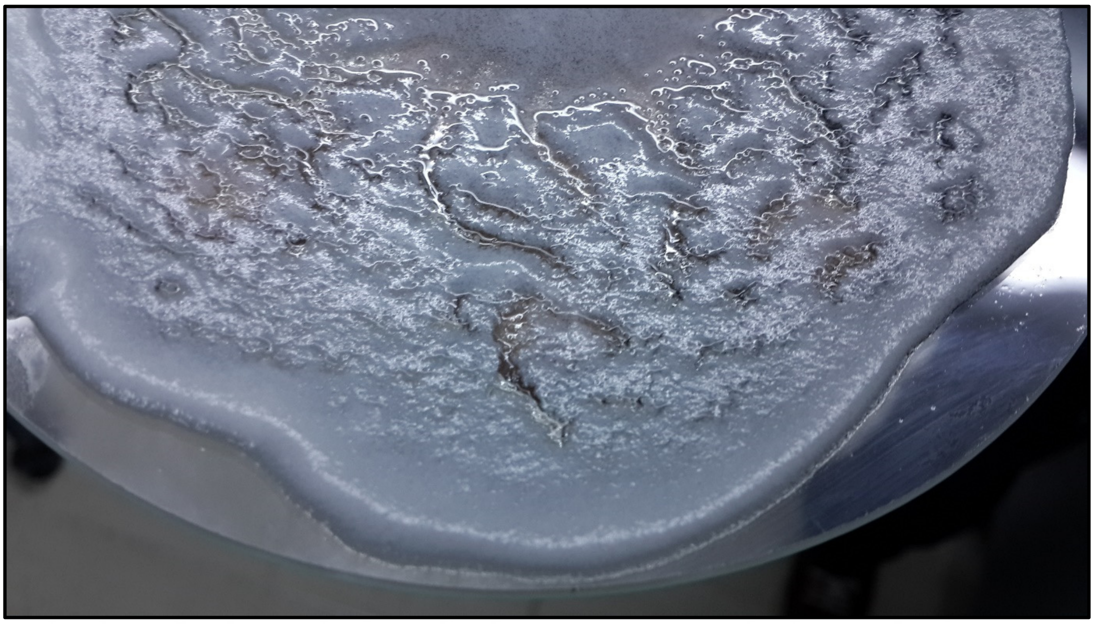

Figure 9.2 The particles transferred to watch glasses for drying process (Personal archive, 2016)

9.1.2 Results and Discussion

The problems described in detail above were valid in all experiments. It was not possible to solve the problem completely by changing any parameters. In Figure 9.3, SEM images of the products obtained from some experiments that can relatively represent the results of all experiments are presented. As can be seen, it is not correct to consider these irregular-shaped particles as microcapsules. It can be concluded from many EDS analysis that the products are mainly consist of solidified SS and a little amount of UF polymer formed on them. Figure 9.4 shows spectrums of EDS analysis conducted on some of particles. The EDS analyses revealed that chemical composition of the particles, no matter obtained from which experiment (Table 9.1), consists mainly from Si (49-58%), O (40-46%), and O (0.8-4.5%) elements by weight. As can be seen from Figure 9.5 (c and d), the particles considered as "microcapsules" by Gilford et al. (2014), have irregular shapes similar to the particles obtained in this study. In addition, they have named the particles as "microcapsules" without any elemental analysis in the study. On the other hand, as cam be seen from Figure 9.5 (a and b), it seems that Gilford et al. (2014) could encapsulated successfully the DCPD monomer according to the method proposed by Brown et al. (2003). Although no further analyzes have been presented, successful microencapsulation of the DCPD monomer is evident from SEM images.

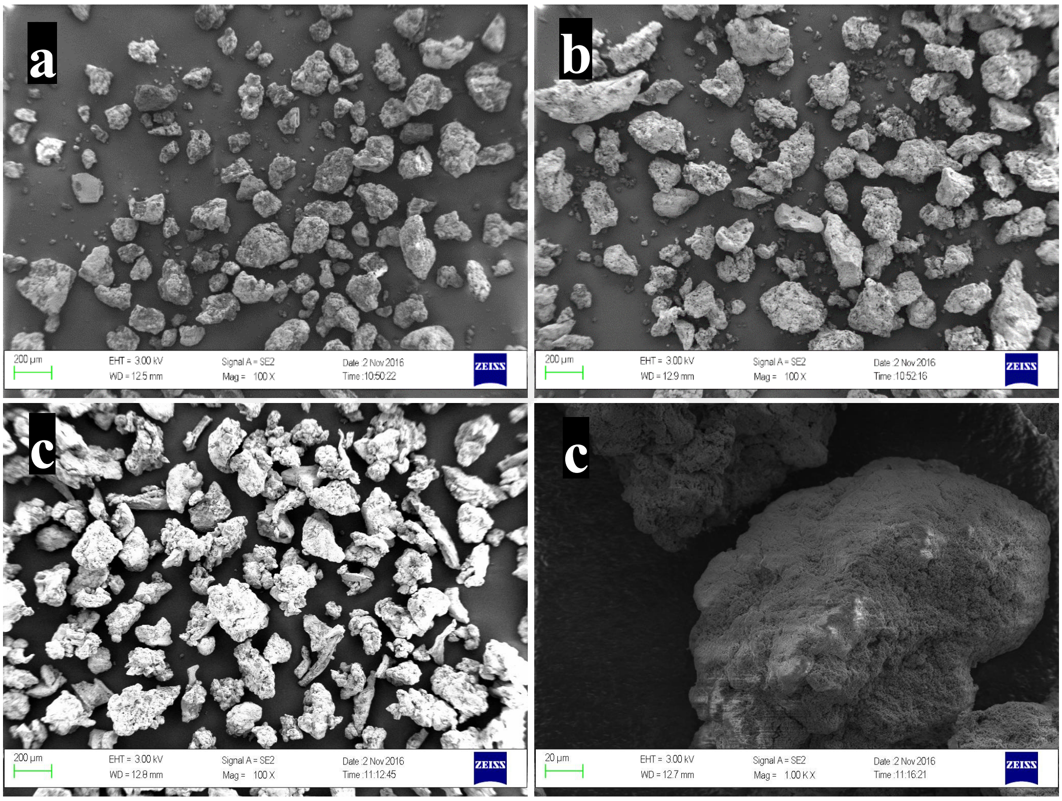

Figure 9.3 SEM images of particles obtained from a) EP2, b) EAR2, and c) ET3 experiments

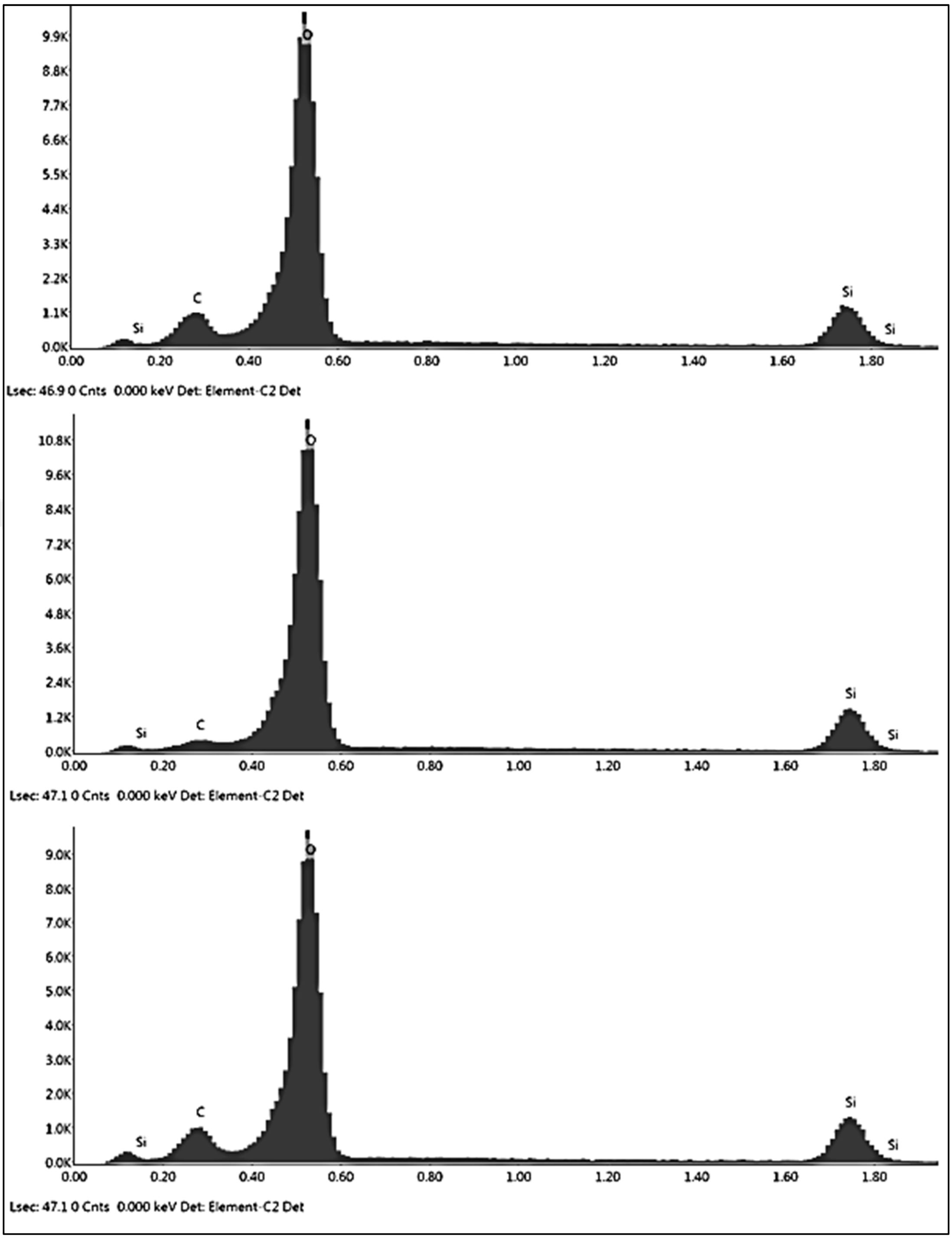

Figure 9.4 EDS spectrum of some particles obtained from a) EP2, b) EAR2, and c) ET3 experiments

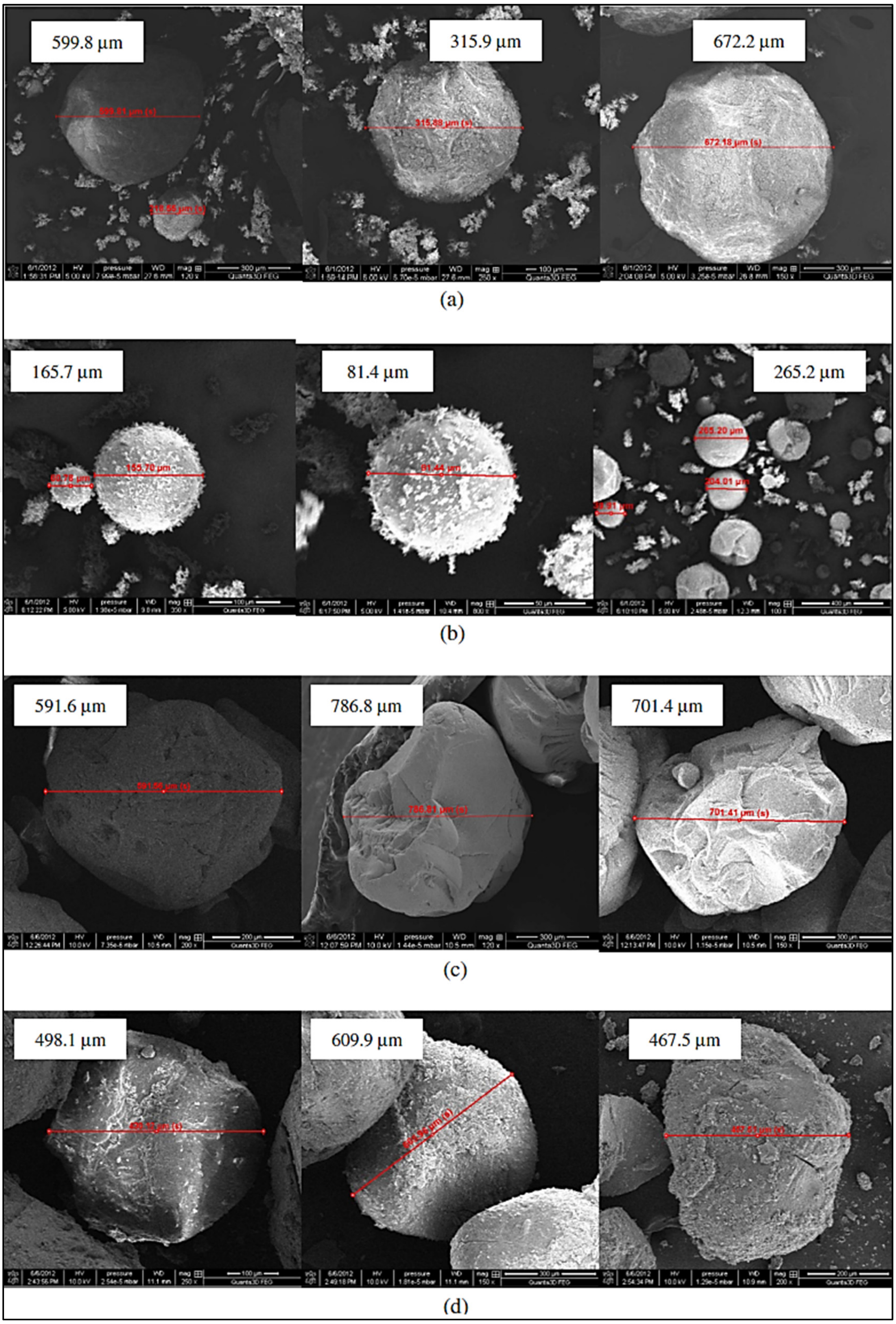

Figure 9.5 SEM images of microencapsulation results of DCPD (a and b) and sodium silicate (c and d) as healing agents (Gilford et al., 2014)

9.2 Microencapsulation with Polyurethane Polymer

As mentioned in previous chapters Pelletier et al. (2011) have prepared aqueous SS-loaded polyurethane microcapsules according to the method suggested by Saihi et al. (2006). Pelletier et al. (2011) have used a certain amount of shell-forming monomer in their synthesis procedure. However, it is well known that the amount of shell-forming monomer is a key factor in terms of the characteristics of microcapsules. Therefore, initially, various amounts of shell-forming monomer, methylene diphenyl diisocyanate (MDI) were used in the synthesis of SS bearing poly(urea-urethane) microcapsules.

Moreover, Pelletier et al. (2011) have not studied the characterization of microcapsules in detail. The microcapsules synthesized with various amount of MDI were characterized through different analyses. Besides, the fracture behavior of the optimized microcapsule was examined in a cement paste matrix. This optimization study has been published as a paper titled “Sodium silicate/polyurethane microcapsules used for self-healing in cementitious materials: Monomer optimization, characterization, and fracture behavior” in journal of Construction and Building Materials (Beglarigale, Seki, Demir, & Yazici, 2018).

Some of the optimization tests were carried out using more materials in 250 mL beaker by using various type of magnetic cylindrical stirrer bars. The effect of parameters such as emulsification and polymerization speeds were examined.

9.2.1 Optimization of Shell-Forming Monomer - Characterization of Microcapsules

Based on the preliminary test results, various amounts of MDI were used in this study to determine the effect of diisocyanate monomer on the properties of the microcapsules. Therefore, four different mixtures (hereafter called MDI-1, MDI-2, MDI-3, and MDI-4) were prepared by using 7.5, 10, 12.5, and 15 g of MDI, respectively. It must be noted that shell-forming monomer to core material ratios of

MDI-1, MDI-2, MDI-3, and MDI-4 mixtures are 0.50, 0.67, 0.83, and 1.00, respectively. The synthesis process was described in details at section 3.2.2.

9.1.1.1 Synthesis

The microencapsulation was carried out by the emulsification of healing agent in the organic medium (toluene) using POEDO and Span 85 surfactants and then, followed by an interfacial polymerization on the emulsion droplets. After vacuum filtration, sufficient washing, and drying in air, a free-flowing white powder of microcapsules was obtained (Figure 9.6).

Figure 9.6 Image of 0.4 g of MDI-3 microcapsules powder spread over a watch glass with 80 mm diameter (Personal archive, 2017)

As expected, it was observed that the viscosity of the emulsion increased by using more MDI. To our observations, this phenomenon adversely affects the microencapsulation process of MDI-3 and MDI-4 mixtures. Excessive viscosity leads to an improper agitation; therefore, an inhomogeneous polymerization process takes place.

Microencapsulation yields (%) MY were calculated by the following equation (Saihi et al., 2006):

$$MY(\%) = \frac{W_M}{W_{HA} + W_{MDI} + W_{SPAN}} \tag{9.1}$$

Where W_M, W_{HA}, W_{MDI}, and W_{Span} are the weights of dried microcapsules powder, healing agent (SS + deionized water), MDI, and Span surfactant, respectively. As can be seen from Figure 9.7, the highest yield was obtained in the MDI-2 mixture. It seems that excessive viscosity of MDI-3 and MDI-4 affected negatively the microencapsulation yields.

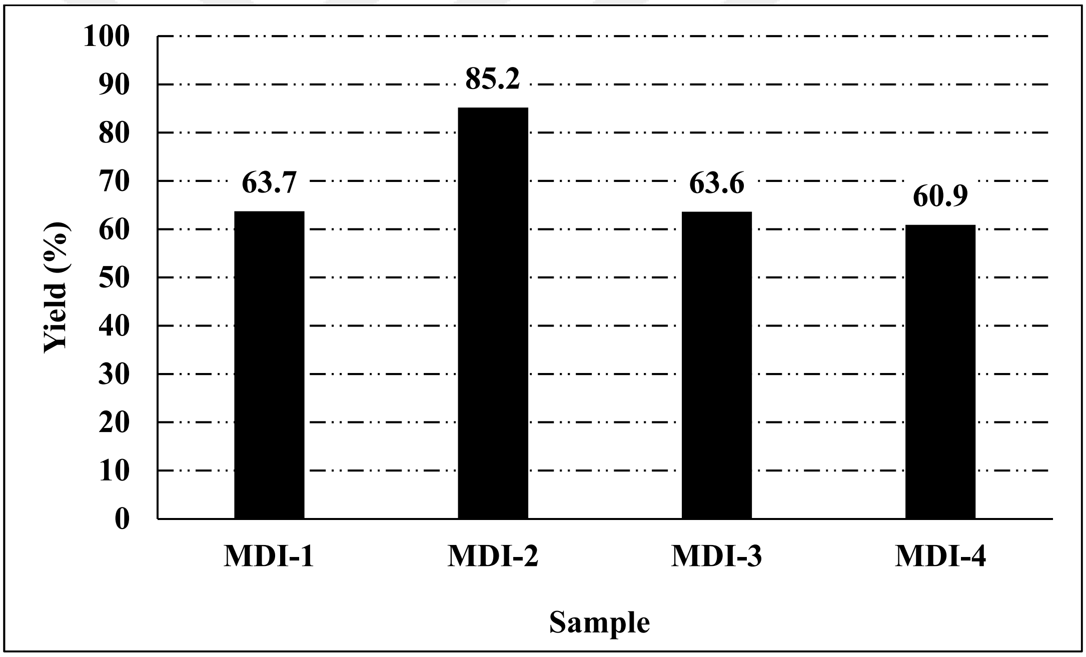

Figure 9.7 Yield values of microcapsules

9.1.1.2 FTIR Analysis Results

FTIR spectra of the microcapsules are presented in Figure 9.8. As can be seen from Figure 9.8, the FTIR spectra of MDI-based microcapsules are almost similar. The amount of MDI within the microcapsules did not considerably affect the FTIR spectra of the microcapsules. In the spectrum of MDI-1, the peaks at 2925 cm^{-1} is assigned to

CH_2 groups. (C=O) free and bonded (urea group) were seen at 1690–1660 cm^{-1}. Aromatic groups of MDI have peaks at 1596, 1411, and 857 cm^{-1}. A weak shoulder at about 1750 cm^{-1} and peaks at 1433 cm^{-1} and 1109 cm^{-1} may be due to C=O, C=C, and C-O-C groups of Span 85, respectively. The presence of peak of isocyanate function at 2296 cm^{-1} indicates that the diisocyanate has not completely reacted with Span 85 to form polyurethane (PU) (Saihi et al., 2006). The peaks at 3302 cm^{-1}, 1540 cm^{-1}, and 1230 cm^{-1} correspond to N-H groups. It is known that hydrogen bonded NH groups with ether oxygen are seen in 3290-3310 cm^{-1}. Hydrogen bonded NH groups with ether oxygen were seen at 3302 cm^{-1} in the spectrum of MDI-1 in this study, which indicates that hydrogen bond has formed in PU chain (Badri et al., 2010). The peaks belonging to C-N groups were observed at 1508 cm^{-1} and 1230 cm^{-1}. Microcapsules exhibit the characteristic peak at 1018 cm^{-1}assigned to Si–O–Si bonds (Kanellopoulos et al., 2017).

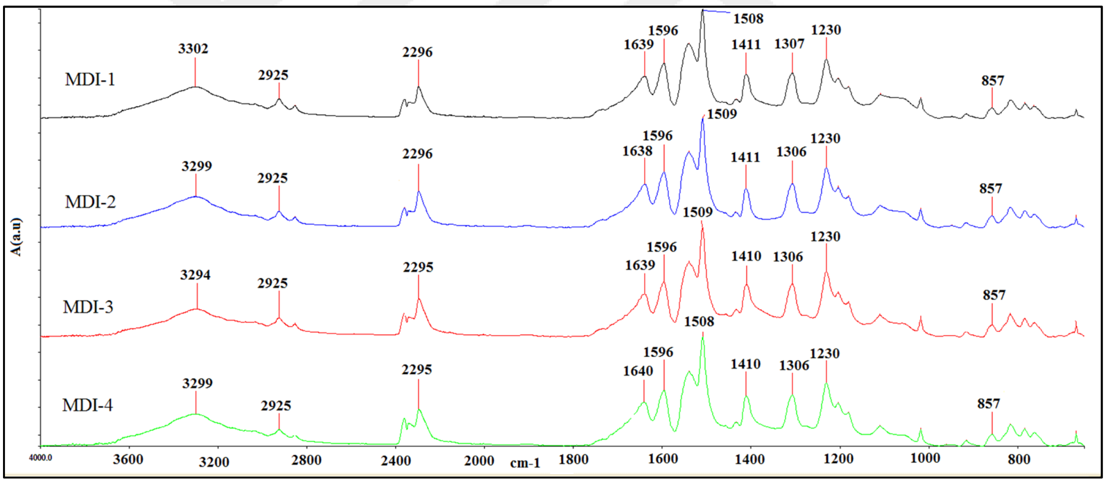

Figure 9.8 FTIR spectra for the microcapsules

9.1.1.3 TG Analysis Results

TGA curves of the samples are shown in Figure 9.9. As shown in Figure 9.9, three main degradation steps, first step up to 110°C, second step in the range 200-400°C, third step in the range 400-570°C, are present for the microcapsules. Mass loss values up to 110°C, which are due to moisture within the samples, were calculated to be 25.6, 38.5, 11.5, and 23.8% for MDI-1, MDI-2, MDI-3, and MDI-4, respectively. Higher moisture content may be due to higher content of inner material (SS + deionized water). From these results, it can be deduced that MDI-2 may have capsulated more inner material than the others. The second step between 280-320°C may be due to MDI evaporation (Litina, Kanellopoulos, & Al-Tabbaa, 2014). The third step corresponds to the extensive decomposition of shell wall material (Litina et al., 2014). It is known that above 500°C, all urea groups are decomposed (Saihi et al., 2006).The temperatures for MDI-1, MDI-2, MDI-3, and MDI-4 at 5% mass loss are 51.0, 51.4, 60.7, and 52.1°C, respectively (Table 9.2). Maximum degradation temperatures were determined to be 345, 344, 346, and 351°C, respectively. The temperatures for MDI-1, MDI-2, MDI-3, and MDI-4 at 50% mass losses were obtained to be 341, 309, 370, and 355°C, respectively. Residue masses for MDI-1, MDI-2, MDI-3, and MDI-4 are 21.6, 17.7, 26.2, and 23.1, respectively. There is one small step in second stage in the range 240-260°C. This step may be attributed to the depolymerisation of PU to produce the starting monomers (Saihi et al., 2006).

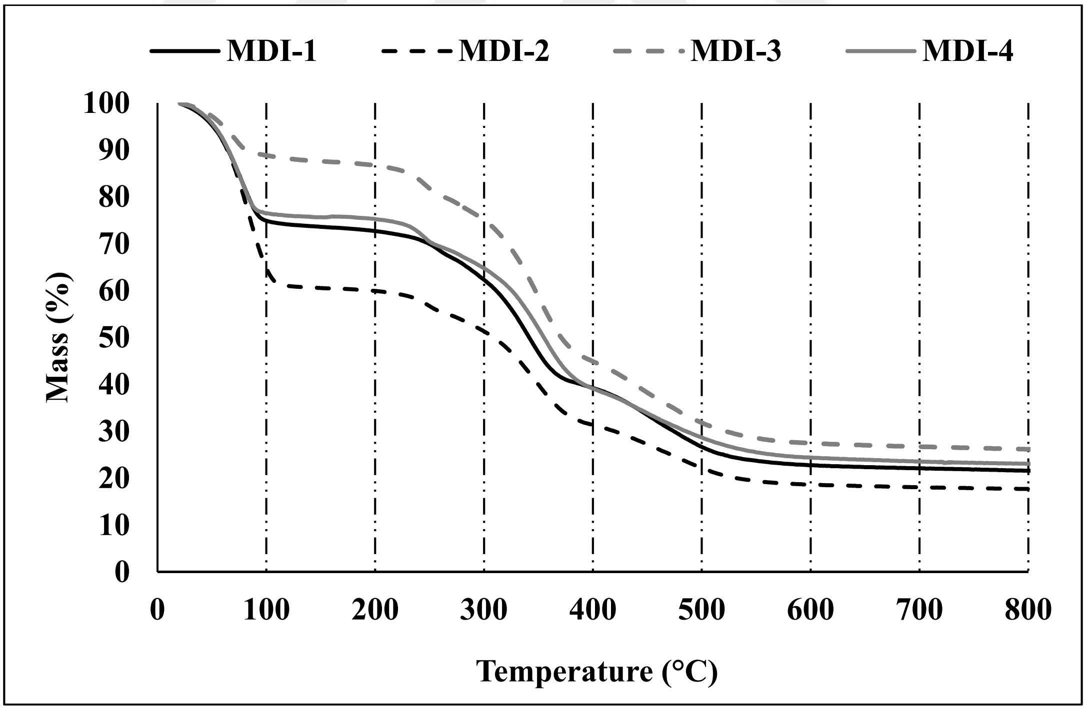

Figure 9.9 TGA curves for the microcapsule

Table 9.2 TGA data for the microcapsule samples

Sample	Temperature at 5% mass loss (°C)	Mass loss up to 100°C (%)	Temperature at 50% mass loss (°C)	T_{MAX} (200-400°C)	Residue Mass (at 800 °C)
MDI-1	51.0	25.6	341	345	21.6
MDI-2	51.4	38.5	309	344	17.7
MDI-3	60.7	11.5	370	346	26.2
MDI-4	52.1	23.8	355	351	23.1

9.1.1.4 XRD Analysis Results

XRD diffractograms of microcapsules are shown in Figure 9.10. MDI-1 exhibits a broad peak positioned at about 2θ=21.2°, which indicates amorphous characteristic of the sample (Ferreira, Santos, Bonacin, Passos, & Pocrifka, 2015). Although all microcapsules show similar XRD patterns, MDI-2, MDI-3, and MDI-4 exhibit a weak doublet-type peak profile located at 21.3° and 18.3°, 21.2° and 18.6°, and 21.1° and 18.4°, respectively. With increasing the amount of MDI, the peak located at about 18° becomes more apparent.

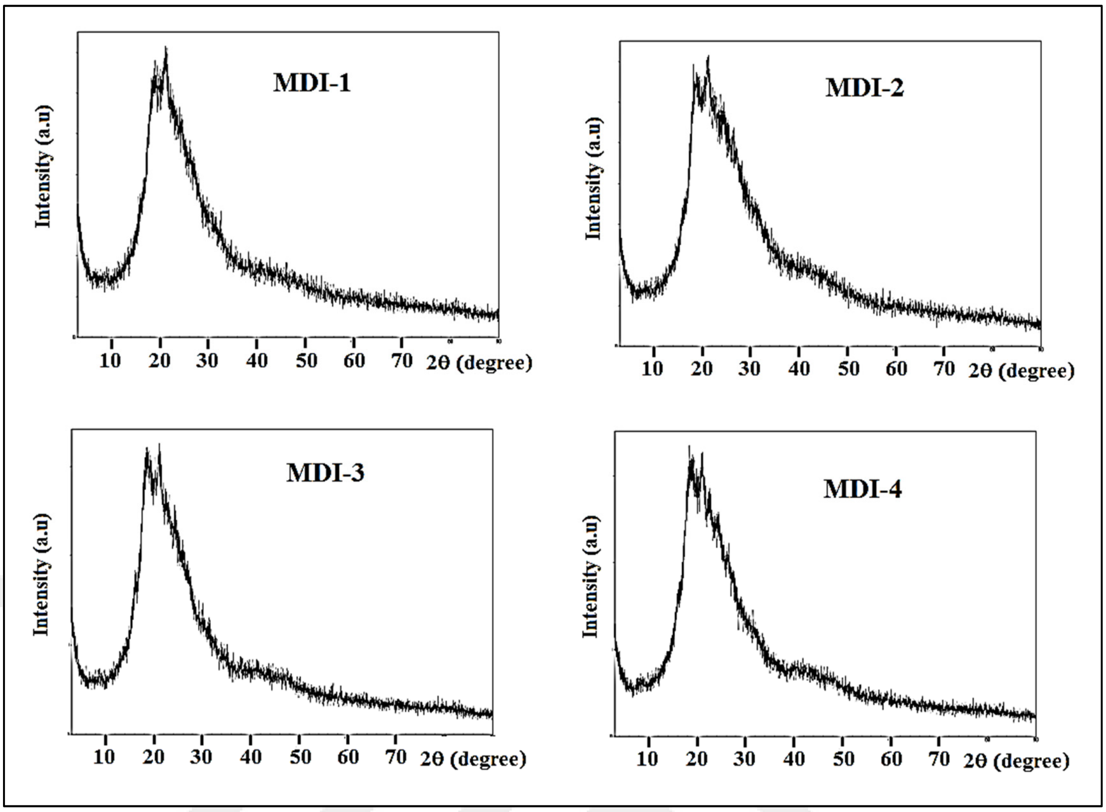

Figure 9.10 XRD patterns of microcapsule samples

9.1.1.5 SEM/EDS Analysis Results

It can be seen from Figure 9.11 that most of the microcapsules are spherical shaped and free-flowing powder. However, the particles with irregular shapes can be found among the microcapsules. The irregular particles increased as the MDI amount was increased. A typical EDS analysis of spherical shaped microcapsules are presented in Figure 9.12. The EDS shows that the microcapsule consists of C, O, Na and, Si elements. Therefore, it revealed the existence of polyurethane (shell material) and sodium silicate (core material).

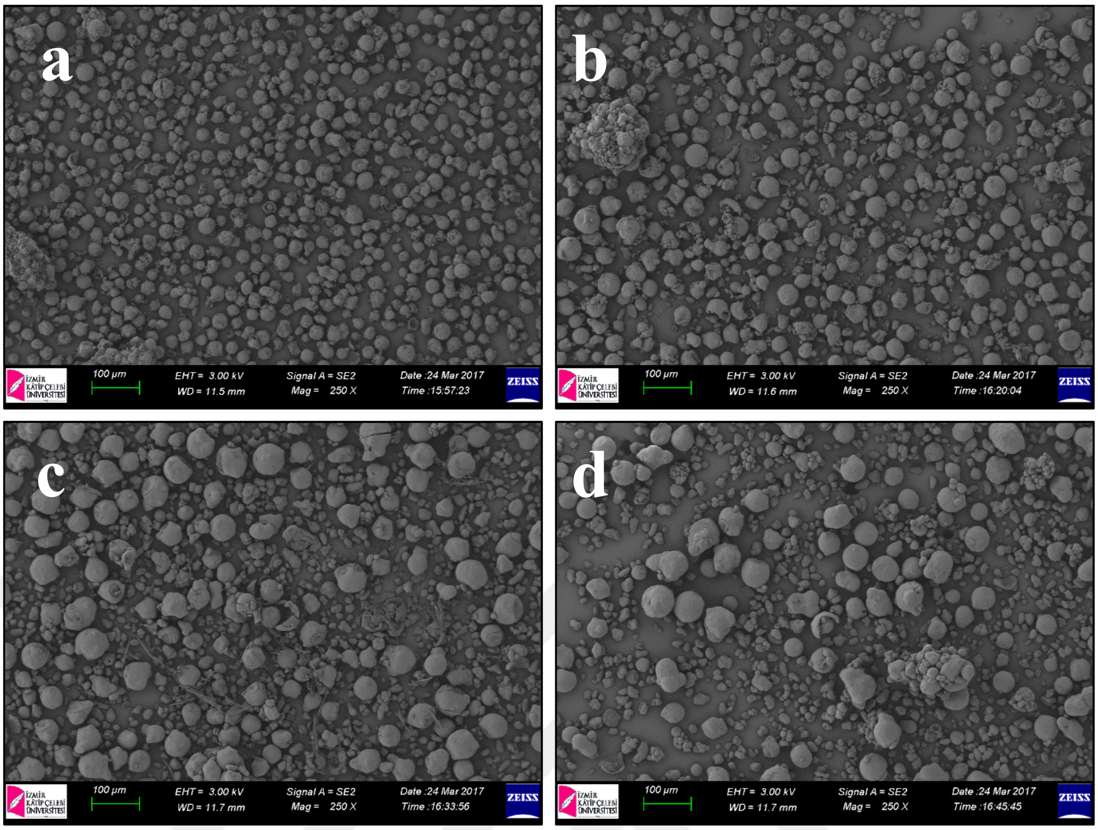

Figure 9.11 SEM images of (a) MDI-1, (b) MDI-2, (c) MDI-3, and (d) MDI-4 microcapsules

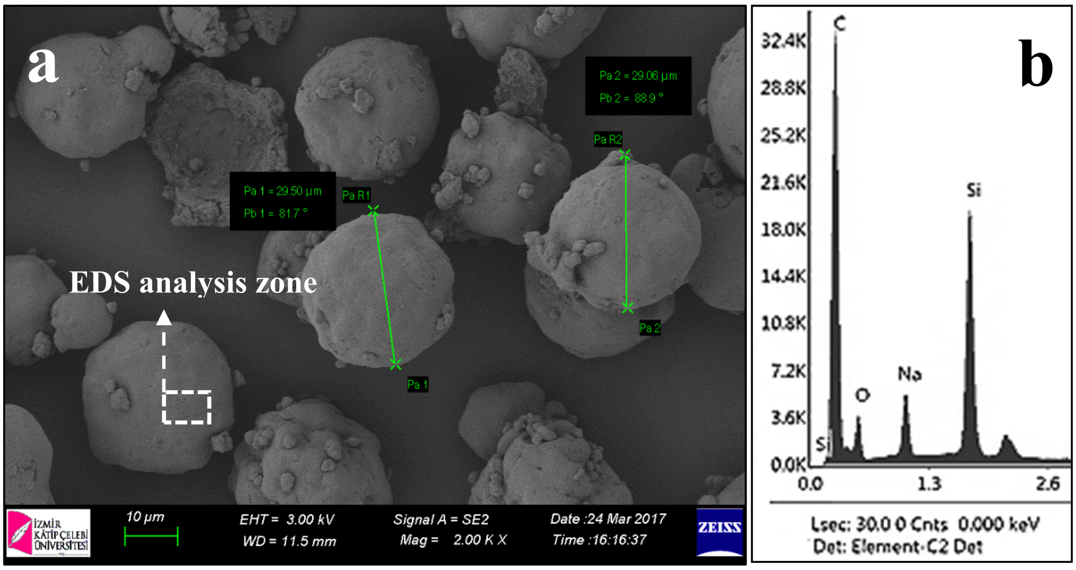

Figure 9.12 SEM image of the MDI-1 microcapsules. (b) The EDS spectrum presenting the chemical composition of a MDI-1 microcapsule

In very few of crushed microcapsule, no matter what amount of MDI was used in microcapsules, the core material (sodium silicate) seems to be a porous spherical solid particle (Figure 9.13).

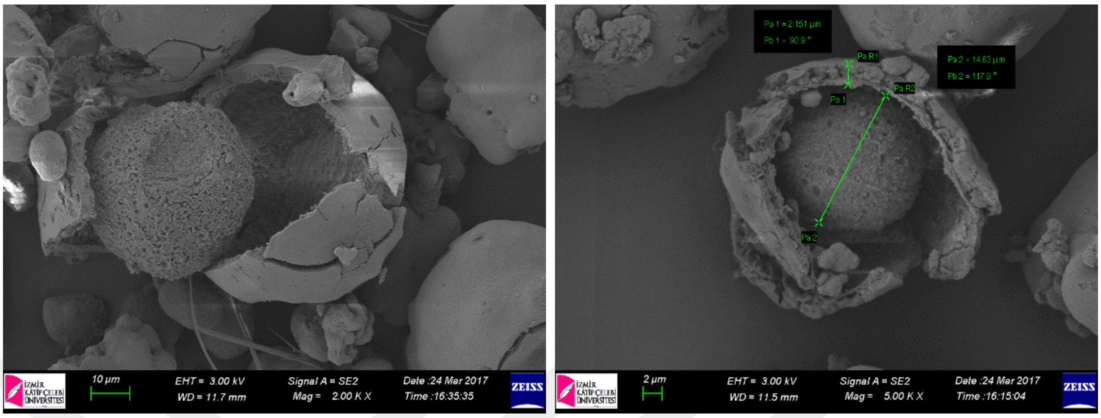

Figure 9.13 Crushed microcapsules

The EDS analyses were performed on the crushed shell of microcapsule and the solid particle (Figure 9.14). As expected, the EDS analyses conducted on the shell revealed that chemical composition of the shell consists mainly from C (59.5%), N (18.7%), and O (17.0%) elements by weight. In addition, Na (3.5%) and Si (1.3%) elements by weight were observed in the EDS analysis of the shell. On the other hand, the main elements of solid spherical particle are O (45.7%), Si (21.8%), Na (4.5%), and C (28.0%).

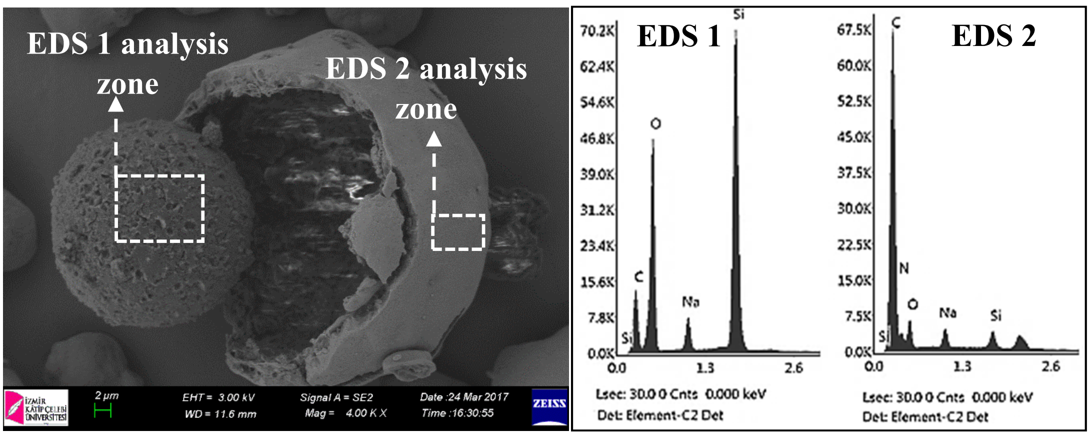

Figure 9.14 The EDS analyses conducted on a crushed microcapsule

It is obvious that this solid particle mainly includes the core material. There are two possibility as follows: 1) these kind of microcapsules have cracks on their shell, so the liquid sodium silicate solution may become hard by the air drying process, 2) a thin membrane of polyurethane may covered the liquid SS based on the EDS analysis which showed C (28%) element on the solid spherical particle. However, it seems that the first hypothesis is more likely reasonable.

The average diameters of microcapsules were obtained by measuring of at least 50 microcapsules. The average diameter of microcapsules was 22, 29, 40, and 47 μm for MDI-1, MDI-2, MDI-3, and MDI-4 respectively. It is obvious that average diameter of microcapsules increased by using more MDI.

It can be concluded from the yield, SEM, and TG analyses that the optimum shell-forming monomer to core material ratio is 0.67 (MDI-2). Therefore, the MDI-2 microcapsules were used in the next section to analyzed the fracture behavior of these microcapsules in cementitious matrix.

9.1.1.7 Fracture Behavior of Microcapsules in Cementitious Matrix

Fracture behavior of microcapsules was analyzed in cement paste matrix. The MDI-2 microcapsules were added in a cement paste mixture (water/cement ratio=0.3) at a concentration of 5% with respect to cement weight. As mentioned earlier, the disk-shaped specimens were split and then, SEM/EDS analyses were performed on the fracture surface of the specimens. The SEM images presented in Figure 9.15, shows many fractured microcapsules embedded in the cement paste matrix. These fractured microcapsules exhibited many dome-shaped empties throughout the fractured surface of the specimens. It is obvious that there is sufficient interfacial bond strength between the shell of microcapsules and matrix. Figure 9.16 shows the details of a fractured microcapsule embedded in the matrix. As mentioned earlier, most of the microcapsules were completely bonded to the cement paste, while in few cases a small part of the shell was debonded from matrix. In spite of those limited debonded region, the crack induced by the splitting ruptured these microcapsules. This behavior promotes the release of healing agents of microcapsules. In addition, the inner surface of most of the microcapsules seemed well-shaped and crack-free (Figure 9.17). However, cracks can be seen in few cases like the fractured microcapsule shown in Figure 9.16.

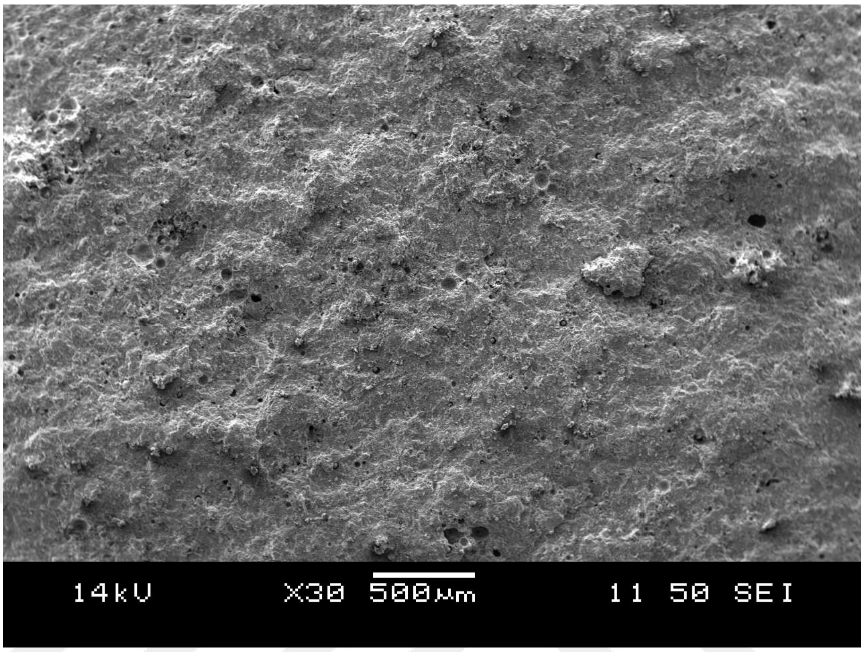

Figure 9.15 SEM image of fractured surface of the disk-shaped specimens

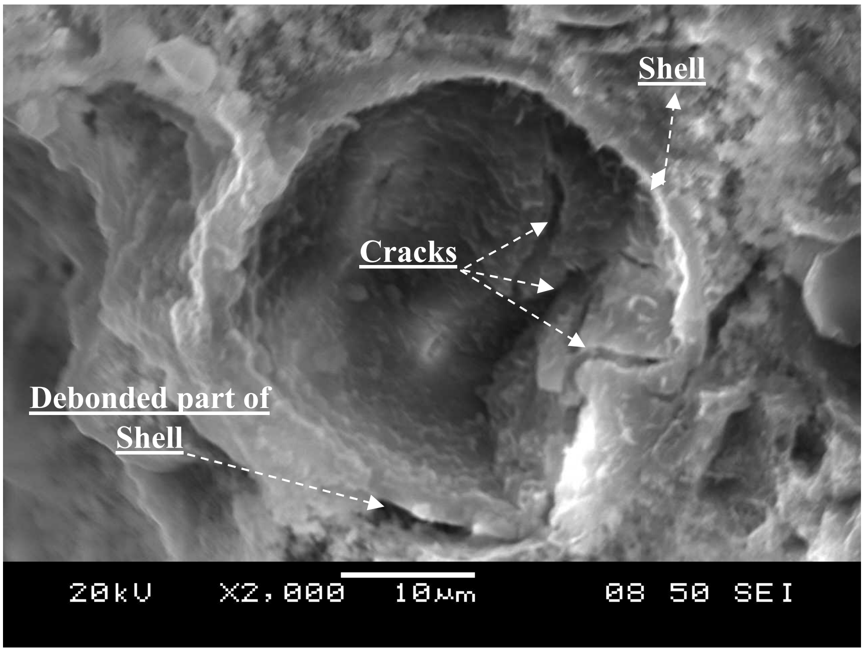

Figure 9.16 Closer examination of a fractured microcapsule

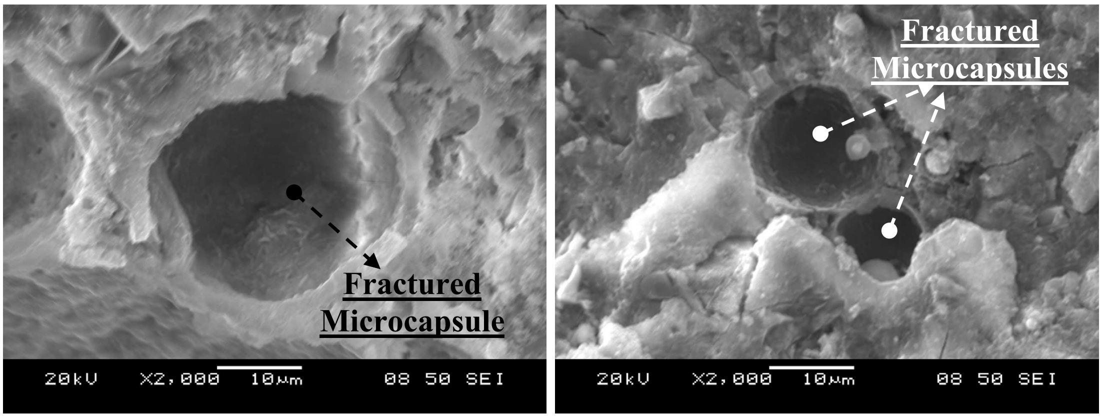

Figure 9.17 SEM images of fractured microcapsule (×2000)

The solid core phenomenon, discussed earlier in the SEM analyses of microcapsules, was also observed in the few fractured microcapsules embedded in matrix (Figure 9.18). These kinds of microcapsules may have cracks on their shell, so the liquid sodium silicate solution may have become solid material with the air-drying process. The EDS analyses conducted on the shell of these fractured microcapsules revealed a 0.2–0.69 Si/C ratio. However, Si/C ratio of solid spherical part of microcapsule was calculated to be 4.1–4.6, which indicates their high Si content. Therefore, it can be noted that spherical material which consist of mostly silicate shows the dried inner material of microcapsule.

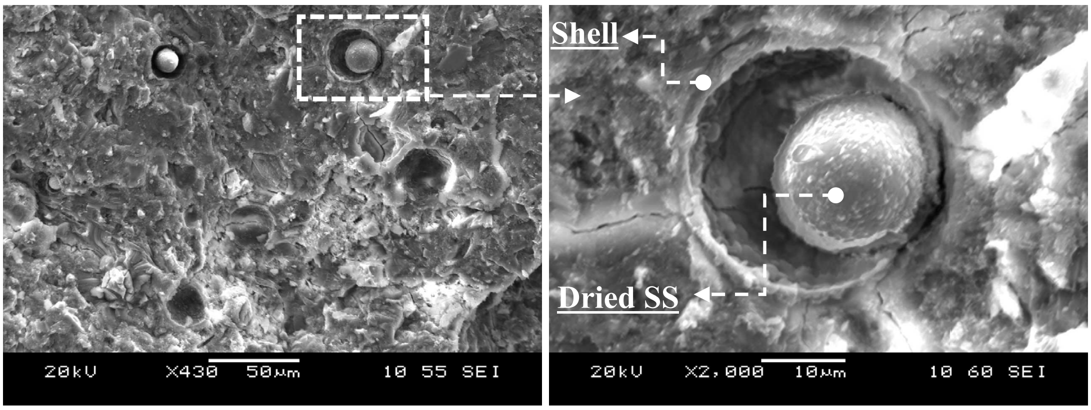

Figure 9.18 SEM images of fractured microcapsules (×430 and ×2000)

9.2.2 Optimization of Core Material Components

In order to describe the core material components optimization procedure, it is necessary to remind the solutions used in the synthesis process of previous section. Three solutions were prepared in the synthesis process as follows: 1) S1 is a solution of surfactants, which are Span 85 (2 g) and POEDO (1 g), in 45 mL of toluene, 2) S2 is a solution of shell-forming substances, which is monomer (MDI) and a few droplets of catalyst, in 7.5 mL of S1 and 12.5 g of additional toluene, and 3) S3 is solution of SS (7.5 g) in 7.5 mL of deionized water, called core material.

In previous section, four different S2 solution were prepared by using 7.5, 10, 12.5, and 15 g of MDI. The shell-forming monomer to core material ratios were 0.50, 0.67, 0.83, and 1.00, respectively. It was concluded from the yield, SEM, and TG analyses that the optimum shell-forming monomer to core material ratio was 0.67 (MDI-2 mixture). In this section, the components of S3 solution (core material), the SS and deionized water, were optimized through the yield and SEM analyses. For this purpose, four different S3 solutions were prepared by the SS to water ratios (by weight) of 1.00, 0.75, 0.25, and 0.00. It should be noted that the 0.50 ratio (MDI-2, the optimized mixture) was already used in the previous section. Therefore, four different microcapsules, hereafter called SS/W-100, SS/W-75, SS/W-25, and SS/W-0, were synthesized in this section. The synthesis process was described in details at section 3.2.2.

Microencapsulation yield values were calculated by the Equation 9.1. As can be seen from Figure 9.19, the yield value of SS/W-50 microcapsules (MDI-2), which was synthesized in previous section, is much higher than the other samples. On the other hand, the lowest yield value was obtained in the SS/W-0 sample. It should be noted that the core material solution of SS/W-0 was 100% water. It can be seen from the yield analysis results that increasing and especially decreasing the SS portion of core material solution has affected adversely the microencapsulation synthesis.

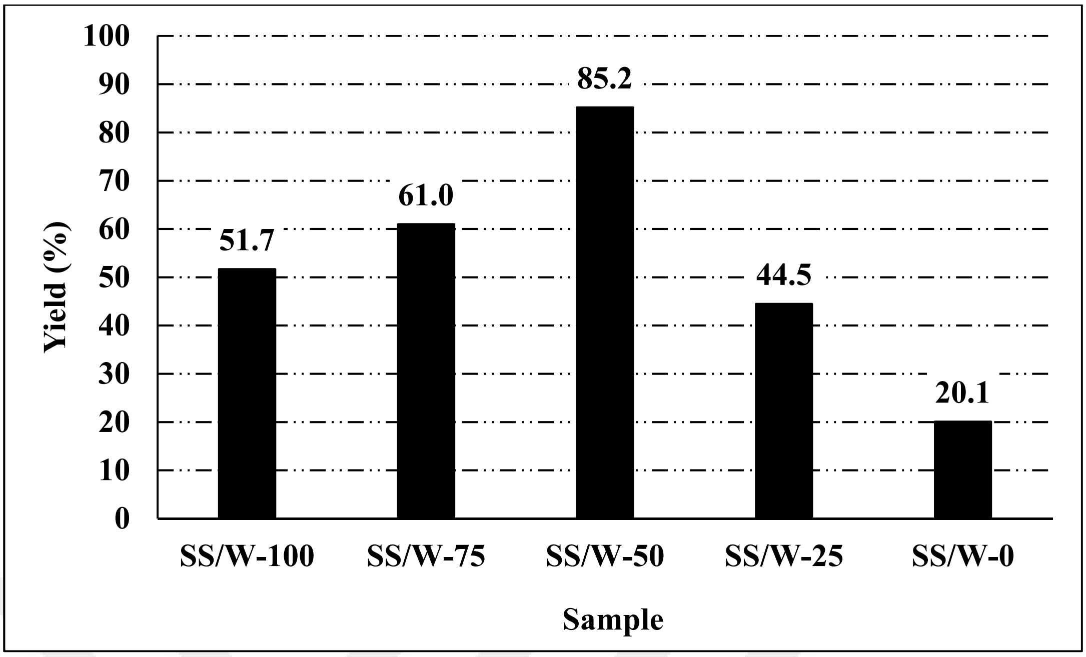

Figure 9.19 Yield values of microcapsules

Figure 9.20 shows SEM images of SS/W-5 (MDI-2) microcapsules synthesized in previous section. As can be seen from the figures, most of the microcapsules are spherical shaped. In addition, as described in previous section, the final dried sample was totally free-flowing powder with minimum clumping of microcapsules. The yield value of this mixture was 85.2%.

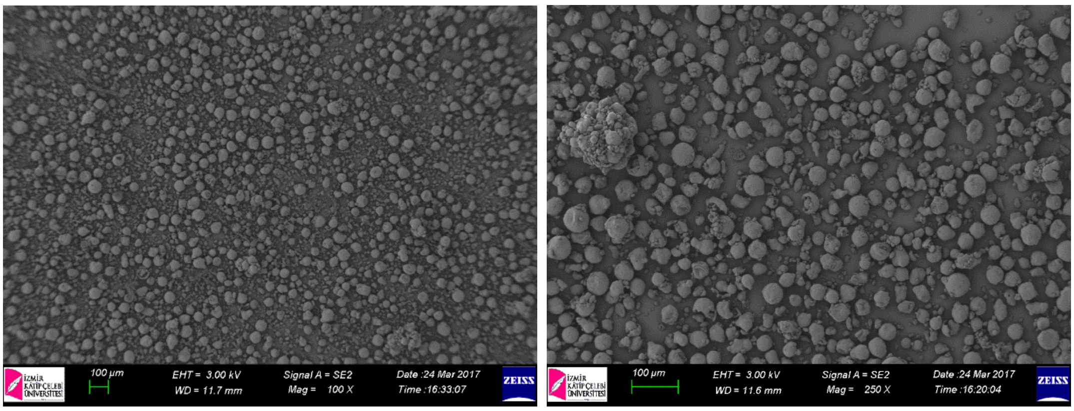

Figure 9.20 SEM images of SS/W-50 (MDI-2) microcapsules

Figure 9.21 shows SEM images of SS/W-75 microcapsules. As can be seen from the figures, most of microcapsules are not well-shaped and homogeneous. In addition, the particles with irregular shapes among the microcapsules increased as compared to the SS/W-50 mixture. Aggregation and clumping of microcapsules can also be seen in the SS/W-75 mixture. On the other hand, the microcapsules that be formed in SS/W-100 mixture were spherical shaped, but not homogeneous (Figure 9.22). In addition, the irregular-shaped particles extremely increased in this mixture. The yield value of SS/W-75 and SS/W-100 mixtures were 61%and 51.7%, respectively. It is obvious that increasing the SS portion of core material solution (S3) were adversely affected the yield and morphology of the sodium silicate/polyurethane microcapsules.

.

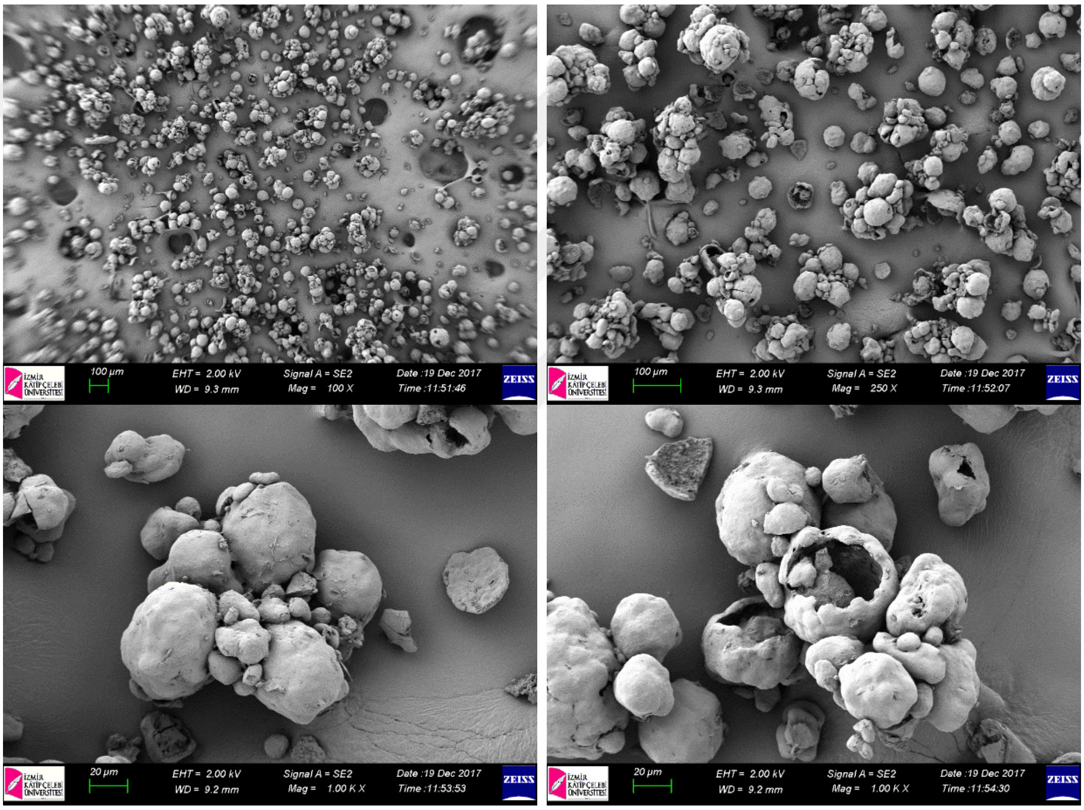

Figure 9.21 SEM images of SS/W-75 microcapsules

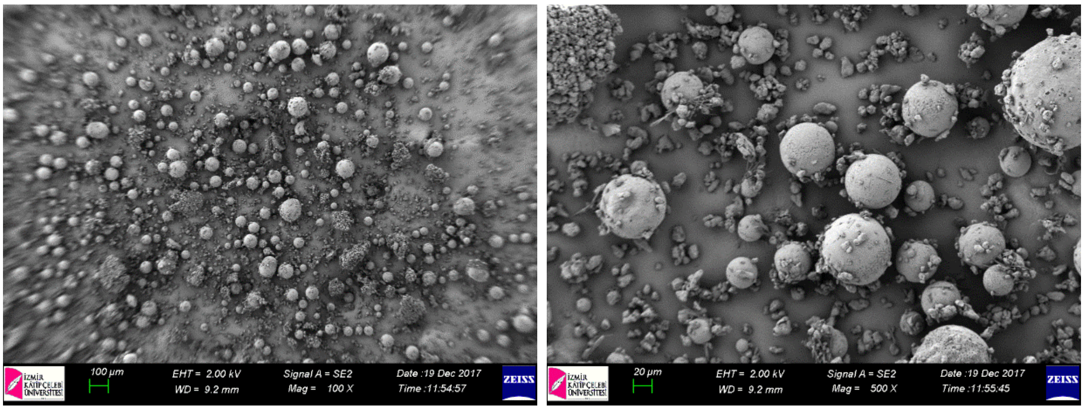

Figure 9.22 SEM images of SS/W-100 microcapsules

Figure 9.23 shows SEM images of SS/W-25 microcapsules. As can be seen from figures the microcapsules can be seen rarely. In other words, microencapsulation efficiency was adversely affected by decreasing the SS portion of SS core material solution from 0.5 to 0.25 (increasing the water content).

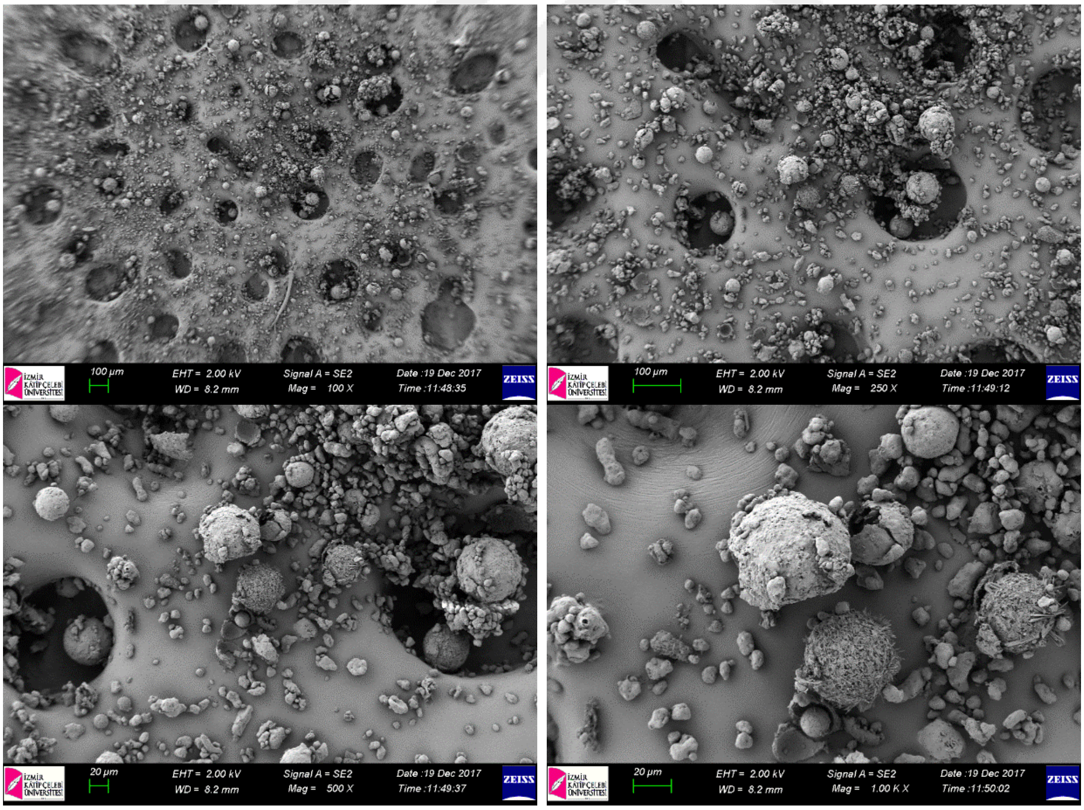

Figure 9.23 SEM images of SS/W-25 microcapsules

Figure 9.24 shows SEM images of SS/W-0 microcapsules. It can be seen from the figures that most of the microcapsules are not well-shaped and homogeneous. It should be noted that core material of these microcapsule was only water. The yield value of SS/W-25 and SS/W-0 mixtures were 44.5% and 20.1%, respectively. It is obvious that decreasing the SS portion of core material solution (S3) was also adversely affected the yield and morphology of the sodium silicate/polyurethane microcapsules.

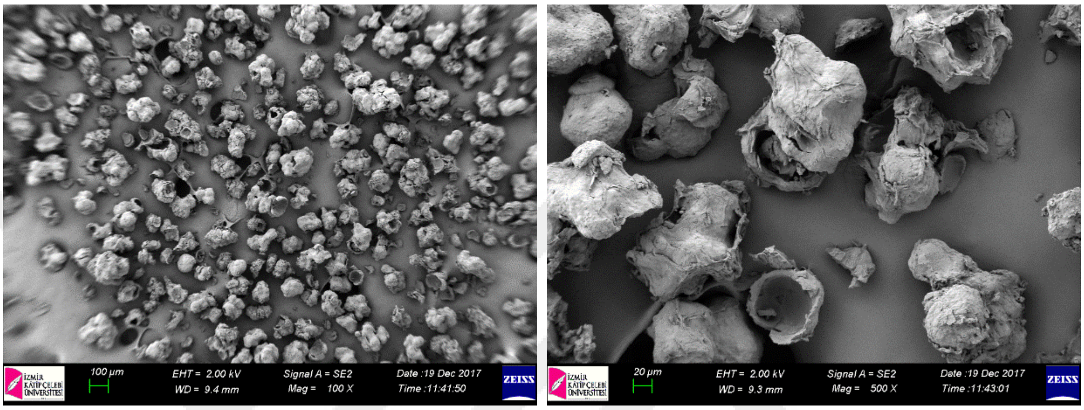

Figure 9.24 SEM images of SS/W-0 microcapsules

9.2.3 Optimization of Stirring Speed

The optimized SS/W-50 or MDI-2 microcapsules with shell-forming monomer to core material ratio of 0.67 and SS to water ratio of 0.5 was used in the continuation of the research program. To produce more microcapsules in a single batch, the amounts of all materials used in the synthesis process were doubled. Therefore, the syntheses were carried out in 250 mL beaker instead of 100 mL beaker. As discussed earlier, a magnetic cylindrical stirrer bar with 30 mm length were used for agitation. However, it was observed that this cylindrical stirrer bar was not appropriate for the agitating of the new batch (doubled materials). In addition, the length of stirrer bar (30 mm) was not enough due the higher diameter of the 250 mL beaker. Oval and cylindrical stirrer bars with 30, 35, and 40 mm length were tested for the agitation. The oval one with 40 mm length was the most suitable stirrer bar among the other bars. The mixtures could be homogeneously stirred by the 40 mm oval stirrer bar at even high speed. However, the morphology and the yield values of microcapsules highly changed due to the different beaker and stirring bar. The microencapsulation is a complex process and any change in the process can affect the results.

As can be seen from Table 9.3, based on the preliminary tests nine different stirring procedures were carried out to obtain optimum stirring speeds. As described in details at Section 3.2.2.2, the stirring speed for emulsification (SS-E), stirring speed for formation of primary membrane (SS-FPM), and stirring speed for polymerization (PS) were 1000 rpm, 900 rpm, and 800 rpm, respectively. Except the EP3 experiment, in which the PE was very low (300 rpm), the microcapsules formed in all experiments.

Table 9.3 The stirring procedures performed in each experiment

Experiment Code	SS-E (rpm)	SS-FPM (rpm)	SS-P (rpm)	Description
Control	1000	900	800	Same speeds with previous sections.
EP1	800	700	600	Decreasing of speeds.
EP2	700	600	500	Decreasing of speeds.
EP3	500	400	300	Too low PE speed. Experiment was failed
EP4	600	600	600	Constant speed.
EP5	500	500	500	Constant speed.
EP6	600	600	800	Higher and constant ES and SSFPM speeds
EP7	600	500	500	Lower and constant SSFPM and PE speeds
EP8	600	700	700	Higher and constant SSFPM and PE speeds

Microencapsulation yield values were calculated by the Equation 9.1. As can be seen from Figure 9.25 the yield value of microcapsules decreased from 85.2% (see figures 9.7) to 57.4%. The highest yield value (75.9%) was obtained in the EP7 experiment. The yield value is one of the most important criteria that can give an opinion about the efficiency of microencapsulation. On the other hand, after vacuum filtration, sufficient washing, and drying in air, a more free-flowing powder of microcapsules was obtained in the EP7 experiment. In other words, the aggregation and clumping of microcapsules was rarely observed in the EP7 experiment. However, a large amount of aggregation and clumping of microcapsules was observed in some of the samples such as the EP6 and EP8 experiments. To give an opinion a SEM image of the microcapsules obtained from the EP6 experiment is presented in Figure 9.26.

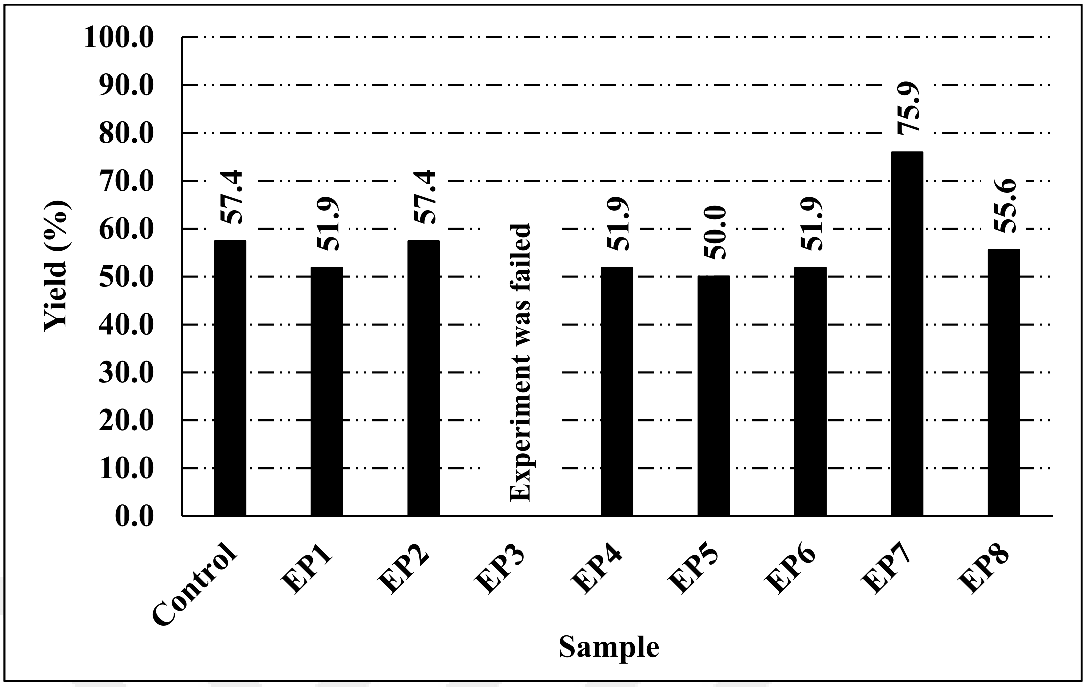

Figure 9.25 Yield values of microcapsules

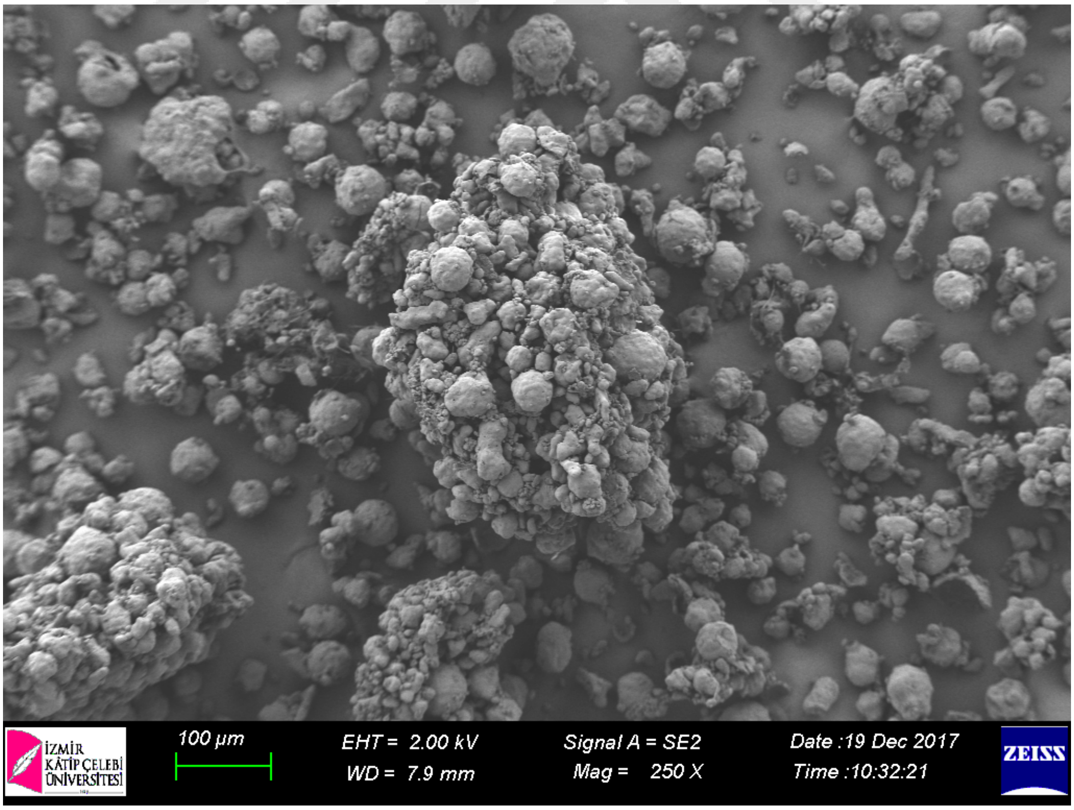

Figure 9.26 The microcapsules synthesized via the EP6 procedure

Many SEM/EDS analyzes were conducted on the microcapsules. The most well-shaped microcapsules were also observed in the EP7 sample. However, the microcapsules with random shapes can be seen among the spherical microcapsules. For example, the EDS analyzes of two microcapsules with spherical and random shapes are presented in Figure 9.28. The EDS shows that both of the microcapsules consist of C, O, Na and, Si elements. Therefore, it revealed the existence of polyurethane (shell material) and sodium silicate (core material).

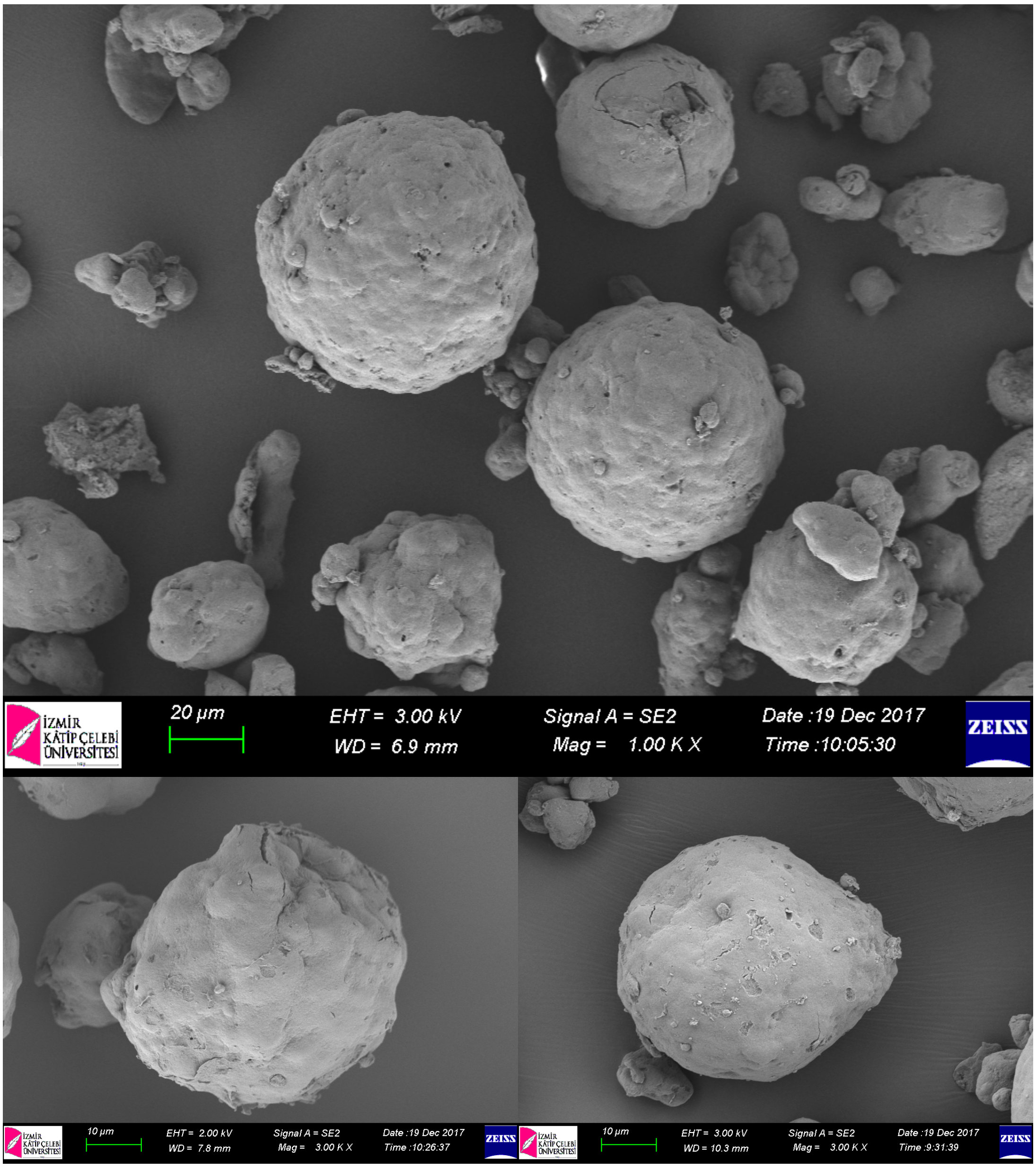

Figure 9.27 The microcapsules synthesized via the EP7 procedure

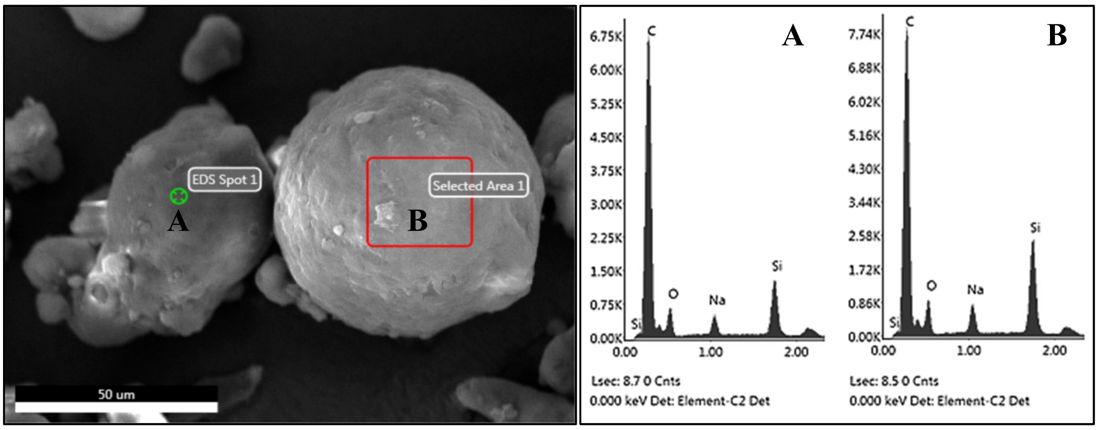

Figure 9.28 The EDS spectrums presenting the chemical composition of EP7 microcapsules

In addition, the particles with irregular shapes can be found among the microcapsules. This particles were also observed in the previous sections. It can be concluded from EDS analysis that these particles consist mainly of polymer (Figure 9.29). Furthermore, Figure 9.30 shows the EDS spectrums of a cylindrical-like particle and a well-shaped spherical microcapsule. The EDS analysis revealed that the cylindrical-like particle has also consist mainly of shell-forming material.

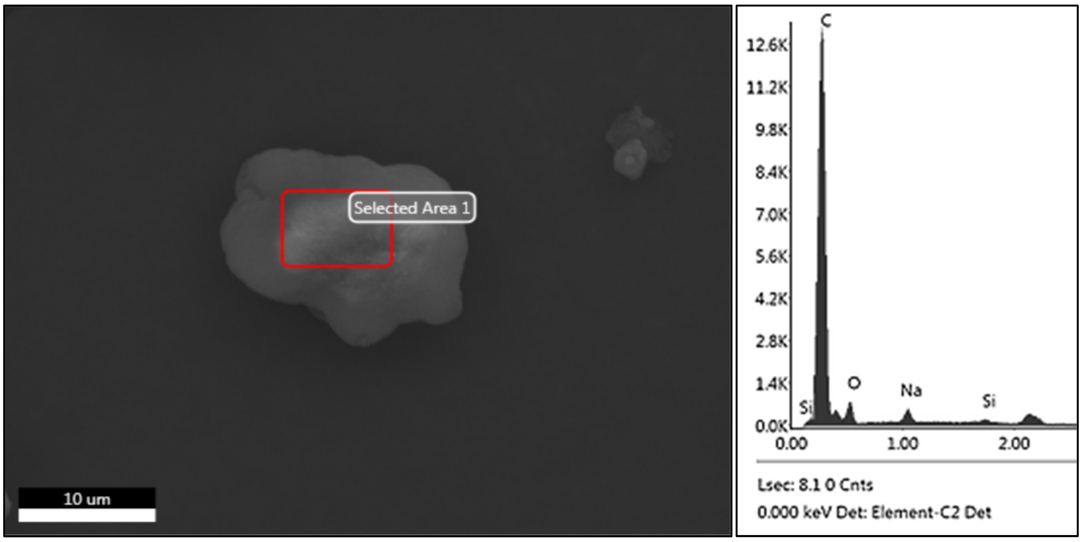

Figure 9.29 The EDS spectrum presenting the chemical composition of irregular-shaped particles

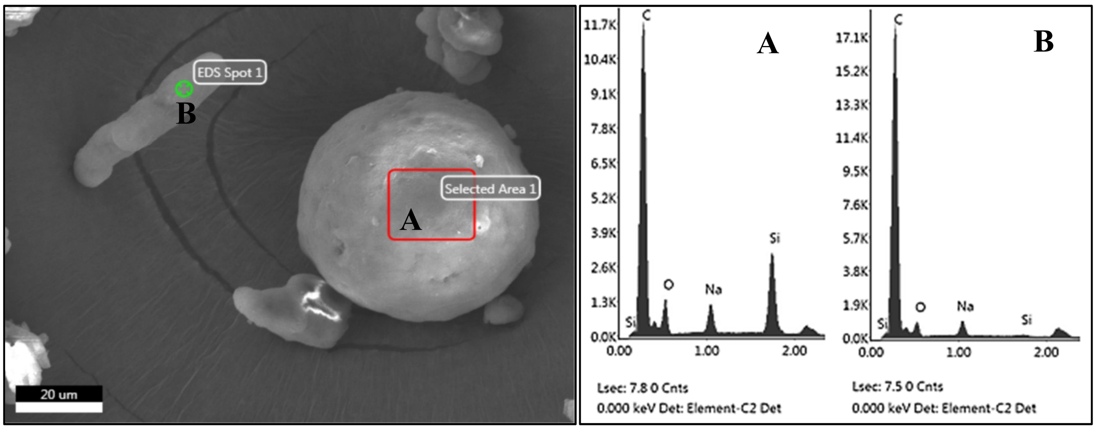

Figure 9.30 The EDS spectrum presenting the chemical composition of cylindrical-like particle

Besides the yield and the morphology of the microcapsules, the average diameter of them has also changed with the new procedure. The average diameters of microcapsules were obtained by measuring of at least 50 microcapsules. The measuring were also carried out on the digital microscope images (9.31). As discussed earlier the average diameter of optimized microcapsules (SS/W-50 or MDI-2) was 29 µm. However, the measurements conducted on the SEM and digital microscope images revealed that the average diameter of the microcapsules synthesized via the EP7 procedures increased to 65 µm. The diameter microcapsules can increase by decreasing the SS-E (Brown et al., 2003).

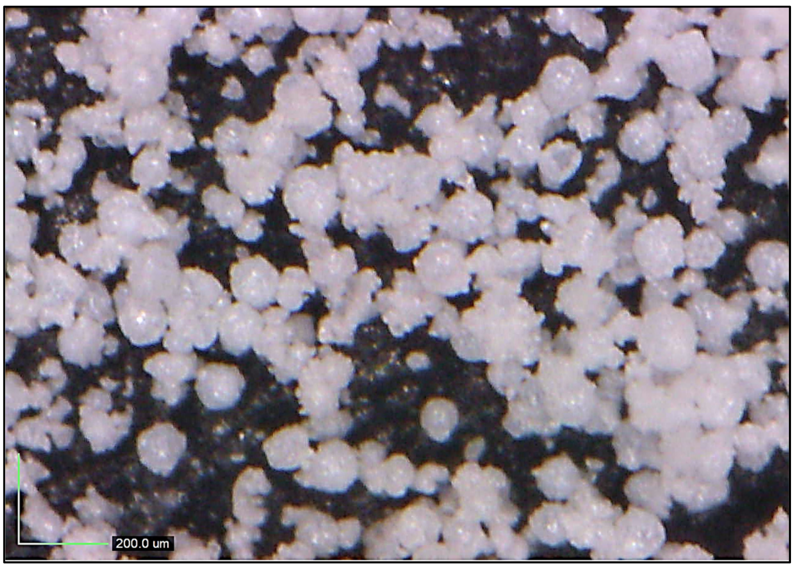

Figure 9.31 A digital microscope image of the microcapsules synthesized via the EP7 procedures

The measurements of the shell thickness of microcapsules were performed on the fractured microcapsules (Figure 9.32). The measurements showed that the shell thickness of microcapsules has not considerably changed. It should be noted that the measurements were performed on at least six well-shaped spherical microcapsules (Figure 9.33). Similar to the previous sections, the average shell thickness was 3 µm. In other words, applying different stirring procedure, increasing the amount of raw materials (doubled materials), and using different beaker/stirring bar did not affect remarkably the shell thickness of microcapsules.

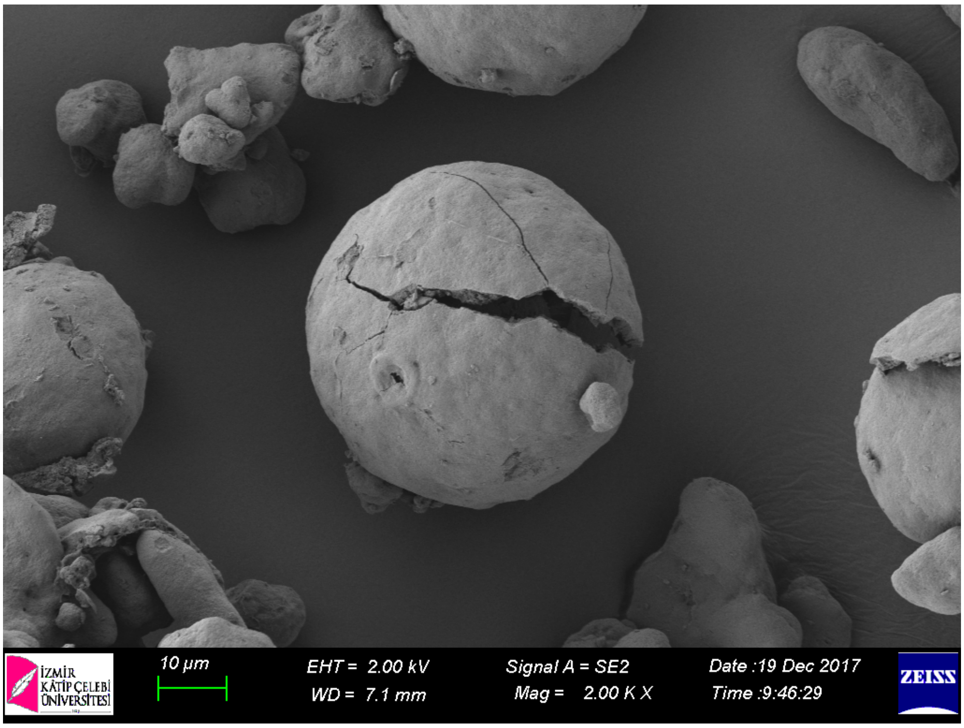

Figure 9.32 A fractured microcapsule synthesized via the EP7 procedures

As can be seen from the cross section of shell, the porosity of shell is higher near the inner face. Furthermore, it can be seen that the inner face is highly rough. Similar properties were also seen in the microcapsules synthesized in previous sections.

It can be concluded that applying different stirring procedure, increasing the amount of raw materials (doubled materials), and using different beaker/stirring bar have affected only the yield value and the average diameter of the microcapsules (SS/W-50 or MDI-2).

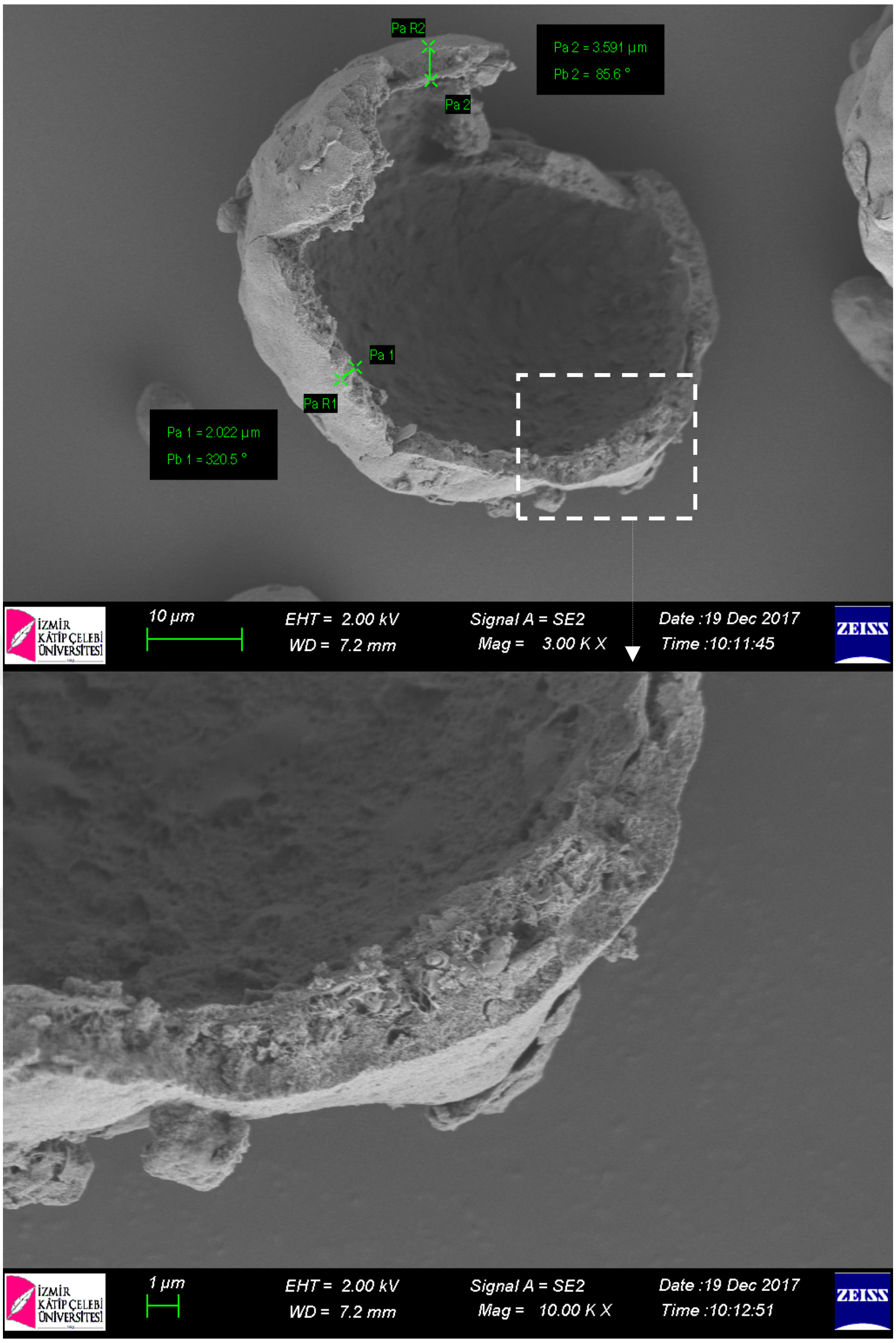

Figure 9.33 Cross section of a fractured microcapsule synthesized via the EP7 procedures

9.3 Incorporation of SS-loading Microcapsules in UHPC Mixtures

In this section of thesis, the sodium silicate/polyurethane microcapsules, which its synthesis parameter such as shell-forming monomer, core material (healing agent), and stirring procedures had been optimized, were incorporated in the UHPC mixtures.

9.3.1 Second Washing/Drying Process of Microcapsules

As described in details at section 3.2.2.2, after vacuum filtration, sufficient washing, and drying in air, a free-flowing powder of microcapsules can be obtained. In other words, the aggregation and clumping of microcapsules was rarely observed in the optimized microcapsules. However, a certain amount of clumping can be seen even in well optimized and washed microcapsules, especially in the doubled materials batches (Figure 9.34). The clumping of microcapsules can lead to an inhomogeneous dispersion of microcapsules in UHPC mixtures. Therefore, the microcapsules were subjected to second washing/drying process as discussed in the following paragraphs.

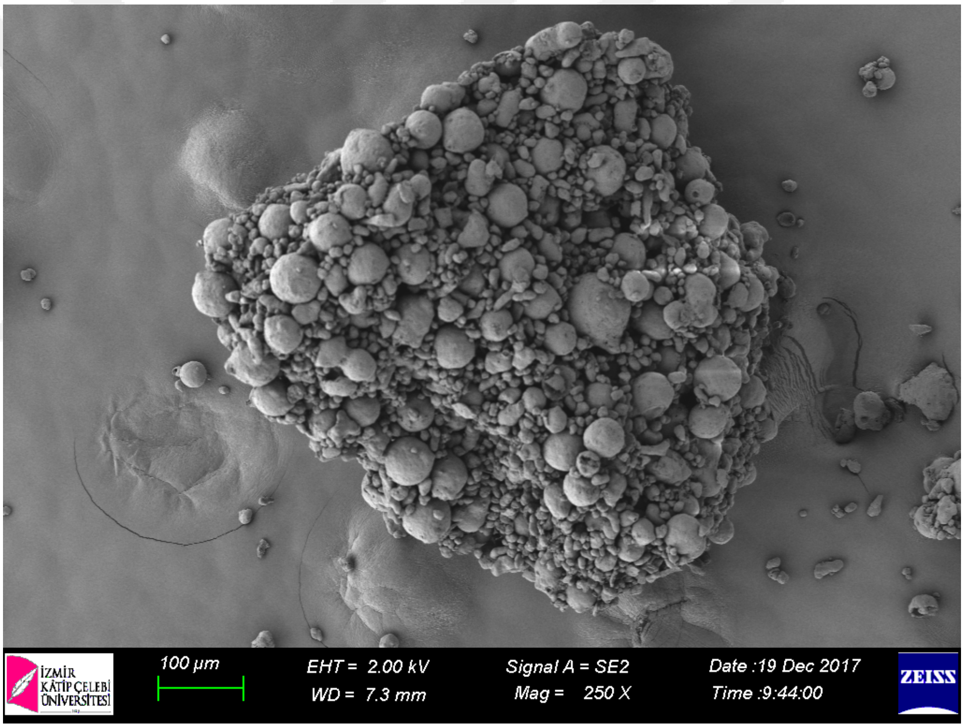

Figure 9.34 The aggregation and clumping of microcapsules synthesized via the EP7 procedures

In order to obtain homogeneous and more free-flowing powder, the microcapsules synthesized in separate batches (doubled materials) were mixed with each other and then, were dispersed in certain amount of toluene (1000 mL beaker). The slurry of microcapsules was agitated with the magnetic stirrer for 20 minutes (Figure 9.35). The microcapsules were vacuum filtered, and then washed with ethanol/water. The wet microcapsules were transferred to watch glasses and then, were dried at room temperature for 48 h (Figure 9.35). As can be seen from figure 9.36, the dried microcapsules were highly homogeneous and free-flowing powder.

Figure 9.35 The second washing/drying process of microcapsules (Personal archive, 2018)

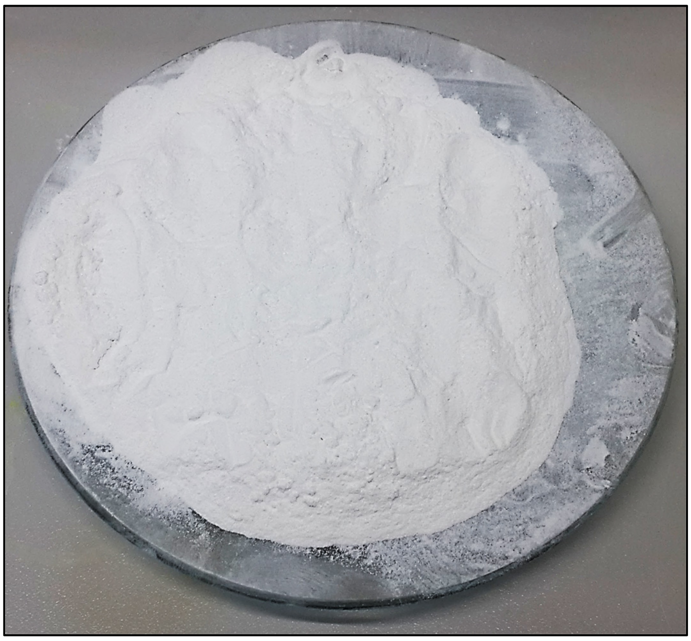

Figure 9.36 Microcapsules powder after the second washing/drying process (Personal archive, 2018)

EDS image and spectrum of a microcapsule, which was analyzed after the second washing/drying process, is presented in Figure 9.37. Similar to the previous sections, the EDS shows that the microcapsules consist of C, O, Na and, Si elements. Therefore, it revealed the existence of polyurethane (shell material) and sodium silicate (core material).

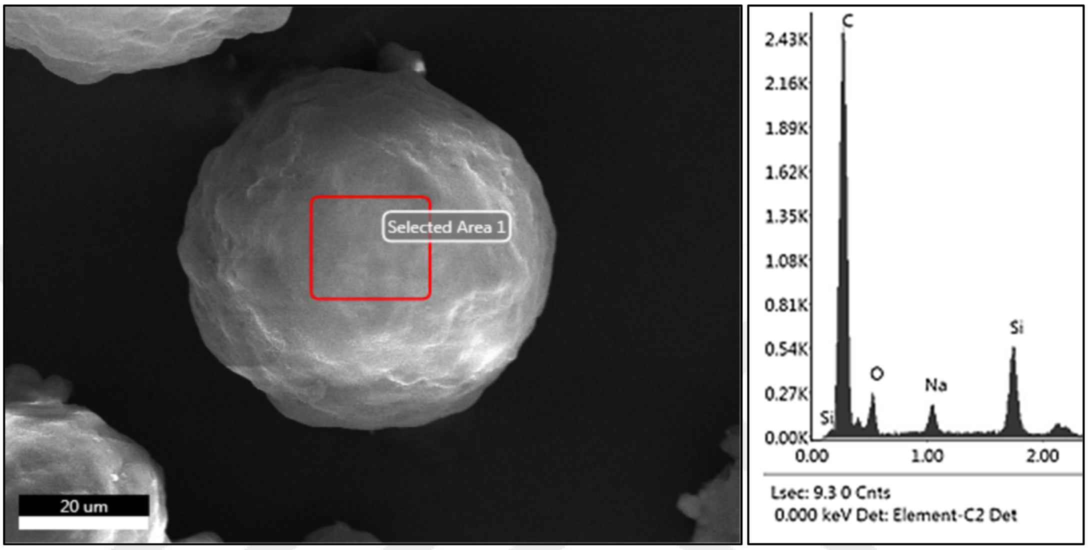

Figure 9.37 EDS image and spectrum of a microcapsule after the second washing/drying process

9.3.2 Mix Designs and Fresh Properties of Microcapsule Containing Mixtures

The SS-loading polyurethane microcapsules were incorporated in the Control and GGBFS-G1 mixtures. Two different microcapsule bearing Control mixtures were prepared as follows:

- WM_Control: In this mixture, firstly the microcapsules were dispersed in water of mixture (approximately 90% of the required water). The mixture was agitated with the magnetic stirrer until to achieve a homogeneous water-microcapsules suspension. The microcapsules were successfully suspended in water due to their small size and also similar specific gravity with water. This application was done to ensure that the microcapsules remained hydrated and no clusters were formed in UHPC mixtures. Kanellopoulos et al. (2017) have also dispersed SS-loading gelatin/acacia gum microcapsules in the water for above-mentioned purposes. In addition, this application might lead to homogeneous dispersion of microcapsule in cementitious matrix. Half of the required superplasticizer (SP) was also added to the water-microcapsule suspension. It was observed that a more homogeneous suspension could be obtained by adding superplasticizer. Dry ingredients of mixtures were premixed for five minutes. Then, the suspension was added to the dry mixture. The remaining water (approximately 10%) was mixed with the remaining SP and then, poured into the mixer. It should be noted that any microcapsules remaining in the suspension beaker were also poured into the mixer using the remaining water/SP mixture. After normal speed for about 5 minutes, mixing continued for another 15 min in high speed.

- DM_Control: In this mixture, the microcapsules were directly added to the other dry ingredients of mixtures. Same procedure were carried out in the case of the M_GGBFS-G1 mixture

Microcapsules were used in a concentration of 5% with respect to cement weight (40 kg/m^3). The mix designs of microcapsules bearing UHPC mixture are presented in Table 9.4. The dosages of water, cement, GGBFS, and micro fibers were kept constant in the microcapsule bearing mixtures. In other words, the required volume for microcapsules was provided by reducing the amount of aggregate. The specific gravity of microcapsule was considered 1.00. This assumption were based on the specific gravity of raw materials and the high stability of water-microcapsules suspension. This assumption in mix design was also checked by comparing the volume and the unit volume weight of the calculated and the real fresh mortar. Furthermore, Kanellopoulos et al. (2016) have used a value of ~0.98 g/cm^3 for density of a SS-loaded microcapsule.

As expected, the microcapsules have increased the SP demand, especially in GGBFS-G1 mixture (Table 9.4). The SP demand of WM_Control mixture were 2 kg/m^3 lower than the DM_Control mixture. This behavior may be attributed to the better dispersion of microcapsules in WM_Control mixture. As mentioned earlier the required amount of superplasticizer was used to achieve 260 ±10 mm free flow value.

Table 9.4 Mix design of microcapsule containing UHPC mixtures

Mixtures	Water	Cement	Fiber	GGBFS	Microcapsule	Quartz aggregate			SP
						0-0.4 (mm)	0.4-1 (mm)	1-3 (mm)	
Control	176	800	143	-	-	330	463	529	23
WM_Control	176	800	143	-	40	305	427	489	28
DM_Control	176	800	143	-	40	305	427	489	30
GGBFS-G1	264	800	143	400	40	189	265	303	11
M_GGBFS-G1	264	800	143	400	40	165	230	264	17

9.3.3 The Effect of Microcapsules on Compressive Strength of UHPC mixtures

The compressive strength test results are the average of three 50×50×50 mm cubic specimens. The 7-day and 28-day compressive strengths of all mixture are presented in Figure 9.38. It should be noted that the 7-day compressive strength of Control and GGBFS-G1 mixture were determined in previous Chapters. It can be seen from test results that the incorporation of microcapsules decreased (13-14.6%) the compressive strength of Control and GGBFS-G1 mixture at 7 days. As mentioned earlier, the required volume for microcapsules was provided by reducing the amount of aggregate. Therefore, it is expected result that the replacing a part (7.6% in Control mixture - 12.95% in GGBFS-G1 mixture) of such a high strength aggregate like quartz with microcapsules leads to decreasing in compressive strength of UHPC mixtures.

As can be seen from Figure 9.38, the 28-day compressive strength of WM_Control mixture and Control mixture are almost the same. In other words, the negative effect of microcapsules in compressive strength (13% reduction) of Control mixtures was not observed at 28 days. However, the 28-day compressive strength of DM_Control mixture was 5.3% less than the Control mixture strength. This difference between WM_Control and DM_Control mixtures can also be attributed to the better dispersion of microcapsules in WM_Control mixture. The 28-day compressive strength of M_GGBFS-G1 mixture was only 2.7% less than the GGBFS-G1 mixture strength.

As discussed earlier the average diameter of microcapsules incorporated in the UHPC mixtures was 65 µm. It is seems that the using of such small microcapsules in UHPC mixture has negligible effects on the compressive strength. Kanellopoulos et al. (2016) have also reported the lower effects of small microcapsules (not too small like 5 µm) on compressive strength.

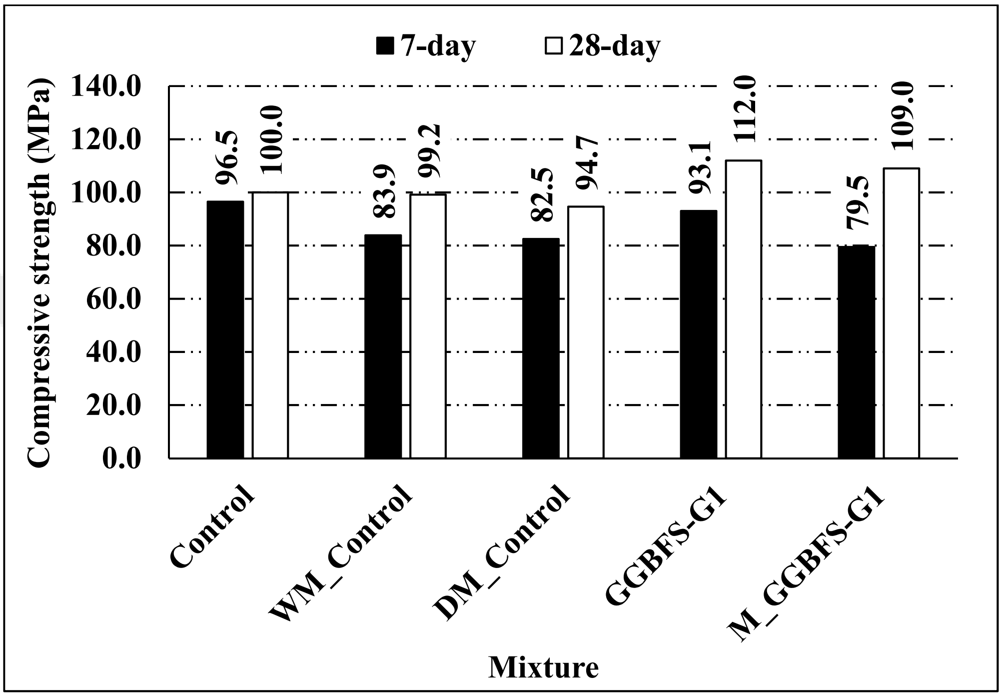

Figure 9.38 Compressive strengths of microcapsule containing UHPC mixtures

9.3.4 Evaluation of Self-Healing Mechanism Using Crack Closing Test

The crack closing or self-healing ratios of 7-days specimens (cracked after 7 days water curing) after 15-day and 30-day healing periods are presented in Figure 9.39. It should be noted that the crack closing ratios of Control and GGBFS-G1 mixture were determined in previous Chapters. The crack closing ratio of the GGBFS-G1 mixture was already 100%. Therefore, the effect of microcapsules on the self-healing ability of this mixture cannot be observed. As expected the crack closing ratio of the M_ GGBFS-G1 mixture was also 100%.

The positive effect of microcapsules can be seen in Control mixture. The contribution of sodium silicate, which is the core material of microcapsules, in the reactions at the cracked surfaces is obvious. The reaction between of SS and $Ca(OH)_2$ in the case of presence of water is given as follow (Alghamri et al., 2016; Giannaros et al., 2016; Pelletier et al., 2011):

$$Na_2SiO_3 + Ca(OH)_2 + H_2O \rightarrow {}_X(CaO \cdot SiO_2)H_2O + Na_2O \qquad (9.2)$$

It can be seen that the reaction between calcium hydroxide, a product of cement hydration, and SS can produce secondary calcium-silica-hydrate (C-S-H) gel.

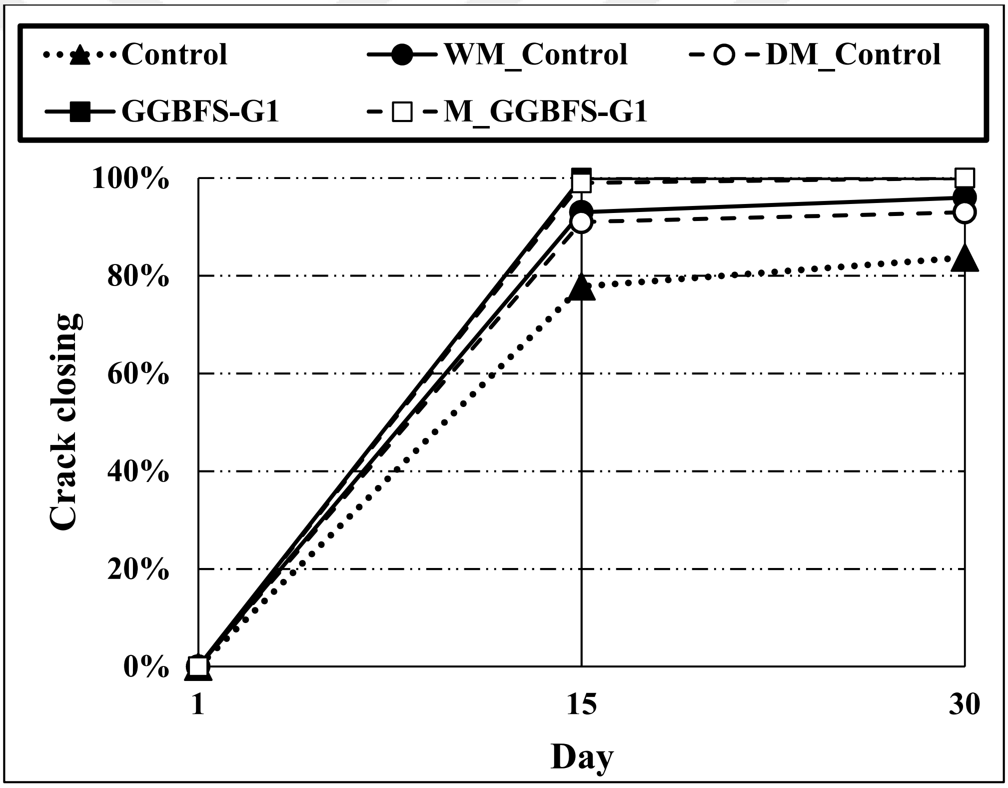

Figure 9.39 The crack closing ratios

After 30 days healing period, the cylindrical specimens were split by hand from the cracks. SEM/EDS analysis were conducted on the fractured surfaces to observe the healing products as well as the fracture microcapsules. As can be seen from Figure 9.40, various products were formed throughout the fractured surfaces of WM_Control mixture during the 30 days healing period. In other words, the healing products have covered the entire surfaces. Therefore, most of the fractured microcapsules cannot be observed in the surfaces. Ettringite clusters as well as individual ettringite crystals can be seen throughout the fractured surfaces (Figures 9.41 and 9.42). Secondary C-S-H gels can also be detected among Ca-rich products and ettringite crystals (Figure 9.41). $CaCO_3$ formation was also one of the main healing products Figures 9.43 and 9.44. The $CaCO_3$ was also formed on the fractured quartz aggregate. (Figure 9.43). Furthermore, massive Ca rich products with rose petal-like morphology were formed on many of the $CaCO_3$ crystals (Figure 9.44). As can be seen from Figure 9.45 similar crystals and products can be seen in many dome-shaped empties throughout the fractured surface. These empties can be air voids or fractured microcapsules. It is more likely to be fractured microcapsules. Figure 9.46 shows the SEM image of two dome-shaped empties close to each other captured at the M_GGBFS-G1 mixture. The fractured surface and one of the dome-shaped empty were covered by massive healing products, mainly $CaCO_3$. The other empty is absolutely a typical air void according to the EDS analysis and its appearance. The other one may be a fractured microcapsule that healing products were formed in its inner face after releasing the core material (SS). It can explained by the fact that the inner face of these microcapsules is highly rough. On the other hand, the inner surface of air voids is highly smooth (Figure 9.46). This finding were also observed in many regions of the fractured surfaces.

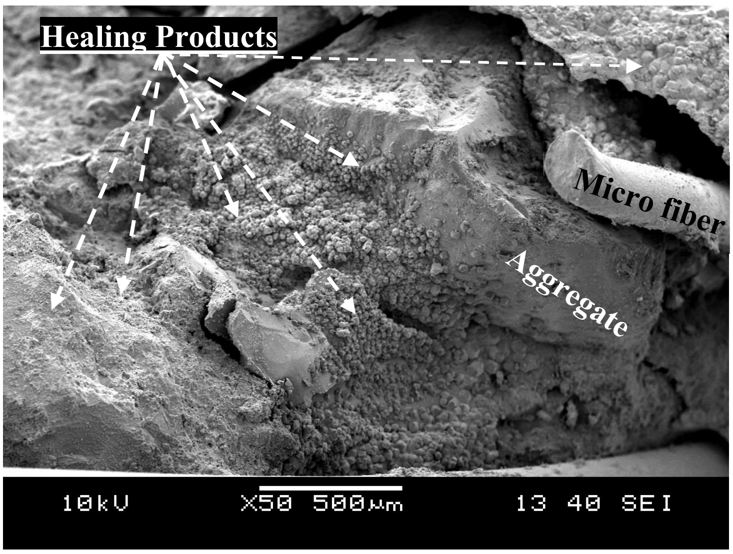

Figure 9.40 SEM image captured from fractured surface of WM_Control mixture after healing period

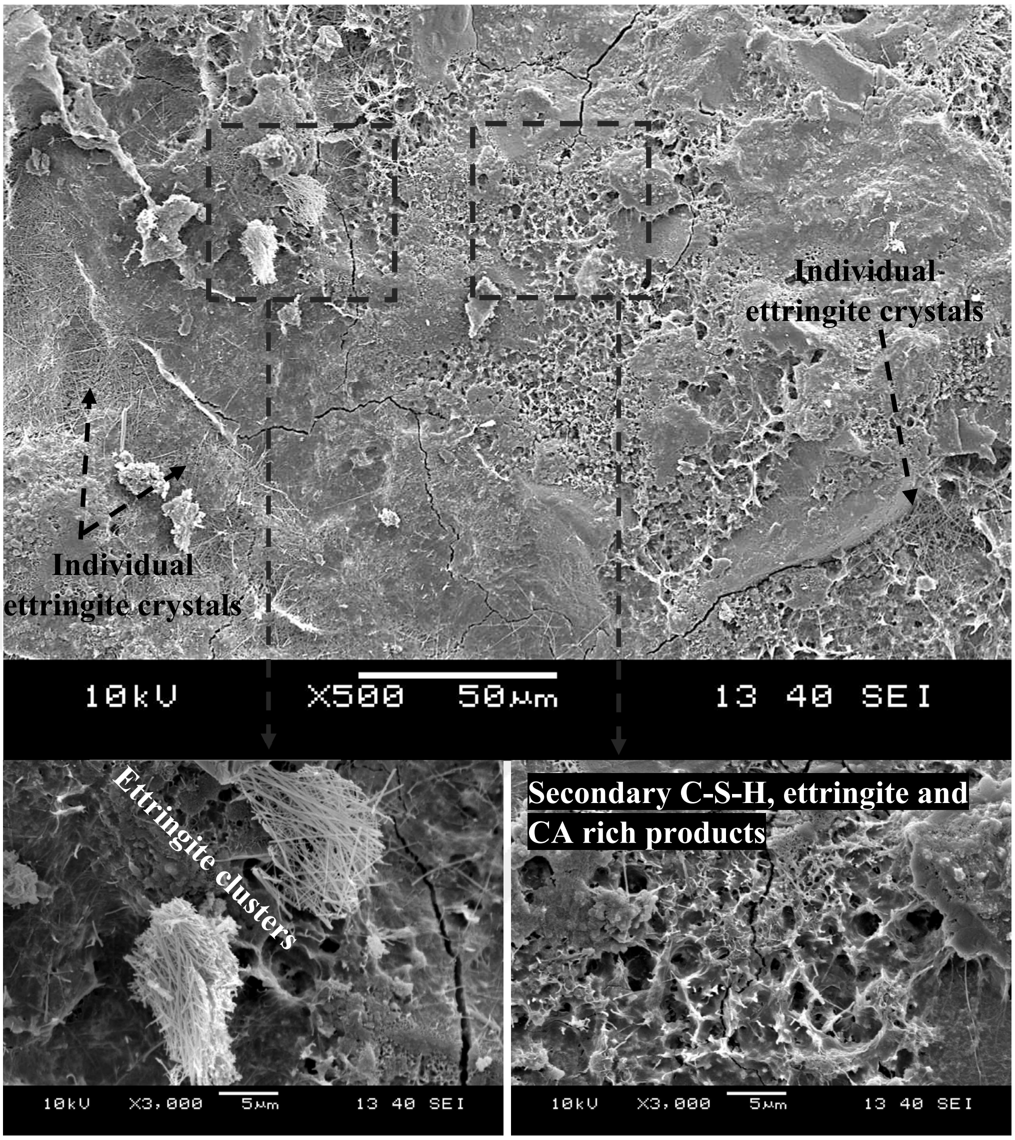

Figure 9.41 Healing products at the fractured surfaces of WM_Control mixture

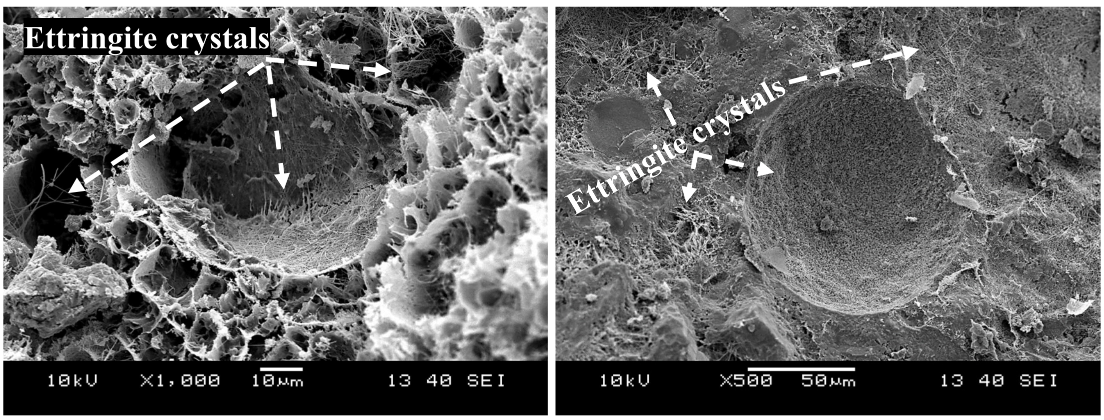

Figure 9.42 Healing products like Ettringite at the fractured surfaces of WM_Control mixture

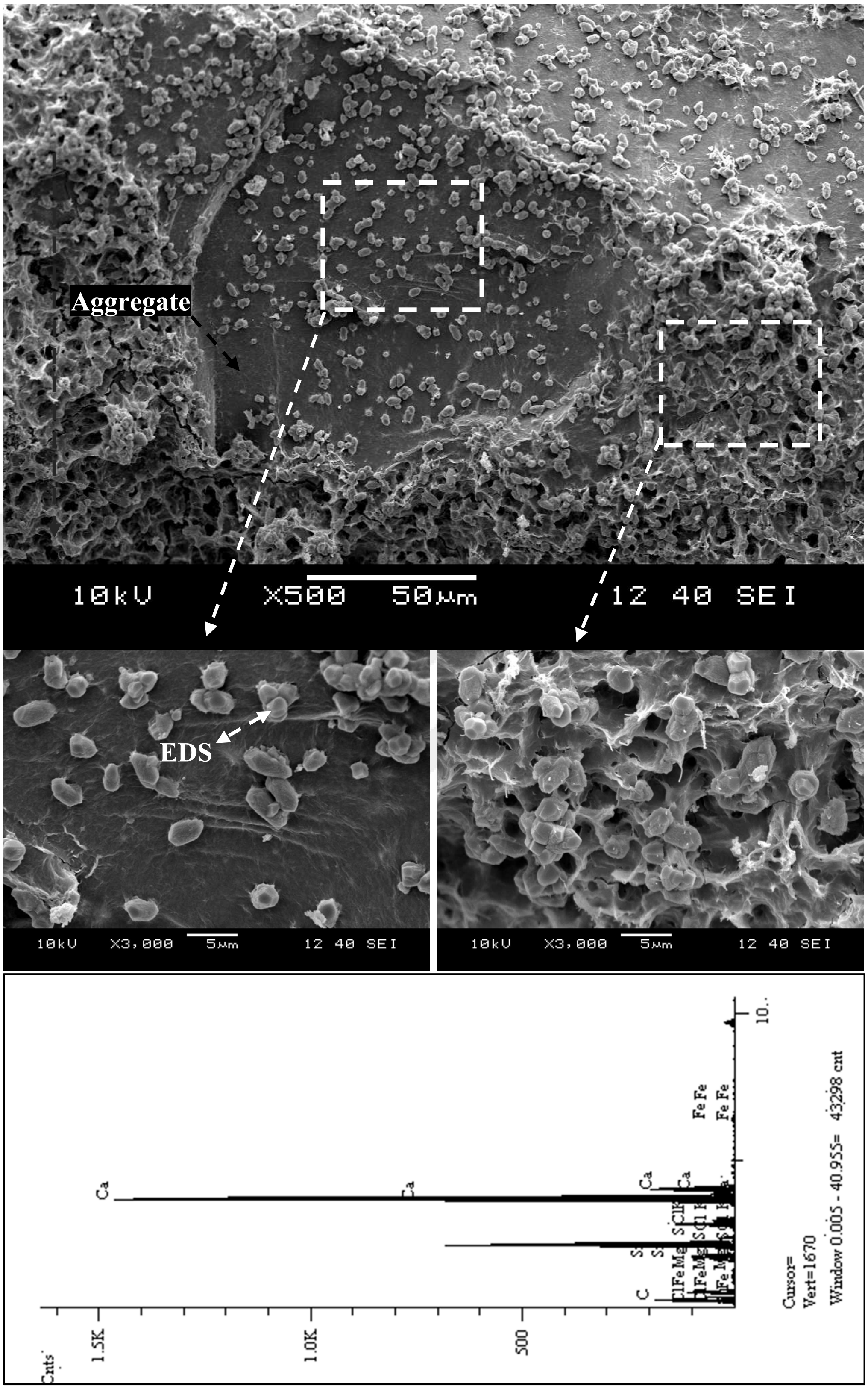

Figure 9.43 Healing products (mainly $CaCO_3$) formed at the surface of a fractured aggregate

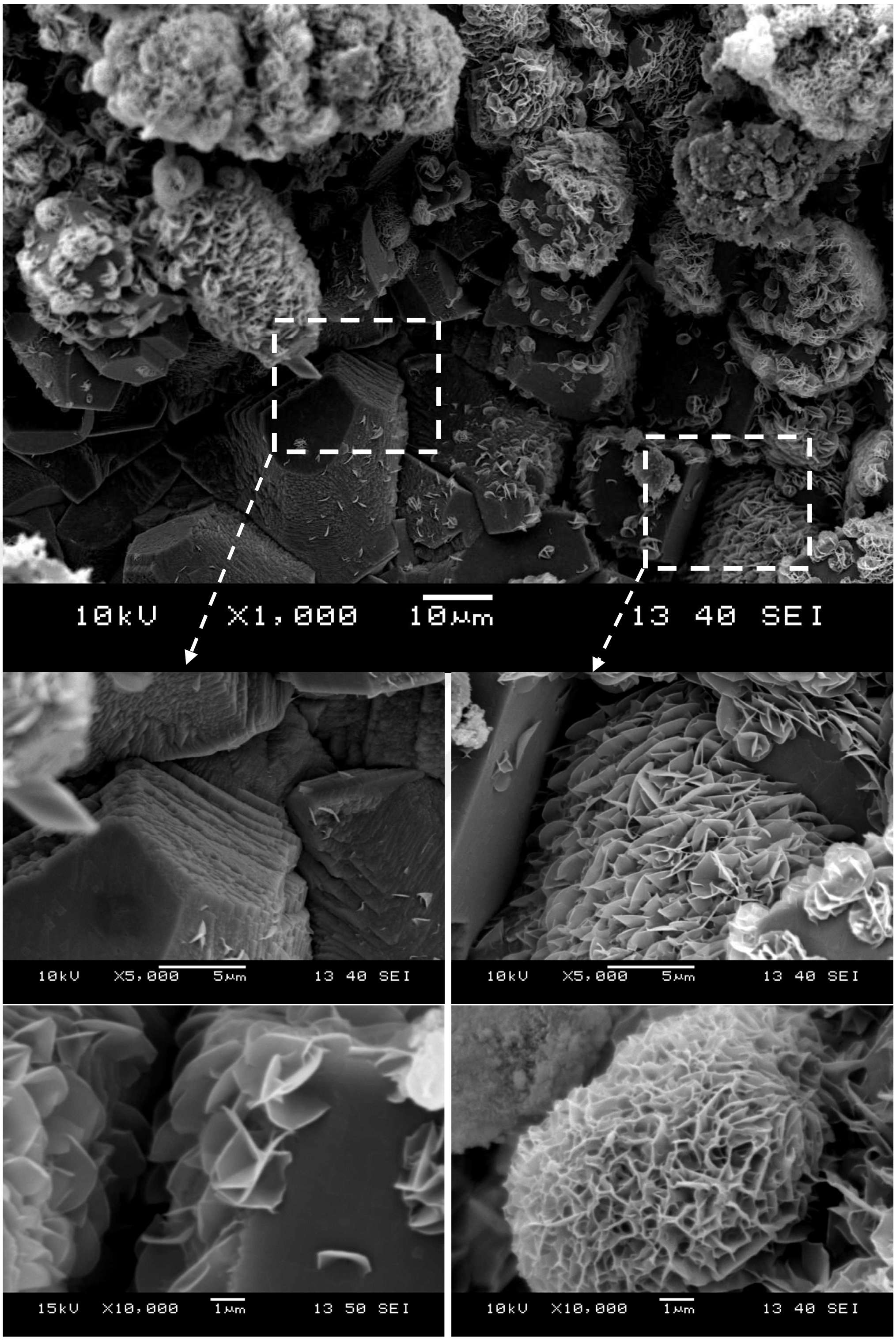

Figure 9.44 Massive $CaCO_3$ formation; and Ca-rich products with rose petal-like morphology

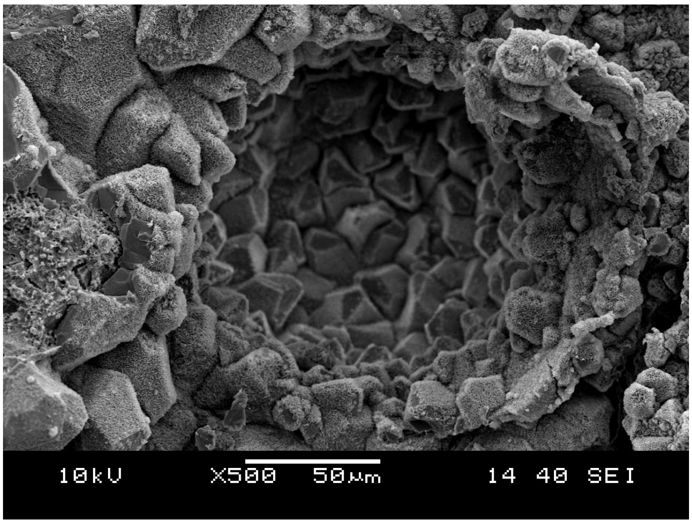

Figure 9.45 A dome-shaped empty covered by massive healing products

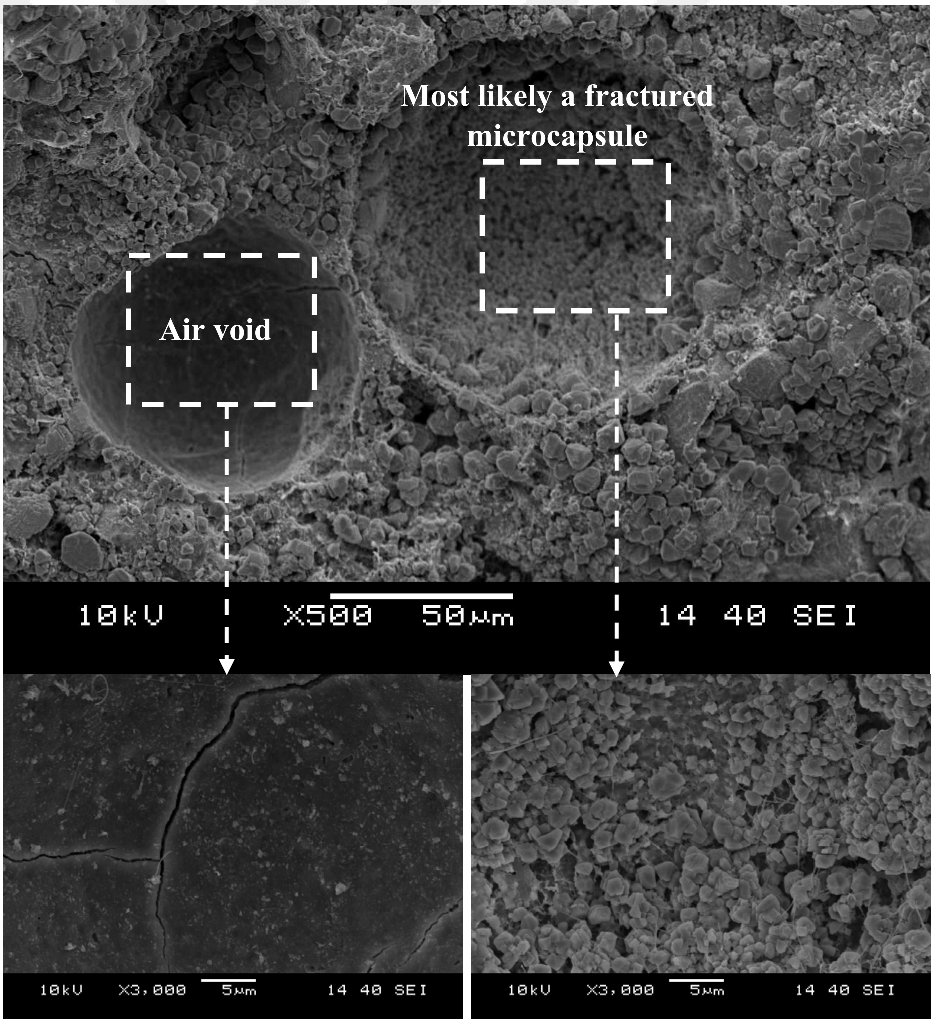

Figure 9.46 SEM image of two dome-shaped empties captured at the M_GGBFS-G1 mixture

CHAPTER TEN
MICROENCAPSULATION OF ISOPHORONE DIISOCYANATE

As discussed earlier, isophorone diisocyanate (IPDI), a monomeric aliphatic diisocyanate, has been used as a catalyst free healing agent in a few studies since 2008. The liquid phase diisocyanate monomer healing agent, IPDI, was microencapsulated for the first time via interfacial polymerization of polyurethane in a stabilized aqueous emulsion by J. L. Yang et al. (2008). J. L. Yang et al. (2008) have emphasized that "diisocyanates are reactive with water, introducing the possibility of one-part, catalyst-free self-healing system that is functional in an aqueous or moisture-laden environment" (p. 9650). As discussed in details earlier, the IPDI have been microencapsulated in a few studies with various polymeric shells for self-healing purposes in polymer based materials. However, IPDI have not been used as healing agent (in the form of core material of a microcapsule) in cement based composites up to now. On the other hand, the shell material of the IPDI-loaded microcapsules reported in literature are polymeric (organic).

In this chapter, microcapsules based on IPDI core (healing agent) and silica shell were synthesized via the interfacial polycondensation of a silica precursor (TEOS). Z. X. Yang et al. (2011) have encapsulated methylmethacrylate monomer and triethylborane as the healing agent with silica based shell through an interfacial self-assembly process. They have stated that the silica based shell of microcapsules form a stronger bond with the cementitious matrix. The shell can chemically and physically bonded to the matrix, allowing the microcapsule to remain stable for years without deterioration. Therefore, this study has dealt with the idea of possible microencapsulation of IPDI as a self-healing agent with silica-based shell for the first time in the literature.

As mentioned earlier, IPDI was microencapsulated via the interfacial polycondensation of a silica precursor (TEOS). This method has two main steps as follows: 1) dispersion of the oil phase (IPDI+TEOS) in water phase, 2) reducing the pH of emulsion to desired value solution to initiate the condensation of silica hydrolysates. Similar procedures have also carried out by H. Z. Zhang et al. (2011) for encapsulation of n-octadecane (a phase change material) with inorganic silica. As can be seen from Figure 10.1, H. Z. Zhang et al. (2011) have provided a nice schematic illustration of synthesizing silica based microcapsules through interfacial polycondensation. They have described the mechanism as follows: an oil mixture of TEOS and core material is dispersed in the aqueous solution containing surfactant to obtain an oil/water emulsion. Then, the HCl aqueous solution, catalyst, should be added into the emulsion. The water molecules/acidic catalyst can access to the surface of oil droplets (TEOS/core material) by penetration into the micelles. In the catalysis of acid, hydrolysis and condensation of the TEOS molecules on the surface of oil droplets begins (H. Z. Zhang et al., 2011).

H. Z. Zhang et al. (2011) have nicely summarized the process as follow:

> During this process, one ethoxyl group of TEOS first hydrolyzed to hydroxyl group while the other ethoxyl groups were difficult to hydrolyze, because the hydroxyl group is unfavorable to the stability of the positive charge of the silica oligomers obtained by TEOS hydrolysis. In this case, the number of hydroxyl groups on the silica oligomers is always less than two. These partially hydrolyzed TEOS molecules are amphiphilic, inclining to aggregate onto the surface of … droplets (H. Z. Zhang et al., 2011, p. 106).

They have emphasized that the polycondensation of the silica oligomers occurs with increasing the pH value. H. Z. Zhang et al. (2011) have stated that the TEOS molecules inside the droplets also "diffused continuously toward the interface and agglomerated on the surface of the oil droplets due to the concentration difference of TEOS between the surface and interior of the oil droplets" (p. 107).

Finally, a silica shell of microcapsules can be formed on the oil droplets by gradually increasing of deposition of SiO_2 gels derived from silica polycondensation.

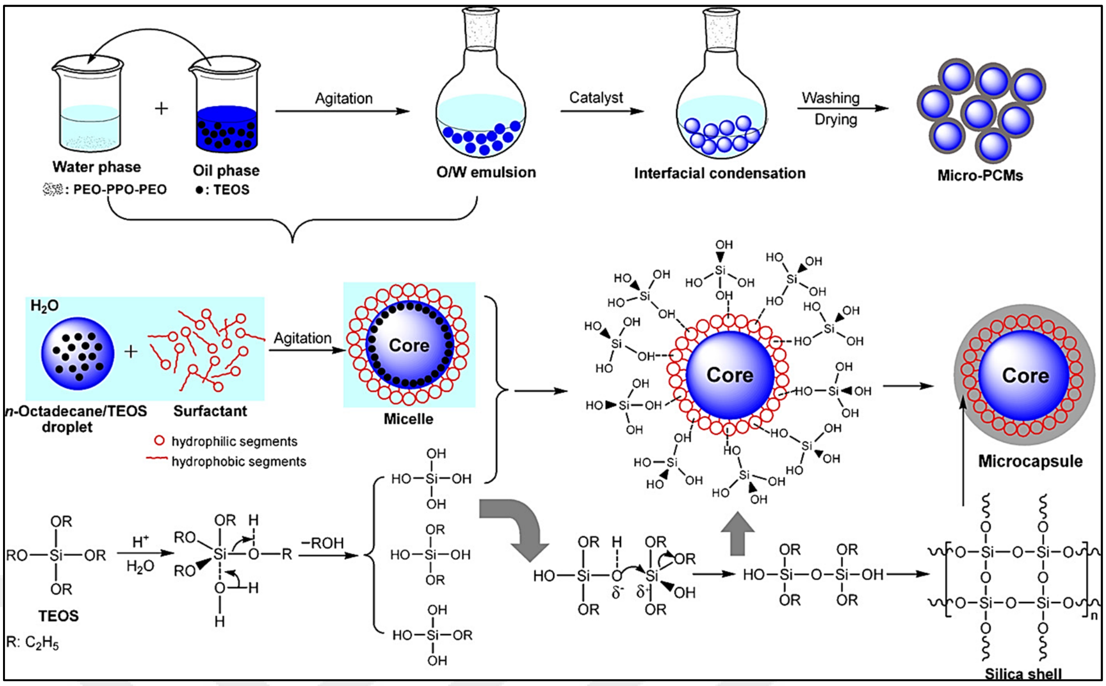

Figure 10.1 Schematic illustration of preparing silica shell-based microcapsules via interfacial polycondensation (H. Z. Zhang et al., 2011)

As mentioned earlier H. Z. Zhang et al. (2011) have microencapsulated the n-octadecane (a phase change material) with silica-based shell through interfacial polycondensation. However, in this study, it was aimed to encapsulate a reactive monomeric aliphatic diisocyanate (IPDI) with the silica shell. Although the principle was similar, but the parameters were highly different.

10.1 Preliminary Tests

It must be noted that many preliminary tests were carried out to find out the material ratios, pH values, and stirring speeds. Only some of the systematic preliminary tests were discussed in this section. Parameter such the amounts of core material (IPDI), shell-forming material (TEOS), and surfactant (Tween80) as well as the stirring speed for emulsification (SS-E) and the stirring speed for polycondensation (SS-P) were examined. The synthesis process were discussed earlier at Section 3.2.3.2.

It must be noted that, the measurement of pH value and adjusting pH continuously to desired value after raising temperature to 40 °C has remarkably positive effect on microencapsulation. However, this finding was obtained in the next section. Therefore, it was not applied in the preliminary tests.

The parameters that were examined in this section are presented in Table 10.1. It can be seen from Table 10.1 that the P-EP1, P-EP2, and P-EP2 experiment were failed. Many similar tests with various amount of IPDI and TEOS were also carried out. However, most of them were failed due to the low amount of surfactant or insufficient oil/water ratios.

Table 10.1 The parameters examined in the preliminary tests

Pre-Experiment Code	IPDI (g)	TEOS (g)	T80 (g)	SS-E (rpm)	SS-P (rpm)	pH	Description, Yield (%)
P-EP1	2	2	0.3	800	500	2.8	Failed
P-EP2	2	1	0.3	800	500	2.8	Failed
P-EP3	4.5	4.5	0.3	800	500	2.8	Failed
P-EP4	4.5	4.5	0.5	500	300	2.8	59.2%
P-EP5	4.5	4.5	0.8	500	300	2.8	61.1%
P-EP6	4.5	4.5	0.9	500	300	2.8	59.0%
P-EP7	4.5	4.5	1.2	500	300	2.8	58.5%
P-EP8	4	3	0.8	500	300	2.8	55.0%

As can be seen the yield value of P-EP4 synthesis was 59.2%. However, the SEM and digital microscopy (DM) analyses revealed that the obtained powder from this synthesis was mainly not microcapsules. For example, Figure 10.2 shows a SEM/EDS image of the P-EP4 sample. Irregular-shaped particles with mainly consist of C element can be seen in the figure. However, few microcapsules were also seen in this sample (Figures 10.3 and 10.4). As can be seen from the EDS spectrum, the microcapsule consists of Si (indicates silica shell), C (indicates core material, IPDI monomer), and O elements. Therefore, it revealed the existence of silica (shell material) and IPDI (core material).

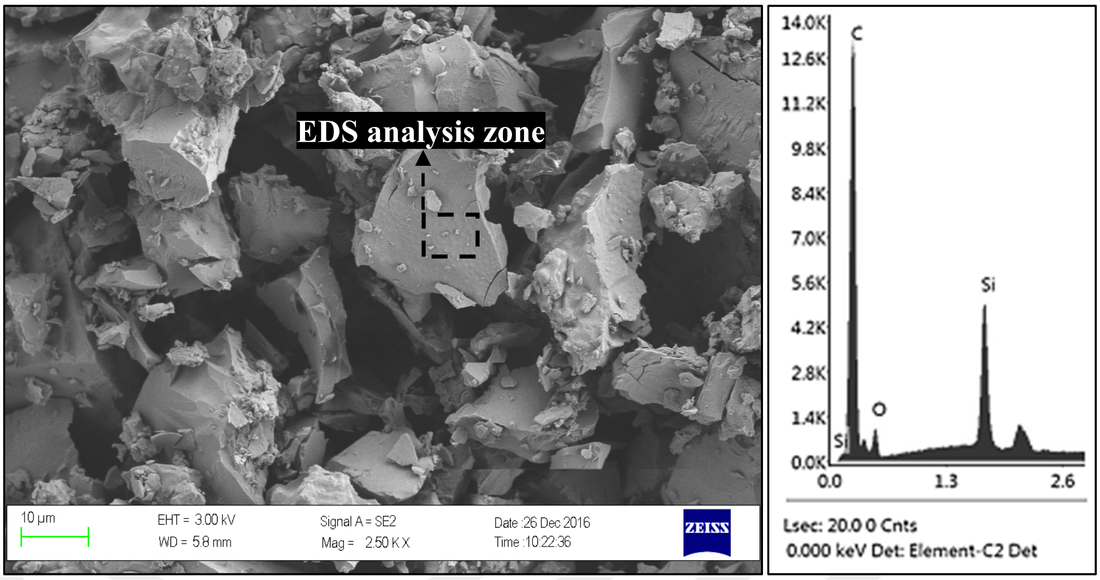

Figure 10.2 SEM/EDS spectrum images of the particles (possible microcapsules) synthesized via the P-EP4 experiment

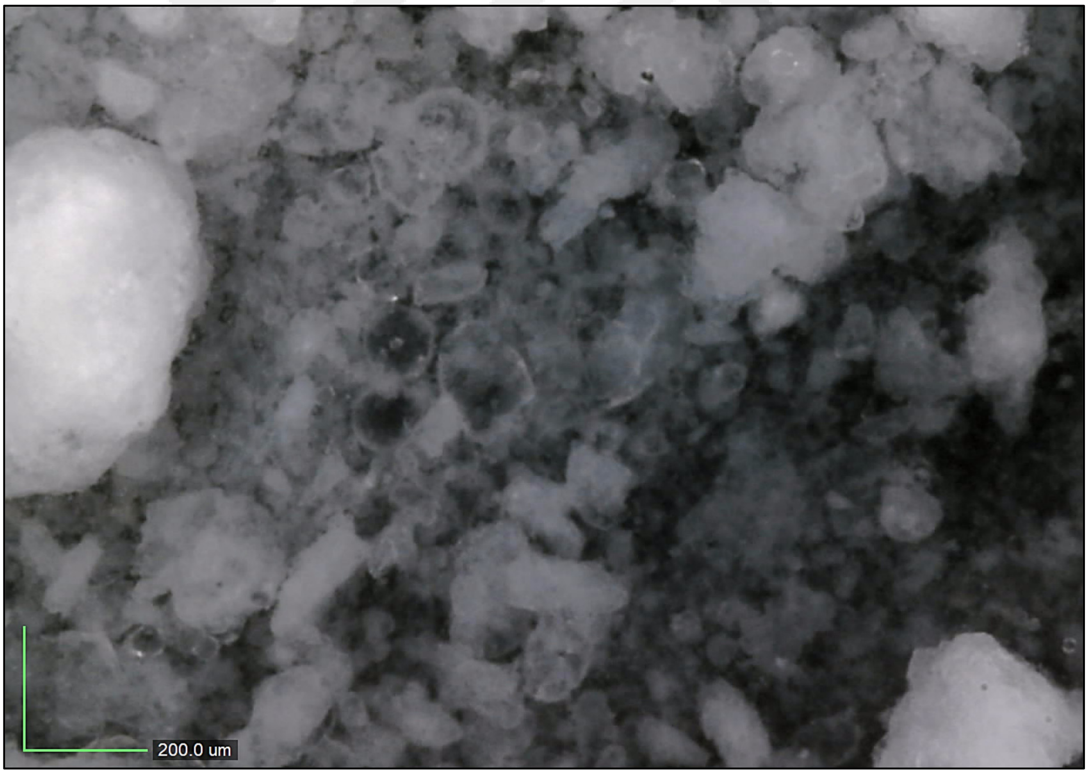

Figure 10.3 DM image of the particles/microcapsules synthesized via the P-EP4 experiment

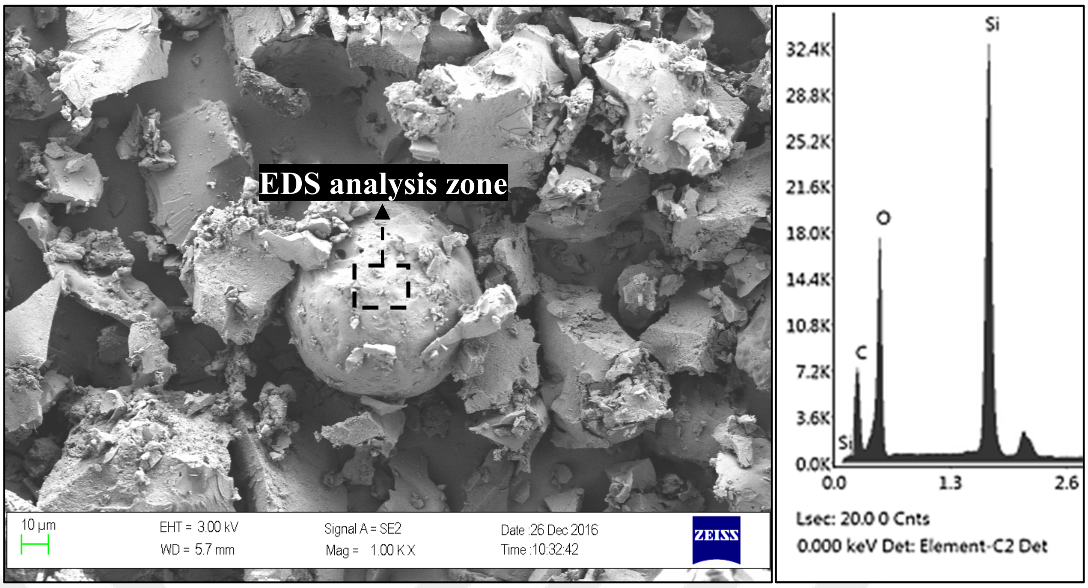

Figure 10.4 SEM/EDS spectrum images of a microcapsule synthesized via the P-EP4 experiment

Increasing the Tween80 weight from 0.5 g to 0.8 g were affect positively the synthesis process. Figure 10.5 shows the DM and SEM images of the P-EP5 samples. As can be seen from the images the number of microcapsules remarkably increased in this synthesis.

To avoid damaging the scanning electron microscopy during the vacuuming, immediately after the microcapsules are poured onto the carbon tape, the sample stub should be hit to anywhere several times to make sure that the unbonded particles are removed. This necessary application leads to a significant loss of spherical capsules from the stub. On the other hand, the irregular smaller particles, which have more contact point and area with the carbon tape, were more difficult to fall out from the carbon bond. Therefore, the SEM images were not as realistic as the optical microscope images. The average diameters of microcapsules were obtained by measuring of at least 50 microcapsules on the digital microscope images. The average diameter of microcapsules were 160 µm. Figure 10.6 shows EDS spectrum of a microcapsule synthesized in the P-EP5 experiment. The microcapsule consists of Si (indicates silica shell), C (indicates core material, IPDI monomer), and O elements. Therefore, it revealed the existence of silica shell and IPDI. It should be noted that the maximum yield value were obtained in the in the P-EP5 experiment.

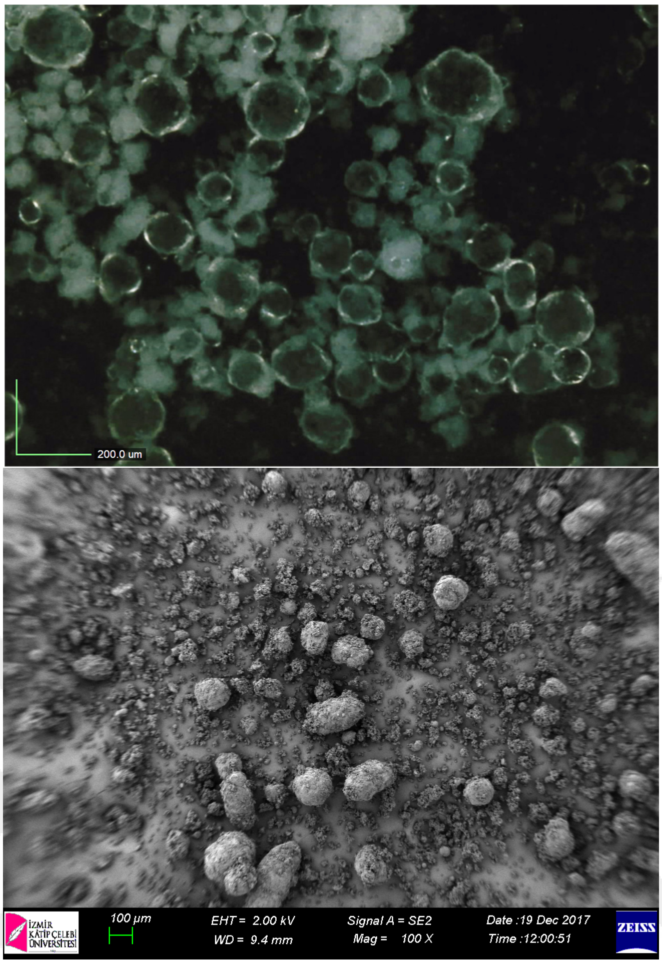

Figure 10.5 DM and SEM images of the microcapsule synthesized via the P-EP5 experiment

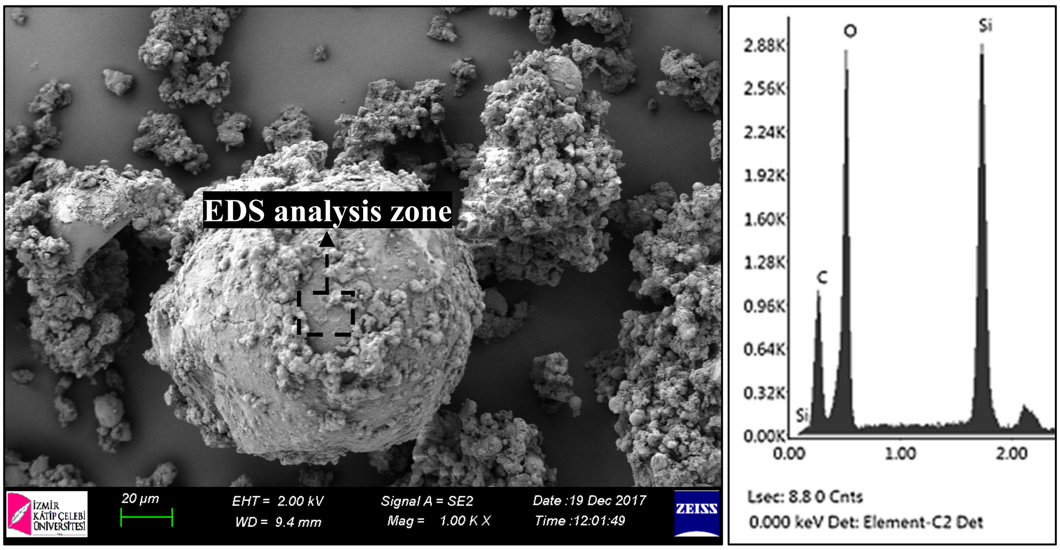

Figure 10.6 SEM/EDS spectrum images of a microcapsule synthesized via the P-EP5 experiment

The other samples (P-EP6, P-EP7, and P-EP8) were not better than the P-EP5 samples. Therefore, the P-EP5 was tried to be systematically optimized in the continuation of this chapter.

10.2 Optimization of IPDI/Silica Microcapsules

Based on the preliminary tests the following parameters were kept constant in the optimization process;

- The stirring speed for polycondensation: 500 rpm
- Emulsion temperature: 40°C
- Polycondensation time: 24 hours
- The ratio (by weight) of core material (IPDI) to shell-forming material (TEOS): 1.0
- The ratio (by weight) of oil phase (IPDI+TEOS) to aqueous phase (water, continuous phase): 0.18

The synthesis process was discussed earlier at Section 3.2.3.2. The effect of Tween80 (surfactant) weight ratio, pH value, and stirring speed for emulsification (SS-E) were examined through the yield, microscopy, TGA, and FTIR analysis.

10.2.1 The Effect of Tween80 Weight Ratio on Properties of Microcapsules

In this section, the effects of Tween80 (surfactant) on IPDI/Silica microcapsules were examined. Firstly, the Control samples should be described. Based on the preliminary tests the following procedure was carried out in synthesis of Control sample;

Two solutions were prepared in the synthesis process as follows: 1) S1 is a solution of surfactant, Tween80 (0.8 g), in 50 mL of deionized water. 2) S2 is a solution of

4.5g of shell-forming (TEOS) and 4.5 g of core material (IPDI). S2 was emulsified in S1 solution at a speed of 800 rpm for 20-30 min. After dispersion and stabilization of TEOS/IPDI micro droplets in the water phase, the pH value of emulsion was adjusted to 2.8. The emulsion was continuously stirred (500 rpm) at 40 °C for 24 h to complete the interfacial polycondensation of silica precursor. As mentioned earlier, adjusting the pH value continuously to desired value for at least 30 min after raising temperature to 40°C has remarkably positive effect on microencapsulation. Therefore, this finding were applied in the syntheses process.

In order to examine the effect of Tween80 weight ratio on microcapsules two different samples were synthesized. As can be seen from Table 10.2, the Tween80 weight was increased to 1.0 g in sample M-TW1.0. In other words, the ratio of surfactant (Tween80) to oil phase (IPDI+TEOS) was increased from 0.088 to 0.11. On the other hand, the Tween80 weight was decreased to 0.6 g in sample M-TW0.6. In other words, the ratio of surfactant to oil phase was decreased from 0.088 to 0.66.

After vacuum filtration, sufficient washing, and oven drying, a free-flowing white powders were obtained. However, the Control sample was more free-flowing powder than the M-TW1.0 and M-TW1.0 samples.

Microencapsulation yields (%) MY were calculated by the following equation:

$$MY(\%) = \frac{W_M}{W_{TWEEN80} + W_{IPDI} + W_{TEOS}} \tag{10.1}$$

Where W_M, $W_{TWEEN80}$, W_{IPDI}, and W_{TEOS} are the weights of dried microcapsules powder, Tween80 (surfactant), core material (IPDI), and shell-forming material (TEOS), respectively. As can be seen from Table 10.2 there is not significant differences between yield values of samples.

Table 10.2 Sample codes, varieties, and yield values (effect of Tween80)

Sample Code	**Tween 80 (g)**	**Stirring speed (rpm)**	**pH**	**Yield (%)**
Control	0.8	500	2.8	62.3
M-TW1.0	1.0	500	2.8	65.0
M-TW0.6	0.6	500	2.8	60.4

Based on many digital microscopy and SEM analyses the most well-shaped microcapsules were formed in the Control sample. The average microcapsules diameter was 153 μm. The digital microscope and SEM/EDS analysis of the sample with better morphology are presented in this section. Figure 10.7 shows a digital microscope image of Control sample. Figure 10.8 shows SEM/EDS image of a Control microcapsule. It can be seen from the EDS spectrum that the microcapsule consists of Si (indicates silica shell), C (indicates core material, IPDI monomer), and O elements. Therefore, it revealed the existence of silica shell and IPDI.

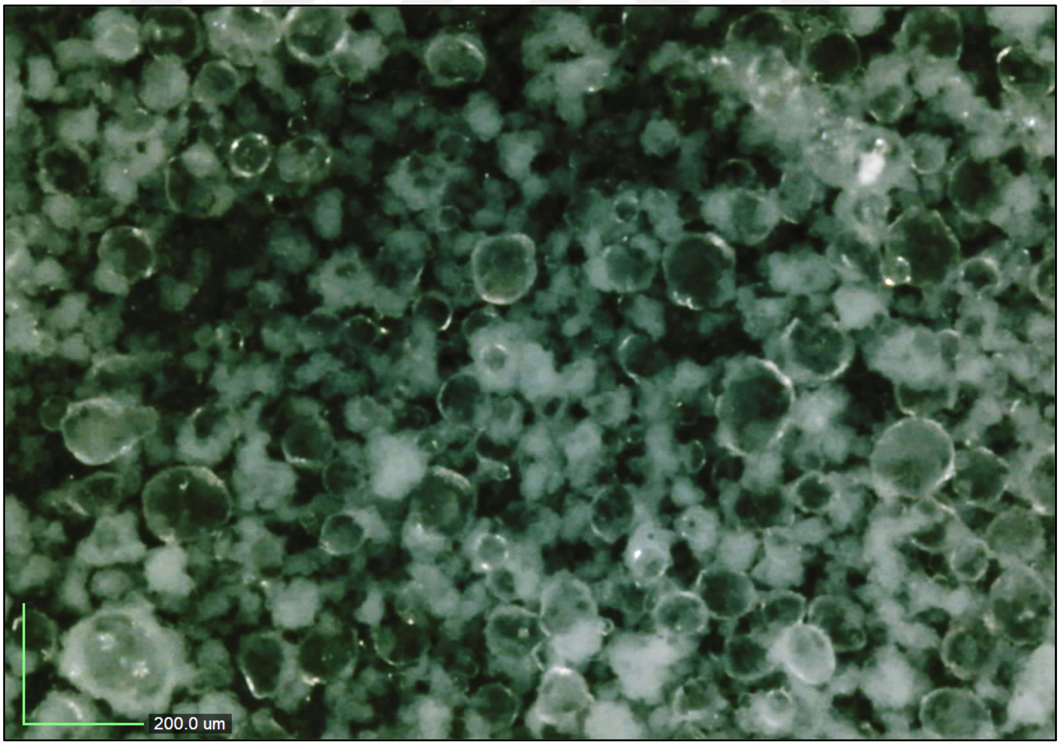

Figure 10.7 Digital microscope image of Control microcapsules

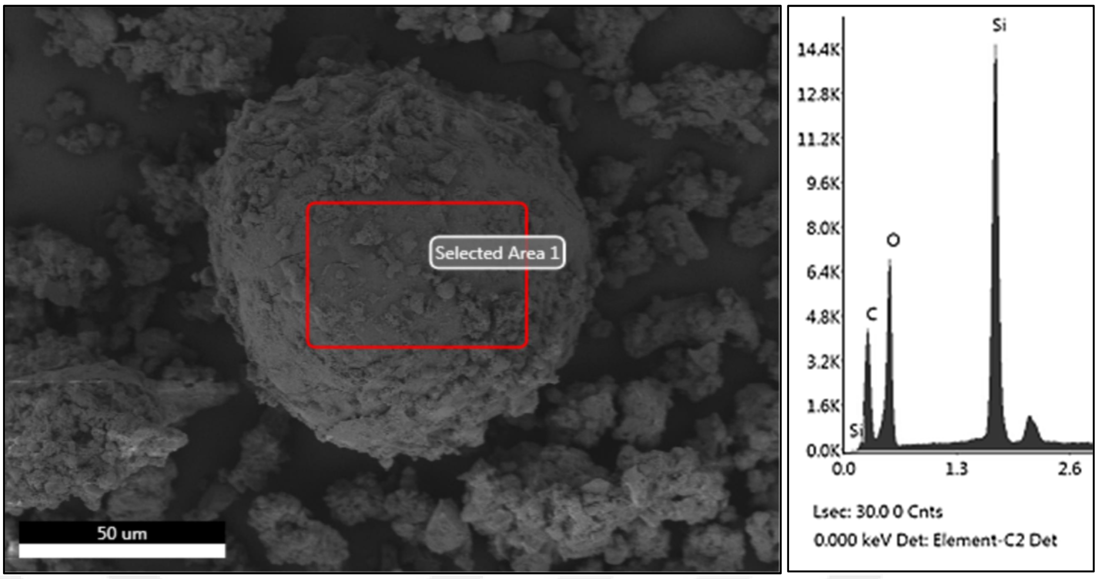

Figure 10.8 SEM/EDS spectrum images of a Control microcapsule

TG data obtained from TGA curve are summarized in Table 10.3. Furthermore, the effect of Tween80 weight ratio on TGA curves of the samples are shown in Figure 10.9. The temperatures at 5% mass loss value decrease with increasing mass of Tween80. The highest residual mass was obtained with higher mass of Tween80. There are three basic mass loss values in thermogram of samples. Mass loss below 150°C is due to moisture content. Encapsulated IPDI evaporation takes place in the temperature range 200-300°C. The maximum degradation rates for Control, M-TW1.0, and M-TW0.6 were obtained to be 293, 296, and 291°C, respectively. The mass loss in the temperature range 300-500°C may be attributed to thermal degradation of silica shell materials. As can be seen from Table 10.3, maximum degradation temperatures for Control, M-TW1.0, and M-TW0.6 were obtained to be 352, 344, and 348°C, respectively. It is probable that SiO_2 shells makes a physical protective barrier on the surface of IPDI

Table 10.3 The effect of Tween80 weight ratio on TGA data

Sample	Mass Loss (up to 110°C)	Temperature at 5% mass loss (°C)	Max Degradation Temperature	Residual Mass (up to 800°C) %
Control	1	205	352	12
M-TW1.0	4	178	344	17
M-TW0.6	4	220	348	19

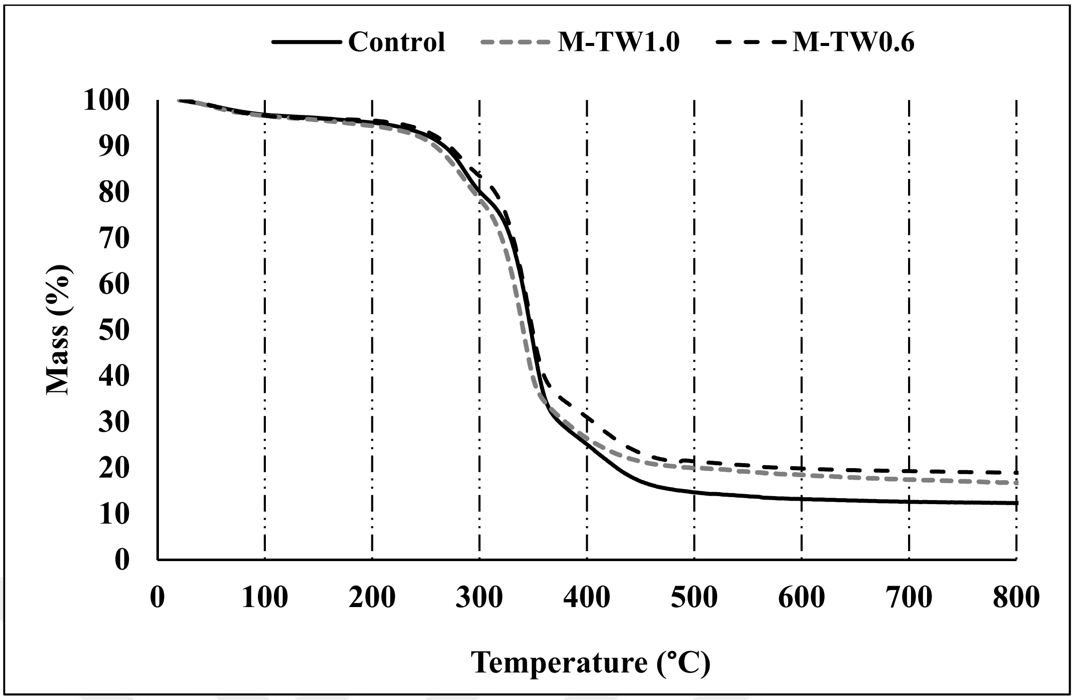

Figure 10.9 TGA curves for the samples (effect of Tween80)

Figure 10.10 shows the FTIR spectra of Control, M-TW1.0, and M-TW0.6 samples. Si-O-Si asymmetric stretching vibration shows a broad band between 1200-1000 cm^{-1}, which confirms the formation of SiO_2. The absorption band around 1630 cm^{-1} may be ascribed to bending vibration of adsorbed water, probably available in the pores of SiO_2 (B. X. Li, Liu, Hu, Wang, & Gao, 2013). C=0 stretching vibration peaks of IPDI can be seen at 1696, 1699, and 1699 cm^{-1} for Control, M-TW1.0, and M-TW0.6, respectively. Figure shows a weak peak in the range 2200-2230 cm^{-1} due to N=C=O group, which shows a little unreacted isocyanate group is in the microcapsule core (Zhan, Chen, Chen, & Hou, 2016). However the peak belonging to N=C=O group is more apparent for M-TW0.6.

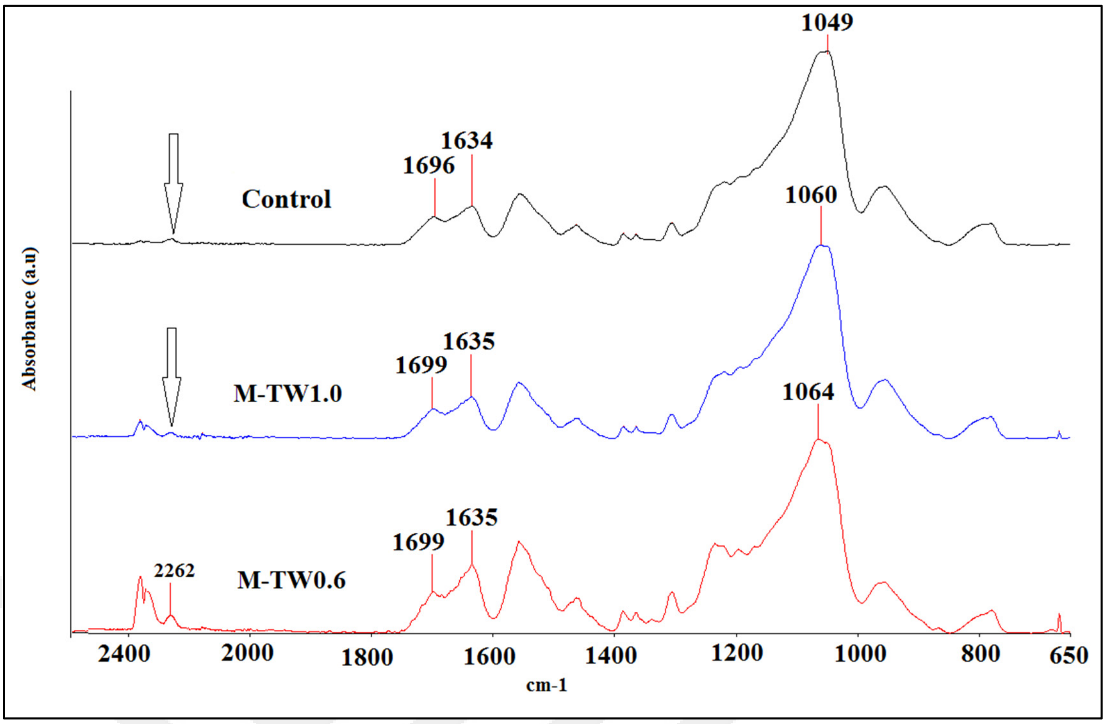

Figure 10.10 FTIR spectra for the samples (effect of Tween80)

10.2.1 The Effect of pH Value of Emulsion on Properties of Microcapsules

In order to examine the effect of pH value of emulsion on microcapsules two different samples were synthesized. As can be seen from Table 10.4, the pH value was increased to 3.0 in M-PH3.0 sample. In other words, the pH value of emulsion was increased from 2.8 to 3.0 in order to modify the rate of interfacial polycondensation of TEOS. On the other hand, the pH value was decreased to 0.6 g in M-PH2.6 sample.

Table 10.4 Sample codes, varieties, and yield values (effect of pH)

Sample Code	Tween 80 (g)	Stirring speed (rpm)	pH	Yield (%)
Control	0.8	500	2.8	62.3
M-PH3.0	0.8	500	3.0	65.1
M-PH2.6	0.8	500	2.6	63.3

After vacuum filtration, sufficient washing, and oven drying, a free-flowing white powder was obtained. However, the M-PH3.0 and M-PH2.6 samples were less free-flowing powder than the Control sample. As can be seen from Table 10.4 the yield value have not highly affected by changing the pH value.

Similar to the previous section, the most well-shaped microcapsules were formed in the Control sample. In other words, increasing or decreasing the pH value of emulsion negatively affected the formation and morphology of microcapsules. For example, the digital microscope and SEM images of M-PH2.6 sample are shown in Figure 10.11. The negative effect of decreasing pH on microencapsulation is obvious in Figure 10.11.

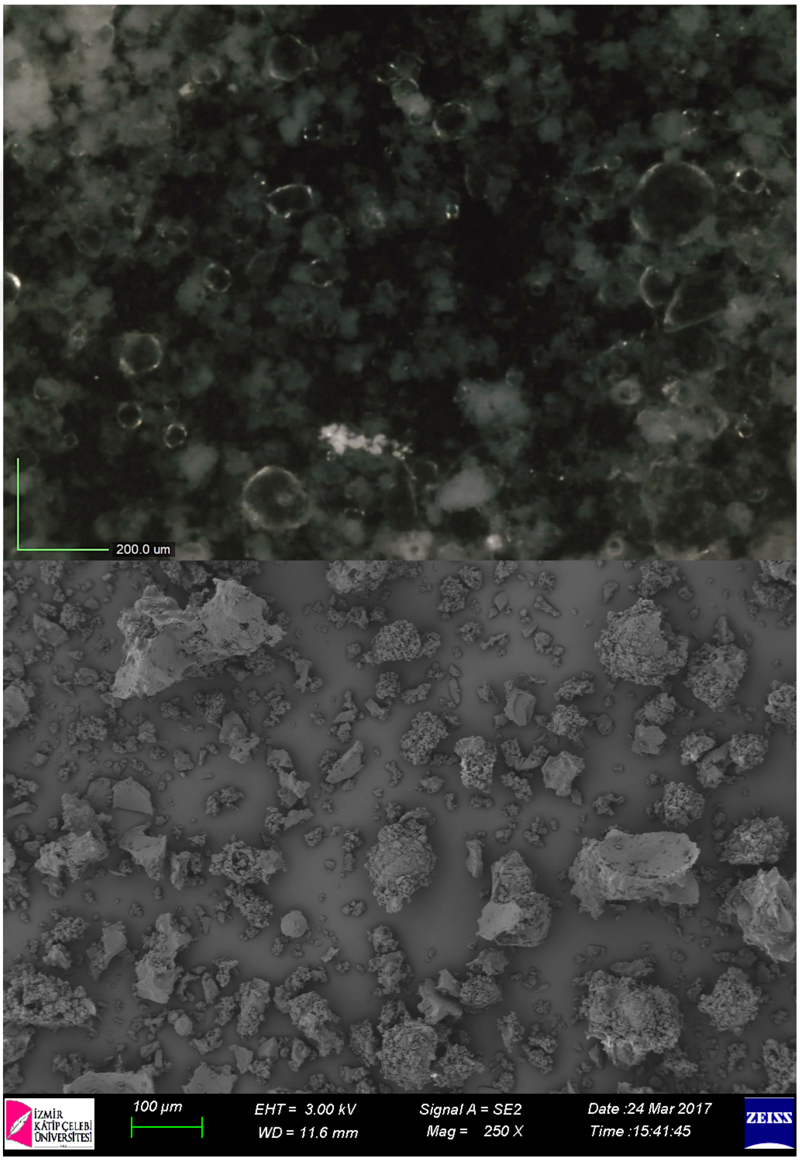

Figure 10.11 Digital microscope and SEM images of M-PH2.6 sample

The effect of pH value of emulsion on TGA curves of the samples is shown in Figure 10.12. TGA results are summarized in Table 10.5. The highest maximum degradation temperature was obtained at the pH values of 2.6 and 2.8 in this study. Besides, the highest temperature at 5% mass loss (°C) and residual mass up to 800°C was obtained when the solution pH was 2.8.

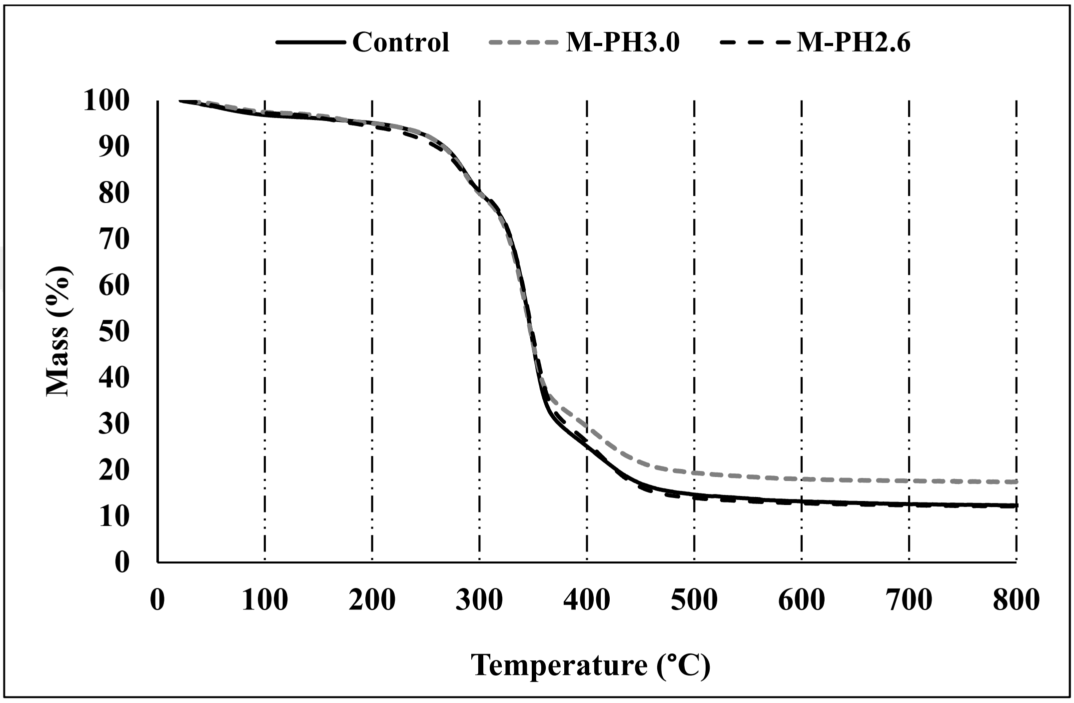

Figure 10.12 TGA curves for the samples (effect of pH)

Table 10.5 The effect of pH value on TGA data

Sample	Mass Loss (up to 110°C)	Temperature at 5% mass loss (°C)	Max Degradation Temperature	Residual Mass (up to 800°C) %
Control	1	205	352	12
M-PH3.0	3	200	349	17
M-PH2.6	3	182	352	12

The effect of pH value of emulsion on chemical structure of the samples is given in Figure 10.13. As can be seen from figure, the peaks at 2262 cm^{-1} for M-PH3.0 and M-PH2.6 corresponds to N=C=O group. While unreacted isocyanate group in the microcapsule core is more apparent for the sample M-PH2.6 (at pH 2.6), the peak for Control (at pH 2.8) is very weak.

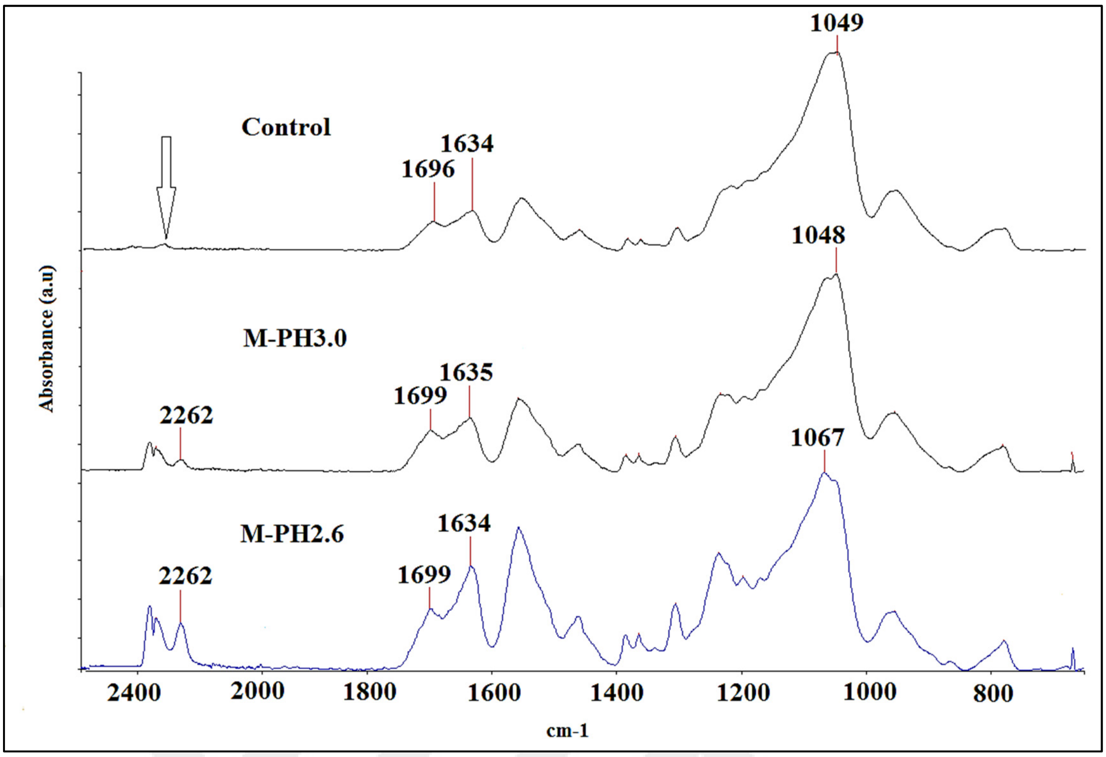

Figure 10.13 FTIR spectra for the samples (effect of pH)

10.2.3 The Effect of Stirring Speed for Emulsification on Samples

In order to examine the effect of stirring speed for emulsification (SS-E) on microcapsules two different samples were synthesized. As can be seen from Table 10.6, the SS-E was increased to 800 rpm and 1100 rpm in M-SE800 and M-SE100 samples, respectively. It is well known that the diameter of droplets in emulsion and as result the diameter of microcapsules can be changed by modifying the SS-E. In addition, the morphology of microcapsules can highly be affected by the SS-E.

Table 10.6 Sample codes, varieties, and yield values (effect of SS-E)

Sample Code	Tween 80 (g)	Stirring speed (rpm)	pH	Yield (%)
Control	0.8	500	2.8	62.3
M-SE800	0.8	800	2.8	64.6
M-SE1100	0.8	1100	2.8	61.4

After vacuum filtration, sufficient washing, and oven drying, a free-flowing white powder was obtained. However, the M-SE800 sample was the most free-flowing powder in this chapter, even better than the Control sample. As can be seen from Table 10.6 the yield values have not highly affected by changing the SS-E.

Figure 10.14 shows SEM image and EDS spectrum of the M-SE800 sample. As can be seen from the figure, the EDS spectrum was not highly changed as compared to Control microcapsules. As discussed earlier, to avoid damaging the scanning electron microscopy during the vacuuming, immediately after the microcapsules are poured onto the carbon tape, the sample stub should be hit to anywhere several times to make sure that the unbonded particles are removed. This necessary application leads to a significant loss of spherical capsules from the stub. On the other hand, the irregular smaller particles, which have more contact point and area with the carbon tape, were more difficult to fall out from the carbon bond. Therefore, the SEM images were not as realistic as the optical microscope images.

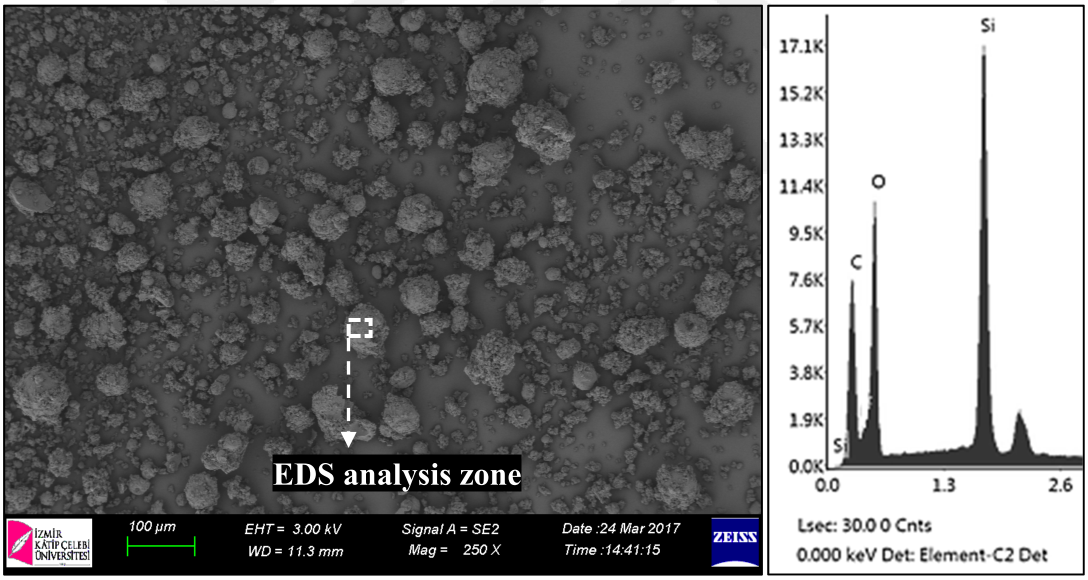

Figure 10.14 SEM image and EDS spectrum of the M-SE800 microcapsules

The digital microscope images of M-SE800 and Control samples are presented in Figure 10.15. As can be seen, the M-SE800 microcapsules were much smaller but more uniform as compared to the Control microcapsules. It can be explained by the fact that increasing the SS-E leads to reduce the diameter of droplets in emulsion and increase in stability of emulsion.

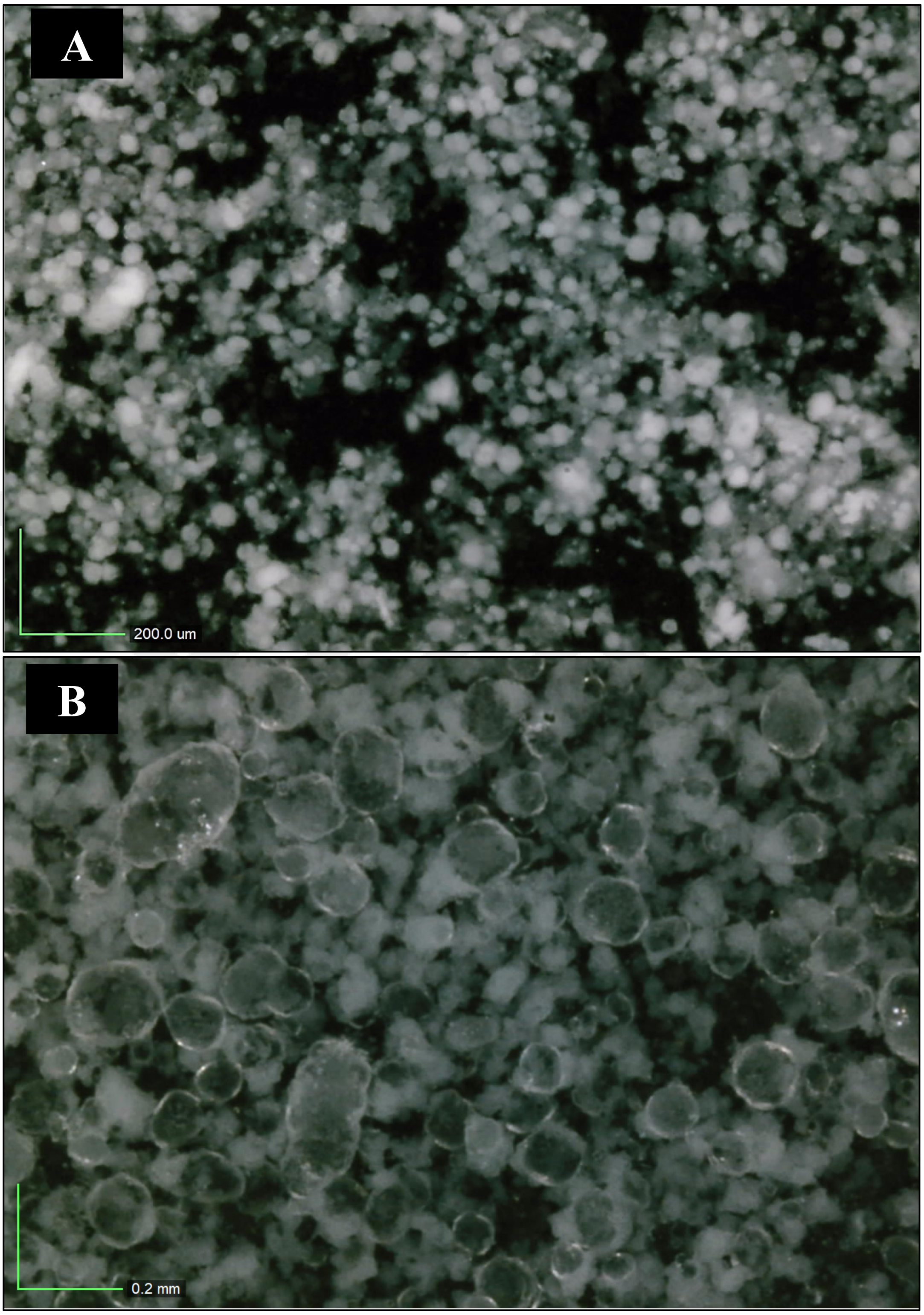

Figure 10.15 Digital microscope images of A) M-SE800 and B) Control microcapsules

As mentioned earlier the average diameter of microcapsules was obtained by measuring of at least 50 microcapsules on the digital microscope images. The average diameter of M-SE800 microcapsules was 42 µm. In other words, increasing the SS-E from 500 rpm to 800 rpm caused to reduce the average diameter of IPDI/silica microcapsules from 153 µm to 42 µm.

As can be seen from Figure 10.16, the M-SE110 microcapsules were the worst sample in this section. It seems that excessive increasing of SS-E affects negatively the emulsification and as a result poor microencapsulation.

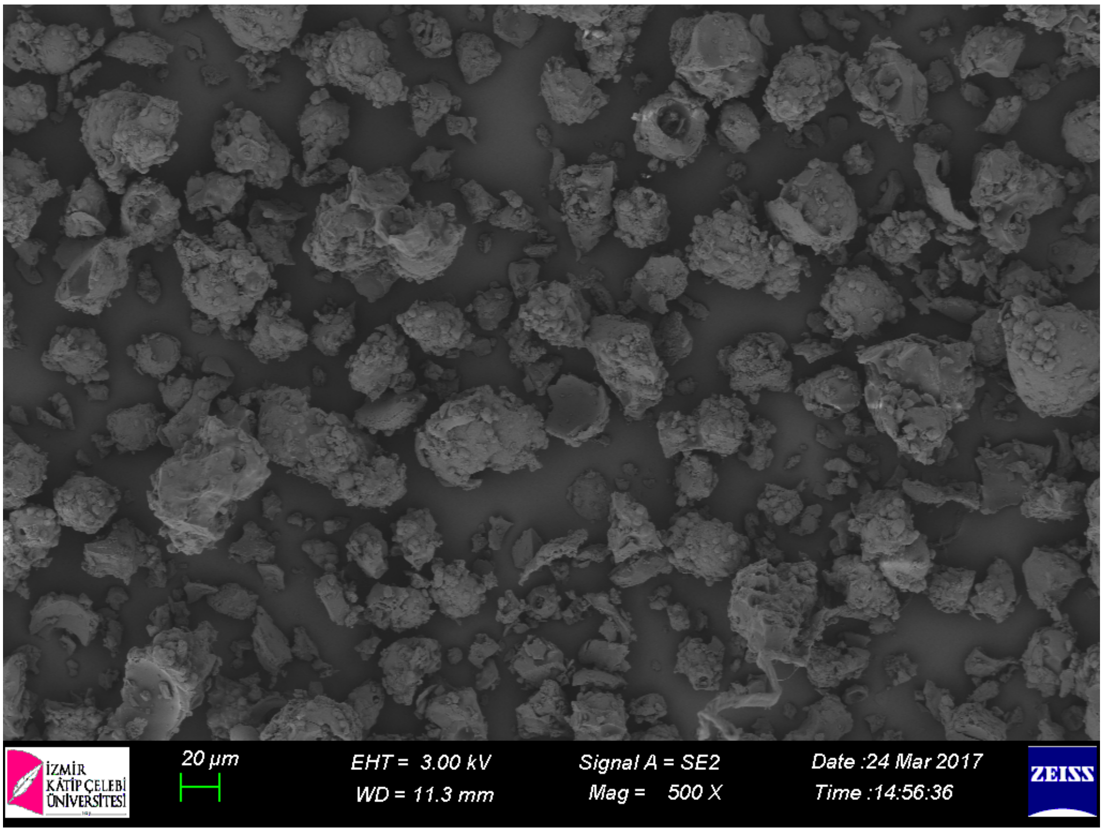

Figure 10.16 SEM image of the M-SE110 sample

The effect of SS-E on thermal properties of samples can be seen in Figure 10.17. TGA data are summarized in Table 10.7. The stirring speed has not affected the maximum degradation temperatures of the samples. However, temperature at 5% mass loss increases as stirring speed increases from 500 to 1100 rpm. The highest residual mass was obtained at 800 rpm.

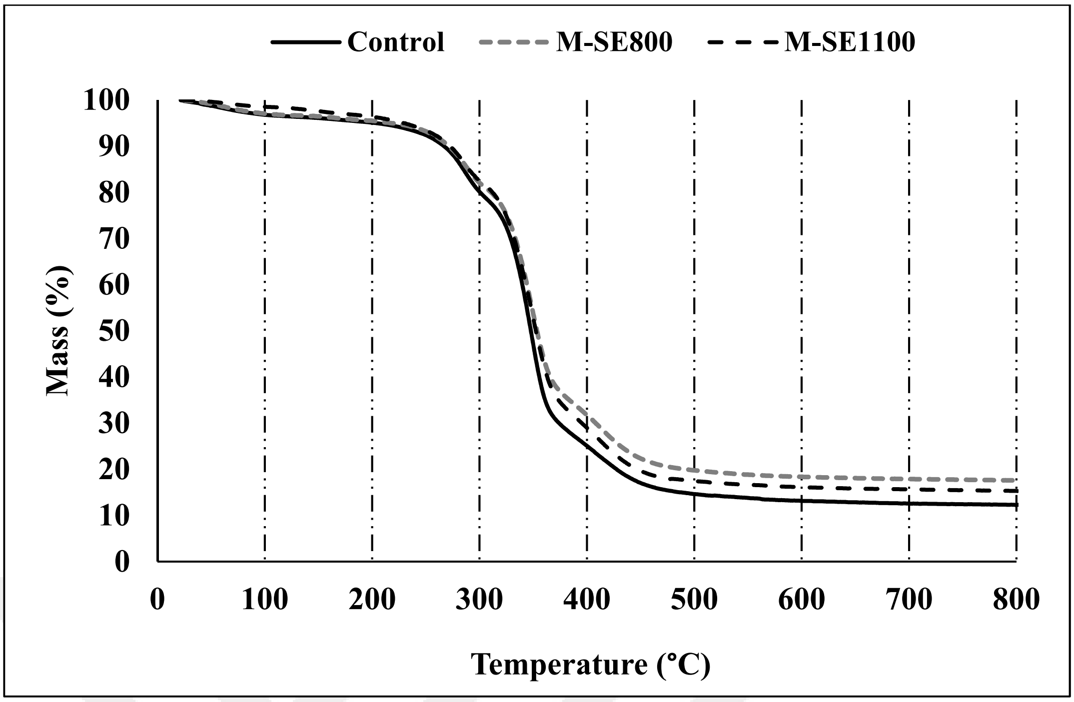

Figure 10.17 TGA curves for the samples (effect of SS-E)

Table 10.7 The effect of SS-E on TGA data

Sample	Mass Loss (up to 110°C)	Temperature at 5% mass loss (°C)	Max Degradation Temperature	Residual Mass (up to 800°C) %
Control	1	205	352	12
M-SE800	3	218	352	18
M-SE1100	2	229	352	15

The effect of SS-E on chemical structure of the samples is given in Figure 10.18. The peaks at 2254, 2264, and 2261 cm^{-1} for Control, M-SE800, and M-SE1100 correspond to N=C=O group. Unreacted isocyanate group in the microcapsule core is more apparent for the sample M-SE1100.

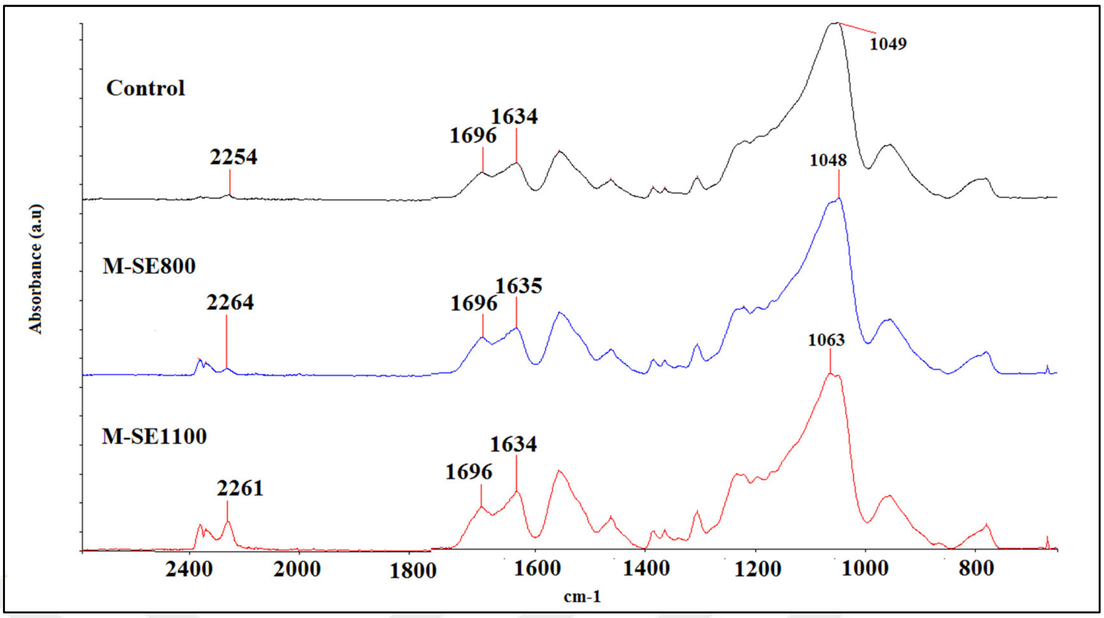

Figure 10.18 FTIR spectra for the samples (effect of SS-E)

CHAPTER ELEVEN
CONCLUSIONS AND RECOMMENDATIONS

Encapsulation of self-healing agents by microencapsulation technology, restriction of the crack width with micro fibers, and ensuring the presence of unreacted cementitious materials in matrix were the self-healing techniques investigated within the scope of this study. The self-healing mechanisms of macro/micro cracks formed under tension and compression loads were investigated by various mechanical, permeability, and microstructure analysis. Furthermore, the microencapsulation of sodium silicate as a self-healing agent with polymeric shell materials was one of the main objectives of this study. The synthesized microcapsules were optimized and characterized by various methods and analyses. This study has also dealt with the idea of possible microencapsulation of isophorone diisocyanate as a self-healing agent with silica-based shell for the first time in the literature.

11.1 Conclusions

Based on the test results of this reasearch, the following conclusions can be drawn:

- The efficiency of autogenous self-healing mechanism can be enhanced by restriction of the crack width. In this study, except the direct tension loads, the crack width and damage level could be controlled successfully by using a micro fiber with 6 mm length. For example, in spite of such a huge preloading level up to ~100% of the average corresponding compressive strength of UHPC specimens, the reduction in strength did not exceed 19%. However, especially in the case of 90-day specimens, the sudden load drops in the direct tension test made crack width control virtually impossible. If it was possible to use 13 mm length micro fibers, consequently it would be possible to obtain mixtures with deformation hardening behavior under direct tension loads. Nevertheless, higher binder dosage must be used for using these fibers. Otherwise, it was observed that the use of 13 mm fibers affected adversely the flow of fresh mixture.

- A part of this dissertation was devoted to the development and application of a novel test method, called “self-bonding’, for studying the self-healing ability of cementitious composites. The principle of this method lies in the bonding capacity of self-healing products under direct tension loads. A special designed cylinder specimen was split after 7 days water curing and then, the two parts of the split specimen were carefully put together immediately. A connector apparatus was designed to keep the surface of each part connected together with equal pressure for “healing” process in water. Therefore, no matter mixture type, the cracks in all of the specimens are continuous with similar widths throughout the cross section, very tight, and under a certain pressure. The suggested test method can be used along with different test methods for assessing self-healing capacity of the cement based materials. It should be noted that the splitting process can be applied on such specimens that have compressive strength value at least below 100 MPa. Determining directly the bonding capacity of healing products can be useful in terms of the assessing self-healing capacity of cementitious mixtures.

- According to the test result of the novel self-bonding and crack closing methods, increasing the binder dosage of UHPC mixture from 800 kg/m^3 cement content to 1200 kg/m^3 by addition of the class C fly ash and GGBFS enhanced remarkably the self-healing capacity of UHPC at early ages.

- The self-healing capacity of three UHPC mixtures, which had been selected from self-bonding test, were determined via various methods. It can be concluded from test results that it is only possible from a correct viewpoint to determine a realistic ratio of self-healing. Especially in the case of compressive strength test, if the undergoing hydration reactions and especially pozzolanic reactions during the healing period were not considered, over-optimistic self-healing ratios could be obtained. In addition, the efficiency of above-mentioned methods can be analyzed in terms of self-healing assessment. The compressive strength, crack-closing, total water absorption and water permeability methods have been used successfully to assess the self-healing behavior of preloaded and/or precracked UHPC specimens. On the other hand, over-optimistic self-healing ratios were obtained in the ultrasonic pulse velocity test. Filling the single crack with even low amount of products such as $Ca(OH)_2$, $CaCO_3$, C-S-H, and the particles and impurities suspended in the water can lead to obtain over-optimistic self-healing ratios with the ultrasonic pulse velocity test. It is also obvious that Torrent air permeability test cannot be used to assess the self-healing ratio of such cracks examined in this study. In the case of direct tension test, as mentioned earlier, the sudden load drops in the direct tension test, which is a very sensitive and difficult experiment due to its nature, negatively affected the examination of the self-healing mechanism.

- The phenomena of self-healing in cement based composite is complex mechanism with many variables. Although the positive effect of SCMs on the self-healing ability of UHPC, it was observed that the self-healing ratios depend on critical parameters such as damage type, deterioration level, and especially methods used to verify the phenomenon of self-healing. In addition, it was observed that SCMs could enhance dramatically the self-healing ability of UHPC mixture preloaded even after 90 days water curing.

- This study showed that sodium silicate can be successfully encapsulated through polyurethane microcapsule by interfacial polymerization of optimum shell-forming monomer on the aqueous sodium silicate droplets. It was observed that most of the microcapsules appear to be spherical shaped and free-flowing powder. It can be indicated from the yield, SEM, and TG analyses that the optimum shell-forming monomer to core material ratio is 0.67. However, from FTIR analyses it was inferred that the reaction of the diisocyanate with Span 85 has not completed to form polyurethane. In addition, SEM and EDS analyses revealed that the liquid core material (aqueous sodium silicate) of some of the microcapsules could become solid due to moisture loss from possible cracks on the shell. Fracture behavior of optimized microcapsule in cementitious matrix demonstrate that there is sufficient interfacial bond strength between the shell of microcapsules and matrix. This mechanism promotes the release of healing agents into cracks.

- The sodium silicate/polyurethane microcapsules, which its synthesis parameter such as shell-forming monomer, core material (healing agent), and stirring procedures have been optimized, were incorporated in UHPC mixtures. It was observed that dispersing the microcapsules in water of mixture before adding to dry ingredients of mixtures has a positive effects on properties of fresh and hardened UHPC mixtures.

- Sodium silicate/polyurethane microcapsules used in a concentration of 5% with respect to cement weight did not affect remarkably the 28-days compressive strength of UHPC mixture. Using of such small microcapsules (65 μm) in UHPC mixture has negligible effects on the compressive strength. On the other hand, the contribution of sodium silicate, which is the core material of the microcapsules, in self-healing ability of UHPC mixtures was obviously observed in crack closing test.

- Microcapsules based on IPDI core (healing agent) and silica shell were synthesized via the interfacial polycondensation of a silica precursor. The optimum core material/shell-forming material, oil phase/aqueous phase, and surfactant/oil ratios were 1.0, 0.18, and 0.08, respectively. Furthermore, the pH value of emulsion should be kept at 2.8 for at least 30 min. The most effective stirring speed for emulsification was found to be 800 rpm.

11.2 Recommendations

Some aspects are suggested for further studies as following;

- Assessing the self-healing capacity of various cement based materials via the "self-bonding" method suggested in this study.

- The phenomena of self-healing in cement based composite is complex mechanism with many variables. Therefore, studies on the standardization of the test methods and the process are highly recommended.

- Further investigations on the self-healing efficiency of sodium silicate/polyurethane microcapsules via various test methods.

- Further investigations should be carried out on the optimization of IPDI/Silica microcapsules.

REFERENCES

Ahn, T.-H., & Kishi, T. (2010). Crack self-healing behavior of cementitious composites incorporating various mineral admixtures. *Journal of Advanced Concrete Technology, 8*(2), 171-186.

Ahn, T. H., & Kishi, T. (2010). Crack Self-healing Behavior of Cementitious Composites Incorporating Various Mineral Admixtures. *Journal of Advanced Concrete Technology, 8*(2), 171-186.

Aldea, C. M., Song, W. J., Popovics, J. S., & Shah, S. P. (2000). Extent of healing of cracked normal strength concrete. *Journal of Materials in Civil Engineering, 12*(1), 92-96. doi:Doi 10.1061/(Asce)0899-1561(2000)12:1(92)

Alghamri, R., Kanellopoulos, A., & A-Tabbaa, A. (2016). Impregnation and encapsulation of lightweight aggregates for self-healing concrete. *Construction and Building Materials, 124*, 910-921. doi:10.1016/j.conbuildmat.2016.07.143

Alizadegan, F., Pazokifard, S., Mirabedini, S. M., Danaei, M., & Farnood, R. (2017). Polyurethane-based microcapsules containing reactive isocyanate compounds: Study on preparation procedure and solvent replacement. *Colloids and Surfaces a-Physicochemical and Engineering Aspects, 529*, 750-759. doi:10.1016/j.colsurfa.2017.06.058

Alyousif, A., Lachemi, M., Yildirim, G., & Sahmaran, M. (2015). Effect of Self-Healing on the Different Transport Properties of Cementitious Composites. *Journal of Advanced Concrete Technology, 13*(3), 112-123. doi:10.3151/jact.13.112

Badri, K. B. H., Sien, W. C., Shahrom, M., Hao, L. C., Baderuliksan, N. Y., & Norzali, N. (2010). FTIR spectroscopy analysis of the prepolymerization of palmbased polyurethane. *ECS J. Solid State Sc, 18*, 1-8.

Beglarigale, A., Seki, Y., Demir, N. Y., & Yazici, H. (2018). Sodium silicate/polyurethane microcapsules used for self-healing in cementitious materials: Monomer optimization, characterization, and fracture behavior. *Construction and Building Materials, 162*, 57-64. doi:10.1016/j.conbuildmat.2017.11.164

Beglarigale, A., & Yazıcı, H. (2015). Pull-out behavior of steel fiber embedded in flowable RPC and ordinary mortar. *Construction and Building Materials, 75*, 255-265. doi:10.1016/j.conbuildmat.2014.11.037

Bhaskar, S., Hossain, K. M. A., Lachemi, M., Wolfaardt, G., & Kroukamp, M. O. (2017). Effect of self-healing on strength and durability of zeolite-immobilized bacterial cementitious mortar composites. *Cement & Concrete Composites, 82*, 23-33. doi:10.1016/j.cemconcomp.2017.05.013

Boh, B., & Šumiga, B. (2008). Microencapsulation technology and its applications in building construction materials Tehnologija mikrokapsuliranja in njena uporaba v gradbenih materialih. *RMZ–Materials and Geoenvironment, 55*(3), 329-344.

Brown, E. N., Kessler, M. R., Sottos, N. R., & White, S. R. (2003). In situ poly(urea-formaldehyde) microencapsulation of dicyclopentadiene. *Journal of Microencapsulation, 20*(6), 719-730. doi:10.1080/0265204031000154160

Cailleux, E., & Pollet, V. (2009). *Investigations on the development of self-healing properties in protective coatings for concrete and repair mortars.* Paper presented at the Proceedings of the 2nd International Conference on Self-Healing Materials, Chicago, IL, USA.

Calvo, J. L. G., Perez, G., Carballosa, P., Erkizia, E., Gaitero, J. J., & Guerrero, A. (2017). Development of ultra-high performance concretes with self-healing micro/nano-additions. *Construction and Building Materials, 138*, 306-315. doi:10.1016/j.conbuildmat.2017.02.015

Choi, Y. W., Oh, S. R., & Choi, B. K. (2017). A Study on the Manufacturing Properties of Crack Self-Healing Capsules Using Cement Powder for Addition to Cement Composites. *Advances in Materials Science and Engineering*. doi:Artn 5187543. 10.1155/2017/5187543

Clear, C. (1985). *The effects of autogenous healing upon the leakage of water through cracks in concrete*. Cement and Concrete Association: Slough, UK.

Çopuroğlu, O., Schlangen, E., Nishiwaki, T., Van Tittelboom, K., Snoeck, D., De Belie, N., & de Rooij, M. R. (2013). Experimental Techniques Used to Verify Healing. In M. de Rooij, K. Van Tittelboom, N. De Belie, & E. Schlangen (Eds.), *Self-Healing Phenomena in Cement-Based Materials: State-of-the-Art Report of RILEM Technical Committee 221-SHC: Self-Healing Phenomena in Cement-Based Materials* (19-63). Dordrecht: Springer Netherlands.

Danner, T., De Weerdt, K., & Geiker, M. R. (2017). *μ-XRF characterisation of chloride ingress and self-healing in cracked concrete.* Paper presented at the XXIIIth Symposium on Nordic Concrete Research & Development. Aalborg, Denmark.

de Rooij, M., Van Tittelboom, K., De Belie, N., & Schlangen, E. (2013). *Self-healing phenomena in cement-Based materials: state-of-the-art report of RILEM technical committee 221-SHC: self-Healing phenomena in cement-Based materials* (Vol. 11): Springer.

Di Credico, B., Levi, M., & Turni, S. (2013). An efficient method for the output of new self-repairing materials through a reactive isocyanate encapsulation. *European Polymer Journal, 49*(9), 2467-2476. doi:10.1016/j.eurpolymj.2013.02.006

Dong, B. Q., Fang, G. H., Ding, W. J., Liu, Y. Q., Zhang, J. C., Han, N. X., & Xing, F. (2016). Self-healing features in cementitious material with urea-formaldehyde/epoxy microcapsules. *Construction and Building Materials, 106*, 608-617. doi:10.1016/j.conbuildmat.2015.12.140

Dong, B. Q., Fang, G. H., Wang, Y. S., Liu, Y. Q., Hong, S. X., Zhang, J. C., . . . Xing, F. (2017). Performance recovery concerning the permeability of concrete by means of a microcapsule based self-healing system. *Cement & Concrete Composites, 78*, 84-96. doi:10.1016/j.cemconcomp.2016.12.005

Dry, C. (1994). Matrix cracking repair and filling using active and passive modes for smart timed release of chemicals from fibers into cement matrices. *Smart Materials and Structures, 3*(2), 118.

Dry, C. (1999). Repair and prevention of damage due to transverse shrinkage cracks in bridge decks. *Smart Structures and Materials 1999: Smart Systems for Bridges, Structures and Highways, 3671*, 253-256. doi:Doi 10.1117/12.348675

Dry, C., & McMillan, W. (1996). Three-part methylmethacrylate adhesive system as an internal delivery system for smart responsive concrete. *Smart Materials & Structures, 5*(3), 297-300. doi:Doi 10.1088/0964-1726/5/3/007

Edvardsen, C. (1999). Water permeability and autogenous healing of cracks in concrete. *ACI Materials Journal, 96*(4), 448-454.

Ferrara, L., Krelani, V., & Moretti, F. (2016). On the use of crystalline admixtures in cement based construction materials: from porosity reducers to promoters of self healing. *Smart Materials and Structures, 25*(8). doi:Artn 084002. 10.1088/0964-1726/25/8/084002

Ferreira, C. S., Santos, P. L., Bonacin, J. A., Passos, R. R., & Pocrifka, L. A. (2015). Rice Husk Reuse in the Preparation of SnO2/SiO2Nanocomposite. *Materials Research, 18*, 639-643.

Freyermuth, C. L. (2001). Life-Cycle Cost Analysis for Large Bridges. *Concrete International, 23*(02), 89-95.

Ghosh, S. K. (2009). *Self-healing materials: fundamentals, design strategies, and applications*: John Wiley & Sons.

Giannaros, P., Kanellopoulos, A., & Al-Tabbaa, A. (2016). Sealing of cracks in cement using microencapsulated sodium silicate. *Smart Materials and Structures, 25*(8). doi:Artn 084005. 10.1088/0964-1726/25/8/084005

Gilabert, F. A., Van Tittelboom, K., Van Stappen, J., Cnudde, V., De Belie, N., & Van Paepegem, W. (2017). Integral procedure to assess crack filling and mechanical contribution of polymer-based healing agent in encapsulation-based self-healing concrete. *Cement & Concrete Composites, 77*, 68-80. doi:10.1016/j.cemconcomp.2016.12.001

Gilford, J., Hassan, M. M., Rupnow, T., Barbato, M., Okeil, A., & Asadi, S. (2014). Dicyclopentadiene and Sodium Silicate Microencapsulation for Self-Healing of Concrete. *Journal of Materials in Civil Engineering, 26*(5), 886-896. doi:10.1061/(Asce)Mt.1943-5533.0000892

Glanville, W. H. (1931). *The permeability of Portland cement concrete*: [HM Stationery Office [printed by Harrison and sons, Limited].

Hager, M. D., Greil, P., Leyens, C., van der Zwaag, S., & Schubert, U. S. (2010). Self-Healing Materials. *Advanced Materials, 22*(47), 5424-5430. doi:10.1002/adma.201003036

Haghayegh, M., Mirabedini, S. M., & Yeganeh, H. (2016a). Microcapsules containing multi-functional reactive isocyanate-terminated polyurethane prepolymer as a healing agent. Part 1: synthesis and optimization of reaction conditions. *Journal of Materials Science, 51*(6), 3056-3068. doi:10.1007/s10853-015-9616-6

Haghayegh, M., Mirabedini, S. M., & Yeganeh, H. (2016b). Preparation of microcapsules containing multi-functional reactive isocyanate-terminated-polyurethane-prepolymer as healing agent, part II: corrosion performance and mechanical properties of a self healing coating. *Rsc Advances, 6*(56), 50874-50886. doi:10.1039/c6ra07574f

Hearn, N. (1993). *Saturated permeability of concrete as influenced by cracking and self-sealing.* (Phd Thesis), University of Cambridge, Cambridge.

Hearn, N., & Morley, C. T. (1997). Self-sealing property of concrete - Experimental evidence. *Materials and Structures, 30*(201), 404-411. doi:Doi 10.1007/Bf02498563

Homma, D., Mihashi, H., & Nishiwaki, T. (2009). Self-Healing Capability of Fibre Reinforced Cementitious Composites. *Journal of Advanced Concrete Technology, 7*(2), 217-228.

Huang, H. L., Ye, G., & Damidot, D. (2013). Characterization and quantification of self-healing behaviors of microcracks due to further hydration in cement paste. *Cement and Concrete Research, 52*, 71-81. doi:10.1016/j.cemconres.2013.05.003

Huang, H. L., Ye, G., & Damidot, D. (2014). Effect of blast furnace slag on self-healing of microcracks in cementitious materials. *Cement and Concrete Research, 60*, 68-82. doi:10.1016/j.cemconres.2014.03.010

Huang, H. L., Ye, G., & Pel, L. (2016). New insights into autogenous self-healing in cement paste based on nuclear magnetic resonance (NMR) tests. *Materials and Structures, 49*(7), 2509-2524. doi:10.1617/s11527-015-0664-9

Huang, H. L., Ye, G., Qian, C. X., & Schlangen, E. (2016). Self-healing in cementitious materials: Materials, methods and service conditions. *Materials & Design, 92*, 499-511. doi:10.1016/j.matdes.2015.12.091

Hung, C. C., Su, Y. F., & Hung, H. H. (2017). Impact of natural weathering on medium-term self-healing performance of fiber reinforced cementitious composites with intrinsic crack-width control capability. *Cement & Concrete Composites, 80*, 200-209. doi:10.1016/j.cemconcomp.2017.03.018

Hung, C. C., Su, Y. F., & Su, Y. M. (2018). Mechanical properties and self-healing evaluation of strain-hardening cementitious composites with high volumes of hybrid pozzolan materials. *Composites Part B-Engineering, 133*, 15-25. doi:10.1016/j.compositesb.2017.09.005

Hyde, G., & Smith, W. (1889). Results of experiments made to determine the permeability of cements and cement mortars. *Journal of the Franklin Institute, 128*(3), 199-207.

Isaacs, B., Lark, R., Jefferson, T., Davies, R., & Dunn, S. (2013). Crack healing of cementitious materials using shrinkable polymer tendons. *Structural Concrete, 14*(2), 138-147. doi:10.1002/suco.201200013

Jacobsen, S., Marchand, J., & Boisvert, L. (1996). Effect of cracking and healing on chloride transport in OPC concrete. *Cement and Concrete Research, 26*(6), 869-881. doi:Doi 10.1016/0008-8846(96)00072-5

Jacobsen, S., & Sellevold, E. J. (1996). Self healing of high strength concrete after deterioration by freeze thaw. *Cement and Concrete Research, 26*(1), 55-62. doi:Doi 10.1016/0008-8846(95)00179-4

Jefferson, A., Joseph, C., Lark, R., Isaacs, B., Dunn, S., & Weager, B. (2010). A new system for crack closure of cementitious materials using shrinkable polymers. *Cement and Concrete Research, 40*(5), 795-801. doi:10.1016/j.cemconres.2010.01.004

Jia, Y., Wang, H. Y., Tian, K. S., Li, R. F., Xu, Z. P., Jiao, J., . . . Wu, Y. H. (2016). A combined interfacial and in-situ polymerization strategy to construct well-defined core-shell epoxy-containing SiO2-based microcapsules with high encapsulation loading, super thermal stability and nonpolar solvent tolerance. *International Journal of Smart and Nano Materials, 7*(4), 221-235. doi:10.1080/19475411.2016.1261954

Jonkers, H. M. (2007). Self Healing Concrete: A Biological Approach. In S. van der Zwaag (Ed.), *Self Healing Materials: An Alternative Approach to 20 Centuries of Materials Science* (195-204). Dordrecht: Springer Netherlands.

Joseph, C., Gardner, D., Jefferson, T., Isaacs, B., & Lark, B. (2010). Self-healing cementitious materials: a review of recent work. *Proceedings of the Institution of Civil Engineers-Construction Materials, 164*(1), 29-41.

Joseph, C., Jefferson, A. D., Isaacs, B., Lark, R., & Gardner, D. (2010). Experimental investigation of adhesive-based self-healing of cementitious materials. *Magazine of Concrete Research, 62*(11), 831-843. doi:10.1680/macr.2010.62.11.831

JSCE. (2004). Test methods of surface penetrant (draft). In *Recommendations for design and construction about construction method of surface protection* (58-59). Japan: Concrete Library of JSCE 119.

Kanellopoulos, A., Giannaros, P., & Al-Tabbaa, A. (2016). The effect of varying volume fraction of microcapsules on fresh, mechanical and self-healing properties of mortars. *Construction and Building Materials, 122*, 577-593. doi:10.1016/j.conbuildmat.2016.06.119

Kanellopoulos, A., Giannaros, P., Palmer, D., Kerr, A., & Al-Tabbaa, A. (2017). Polymeric microcapsules with switchable mechanical properties for self-healing concrete: synthesis, characterisation and proof of concept. *Smart Materials and Structures, 26*(4). doi:ARTN 04502510.1088/1361-665X/aa516c

Kardar, P. (2015). Preparation of polyurethane microcapsules with different polyols component for encapsulation of isophorone diisocyanate healing agent. *Progress in Organic Coatings, 89*, 271-276. doi:10.1016/j.porgcoat.2015.09.009

Kim, D. J., Kang, S. H., & Ahn, T. H. (2014). Mechanical Characterization of High-Performance Steel-Fiber Reinforced Cement Composites with Self-Healing Effect. *Materials, 7*(1), 508-526. doi:10.3390/ma7010508

Kishi, T., Ahn, T., Hosoda, A., Suzuki, S., & Takaoka, H. (2007). *Self-healing behaviour by cementitious recrystallization of cracked concrete incorporating expansive agent.* Paper presented at the Proceedings of the First International Conference on Self-healing Materials, 18-20 April.

Kuang, Y. C., & Ou, J. P. (2008a). Passive smart self-repairing concrete beams by using shape memory alloy wires and fibers containing adhesives. *Journal of Central South University of Technology, 15*(3), 411-417. doi:10.1007/s11771-008-0077-9

Kuang, Y. C., & Ou, J. P. (2008b). Self-repairing performance of concrete beams strengthened using superelastic SMA wires in combination with adhesives released from hollow fibers. *Smart Materials and Structures, 17*(2). doi:Artn 025020. 10.1088/0964-1726/17/2/025020

Kunieda, M., Choonghyun, K., Ueda, N., & Nakamura, H. (2012). Recovery of Protective Performance of Cracked Ultra High Performance-Strain Hardening Cementitious Composites (UHP-SHCC) Due to Autogenous Healing. *Journal of Advanced Concrete Technology, 10*(9), 313-322. doi:10.3151/jact.10.313

Lee, H., Wong, H., & Buenfeld, N. (2010). Potential of superabsorbent polymer for self-sealing cracks in concrete. *Advances in Applied Ceramics, 109*(5), 296-302.

Lee, H. X. D., Wong, H. S., & Buenfeld, N. R. (2016). Self-sealing of cracks in concrete using superabsorbent polymers. *Cement and Concrete Research, 79*, 194-208. doi:10.1016/j.cemconres.2015.09.008

Li, B. X., Liu, T. X., Hu, L. Y., Wang, Y. F., & Gao, L. N. (2013). Fabrication and Properties of Microencapsulated Paraffin@SiO2 Phase Change Composite for Thermal Energy Storage. *Acs Sustainable Chemistry & Engineering, 1*(3), 374-380. doi:10.1021/sc300082m

Li, M., & Li, V. C. (2011). Cracking and Healing of Engineered Cementitious Composites under Chloride Environment. *ACI Materials Journal, 108*(3), 333-340.

Li, V. C., & Herbert, E. (2012). Robust Self-Healing Concrete for Sustainable Infrastructure. *Journal of Advanced Concrete Technology, 10*(6), 207-218. doi:10.3151/jact.10.207

Li, V. C., Lim, Y. M., & Chan, Y. W. (1998). Feasibility study of a passive smart self-healing cementitious composite. *Composites Part B-Engineering, 29*(6), 819-827. doi:Doi 10.1016/S1359-8368(98)00034-1

Litina, C., Kanellopoulos, A., & Al-Tabbaa, A. (2014). Alternative repair system for concrete using microencapsulated healing agents. *Concrete Solutions 2014*, 97.

Liu, H. Z., Zhang, Q., Gu, C. S., Su, H. Z., & Li, V. (2017a). Influence of microcrack self-healing behavior on the permeability of Engineered Cementitious Composites. *Cement & Concrete Composites, 82*, 14-22. doi:10.1016/j.cemconcomp.2017.04.004

Liu, H. Z., Zhang, Q., Gu, C. S., Su, H. Z., & Li, V. (2017b). Self-healing of microcracks in Engineered Cementitious Composites under sulfate and chloride environment. *Construction and Building Materials, 153*, 948-956. doi:10.1016/j.conbuildmat.2017.07.126

Liu, X., Yao, W., Zheng, X., & Wu, J. (2005). Experimental study on self-healing performance of concrete. *Journal of Building Materials, 2*, 184-188.

Lv, L., Yang, Z., Chen, G., Zhu, G., Han, N., Schlangen, E., & Xing, F. (2016). Synthesis and characterization of a new polymeric microcapsule and feasibility investigation in self-healing cementitious materials. *Construction and Building Materials, 105*, 487-495. doi:10.1016/j.conbuildmat.2015.12.185

Malinskii, Y. M., Prokopenko, V. V., Ivanova, N. A., & Kargin, V. A. (1970). Investigation of self-healing of cracks in polymers. *Polymer Mechanics, 6*(2), 240-244. doi:10.1007/bf00859196

Mihashi, H., & Nishiwaki, T. (2012). Development of Engineered Self-Healing and Self-Repairing Concrete-State-of-the-Art Report. *Journal of Advanced Concrete Technology, 10*(5), 170-184. doi:10.3151/jact.10.170

Minnebo, P., Thierens, G., De Valck, G., Van Tittelboom, K., De Belie, N., Van Hemelrijck, D., & Tsangouri, E. (2017). A Novel Design of Autonomously Healed Concrete: Towards a Vascular Healing Network. *Materials, 10*(1). doi:ARTN 49 10.3390/ma10010049

Muhammad, N. Z., Shafaghat, A., Keyvanfar, A., Majid, M. Z. A., Ghoshal, S. K., Yasouj, S. E. M., . . . McCaffer, R. (2016). Tests and methods of evaluating the self-healing efficiency of concrete: A review. *Construction and Building Materials, 112*, 1123-1132. doi:10.1016/j.conbuildmat.2016.03.017

Na, S. H., Hama, Y., Taniguchi, M., Katsura, O., Sagawa, T., & Zakaria, M. (2012). Experimental Investigation on Reaction Rate and Self-healing Ability in Fly Ash Blended Cement Mixtures. *Journal of Advanced Concrete Technology, 10*(7), 240-253. doi:10.3151/jact.10.240

Neville, A. (2002). Autogenous healing—A concrete miracle? *Concrete International, 24*(11), 76-82.

Nijland, T. G., Larbi, J. A., van Hees, R. P., Lubelli, B., & de Rooij, M. (2007). *Self healing phenomena in concretes and masonry mortars: a microscopic study.* Paper presented at the In Proceedings of 1st International Conference on Self Healing Materials, The Netherlands.

Nishiwaki, T., Koda, M., Yamada, M., Mihashi, H., & Kikuta, T. (2012). Experimental Study on Self-Healing Capability of FRCC Using Different Types of Synthetic Fibers. *Journal of Advanced Concrete Technology, 10*(6), 195-206. doi:10.3151/jact.10.195

Nishiwaki, T., Kwon, S., Homma, D., Yamada, M., & Mihashi, H. (2014). Self-Healing Capability of Fiber-Reinforced Cementitious Composites for Recovery of Watertightness and Mechanical Properties. *Materials, 7*(3), 2141-2154. doi:10.3390/ma7032141

Nishiwaki, T., Mihashi, H., Jang, B.-K., & Miura, K. (2006). Development of self-healing system for concrete with selective heating around crack. *Journal of Advanced Concrete Technology, 4*(2), 267-275.

Ozbay, E., Sahmaran, M., Lachemi, M., & Yucel, H. E. (2013). Self-Healing of Microcracks in High-Volume Fly-Ash-Incorporated Engineered Cementitious Composites. *ACI Materials Journal, 110*(1), 32-42.

Palin, D., Wiktor, V., & Jonkers, H. M. (2015). Autogenous healing of marine exposed concrete: Characterization and quantification through visual crack closure. *Cement and Concrete Research, 73*, 17-24. doi:10.1016/j.cemconres.2015.02.021

Pelletier, M., Brown, R., Shukla, A., & Bose, A. (2011). Self-Healing Concrete with a Microencapsulated Healing Agent.

http://energetics.chm.uri.edu/system/files/Self%20healing%20concrete%20-7-11.pdf

Perez, G., Erkizia, E., Gaitero, J. J., Kaltzakorta, I., Jimenez, I., & Guerrero, A. (2015). Synthesis and characterization of epoxy encapsulating silica microcapsules and amine functionalized silica nanoparticles for development of an innovative self-healing concrete. *Materials Chemistry and Physics, 165*, 39-48. doi:10.1016/j.matchemphys.2015.08.047

Perez, G., Gaitero, J. J., Erkizia, E., Jimenez, I., & Guerrero, A. (2015). Characterisation of cement pastes with innovative self-healing system based in epoxy-amine adhesive. *Cement & Concrete Composites, 60*, 55-64. doi:10.1016/j.cemconcomp.2015.03.010

Qian, S. Z., Zhou, J., & Schlangen, E. (2010). Influence of curing condition and precracking time on the self-healing behavior of Engineered Cementitious Composites. *Cement & Concrete Composites, 32*(9), 686-693. doi:10.1016/j.cemconcomp.2010.07.015

Ramachandran, S. K., Ramakrishnan, V., & Bang, S. S. (2001). Remediation of concrete using micro-organisms. *ACI Materials Journal-American Concrete Institute, 98*(1), 3-9.

Ramm, W., & Biscoping, M. (1998). Autogenous healing and reinforcement corrosion of water-penetrated separation cracks in reinforced concrete. *Nuclear Engineering and Design, 179*(2), 191-200. doi:Doi 10.1016/S0029-5493(97)00266-5

Reinhardt, H. W., & Jooss, M. (2003). Permeability and self-healing of cracked concrete as a function of temperature and crack width. *Cement and Concrete Research, 33*(7), 981-985. doi:10.1016/S0008-8846(02)01099-2

Sahmaran, M., Keskin, S. B., Ozerkan, G., & Yaman, I. O. (2008). Self-healing of mechanically-loaded self consolidating concretes with high volumes of fly ash. *Cement & Concrete Composites, 30*(10), 872-879. doi:10.1016/j.cemconcomp.2008.07.001

Sahmaran, M., Li, M., & Li, V. C. (2007). Transport properties of engineered cementitious composites under chloride exposure. *ACI Materials Journal, 104*(6), 604-611.

Sahmaran, M., & Li, V. C. (2009). Durability properties of micro-cracked ECC containing high volumes fly ash. *Cement and Concrete Research, 39*(11), 1033-1043. doi:10.1016/j.cemconres.2009.07.009

Sahmaran, M., Yildirim, G., & Erdem, T. K. (2013). Self-healing capability of cementitious composites incorporating different supplementary cementitious materials. *Cement & Concrete Composites, 35*(1), 89-101. doi:10.1016/j.cemconcomp.2012.08.013

Saihi, D., Vroman, I., Giraud, S., & Bourbigot, S. (2006). Microencapsulation of ammonium phosphate with a polyurethane shell. Part II. Interfacial polymerization technique. *Reactive & Functional Polymers, 66*(10), 1118-1125. doi:10.1016/j.reactfunctpolym.2006.02.001

Salama, I., Hilloulin, B., Medjigbodo, S., & Loukili, A. (2017). Influence of Supplementary Cementitious Materials on the Autogenous Self-Healing of Cracks in Cementitious Materials. *Special Publication, 320*, 12.11-12.14.

Sangadji, S., & Schlangen, E. (2012). Self Healing of Concrete Structures - Novel Approach Using Porous Network Concrete. *Journal of Advanced Concrete Technology, 10*(5), 185-194. doi:10.3151/jact.10.185

Sangadji, S., Wiktor, V., Jonkers, H., & Schlangen, E. (2017). The use of alkaliphilic bacteria-based repair solution for porous network concrete healing mechanism. *3rd International Conference on Sustainable Civil Engineering Structures and Construction Materials - Sustainable Structures for Future Generations, 171*, 606-613. doi:10.1016/j.proeng.2017.01.387

Sanghvi, S. P., & Nairn, J. G. (1992). Effect of Viscosity and Interfacial-Tension on Particle-Size of Cellulose-Acetate Trimellitate Microspheres. *Journal of Microencapsulation, 9*(2), 215-227.

Savija, B., Feiteira, J., Araujo, M., Chatrabhuti, S., Raquez, J. M., Van Tittelboom, K., . . . Schlangen, E. (2017). Simulation-Aided Design of Tubular Polymeric Capsules for Self-Healing Concrete. *Materials, 10*(1). doi:ARTN 10 10.3390/ma10010010

Sherir, M. A. A., Hossain, K. M. A., & Lachemi, M. (2016). Self-healing and expansion characteristics of cementitious composites with high volume fly ash and MgO-type expansive agent. *Construction and Building Materials, 127*, 80-92. doi:10.1016/j.conbuildmat.2016.09.125

Sherir, M. A. A., Hossain, K. M. A., & Lachemi, M. (2017a). Development and recovery of mechanical properties of self-healing cementitious composites with MgO expansive agent. *Construction and Building Materials, 148*, 789-810. doi:10.1016/j.conbuildmat.2017.05.063

Sherir, M. A. A., Hossain, K. M. A., & Lachemi, M. (2017b). The influence of MgO-type expansive agent incorporated in self-healing system of Engineered cementitious Composites. *Construction and Building Materials, 149*, 164-185. doi:10.1016/j.conbuildmat.2017.05.109

Siad, H., Lachemi, M., Sahmaran, M., & Hossain, K. M. A. (2017). Mechanical, Physical, and Self-Healing Behaviors of Engineered Cementitious Composites with

Glass Powder. *Journal of Materials in Civil Engineering, 29*(6). doi:Artn 04017016 10.1061/(Asce)Mt.1943-5533.0001864

Singh, M., Hemant, K., Ram, M., & Shivakumar, H. (2010). Microencapsulation: A promising technique for controlled drug delivery. *Research in pharmaceutical sciences, 5*(2), 65.

Sisomphon, K., Copuroglu, O., & Fraaij, A. (2011). Application of encapsulated lightweight aggregate impregnated with sodium monofluorophosphate as a self-healing agent in blast furnace slag mortar. *Heron, 56 (1/2)*, 13–32.

Sisomphon, K., Copuroglu, O., & Koenders, E. A. B. (2012). Self-healing of surface cracks in mortars with expansive additive and crystalline additive. *Cement & Concrete Composites, 34*(4), 566-574. doi:10.1016/j.cemconcomp.2012.01.005

Sisomphon, K., Copuroglu, O., & Koenders, E. A. B. (2013). Effect of exposure conditions on self healing behavior of strain hardening cementitious composites incorporating various cementitious materials. *Construction and Building Materials, 42*, 217-224. doi:10.1016/j.conbuildmat.2013.01.012

Snoeck, D., Steuperaert, S., Van Tittelboom, K., Dubruel, P., & De Belie, N. (2012). Visualization of water penetration in cementitious materials with superabsorbent polymers by means of neutron radiography. *Cement and Concrete Research, 42*(8), 1113-1121. doi:10.1016/j.cemconres.2012.05.005

Tan, N. P. B., Keung, L. H., Choi, W. H., Lam, W. C., & Leung, H. N. (2016). Silica-based self-healing microcapsules for self-repair in concrete. *Journal of Applied Polymer Science, 133*(12). doi:Artn 43090 10.1002/App.43090

Tang, W. C., Kardani, O., & Cui, H. Z. (2015). Robust evaluation of self-healing efficiency in cementitious materials - A review. *Construction and Building Materials, 81*, 233-247. doi:10.1016/j.conbuildmat.2015.02.054

Teall, O., Pilegis, M., Sweeney, J., Gough, T., Thompson, G., Jefferson, A., . . . Gardner, D. (2017). Development of high shrinkage polyethylene terephthalate (PET) shape memory polymer tendons for concrete crack closure. *Smart Materials and Structures, 26*(4), 045006.

Ter Heide, N. (2005). *Crack healing in hydrating concrete.* MSc thesis, Delft University, Delft, The Netherlands.

Termkhajornkit, P., Nawa, T., Yamashiro, Y., & Saito, T. (2009). Self-healing ability of fly ash-cement systems. *Cement & Concrete Composites, 31*(3), 195-203. doi:10.1016/j.cemconcomp.2008.12.009

Torrent, R. J. (1992). A two-chamber vacuum cell for measuring the coefficient of permeability to air of the concrete cover on site. *Materials and Structures, 25*(6), 358-365. doi:10.1007/bf02472595

Tyagi, V. V., Kaushik, S. C., Tyagi, S. K., & Akiyama, T. (2011). Development of phase change materials based microencapsulated technology for buildings: A review. *Renewable & Sustainable Energy Reviews, 15*(2), 1373-1391. doi:10.1016/j.rser.2010.10.006

Van Breugel, K. (2007). *Is there a market for self-healing cement-based materials.* Paper presented at the Proceedings of the First International Conference on Self-Healing Materials, Noordwijk, The Netherlands.

Van Tittelboom, K., & De Belie, N. (2013). Self-Healing in Cementitious Materials-A Review. *Materials, 6*(6), 2182-2217. doi:10.3390/ma6062182

Wang, J., Jonkers, H. M., Boon, N., & De Belie, N. (2017). Bacillus sphaericus LMG 22257 is physiologically suitable for self-healing concrete. *Applied Microbiology and Biotechnology, 101*(12), 5101-5114. doi:10.1007/s00253-017-8260-2

Wang, J. Y., Snoeck, D., Van Vlierberghe, S., Verstraete, W., & De Belie, N. (2014). Application of hydrogel encapsulated carbonate precipitating bacteria for approaching a realistic self-healing in concrete. *Construction and Building Materials, 68*, 110-119. doi:10.1016/j.conbuildmat.2014.06.018

Wang, J. Y., Soens, H., Verstraete, W., & De Belie, N. (2014). Self-healing concrete by use of microencapsulated bacterial spores. *Cement and Concrete Research, 56*, 139-152. doi:10.1016/j.cemconres.2013.11.009

Wang, W., Xu, L. K., Liu, F., Li, X. B., & Xing, L. K. (2013). Synthesis of isocyanate microcapsules and micromechanical behavior improvement of microcapsule shells by oxygen plasma treated carbon nanotubes. *Journal of Materials Chemistry A, 1*(3), 776-782. doi:10.1039/c2ta00612j

White, S. R., Sottos, N. R., Geubelle, P. H., Moore, J. S., Kessler, M. R., Sriram, S. R., . . . Viswanathan, S. (2001). Autonomic healing of polymer composites. *Nature, 409*(6822), 794-797. doi:Doi 10.1038/35057232

Wiktor, V., & Jonkers, H. M. (2011). Quantification of crack-healing in novel bacteria-based self-healing concrete. *Cement & Concrete Composites, 33*(7), 763-770. doi:10.1016/j.cemconcomp.2011.03.012

Wu, M., Johannesson, B., & Geiker, M. (2012). A review: Self-healing in cementitious materials and engineered cementitious composite as a self-healing material. *Construction and Building Materials, 28*(1), 571-583. doi:10.1016/j.conbuildmat.2011.08.086

Xing, F., Ni, Z., Han, N., Dong, B., Du, X., Huang, Z., & Zhang, M. (2008). *Self-healing mechanism of a novel cementitious composite using microcapsules.* Paper presented at the Proceedings of the International Conference on Durability of Concrete Structures, Hangzhou, China.

Xu, J., & Yao, W. (2014). Multiscale mechanical quantification of self-healing concrete incorporating non-ureolytic bacteria-based healing agent. *Cement and Concrete Research, 64*, 1-10. doi:10.1016/j.cemconres.2014.06.003

Yang, J. L., Keller, M. W., Moore, J. S., White, S. R., & Sottos, N. R. (2008). Microencapsulation of Isocyanates for Self-Healing Polymers. *Macromolecules, 41*(24), 9650-9655. doi:10.1021/ma801718v

Yang, Y. Z., Lepech, M. D., Yang, E. H., & Li, V. C. (2009). Autogenous healing of engineered cementitious composites under wet-dry cycles. *Cement and Concrete Research, 39*(5), 382-390. doi:10.1016/j.cemconres.2009.01.013

Yang, Z. X., Hollar, J., He, X. D., & Shi, X. M. (2011). A self-healing cementitious composite using oil core/silica gel shell microcapsules. *Cement & Concrete Composites, 33*(4), 506-512. doi:10.1016/j.cemconcomp.2011.01.010

Yang, Z. X., Holler, J., He, X. D., & Shi, X. M. (2010). Laboratory Assessment of a Self-Healing Cementitious Composite. *Transportation Research Record*(2142), 9-17. doi:10.3141/2142-02

Yi, H., Yang, Y., Gu, X. Y., Huang, J., & Wang, C. Y. (2015). Multilayer composite microcapsules synthesized by Pickering emulsion templates and their application in self-healing coating. *Journal of Materials Chemistry A, 3*(26), 13749-13757. doi:10.1039/c5ta02288f

Yildirim, G., Sahmaran, M., & Ahmed, H. U. (2015). Influence of Hydrated Lime Addition on the Self-Healing Capability of High-Volume Fly Ash Incorporated Cementitious Composites. *Journal of Materials in Civil Engineering, 27*(6). doi:Artn 04014187 10.1061/(Asce)Mt.1943-5533.0001145

Yoshizawa, H., Kamio, E., Hirabayashi, N., Jacobson, J., & Kitamura, Y. (2004). Membrane formation mechanism of cross-linked polyurea microcapsules by phase separation method. *Journal of Microencapsulation, 21*(3), 241-249. doi:10.1080/02652040410001673946

Zhan, S. P., Chen, S. H., Chen, L., & Hou, W. M. (2016). Preparation and characterization of polyurea microencapsulated phase change material by interfacial polycondensation method. *Powder Technology, 292*, 217-222. doi:10.1016/j.powtec.2016.02.007

Zhang, H. Z., Sun, S. Y., Wang, X. D., & Wu, D. Z. (2011). Fabrication of microencapsulated phase change materials based on n-octadecane core and silica shell through interfacial polycondensation. *Colloids and Surfaces a-Physicochemical and Engineering Aspects, 389*(1-3), 104-117. doi:10.1016/j.colsurfa.2011.08.043

Zhang, Z. G., Qian, S. Z., & Ma, H. (2014). Investigating mechanical properties and self-healing behavior of micro-cracked ECC with different volume of fly ash. *Construction and Building Materials, 52*, 17-23. doi:10.1016/j.conbuildmat.2013.11.001

Zhou, S., Zhu, H., & Yan, Z. (2014). Materials, theories and experiments of microcapsule self-healing method—A review. In *Tunneling and Underground Construction* (195-204).

Zhou, Z. H., Li, Z. Q., Xu, D. Y., & Yu, J. H. (2011). Influence of Slag and Fly Ash on the Self-healing Ability of Concrete. *Emerging Focus on Advanced Materials, Pts 1 and 2, 306-307*, 1020-+. doi:10.4028/www.scientific.net/AMR.306-307.1020

Zhu, D. Y., Rong, M. Z., & Zhang, M. Q. (2015). Self-healing polymeric materials based on microencapsulated healing agents: From design to preparation. *Progress in Polymer Science, 49-50*, 175-220. doi:10.1016/j.progpolymsci.2015.07.002